Study of extensive air showers at sea level

Soltanzadeh Mohammad Mahdi Darjazi

STUDY OF EXTENSIVE AIR SHOWERS AT SEA LEVEL

by

Mohammad Mahdi Soltanzadeh Darjazi, B.Sc. (Mashhad)

A thesis submitted to the University of Durham for the degree of Doctor of Philosophy

Department of Physics,
Durham University, U.K.

December, 1983.

CONTENTS

ABSTRACT

The zenith angle distribution of EAS over the size range 10^4 - $1.4.10^6$ particles at sea level has been studied. Representing the zenith angle distribution by $I(\theta) = I(0)\cos^n\theta$ it is found that $n = 8.4 \pm 0.3$ over the size range 5.10^4 - $1.4.10^6$ particles. For the smallest sizes studied $10^4 < N < 5.10^4$ the measurements suggest n decreases to 5.1 ± 1.3.

The design and performance of a prototype plastic scintillation counter of area 80cm x 50 cm = 0.4 m^2 is described. The response of the counter is such that it gives a single particle peak well resolved from the noise when its response to the global cosmic ray flux is displayed on a pulse height analyser. Two such counters of this type were used as local electron density detectors to register the arrival of extensive air showers in a tachyon search experiment.

The tachyon search experiment showed evidence that tachyons may be associated with extensive air showers of local electron density $\geq 25\ m^{-2}$. The evidence is based on the observation of an excess of ionising events (4.4 standard deviations above the background) occurring in the 85-95 μs time domain before the arrival of the main shower front at sea level.

PREFACE

This thesis describes the work performed by the author at Durham University, while under the supervision of Dr. F. Ashton during the period 1979 to 1983.

Initially the author carried out work on the analysis of data obtained using the original Durham Air Shower Array. Subsequently he developed a prototype plastic scintillation counter of area 80cmx50cm = 0.4 cm^2 of high efficiency. Later nine such counters were constructed with the intention of eventually using them in an improved Durham Air Shower Array.

The main work carried out by the author was the experiment to search for evidence for tachyons associated with extensive air showers observed at sea level. This work used two scintillation counters of the type developed by the author as a local electron density trigger plus a further scintillation counter of high efficiency as the tachyon detector.

ACKNOWLEDGEMENTS

I would like to thank Professor A.W. Wolfendale F.R.S. for the privilege of working in his laboratories and for his interest and support.

It is a pleasure to record a deep gratitude to my supervisor Dr. F. Ashton, for his advice, guidance and invaluable suggestions throughout this work.

I would like to thank my colleagues, Dr. H. Najabat and Mr. H.F. Masjed for much helpful assistance and the technical staff of the physics Department, in particular the late Mr. W. Leslie and Mr. K. Tindale and H. Davison.

Thanks are due to Mrs. M. Bell for her careful typing of this thesis.

I wish to express my sincere thanks to my sister and brother-in-law, Mrs. Maleha Sedaght and Faraydon Tahare for their moral and financial support.

Finally, I am indebted to my wife for her continuous encouragement, endurance and patience.

CHAPTER 1

INTRODUCTION

1.1 DISCOVERY OF COSMIC RAYS

Early experiments on the discovery of cosmic rays were carried out by Elster and Geitel. In the year 1900, during experiments to study the conductivity of air, they noticed the existence of a penetrating radiation which continuously ionized the air in an electroscope. Wilson used an ionization chamber and noticed the penetrability of this radiation, even under "many feet of rock" and this led him to agree with Geitel that it seemed to be a property of the air itself. It was also thought that it could be due to some radioactive materials in the earth, so that a measurement of the change of ionization with height was necessary to confirm it. Hess (1911, 1912) flew a balloon to 5 Km and observed a slight decrease up to 1 Km but above this the ionization increased rapidly up to an altitude of 5 Km. From these experiments he concluded that the radiation was of extra terrestrial origin with no significant changes between day and night indicating that the ionization produced did not emanate from the sun. Kolhorster (1913) who extended the data to 9 Km confirmed Hess's work. Millikan (1923, 1926) extended the data up to 15 Km, and some meters under the surface of lakes and measured the absorption of the radiation in water and found an equivalent mass of air and water had the same absorption. In both air and water the results showed a decrease with depth indicating a radiation travelling downwards in the air. The overall results showed this radiation came from above the atmosphere and he called it 'Cosmic radiation'. Subsequently, different detectors such as cloud chambers and Geiger-Muller Counters were used for more investigations showing that in the lower atmospheric levels a large proportion of

the cosmic radiation consisted of charged particles.

The east-west effect shows that more particles arrive from the west than the east, Clay (1927). Johnson and Street (1933) concluded that a significant proportion of primary cosmic rays were positively charged and in 1948 using a high altitude balloon, protons were observed in the primary flux (about 90%). Later, heavy nuclei were also discovered. Progress of cosmic ray radiation studies led to the discovery of many new particles such as the positron (Anderson 1932), which had been predicted by Dirac and muons by Anderson (1937). Particle discoveries continued and in 1947 Rochester and Butler identified in a cloud chamber a neutral particle ($\overset{\circ}{\Lambda}$). In 1962 cosmic x rays and discrete x ray sources were discovered, and subsequently cosmic γ rays and discrete γ ray sources.

1.2 ORIGIN OF THE COSMIC RADIATION

Since the discovery of the cosmic radiation, the origin and acceleration mechanism of very high energy particles coming down continuously were questioned. Three major suggestions for the source of cosmic rays were investigated as follows :

a. Solar origin : It had been believed for a long time that some cosmic rays are of solar origin. The sun can accelerate particles especially at the time of solar flare activity. The results during periods of solar flare activity indicate that there is an acceleration mechanism available on the sun which can produce particles with energies up to ~10 Gev.

One of the obvious arguments against the sun producing all the observed cosmic rays is the comparatively weak interplanetary magnetic fields ($\sim 10^{-5}$ Gauss) which can not confine a proton of 10^{14} ev to the

Solar system. This would result in an anisotropy of the radiation and it is not observed. So, a powerful mechanism of particle acceleration is required. Fermi (1949) postulated that cosmic rays are repeatedly scattered against the clouds of magnetic plasma that move at about 30 Km per sec in interstellar space. This theory does not agree with more recently observed properties.

b. Galactic origin : It was reasonable to assume that other stars like the sun in the galaxy (containing $\sim 10^{11}$ stars) emitted cosmic rays. But it would not be possible for them to produce such an observed flux, so, we have to look for additional sources in other types of star. Several suggestions have been made, for example stars such as magnetic variable stars as well as novae and supernovae seem to be capable of supplying the necessary energies. It seems that, after an initial supernova explosion a shock wave from the core would go out with extreme relativistic velocity and would accelerate particles to energies ranging from 10^{18} to 10^{21} ev. Because supernova are rich in heavy elements this is consistent with the measured cosmic ray composition. However, the energies reached by particles accelerated at their source of origin is likely to be less than the highest energy particles observed. So, an additional acceleration would be necessary. This may be from the collision of cosmic ray particles with randomly moving magnetised gas clouds as they stream through the arms of the galaxy as suggested by Fermi.

c. Universe : At very high energies (above 10^{18} ev) cosmic ray particles producing extensive air showers (E A S) of size $>10^{8}$ particles at sea level have too much energy to be stored in our galaxy, but are coming from outside it. Therefore, they leak from one galaxy to another and contribute an extra galactic component to the cosmic ray

flux. Morrison (1961) mentioned the presence of unusual galaxies which contain a most unusual bright area, that could possibly produce cosmic rays of energy at least as high as 10^{19} ev and perhaps very much higher. This is the most satisfactory composite model at the present time.

1.3 THE SIGNIFICANCE OF COSMIC RAY STUDIES

The study of cosmic rays with individual particles of energy ranging from about 10^{8} ev to 10^{20} ev makes it of interest in the fields of elementary particle physics, as well as astrophysics. Its interactions with the earth's atmosphere has been studied for several decades, and although the gross features are understood, it is likely that new phenomena exist (e.g. quark production in high energy interactions) which have yet to be observed.

Recently cosmic ray studies have expanded to study the current fundamental problems in particle physics as to whether quarks, magnetic monopoles or tachyons exist or not. If they do then it is likely that they are produced in the atmosphere in very high energy cosmic ray interactions or are incident on the earth in the primary cosmic ray flux. Recently Fegan (1981) has produced evidence that a finite flux of tachyons may be produced in high energy cosmic ray interactions. A search for tachyons in the sea level cosmic ray flux is described by the author in Chapter 6.

1.4 PROPAGATION OF COSMIC RAYS THROUGH THE ATMOSPHERE - EXTENSIVE AIR SHOWERS

The primary radiation which is known to be mainly protons and α particles, interacts strongly with the nuclei of the atmosphere and produces a variety of secondary particles. On average, protons travel 70-80 g cm^{-2} of air about 10-30 Km above sea level before making their first interaction with an air nucleus. In this interaction they lose ~50% of their energy and continue a further 70-80 g cm^{-2} before making a second interaction and so on. The secondary particles produced in these interactions are mainly composed of pions with three charge modes (π^+,π^- and π°) which are produced on average in equal numbers as well as kaons, hyperons and nucleon, anti-nucleon pairs. The neutral pions decay almost instantaneously (mean life time $\simeq 10^{-16}$ sec) into two gamma-rays which produce electron-positron pairs by means of the pair production process. The relativistic electrons from pair production produce further gamma rays by bremsstrahlung and the shower of particles resulting is known as an electromagnetic cascade. A primary cosmic ray energy of around 10^{13} ev is sufficient to produce a small extensive air shower (E A S) at sea level containing $\sim 10^3$ electrons.

The produced charged pions can either intract with an air nucleus to produce more pions or can decay to produce muons

$$\pi^+ \rightarrow \mu^+ + \nu_\mu$$
$$\pi^- \rightarrow \mu^- + \bar{\nu}_\mu$$

with a relative probability that depends on their energy and zenith angle. As the energy of the primary cosmic ray particle increases, the number of particles that reach sea level increases and the lateral extent of the shower increases. By measuring the number of particles in the shower an estimate of the primary energy can be

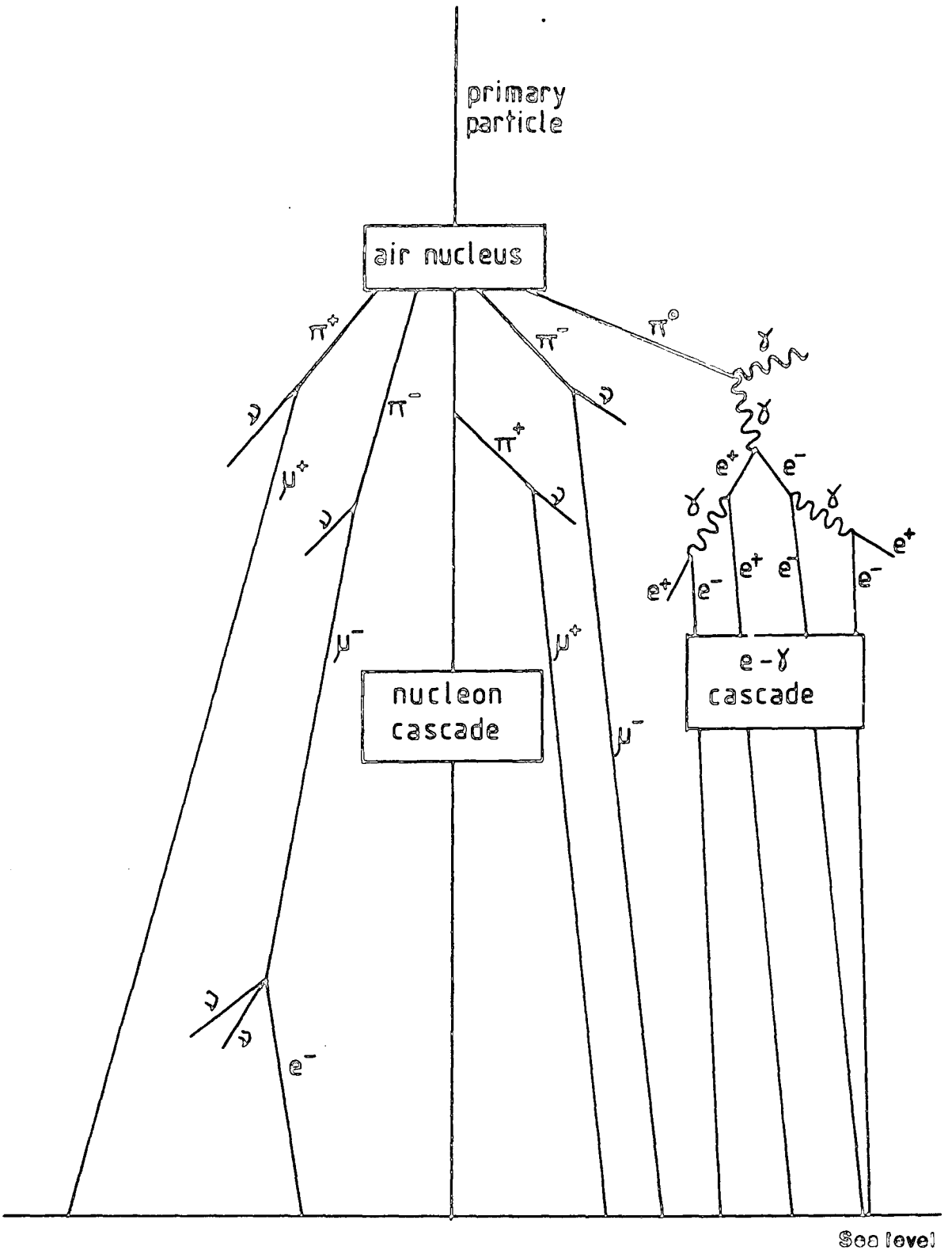

FIGURE 1.1 : Development of an extensive air shower

made. The most important processes for the propagation of cosmic rays through the atmosphere are those shown in Fig. 1.1. The length of the track of π° mesons is infinitesimal in practice and the angles between the various tracks are much smaller than shown. Further the subsequent interactions produced in the nucleon cascade are not shown.

1.5 THE ABSORPTION OF COSMIC RAYS IN THE ATMOSPHERE

It has been remarked already that high energy primary particles mainly consist of protons and α-particles coming from outer space. These primary cosmic ray particles penetrate into the atmosphere and on colliding against oxygen and nitrogen nuclei of the air, lose energy and are gradually absorbed. At the same time secondary rays of lower average energy and of a different nature are produced. This situation is shown in Fig.1.1 which is relevant to primary cosmic rays with energy of a few tens of Gev. The relative intensities of the various components has been measured as a function of altitude in the near vertical direction at 50° geomagnetic latitude by Rossi (1952) as shown in Figure 1.1.2. At the top of the atmosphere (t = o) for protons of energy $\gtrsim$ 1 Gev the intensity is $\sim 10^{-1}$ cm^{-2} Sec^{-1} st^{-1} . With decreasing altitude the intensity of the proton component falls rapidly corresponding to an almost exponential absorption given by $R = Ro \exp -\frac{x}{L}$ (L, the absorption length is = 120 g/cm^2). In contrast the number of electrons and protons increases rapidly and goes through a maximum between (13-20) km and then falls off rapidly with decreasing altitude. The intensity of the meson component (denoted μ) rises rapidly with depth and goes through a maximum in the range (100-200)$g.cm^{-2}$ and then decrease much less rapidly compared with the electron-photon component. This is because μ mesons do not

undergo radiation losses comparable to electrons so with decreasing altitude the number of μ mesons relatively increases until near sea level more than half of the total number of charged cosmic ray particles are μ mesons. Pi-mesons because of their short mean life time ($\sim 2.65 \times 10^{-8}$ sec) are very scarce in the atmosphere. It is noted that for the electron component the peak intensity is much higher than the maximum intensity of the proton or μ-meson components. This is because a high energy π^0 meson can lead to many electrons, via the photon electron cascade compared with a fast charged π meson which can produce only one μ via π-μ decay. The more rapid fall off in intensity of electrons is due to the additional source of energy loss in the form of bremsstrahlung over and above that due to ionisation loss. At the comparatively low primary energies (1 Gev to a few tens of Gev) that produce the main secondary radiation in the atmosphere secondary interactions of the surviving primary nucleon and also of the charged pions that it produces in its first interaction with an air nucleus are comparatively unimportant. However as the primary energy increases (and the rate of arrival of such primaries decreases) secondary and further interactions become more and more important and the effects produced by a primary cosmic ray proton penetrate deeper and deeper into the atmosphere. Ultimately instead of a primary cosmic ray proton producing one or two particles that reach sea level a whole shower of particles arrives simultaneously consisting mainly of electrons but also with significant numbers of muons and hadrons. Roughly speaking a primary proton of energy Eev produces a shower at sea level of size $N=E/10^{10}$ particles. Thus for $E=10^{15}$ ev, $N=10^5$. Such an event (extensive air shower or EAS) has been exploited to signal the arrival of a high energy primary particle as described in later sections of this thesis.

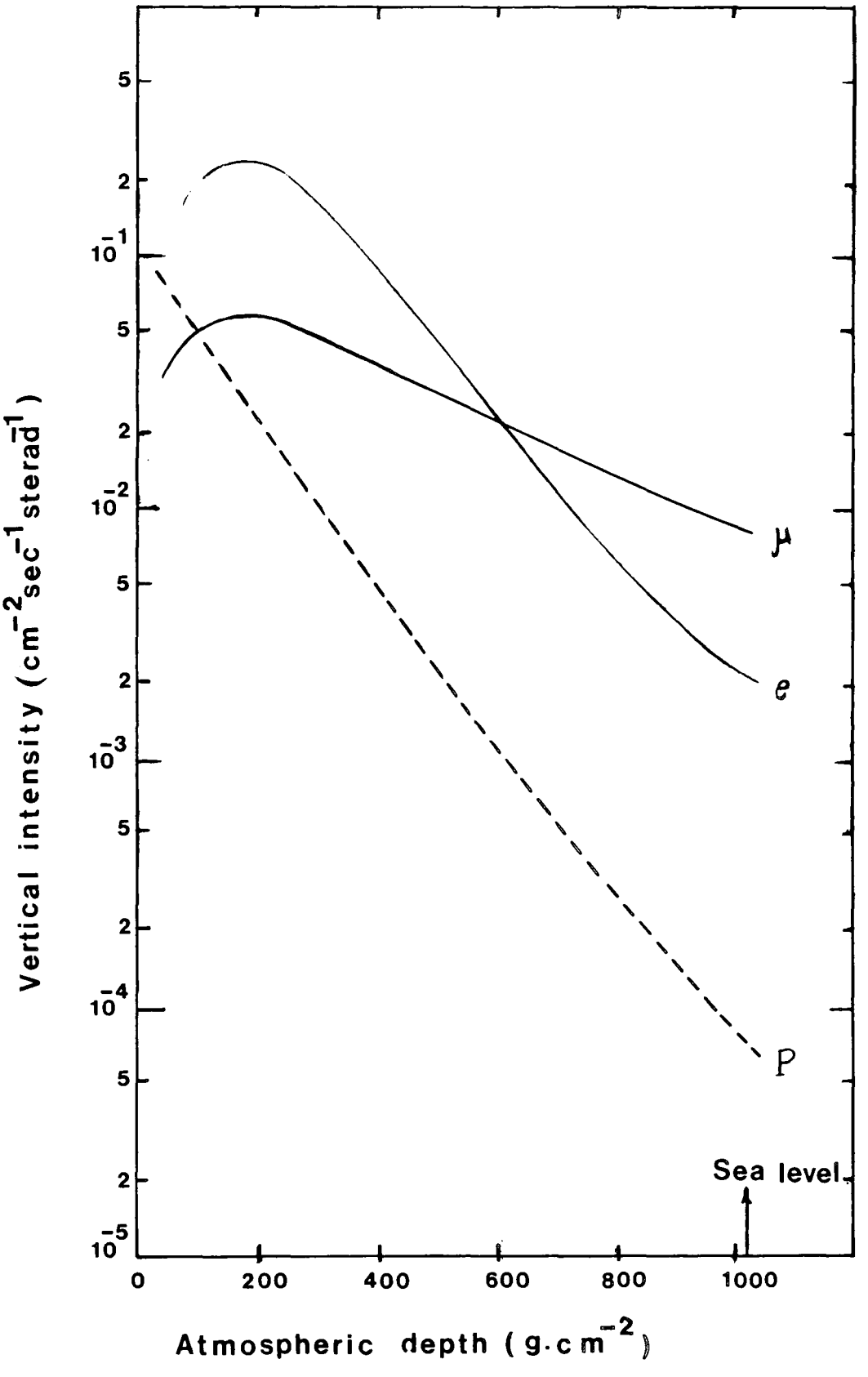

Fig. 1.1.2 Variation of the vertical intensity with altitude. (μ and e after Rossi (1952), p estimated).

1.6 INTENSITY OF PRIMARY COSMIC RAYS

The wide range of energy and intensities of cosmic rays is one of the most important parameters. Wolfendale (1973) summarised measurements of the primary cosmic ray spectrum as shown in Fig.1.2. The overall primary energy can be characterised over a wide range of energies by $I(>E) = KE^{-\gamma}$ where K is a constant and E is the primary energy, γ is the slope of the spectrum and I is the intensity. Greisen (1965) expressed the variation of the integral spectrum intensitieswith particle energy in ev as

$I(>E) = KE^{-\gamma}$

10^{10} ev < E < 10^{15} ev	$I(>E) = 2.5 \times 10^{18} E^{-1.6}$	
10^{15} ev < E < 10^{18} ev	$I(>E) = 5.0 \times 10^{27} E^{-2.2}$	$m^{-2}sec^{-1}st^{-1}$
10^{18} ev < E	$I(>E) = 4.0 \times 10^{16} E^{-1.6}$	

Four different regions of the spectrum have been considered below. In the energy range from a few hundred Mev to $\sim 10^3$ Gev all measurement information comes mainly from satellite and balloon experiments. Between 10^{10} up to 10^{15} ev the slope is -1.6. In this region, the highest direct energy measurements have been done and reported by Grigorov et al (1971). Above 10^{14} ev all information is provided from E.A.S studies where the atmosphere is a part of the detector system. Around 3×10^{15} ev the slope changes from

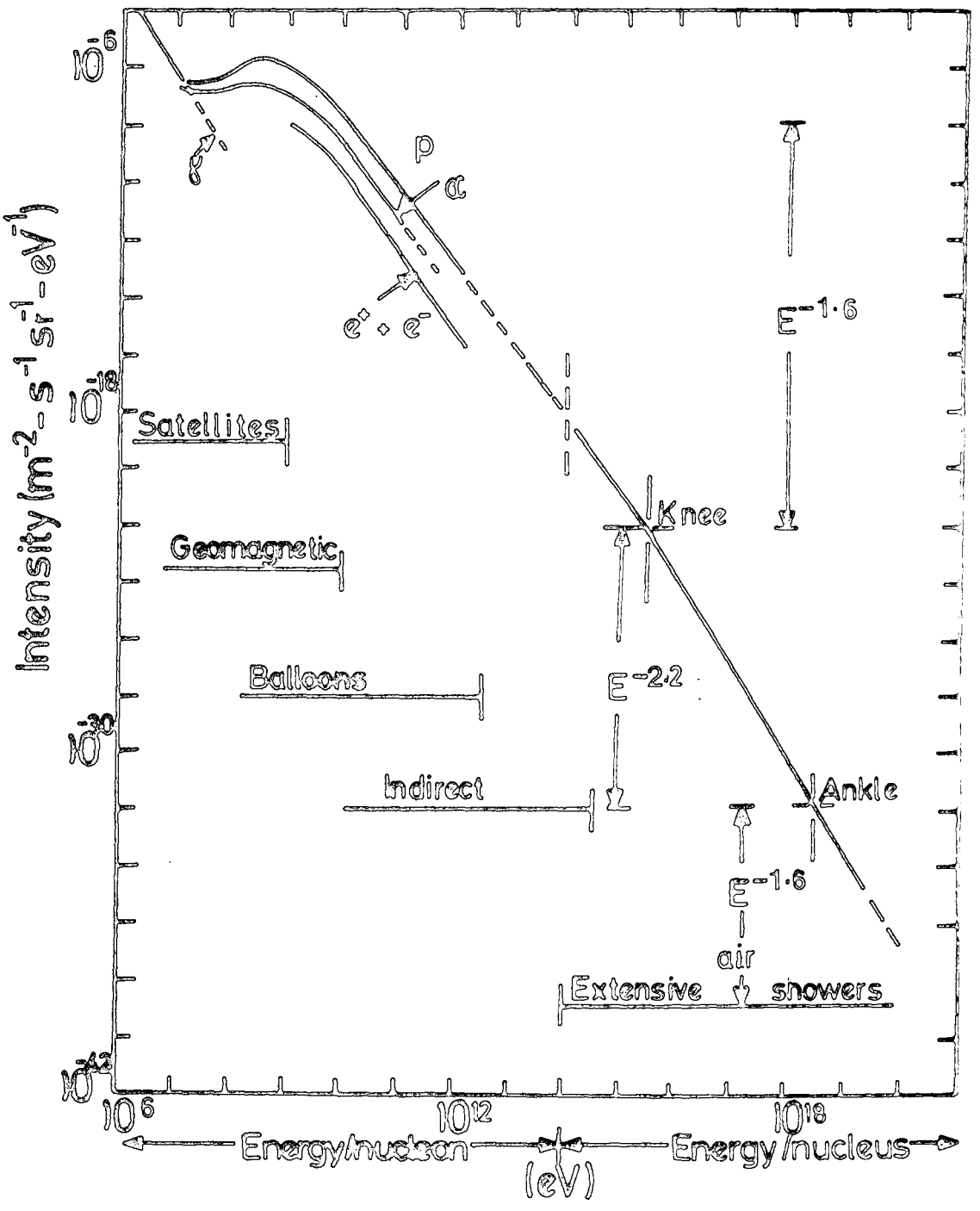

Figure 1.2 : Summary of measurements of the primary spectrum of protons and nuclei in the cosmic radiation (After Wolfendale, 1973).

-1.6 to -2.2. It is believed that this change is due to the inability of the galactic magnetic fields to contain various types of particles as their containment rigidities are exceeded. At around 3.10^{18} ev the slope changes to -1.6 again. This change may be produced by extra-galactic sources of radiation but more recent data from air shower experiments has increased doubts about this "kink" in the spectrum.

Greisen (1966) suggested a cut off in the cosmic ray spectrum at about 6×10^{19} ev, this has not been confirmed. Fig. 1.3 by Hillas (1981) shows the recently accepted form of the integral energy spectrum. Between 10^{10} ev till 10^{15} ev $\gamma \simeq 1.6$ and around 3×10^{15} ev. it changes to $\gamma \simeq 2$.

1.7 THE NATURE OF THE COSMIC RADIATION

At the present time considerable effort is being made to study the nature of cosmic rays. The primary cosmic ray composition contains nuclear (i.e. nuclei), electronic (i.e. electrons and positrons) and electro-magnetic (i.e. x-rays and γ-rays) components. The measurement of nuclei in primary cosmic rays now extends up to 10^{20} ev. For low energies ($< 10^{13}$ ev) direct measurements have been made by using balloons and satellites. In the energy region 10^{10} - 10^{13} ev the composition of the primary flux is shown in table 1.1 (after Juliussen 1975) and normalized to a percentage of the total.

Figure 1.4 compares the solar system abundance and the abundance of elements in cosmic rays in the range of a few hundred Mev per nucleon to about 1 Gev per nucleon from hydrogen up to iron as given by Meyer et al (1974). A comparison between the two abundances shows an excess of light (L) nuclei (Li, Be, B), in the primary cosmic rays (about 10^6 times more) which is believed to be due to the fragmentation of heavier nuclei in penetrating the small amount of matter (~ 4 g cm^{-2})

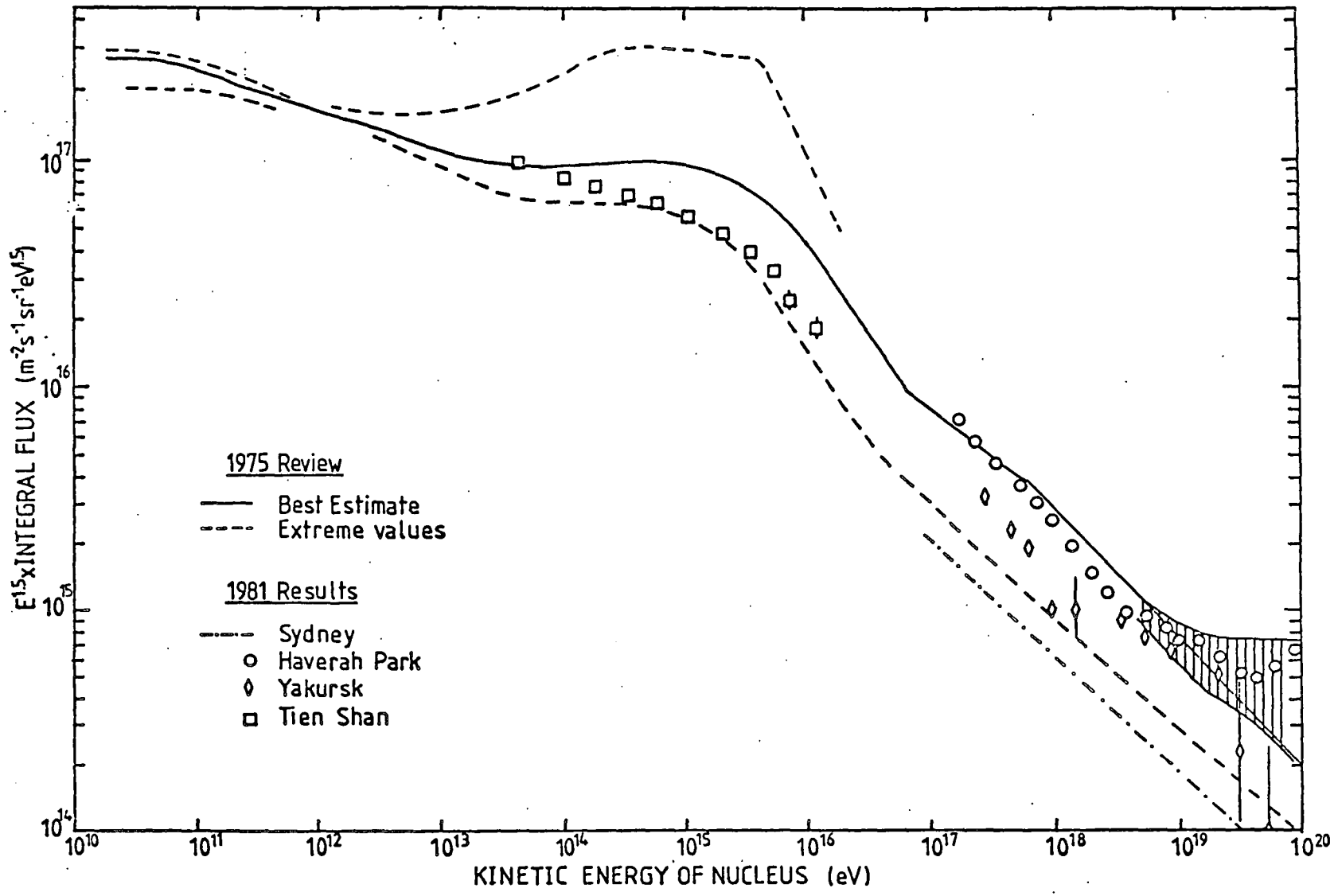

FIGURE 1.3 : Integral Energy Spectrum of the Primary Radiation (after Hillas 1981)

Z Elements	Kinetic energy per nucleus (eV)			
	10^{10}	10^{11}	10^{12}	10^{13}
1 Hydrogen	58 ± 5	47 ± 4	42 ± 6	24 ± 6
2 Helium	28 ± 3	25 ± 3	20 ± 3	15 ± 5
3-5 Lightnuclei	1.2 ± 0.1	1.1 ± 0.1	0.6 ± 0.2	-
6-8 Medium nuclei	7.1 ± 0.4	12.2 ± 0.8	14 ± 2	-
10-14 Heavy nuclei	2.8 ± 0.2	6.7 ± 0.5	10 ± 1	-
16-24 Very heavy nuclei	1.2 ± 0.2	3.6 ± 0.4	4 ± 1	-
26-28 Iron group nuclei	1.2 ± 0.2	4.5 ± 0.5	10 ± 2	24 ± 7
$\geqslant$ 30 Very very heavy nuclei		0.007 ± 0.004		

TABLE 1.1 : Composition of the cosmic rays at different primary energies (after Julliusson et al, 1975)

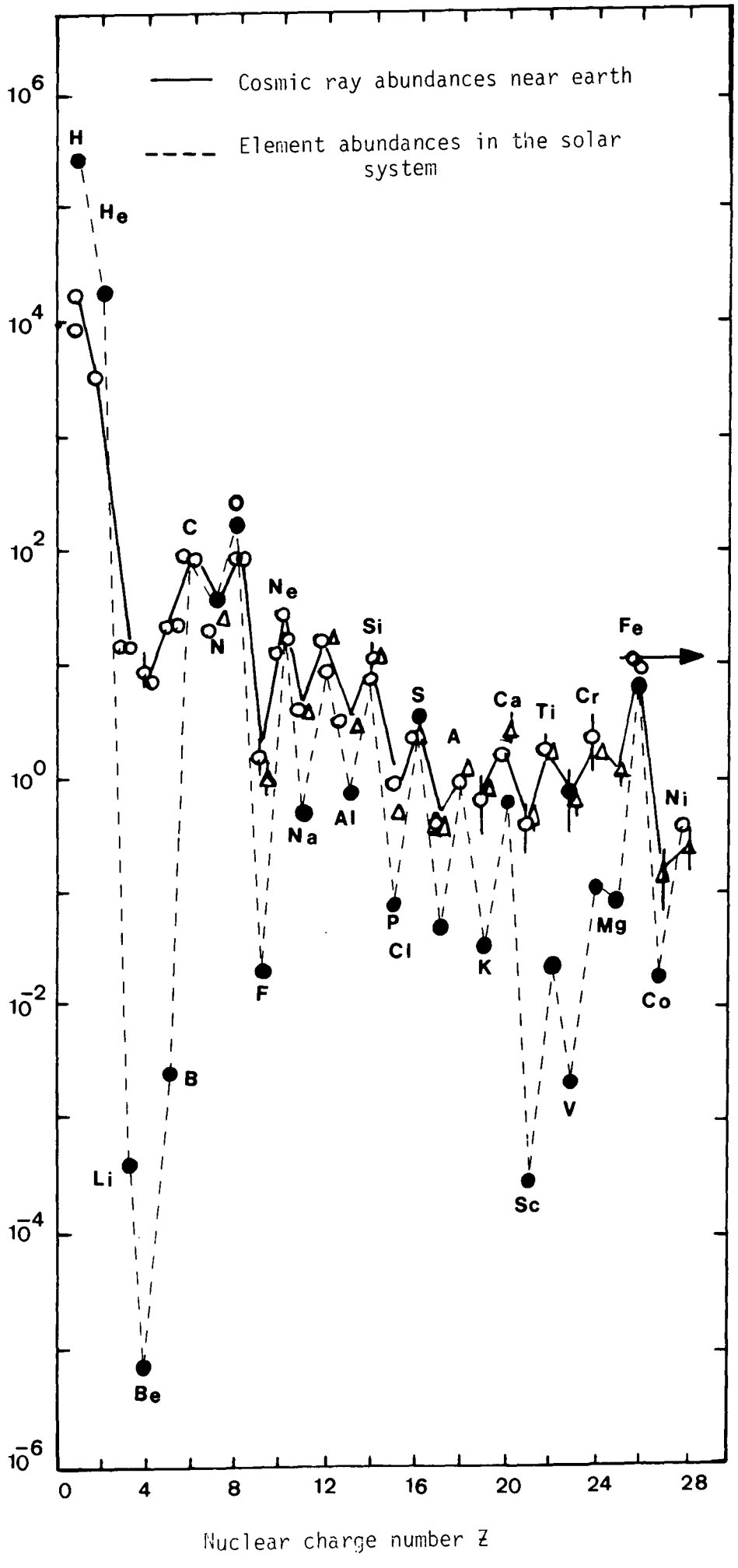

Figure 1.4 : Relative abundance of the elements from hydrogen to the iron group normalized to that of carbon (c = 100) (After Meyer et al, 1974).

between their source and the earth in space which contains ~1 H atom cm^{-3}. Another point is an increase in the relative abundance of heavy nuclei with increasing primary energy. The increase in abundance, especially for iron with an energy of 10^{13} ev is probably due to the production mechanism of iron at the source.

However, other observations of the relative abundance of L nuclei suggests that cosmic rays have traversed ~2.5 g cm^{-2} of interstellar hydrogen which means the average travelling time of cosmic ray nuclei is a few million years in the energy range where relative abundances have been measured.

1.8 SCINTILLATION COUNTERS

One of the most common detectors used in the detection of ionizing radiation is the scintillation counter and this technique has been used by the author in subsequent work. Basically the detector consists of a phosphor which is viewed by photomultipliers using a suitable light guide.

When an ionizing particle impinges on a phosphor which possesses the property of luminescence, part of its energy which is dissipated in molecular excitation and ionization is re-emitted as visible or ultra-violet photons. Some of these photons fall on the photo cathodes of the viewing photomultiplier tubes and produce a number of photo-electrons. These electrons are then accelerated through the dynode structure of the tube and at each dynode electron multiplication takes place. Finally an electron avalanche arrives at the collector plate and produces a voltage pulse which may be used for detection and measurement. Figure (1.5) shows schematically the operation of a scintillation counter.

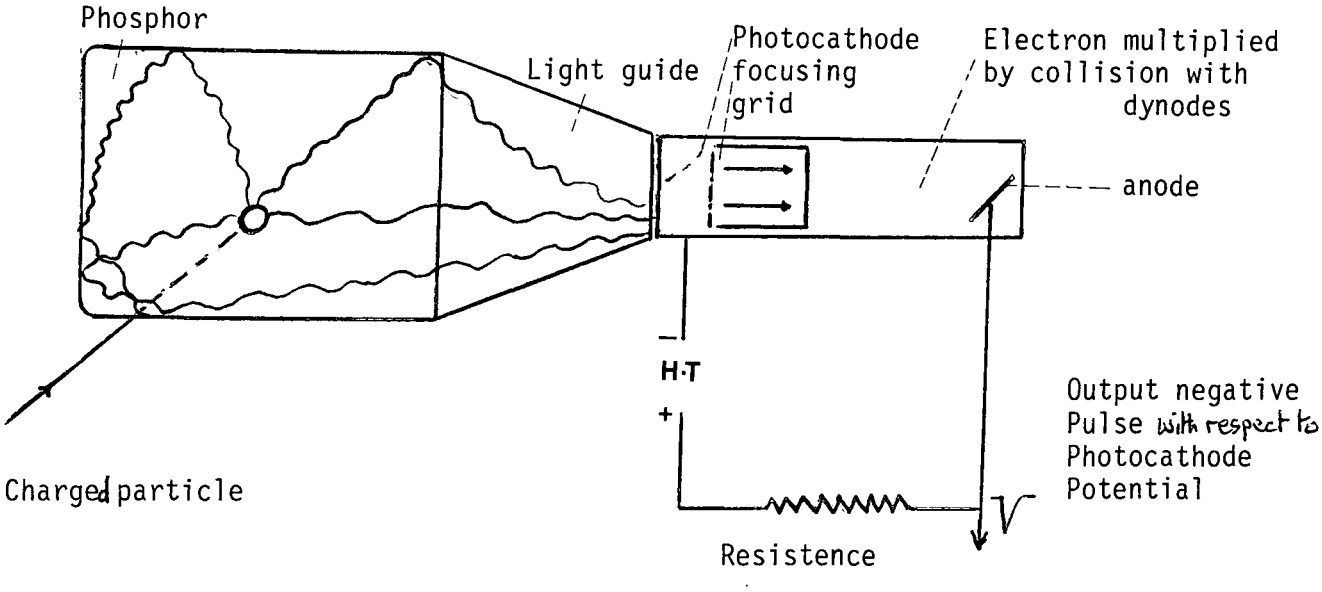

Fig.1.5 : Diagram illustrating the principle of operation of a scintillation counter

The ideal scintillation counter should be able, when exposed to the global cosmic ray flux yield a pulse height distribution (produced by the passage of relativistic cosmic ray particles through the phosphor) whose peak is well resolved from the distribution produced by single thermal electrons leaving the photocathodes of the photomultipliers used to view the phosphor. The thermal emission of electrons from the photo cathodes provides the main background of "noise" pulses which are not uniform in amplitude but form a distribution with a peak at very small pulse heights (which is not normally observable) with a long tail to the distribution extending to the region of much larger pulse heights produced by cosmic ray particles. The rate of noise pulses depends on the work function of the photocathodes used, their area and temperature. In a good scintillation counter used for cosmic ray work it is required that the pulse height distribution produced by the passage of the global cosmic ray flux through the phosphor is well resolved from the thermal electron noise distribution. The design of a large area counter (80cm x 50cm) satisfying this requirement is described in Chapter 4. The response of one counter constructed (scintillator C) is shown for illustration in Figure 1.6.

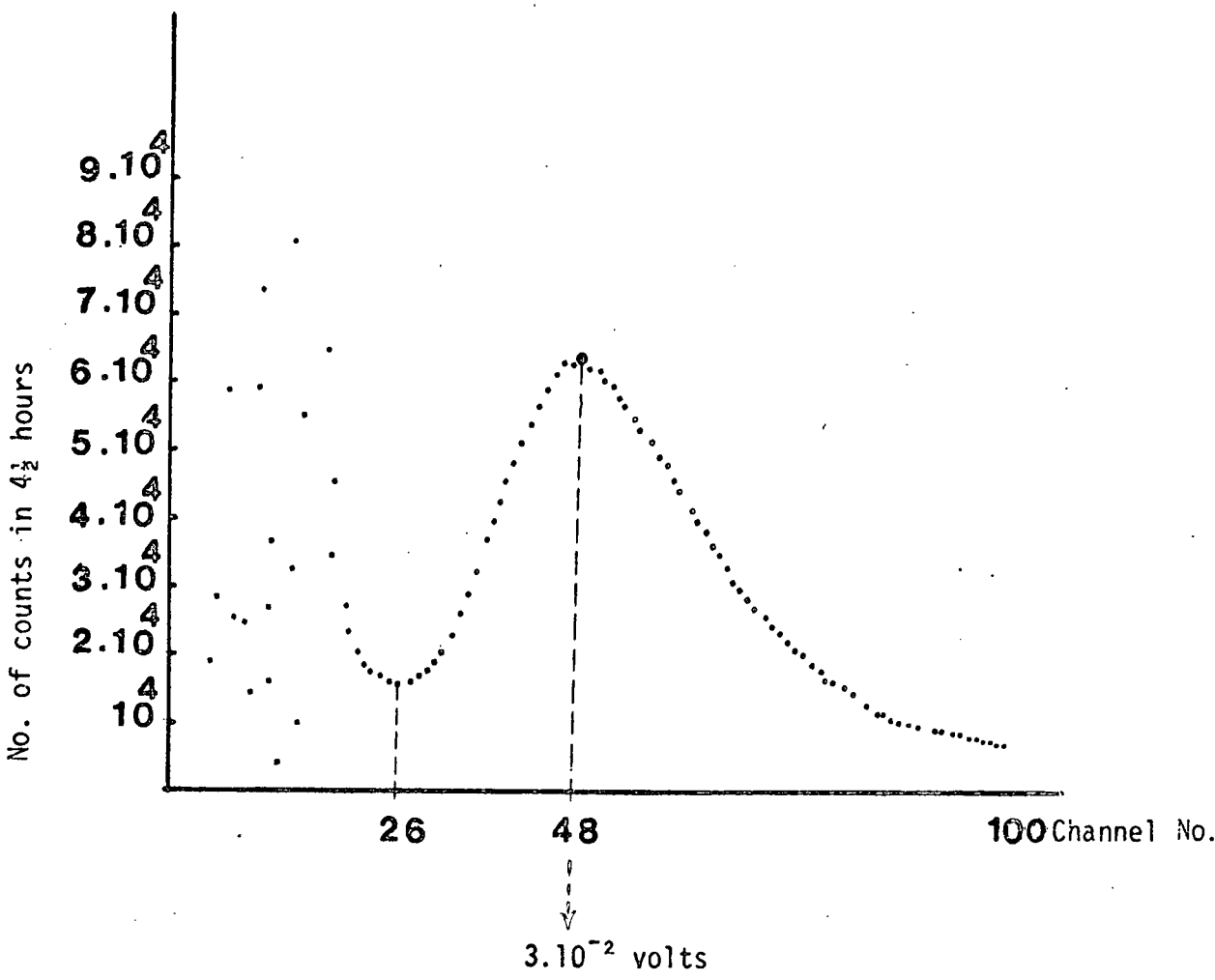

Figure 1.6 : Typical single particle cosmic ray peak as displayed on the pulse height analyser for scintillator C.

1.9 TACHYONS; PARTICLES MOVING WITH VELOCITIES GREATER THAN THE SPEED OF THE LIGHT

It has generally been believed that no particles can exceed the speed of light in vaccum, $c = 3 \times 10^8$ m sec^{-1} . This limitation is a direct consequence of the special theory of relativity. The relation between the total energy E and momentum P and velocity v that must be satisfied by any object obeying the special theory of relativity is given by:

$$E = \frac{moc^2}{\sqrt{(1-\frac{v^2}{c^2})}} \qquad (1.1)$$

$$P = \frac{mo\,v}{\sqrt{(1-\frac{v^2}{c^2})}} \qquad (1.2)$$

where mo is the rest mass. The relation between energy and velocity implied by relativity is such that as the velocity of a particle approaches c its energy becomes infinite. Since this energy must be supplied by whatever is accelerating the particle, an infinite source of energy would be needed to increase the velocity of a particle to the value c or greater and such an infinite energy source cannot be available. However, it is noted that photons or neutrinos (zero rest mass particles) when they are created in atomic or nuclear processes take off right away with the velocity of light and have not been speeded up to c from a lower speed. The next question is can there exist in nature particles that move with velocities exceeding the velocity of light in vaccum? Particles with such velocities $v > c$ have come to be known as "tachyons". Feinberg (1967) points out that since the advent of relativistic quantum field theory, it is no longer necessary to accelerate a particle through the "light barrier" in order to obtain a tachyon. Tachyons can be created in pairs without contradicting special relativity just as the photon or neutrino is produced and absorbed, always having a velocity $v \geq c$. This restriction implies that $1 - \frac{v^2}{c^2}$ takes negative values, so all physically observable and experimentally measurable characteristics

of particles, whose expressions contain the relativistic factor $\gamma = \frac{1}{\sqrt{1-\frac{v^2}{c^2}}}$ become imaginary. In order to make E a real number mo must be an imaginary number, say mo = $\mu o \sqrt{-1}$ and consequently equation 1.1, 1.2 may be rewritten as

$$E = \frac{\mu o c^2}{\sqrt{\frac{v^2}{c^2} - 1}} \qquad 1.3 \qquad P = \frac{\mu o v}{\sqrt{\frac{v^2}{c^2} - 1}} \qquad 1.4$$

Since the tachyon could not cross a lower limit value of c then the rest mass being imaginary would not necessarily create a problem but its energy and momentum would remain real. It is seen for ordinary particles, as their speed increases, their energy also increases. For tachyons in contrast, an increase in speed results in a decrease in energy. Hence a tachyon which loses energy by interacting with matter or by radiating light would speed up and in the limiting case of infinite speed its total energy would be zero, although its momentum would remain finite.

1.10 POSSIBLE OBSERVATION OF TACHYONS ASSOCIATED WITH EXTENSIVE AIR SHOWERS

One of the recent searches has been conducted in extensive air showers with three assumptions based on the Clay and Crouch experiment (1974). First, it is assumed that tachyons are produced as particle-antiparticle pairs in interactions when high energy primary cosmic ray protons with energies of 10^{15}ev. or greater collide with a nucleus at an atmospheric depth of 80 g cm^{-2} the surviving nucleon subsequently generating an air shower $P + N \rightarrow N + N + t + \bar{t}$ + mesons.....

Tachyons, due to their superluminal speeds would arrive at sea level earlier than the main shower front (consisting predominantly of relativistic electrons) which propagates down through the atmosphere

with a velocity very close to the velocity of light. The second assumption is that at least some of the produced tachyons survive for long enough to reach sea level. Any tachyon produced would reach sea level at some time in the 59 μs (this time corresponding to tachyons moving with infinite velocity) time period before the arrival of the main electron photon shower front. For showers incident at a zenith angle of 60° the relevant time interval is 150μs. The third assumption is that a tachyon itself will loose energy in a scintillator or will be detected by the production of secondary particles which traverse the scintillator and can be detected. A search for tachyons associated with extensive air showers produced by primary cosmic rays of energy $>10^{15}$ev. has been carried out by the author along these lines and his work is described in Chapter 6.

1.11. SUMMARY

Although many elaborate and well designed accelerator experiments are in operation or under construction, which enable controlled experiments to be made at collision energies up to $\sim 10^{14}$ev, cosmic rays will be in use for many years to come simply because it is a cheap high energy beam of particles. Also, because the primary cosmic rays themselves originate from violent events in the universe it is quite possible that the lower energy primary radiation itself may contain a significant flux of new types of particle (tachyons,quarks etc.). The study of the primary and secondary radiations provides a good opportunity for nuclear physicists to investigate the characteristics of particles and the nature of high energy interactions.

EAS provide the only means of investigating the properties of what occurs at energies in excess of 10^{14}ev. and it appears as though

they will be the main contributor to this sector for a long time. Also such studies provide a valuable tool for investigating the condition of the galaxy and beyond and it is to these two ends that the extensive air shower needs to be pursued.

CHAPTER 2

THE DURHAM EXTENSIVE AIR SHOWER ARRAY

2.1 INTRODUCTION

The Durham extensive air shower array with a radius of 60 m has been set up around the physics department. The array consists of 14 plastic scintillators in a geometric pattern and detectors with the same area have been placed at the equivalent positions within the array to enhance the symmetry. Figure 2.1 shows the location of the detectors in the array and Table 2.1 gives the exact areas and coordinates of all the detectors.

Each scintillator is housed in a wooden box and for prevention of electrical interference the head amplifier is located in an aluminium box and the E.H.T distibutor unit is recessed into the scintillator box. The detector box rests on an angle iron bed to prevent damp, the whole detector being covered by a weather proofed wooden hut as shown in Figure 2.2. Four cables have been supplied from the laboratory to each detector; the first for the photomultiplier tube E.H.T; the second carrying 24 volts DC for the head amplifier; the third cable for carrying the photomultiplier tube output to the laboratory, and the last is kept as a spare. Figure 2.3 shows the arrangement of the detector supply cables.

2.2 THE PLASTIC SCINTILLATOR DETECTORS

The 14 detectors with four different areas are identified as 2 m^2(11, 31, 51, 13, 33, 53), 1.6 m^2(12, 42, 61, 62), 1 m^2(32, 41, 52) and 0.75 m^2(C). According to the purpose, each detector has been designed to perform either shower density and timing measurements or shower density only.

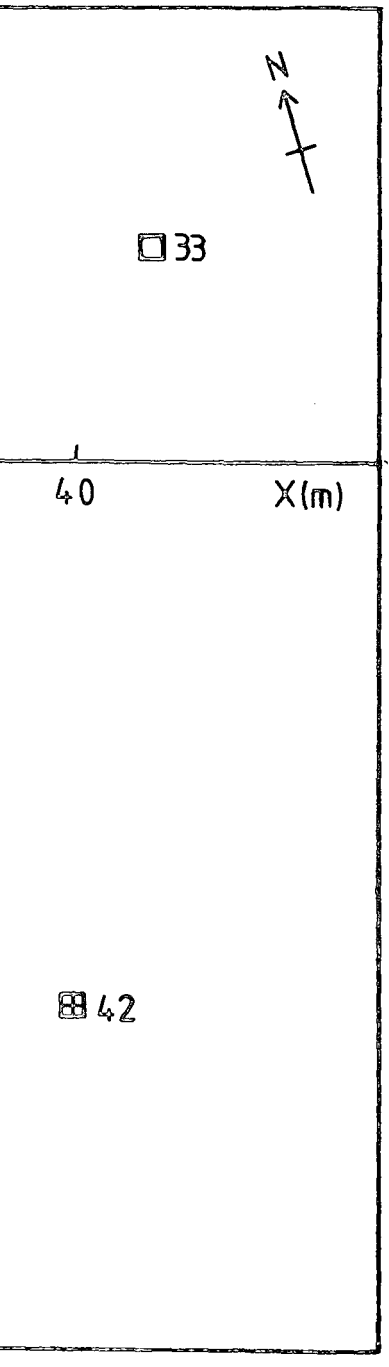
N
33
40
X(m)
42

DETECTOR	AREA (m^2)	COORDINATES (metres) X	Y	Z
C	0.75	0	0	0
11	2.0	-12.30	- 5.64	- 4.83
31	2.0	14.80	3.10	0.16
51	2.0	0.30	-26.80	0.18
13	2.0	-45.0	29.5	-13.5
33	2.0	45.0	14.0	0.2
53	2.0	- 5.0	-58.5	- 8.7
12	1.6	-24.0	7.5	-12.8
42	1.6	39.5	-36.5	- 8.3
61	1.6	- 7.9	- 5.1	- 4.9
62	1.6	-41.0	-18.2	-11.1
32	1.0	25.5	8.5	0.7
41	1.0	22.0	-17.0	-11.4
52	1.0	- 0.5	-17.0	0.67

TABLE 2.1 : Areas and coordinates of detectors

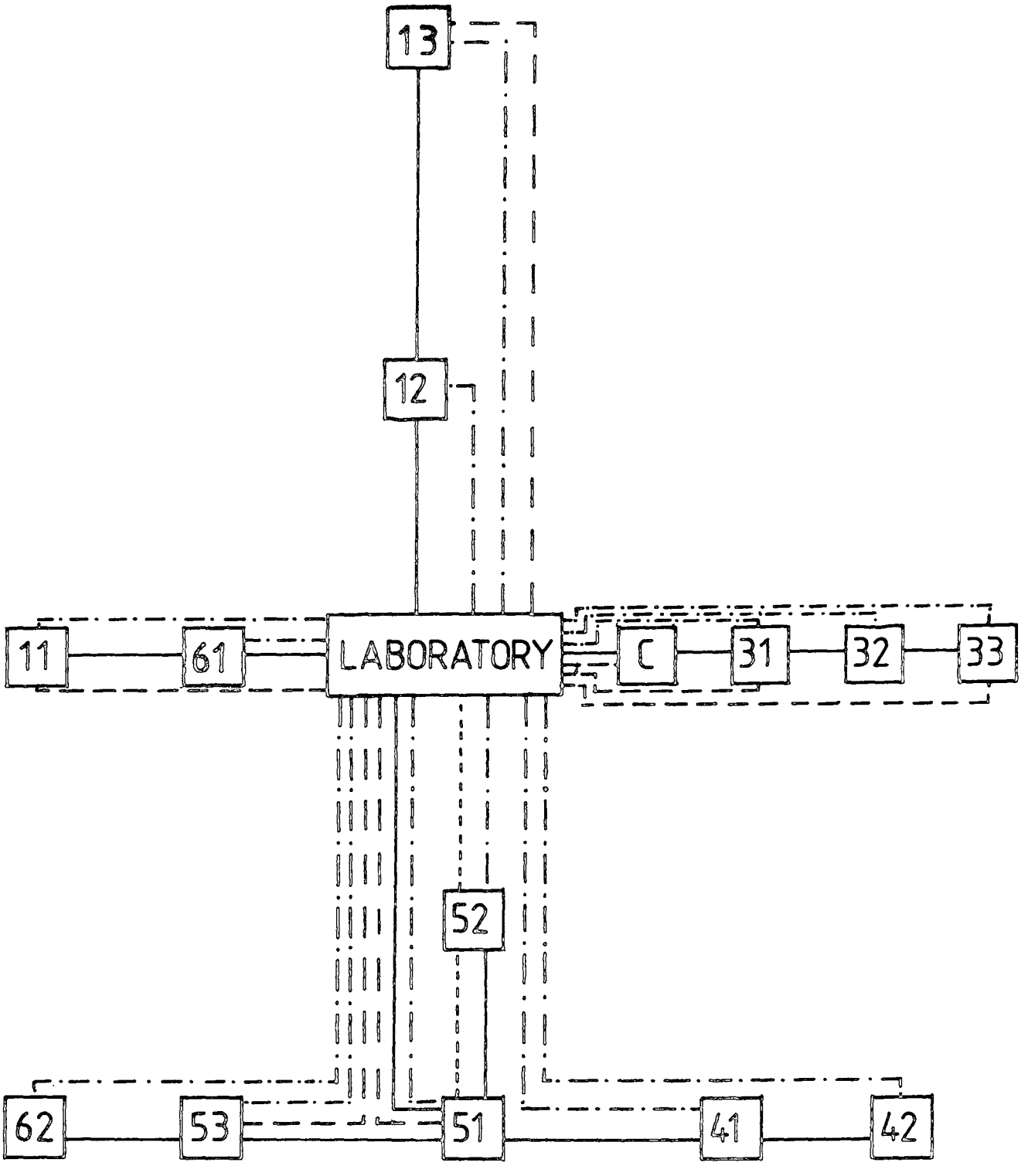

FIGURE **2.3** : Layout of cables supplying detectors

Showers of size between 10^4 to 5×10^6 particles are detected by the array. In general each of the detectors has four photomultiplier tubes (P.M.T), observing the plastic scintillator except the central and 2 m^2 ones which have one extra photomultiplier for fast timing measurements. Figure 2.4 shows the detector features.

a) The central detector c

The central detector c is located at the centre of the array and is situated on the roof of the physics department. It consists of two separate rectangular slabs of 5 cm thick NE 102A plastic scintillator of total area 0.75 m^2. Each slab is viewed by two Phillips 53 AVP P.M.T for density measurement and these are attached to the perspex light guides (using NE 580 optical cement) at each end. A single fast timing tube, Phillips 56 AVP, is attached to a light guide at one end giving the zero time pulse comparison with the fast timing pulses from other detectors.

b) The 2.0 m^2 detectors

These six detectors individually consist of 2 m x 1 m x 2.5 cm slabs of NE 110 plastic scintillator. Each is observed by a total of five P.M.Ts, four EMI 9579 B, 5" diameter tubes for particle density measurements and a single Phillips 56 AVP 2" diameter tube for fast timing measurements as shown in Figure 2.4. The 2 m^2 detectors are used as triggers to select E.A.S. that are recorded by the array. For preserving symmetry and uniformity two triangular arrays are formed with detectors placed at each corner of an approximately equilateral triangle. Three detectors (13, 33, 53) forming an outer equilateral triangle and another three detectors (11, 31, 51) forming an inner triangular arrangement. A coincidence

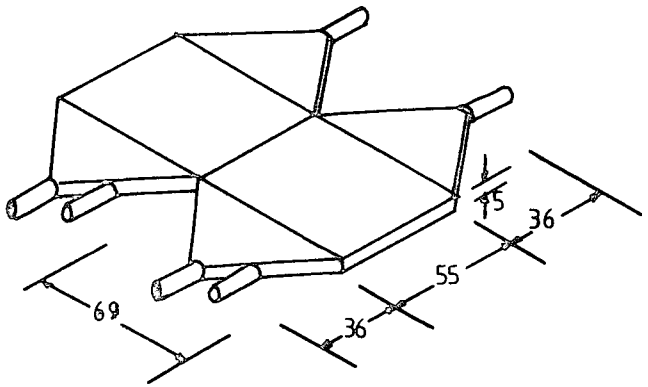

(i) 0.75 m^2 detector

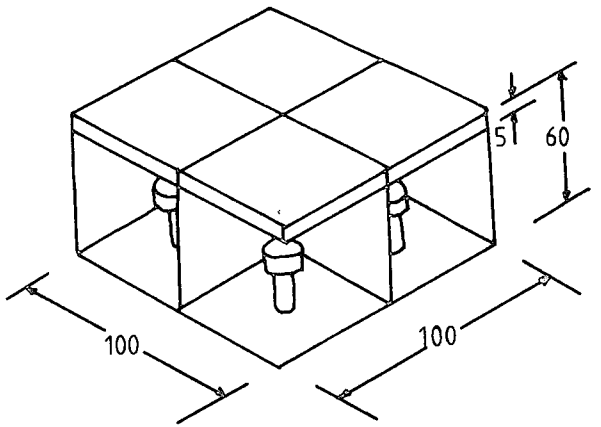

(ii) 1.0 m^2 detector

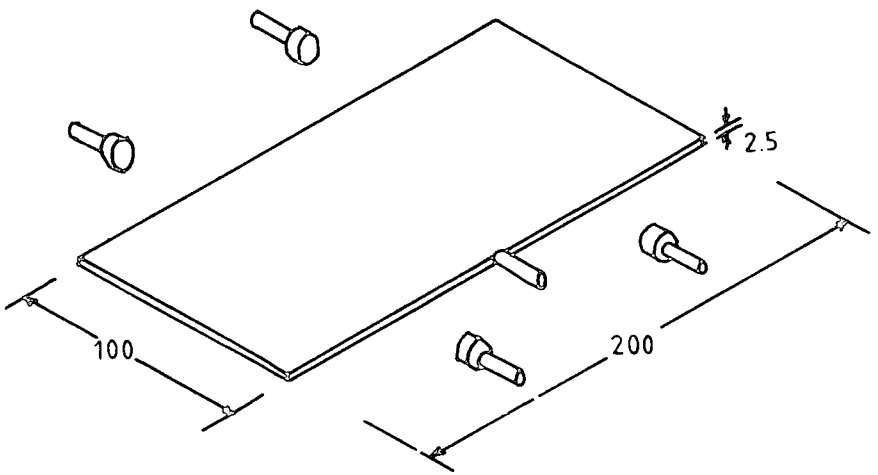

(iii) 2.0 m^2 detector

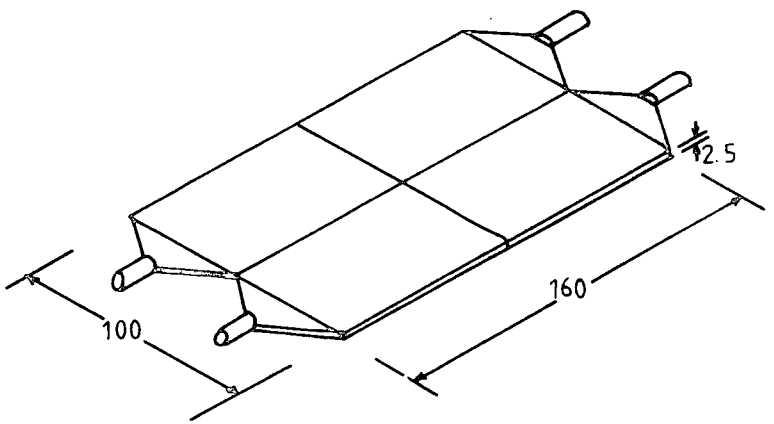

(iv) 1.6 m^2 detector

FIGURE 2.4 : Arrangement of scintillators in detectors (all dimensions in cm)

between the central detector and (13, 33, 53) is called the outer ring trigger and a coincidence between the central detector and (11, 31, 51) is called the inner ring trigger. Coaxial cables are used to transfer all the pulses to the laboratory and by using the appropriate lengths of cable the fast timing signal from the central detector always arrives at the recording equipment before the other fast timing pulses.

c) 1.6 m^2 detectors

Each detector with this area consists of four identical individually light proofed quarters each with area 0.4 m^2. The slabs are 2.5 cm thick and of area 0.4 m^2 and consist of NE 102 A plastic scintillator. A Phillips 53 AVP P.M.T by way of perspex light guide is attached to each quarter. Each quarter operates independently of the other three and a single output pulse is achieved from all quarters by using a mixer amplifier.

d) 1.0 m^2 detector

The detectors with 1.0 m^2 area, again, consist of four individually light proofed slabs. The slabs are 5 cm thick and each is of area 0.25 m^2 . They are viewed on their broad face by a single E.M.I 9579 B P.M.T - see Figure 2.4. Pulses from independent quarters are added in a mixer amplifier at the detector and transferred by 50 Ω cable to the laboratory.

2.3 PHOTOMULTIPLIER TUBES

Three types of photomultiplier tubes have been used in the array detectors. E.M.I 9579 B with five inch diameter photo-cathode, Phillips 53 AVP and Phillips 56 AVP both with two inch diameter photo cathodes. The type 56 AVP is used for fast timing, and the other two for density measurements. The tubes are supplied with negative E.H.T. and the outputs of the density tubes are negative with an exponential decay time constant of 20 μsec. The outputs of the fast tubes are negative pulses of time duration 5 n sec (a full width at half maximum). Investigation of the tube linearity and temperature dependence stability has been carried out by Smith (1976) and found to be good. Figure 2.5 shows the values of the resistors and capacitors used in the dynode chains of the different tubes.

2.4 E.H.T SUPPLY UNITS

Two E.H.T. units supply the negative high volage for the P.M.Ts. One supplies the voltage for the electron density measuring P.M.Ts and is set at 2.4 Kv. The other is used for the fast timing P.M.Ts and is set at 2.7 Kv. Since none of the tubes work at exactly the same voltage, a chain of resistors and an adjustable potentiometer (see Figure 2.6) is used at each P.M.T to adjust the tube E.H.T to the appropriate value.

2.5 THE HEAD AMPLIFIERS

Each detector has a mixer amplifier which adds and amplifies the output pulses of the four density P.M.Ts as shown in Figure 2.7. It consists of an emitter-follower for each channel and then all four outputs are added and amplified by a μ A702c operational amplifier

Base circuit for EMI 9579 B P.M.T.

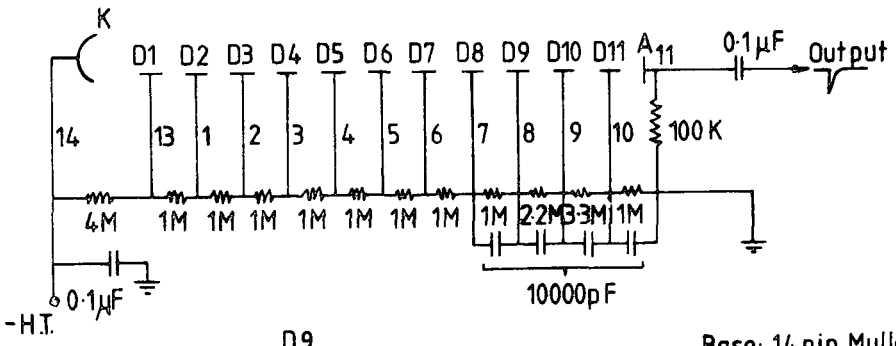

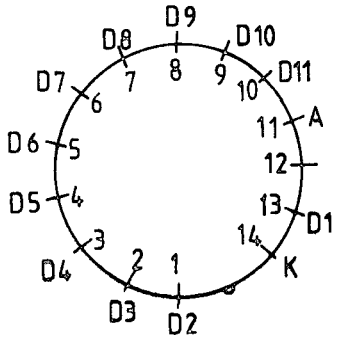

Base: 14 pin Mullard FE 1001
EMI B14A
Viewed from beneath

Base circuit for PHILIPS 53 AVP P.M.T.

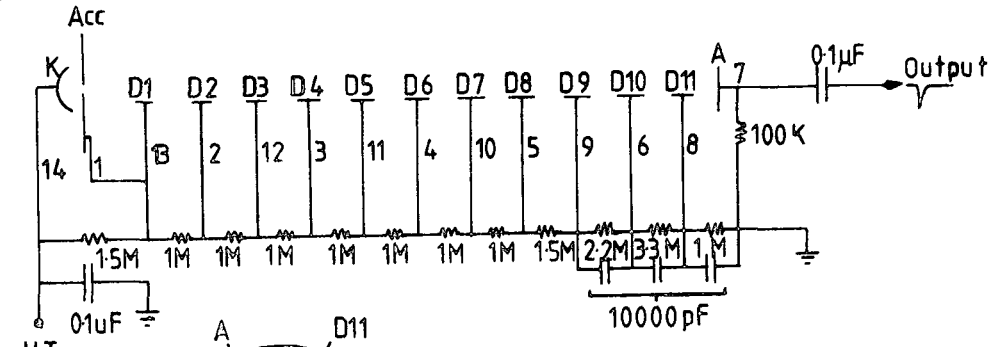

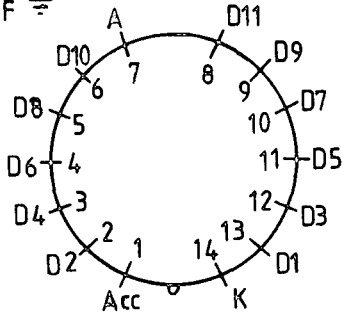

Base: 14 pin Mullard FE1001
EMI B14A
Viewed from beneath

Base circuit for PHILIPS 56 AVP P.M.T.

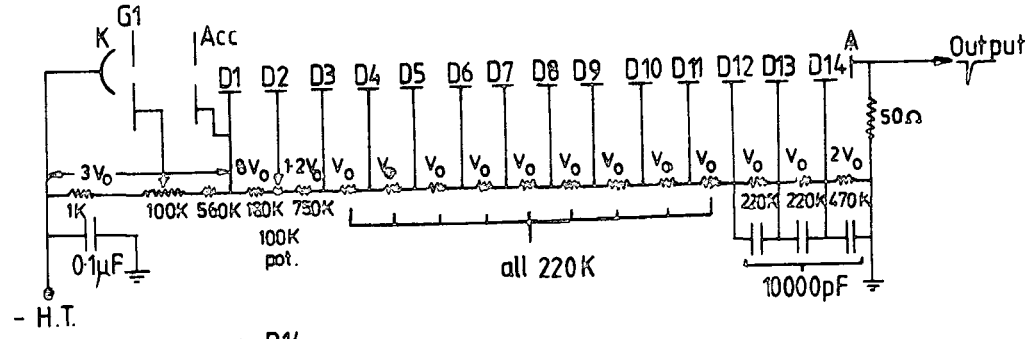

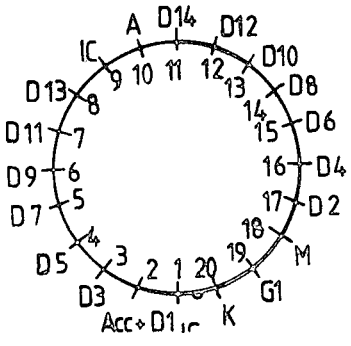

Base: 20 pin Mullard FE 1003
Viewed from beneath

Figure 2.5 : Base circuit for different photomultiplier tubes.

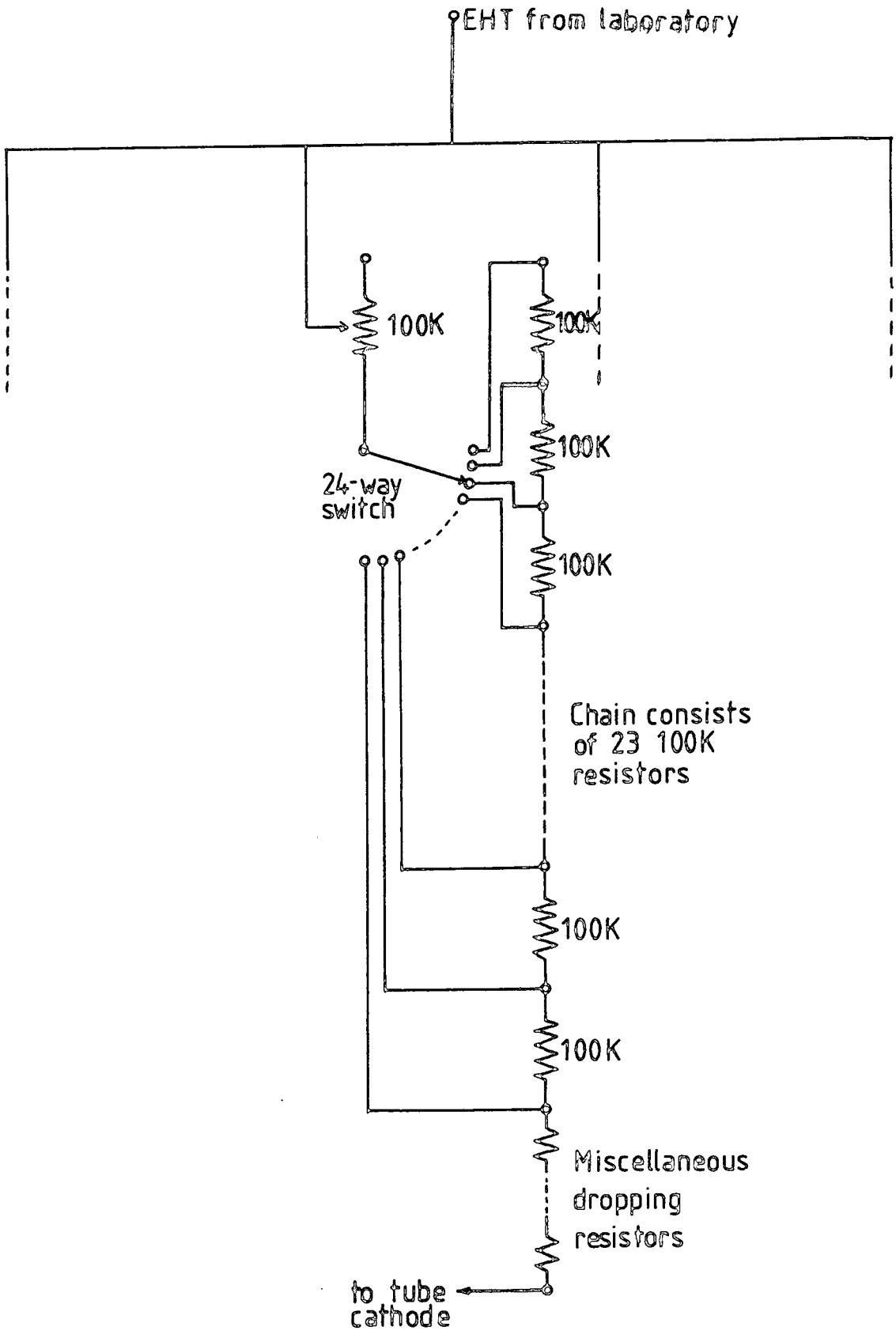

FIGURE 2.6 : EHT distribution at detectors

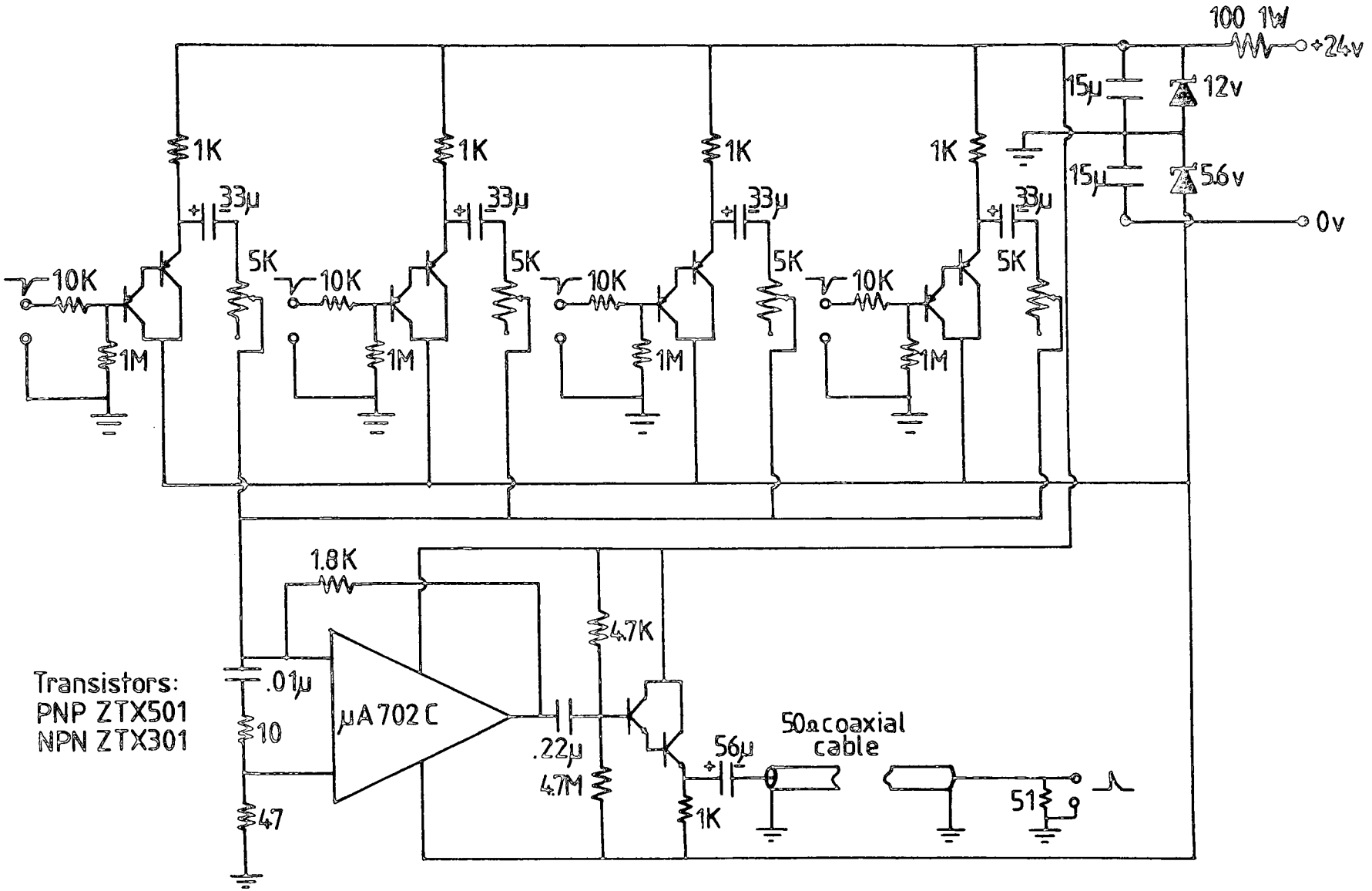

FIGURE 2.7 : Four input head amplifier

and then fed into another emitter follower circuit. The output positive signal is transferred to the laboratory by 50 Ω cable. The response of the amplifier is shown in Figure 2.8. The amplifier is operated by a 24 v, 3A power supply stabilised in the laboratory.

2.6 CALIBRATION TELESCOPE

For calibrating the electron density measuring detectors a subsidiary telescope is used. The telescope consists of a single 23cm x 23cm x 5 cm slab of NE 102A plastic scinti llator. At one edge two Phillips 53 AVP photomultiplier tubes are used to view the phosphor and are supplied with 1.9 kv from the laboratory via a charge sensitive amplifier (C.S.A). Using a C.S.A enables the use of only one cable for each P.M.T because the same cable which takes the E.H.T to the tubes also carries back the output pulses to the laboratory. Tubes and plastic phosphor are positioned in a light tight aluminium box as Figure 2.9 shows.

2.7 CALIBRATION OF THE DETECTORS

As each detector has a different design geometry and consequently different response towards cosmic ray particles, hence each has to be calibrated separately. The number of photons collected by P.M.T depends on the energy loss of the particle in the phosphor and the point and angle which it passes through. Contour maps of each type of detector response have been obtained by Smith(1976). Figure 2.10 shows these maps and also the point on the scintillator where the centre of the calibration telescope should be placed. The pulse height obtained at this point is then used to determine the E.H.T adjustment required to obtain a mean pulse height of 100 mv per particle for the detector.

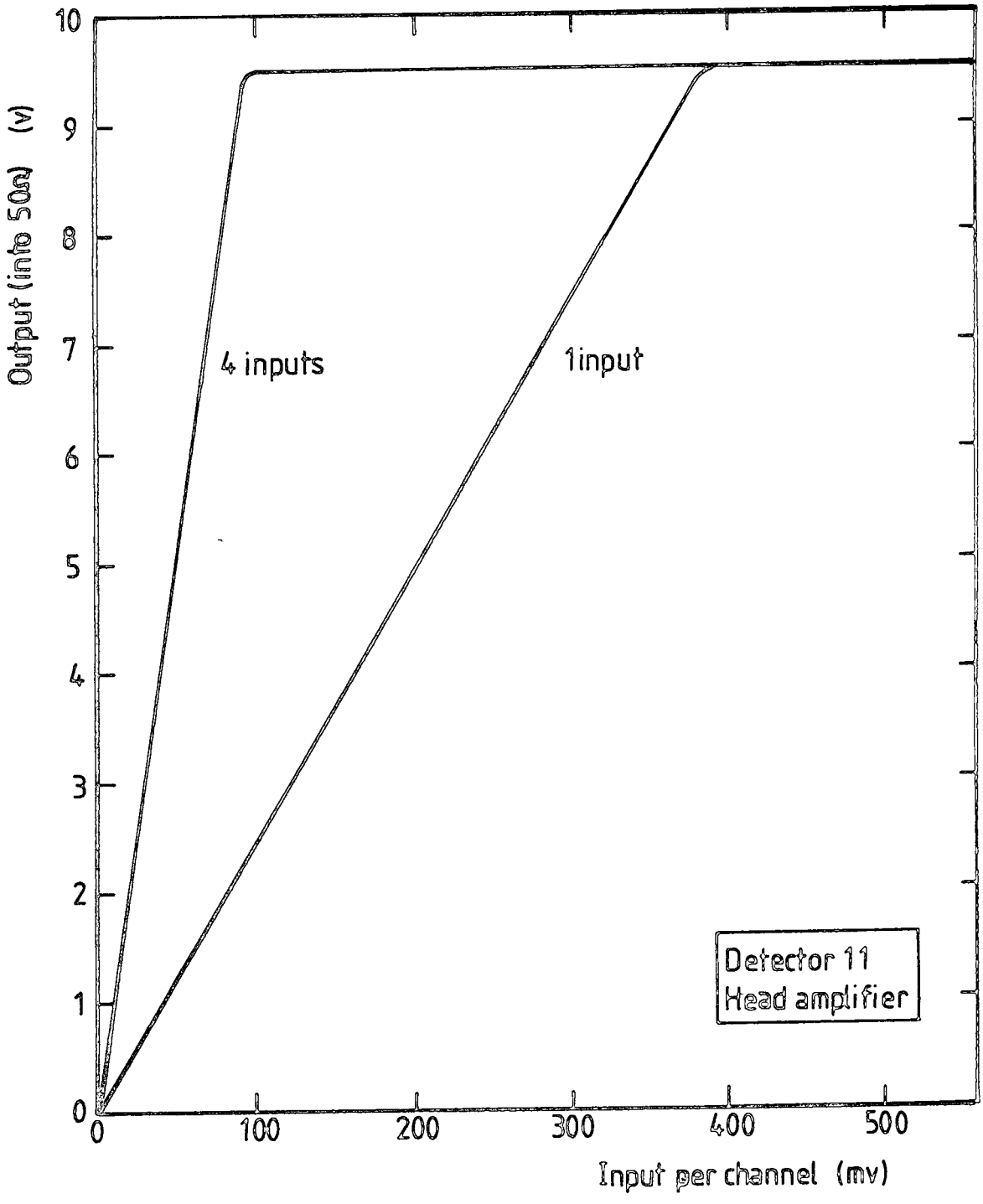

FIGURE 2.8 : Typical head amplifier gain characteristic

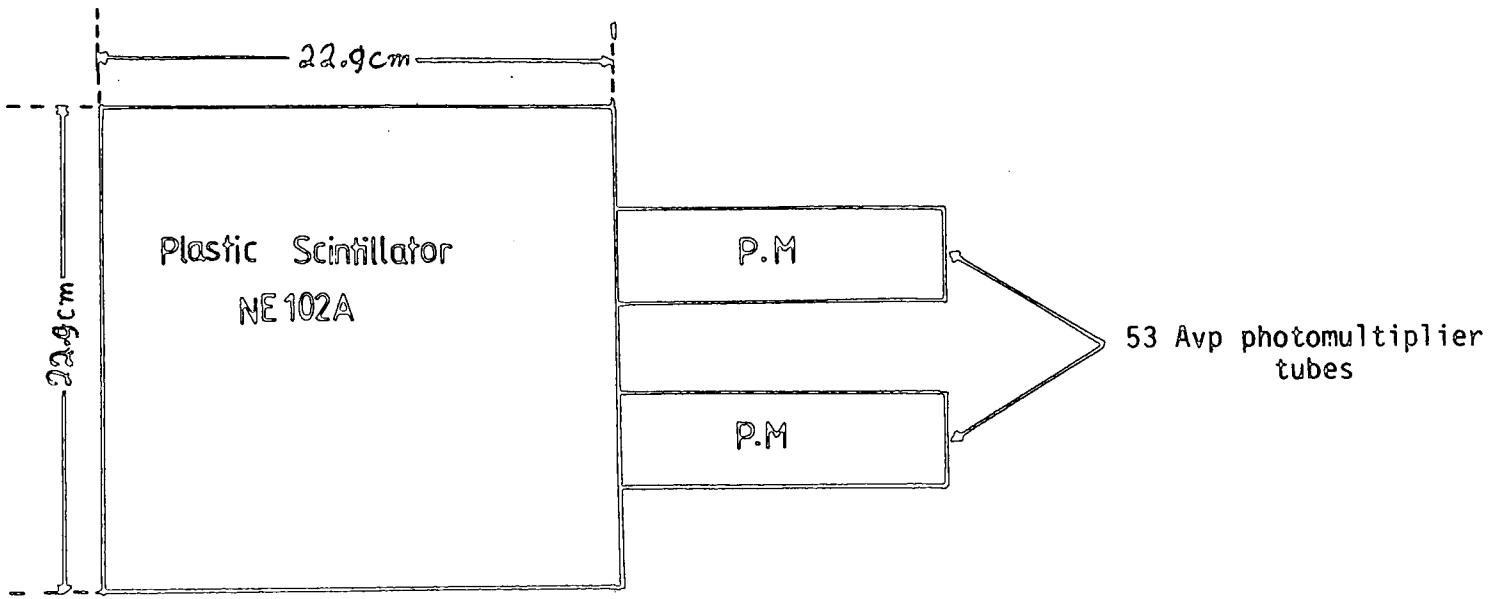

Figure 2.9 :The calibration telescope

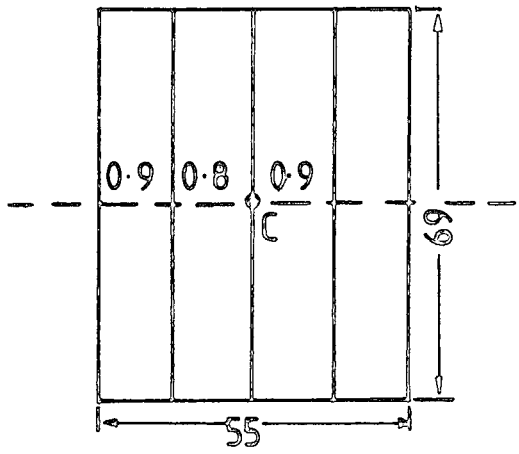

$2 \times 0{\cdot}38\,m^2$ Central Detector

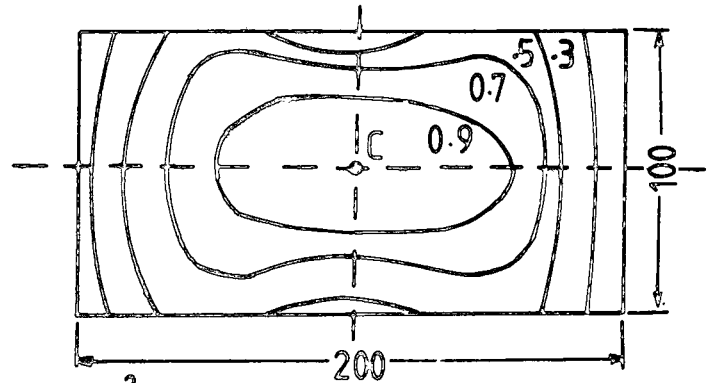

$2m^2$ = Detectors 11, 13, 31, 33, 51 and 53

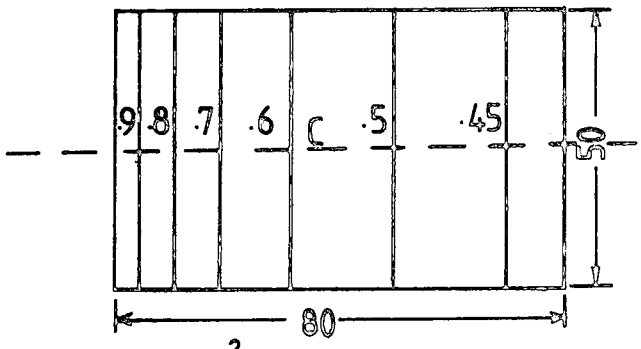

$4 \times 0{\cdot}4\,m^2$ = Detectors 12, 42, 61, and 62

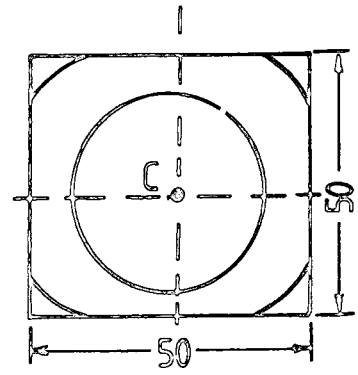

$4 \times 0{\cdot}25\,m^2$ = Detectors 32, 41, 52

Figure 2.10 : Pulse height contour map of the array's scintillators where C represents the calibration points.

2.7.1 Calibration procedure

In practice, when the detector output is connected directly to a pulse height analyser (P.H.A), the single particle peak does not appear as it is masked by noise. The noise pulses are produced by thermal electrons emitted by the photomultiplier photocathodes. In order to detect only pulses produced by cosmic ray particles, a subsidiary telescope is used as described in Section 2.6. The output pulses from the two tubes of the telescope go through a NE 4675 charge sensitive amplifier (C.S.A). Figure 2.11 shows the circuit diagram of it. The signals from the C.S.A are then passed through to a dual discriminator (Figs. 2.12, 2.13), set at a level of 100 mv to remove a large proportion of the noise and then into a two fold coincidence unit between detector and telescope which produce a 2 μs, 5 v rectangular pulse. For gating the 100 channel Laben P.H.A, a 50 Ω termination is applied to the input P.H.A.

To calibrate a given photomultiplier tube, the remaining tubes must be disconnected from the head amplifier and the calibration telescope placed with the centre of its scintillator over the appropriate calibration point and the P.H.A started. After some ten minutes a sufficiently accurate distribution is obtained. The E.H.T is then adjusted by using the resistor chain in series with the specified P.M.T so as to fix the position of the peak near enough to the desired calibration value. When the peak is within $\pm$ 2% of the calibration value, the P.H.A is run overnight to obtain a more accurate distribution. A typical single particle peak and mode determined is shown in Figure 2.14.

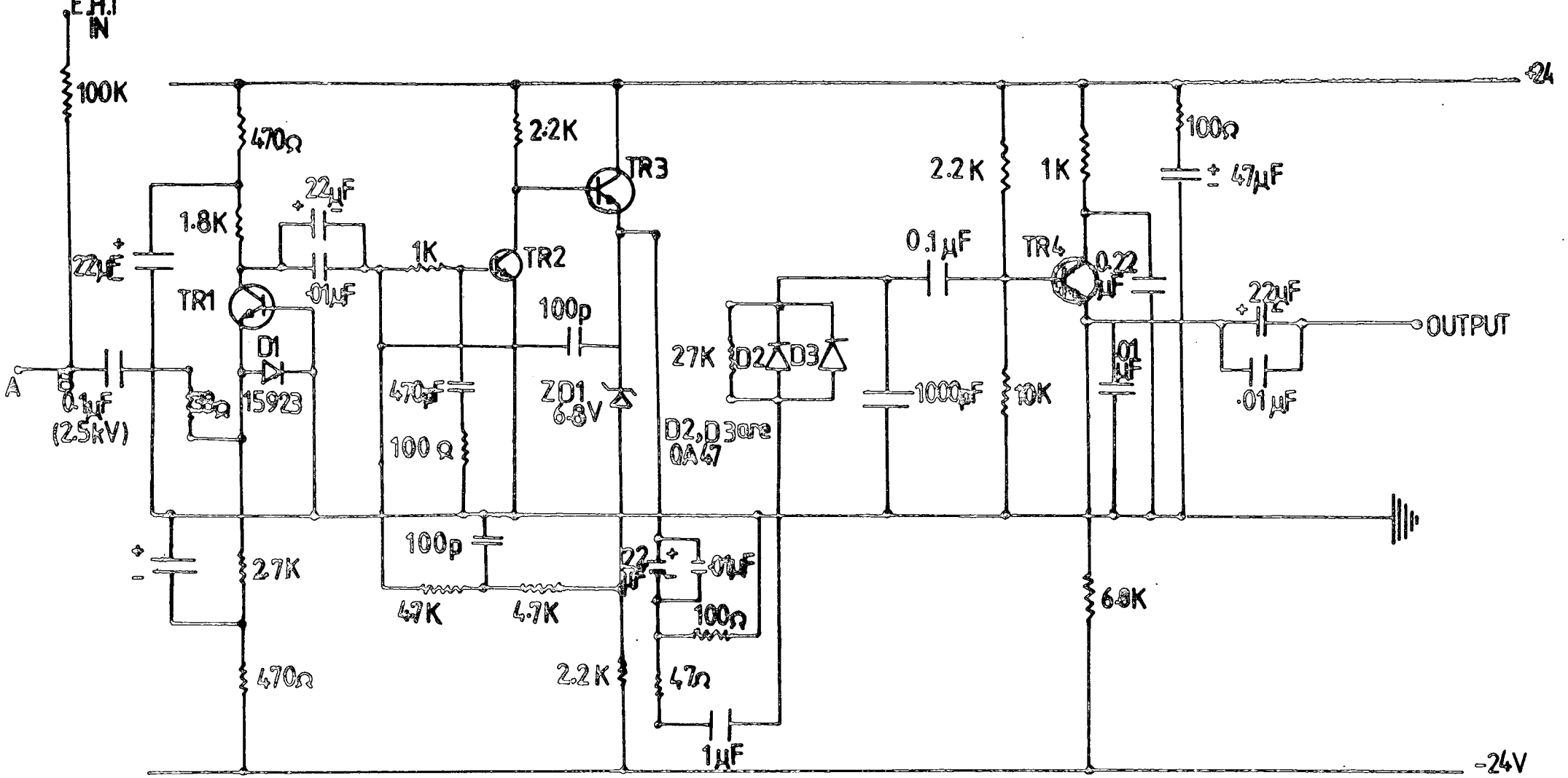

Figure 2.11: Circuit diagram of the charge sensitive amplifiers(C.S.A)used in the calibration telescope.
AB represents the 50m of coaxial cable connecting the CSA to the photomultiplier of the calibation telescope.

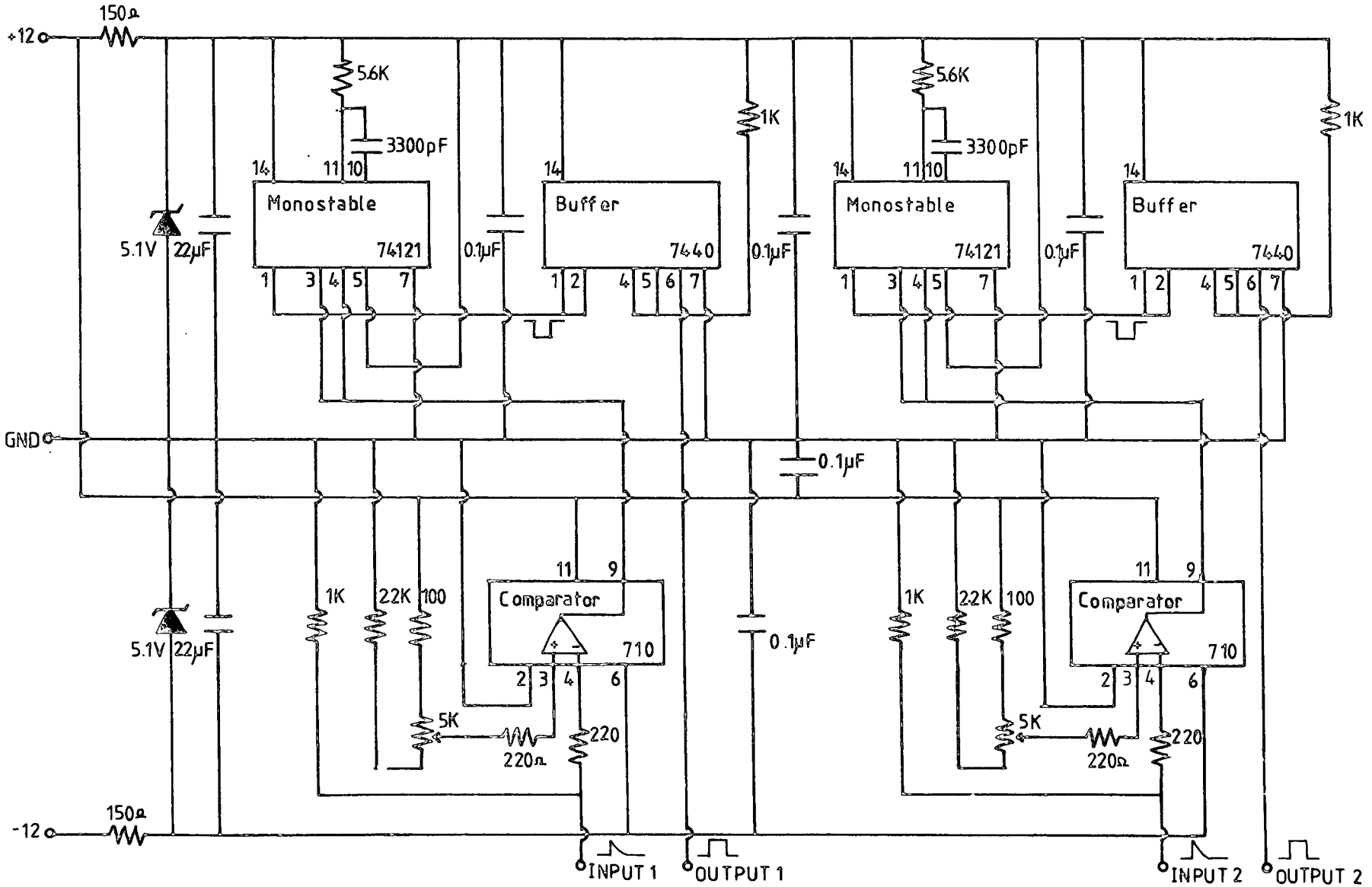

FIGURE 2.12 : Circuit diagram of dual discriminator used in detector calibration

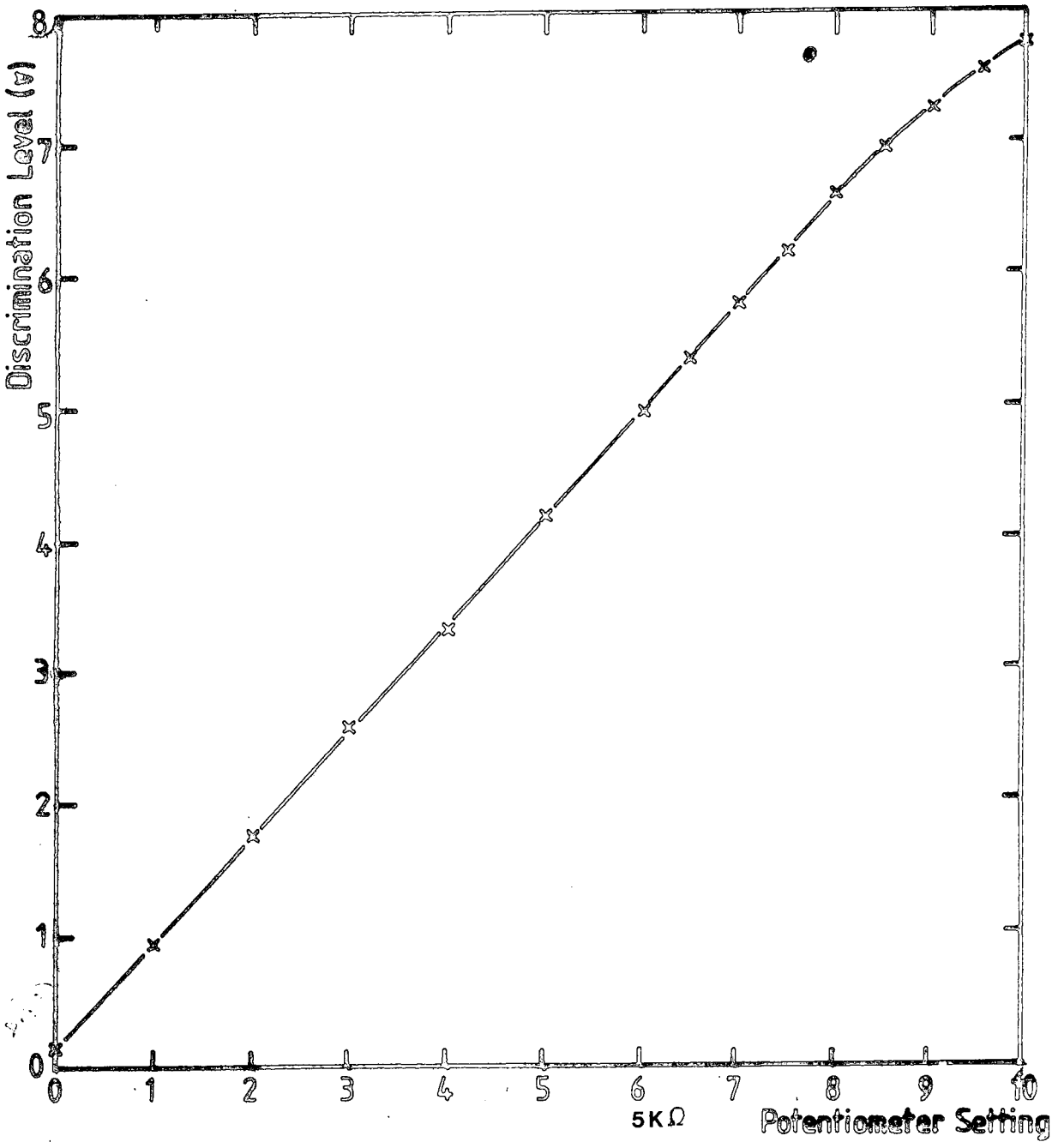

FIGURE 2.13 : Characteristic of circuit shown in figure 2.12

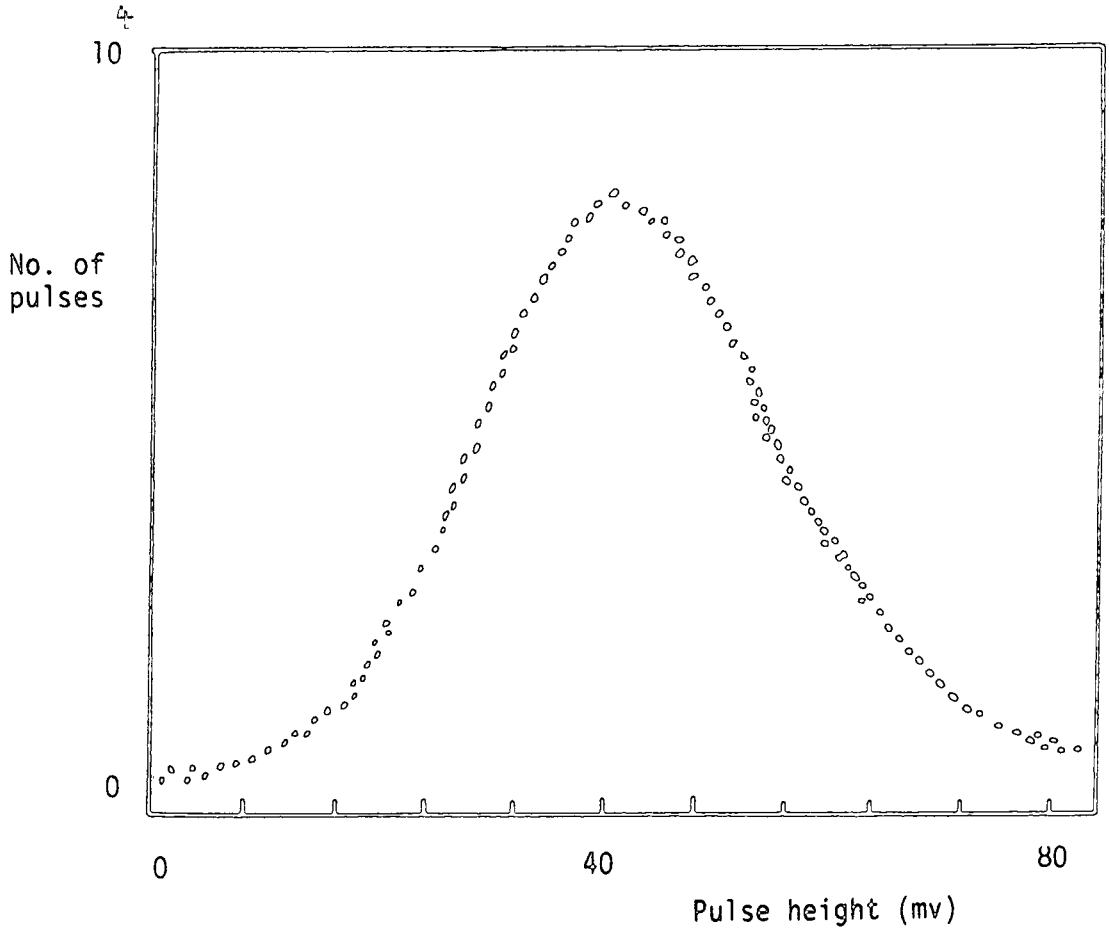

Figure 2.14 : Typical single particle peak as displayed on pulse height analyser.

2.7.2 Method of calculating the calibration pulse height

The aim of calibration is to set all the photomultiplier tubes of each detector to have an identical response such that a summed pulse from them when divided by 100 mν gives the number of particles per square metre at the detector, i.e. the density at the detector. Let A be the total area of a detector (m^2) and n be the number of photomultiplier tubes viewing the same single piece of phosphor. The mean pulse height produced by a single relativistic muon traversing a density detector is adjusted to be $S = \frac{100}{A.n}$ mν per m^2 per photomultiplier tube. In practice the most easily measured quantity that can be related to the average pulse height is the maximum, or mode, of the distribution obtained rather than the mean when measurements are recorded on a pulse height analyser. So, to still retain the desired 100 $\frac{m\nu}{particle.m^2}$ the ratio $\frac{mean}{mode}$ was accurately determined at the calibration point by Smith (1976) and found that this ratio didn't vary more than ± 4% over the total scintillator area of any detector, the use of this ratio, R, modified the calibration pulse height to $S = \frac{100}{A.n.R.} \quad \frac{m\nu}{m^2 \,.\, \text{Photomultiplier tubes.particle}}$ for the mode of single particle distribution.

A number of detectors have a calibration point which is not at the same spot where the mean pulse height occurs and this is because of the phosphor's non-linear response. The ratio of the pulse height at the calibration point to the pulse height at the mean pulse height coordinate, g, becomes another term which has to be applied to the calibration pulse height and has been determined by Smith (1976). Including this correction in the pulse height calibration the equation gives $S = \frac{100}{A.n.R}.g$ mν per particle, per photomultiplier per m^2. The values for R and g are given in table (2.2).

DETECTOR	A	N	n	R	g	S
C	0.75	4	2	1.53±0.01	0.89	38.3
11,31,51, 13,33,53	2.0	4	4	1.83±0.01	1.41	9.6
12,42,61,62	1.6	4	1	1.60±0.01	1.00	39.1
32,41,52	1.0	4	1	1.40±0.01	1.00	71.4

A = Total area of detector (m^2)

N = Total number of photomultiplier tubes in detector

n = Number of photomultiplier tubes viewing each piece of scintillator

R = Mean of pulse height distribution divided by its mode

g = Pulse height at calibration point divided by mean pulse height

S = Calibration pulse height (mV)

TABLE 2.2 : Calibration parameters for density measurement

In the work described in this thesis (Chapter 3), extensive air showers selected by an inner ring trigger coincidence requirement of $\Delta_c(\geq 4m^{-2}).\ \Delta_{11}(\geq 2m^{-2}).\Delta_{31}\ (\geq 2m^{-2}).\Delta_{51}\ (\geq 2m^{-2})$ and an outer ring trigger coincidence requirement of $\Delta_c(\geq 4m^{-2}).\Delta_{13}(\geq 2m^{-2}).\Delta_{33}(\geq 2m^{-2}).\Delta_{53}(\geq 2m^{-2})$ have been investigated. Figures 2.14, 2.15, 2.16, 2.17 show the differential and integral distribution of recorded density in different detectors for both the inner ring and outer ring triggers. Table 2.3 shows the median density recorded by each detector for both the inner ring trigger and outer ring trigger master coincidence requirement. These results indicate that the detectors were in good calibration relative to one another during the period that the basic data was collected. Figure 2.18 shows a diagram of the Durham Air Shower Array with the median particle density recorded by each detector indicated for both outer ring and inner ring trigger data. The minimum shower size detected by the inner ring trigger is 10^4 particles and by the outer ring trigger 10^5 particles respectively. Figure 2.19 shows the shower size distribution recorded by both the inner ring and outer ring triggers respectively. Using the calculation of Kempa (1976) relating the number of particles to primary energy these figures correspond to threshold energies of 10^{14} ev and 8.10^{14} ev respectively.

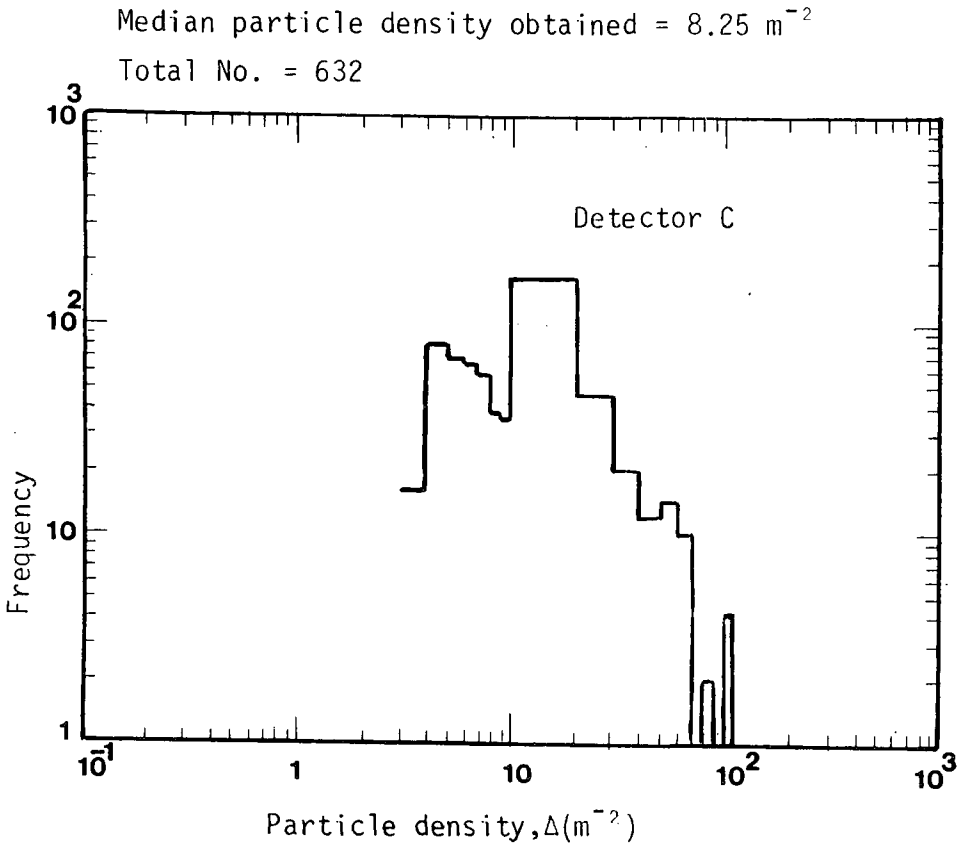

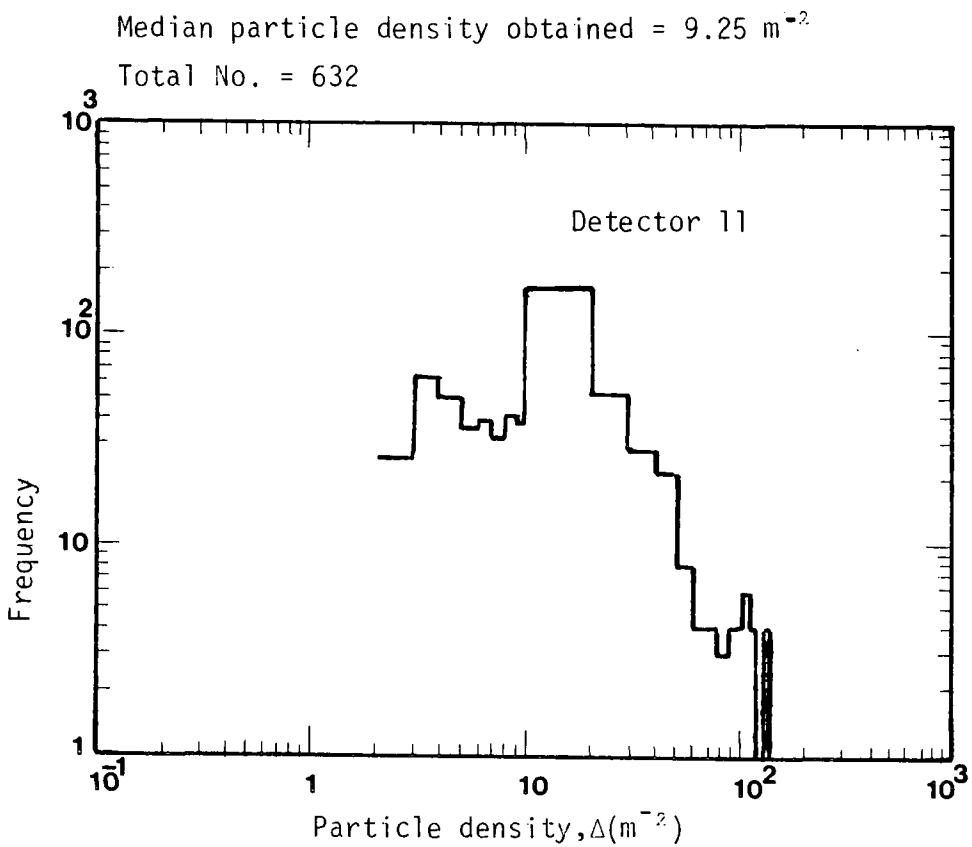

Figure 2.14 Differential frequency distribution of particle density from detectors C and 11 from a sample of 632 shower triggers obtained using the inner ring trigger $\Delta_c(\geq 4m^{-2})$. $\Delta_{11}(\geq 2m^{-2})$. $\Delta_{31}(\geq 2m^{-2})$. $\Delta_{51}(\geq 2m^{-2})$

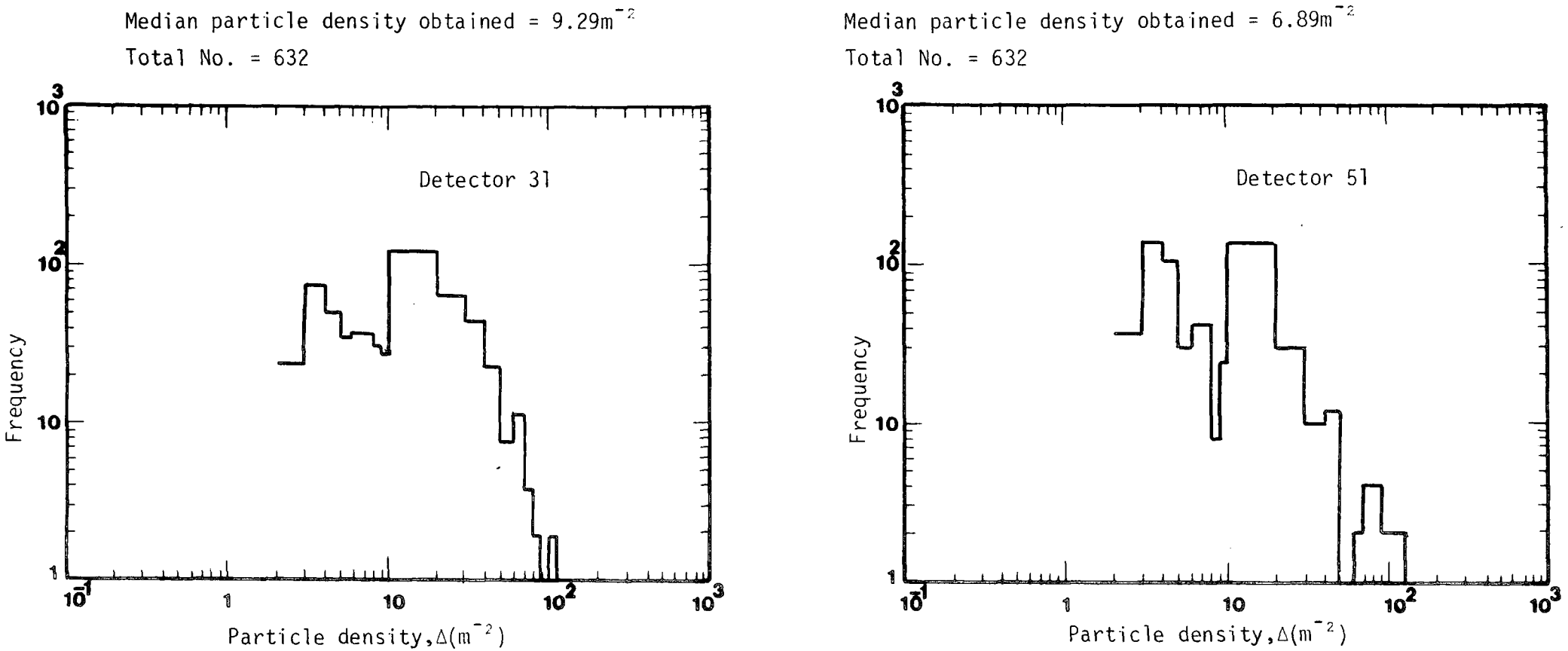

Fig. 2.14 Continued. Differential frequency distribution of particle density from detectors 31, 51 from a sample of 632 shower triggers obtained using inner ring trigger $\Delta_C(\geq 4m^{-2})$. $\Delta_{11}(\geq 2m^{-2})$. $\Delta_{31}(\geq 2m^{-2})$. Δ_{51} $(\geq 2m^{-2})$.

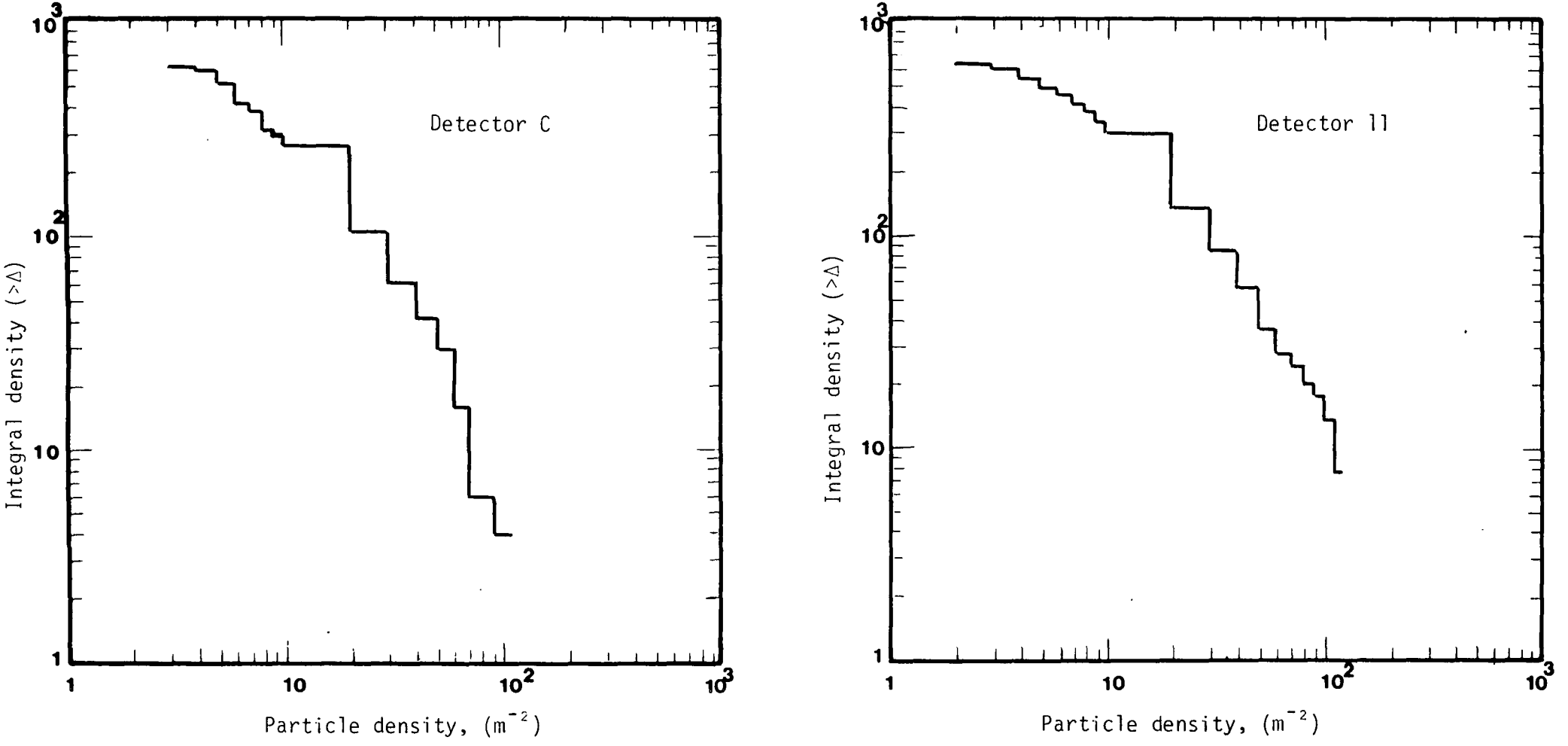

Fig. 2.15 Integral distribution of particle density from detectors C and 11, using the inner ring trigger $\Delta_C(\geq 4m^{-2}).\Delta_{11}(\geq 2m^{-2}).\Delta_{31}(\geq 2m^{-2}).\Delta_{51}(\geq 2m^{-2})$

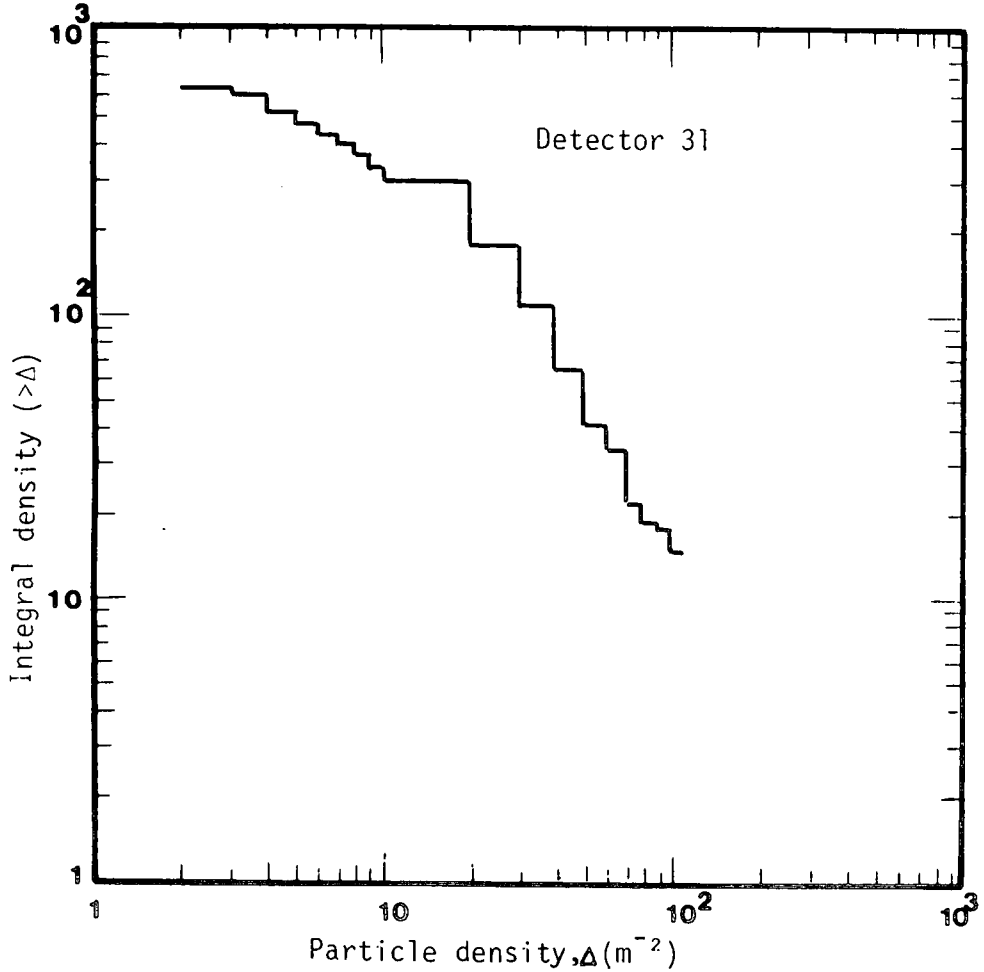

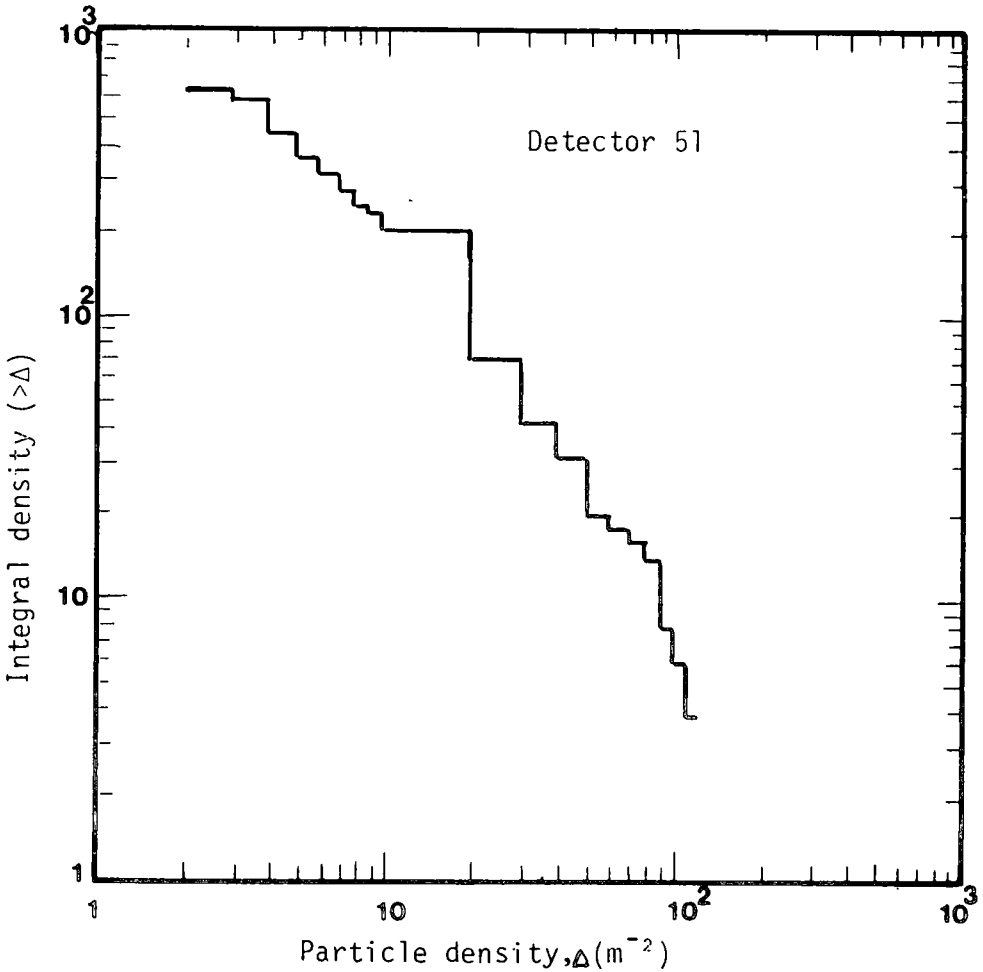

Fig. 2.15 Continued. Integral distribution of particle density from detectors 31, 51, using the inner ring trigger $\Delta_C(\geq 4m^{-2}).\Delta_{11}(\geq 2m^{-2}).\Delta_{31}(\geq 2m^{-2}).\Delta_{51}(\geq 2m^{-2})$

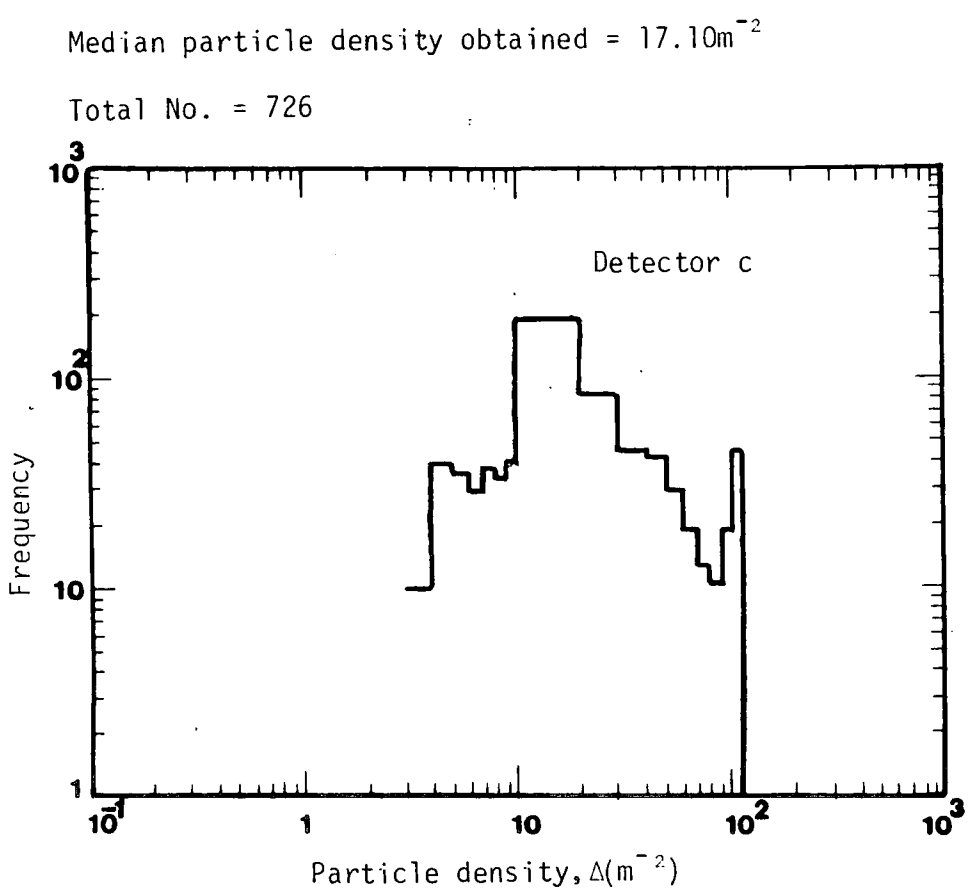

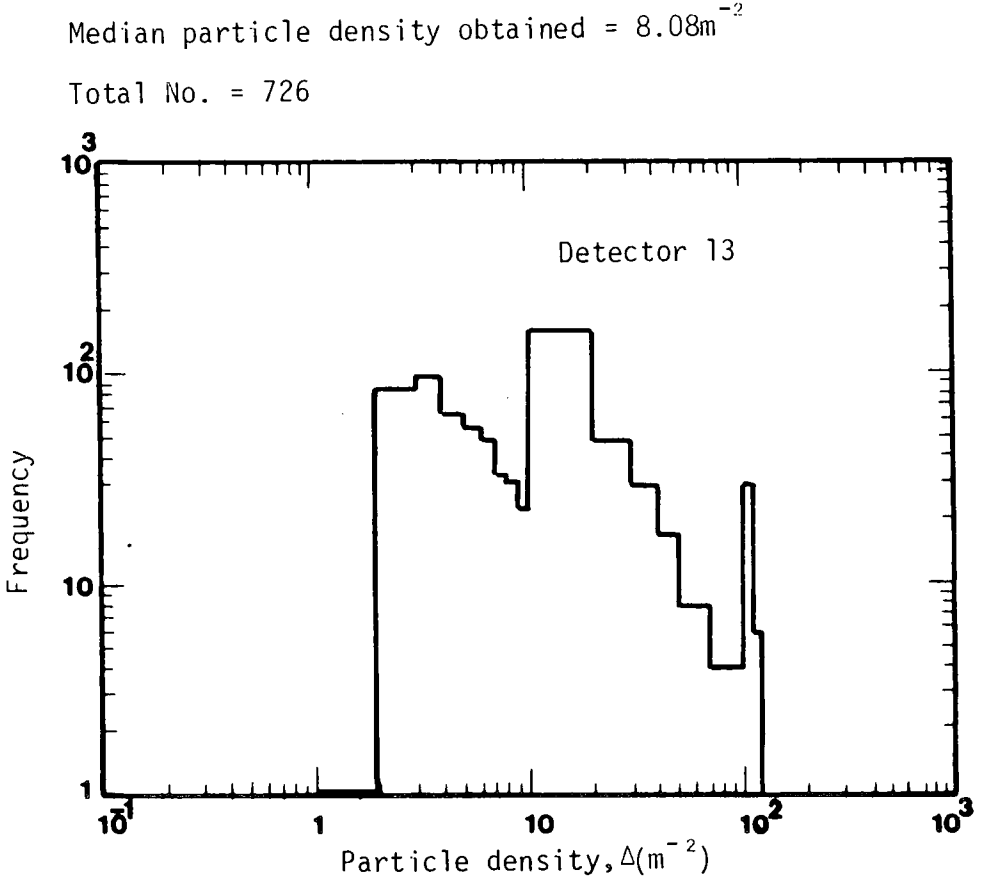

Figure 2.16 Differential frequency distribution of particle density from detectors C and 13 from a sample of 726 shower triggers obtained using the outer ring trigger $\Delta_C(\geq 4m^{-2})$. $\Delta_{13}(\geq 2m^{-2})$. $\Delta_{33}(\geq 2m^{-2})$. $\Delta_{53}(\geq 2m^{-2})$.

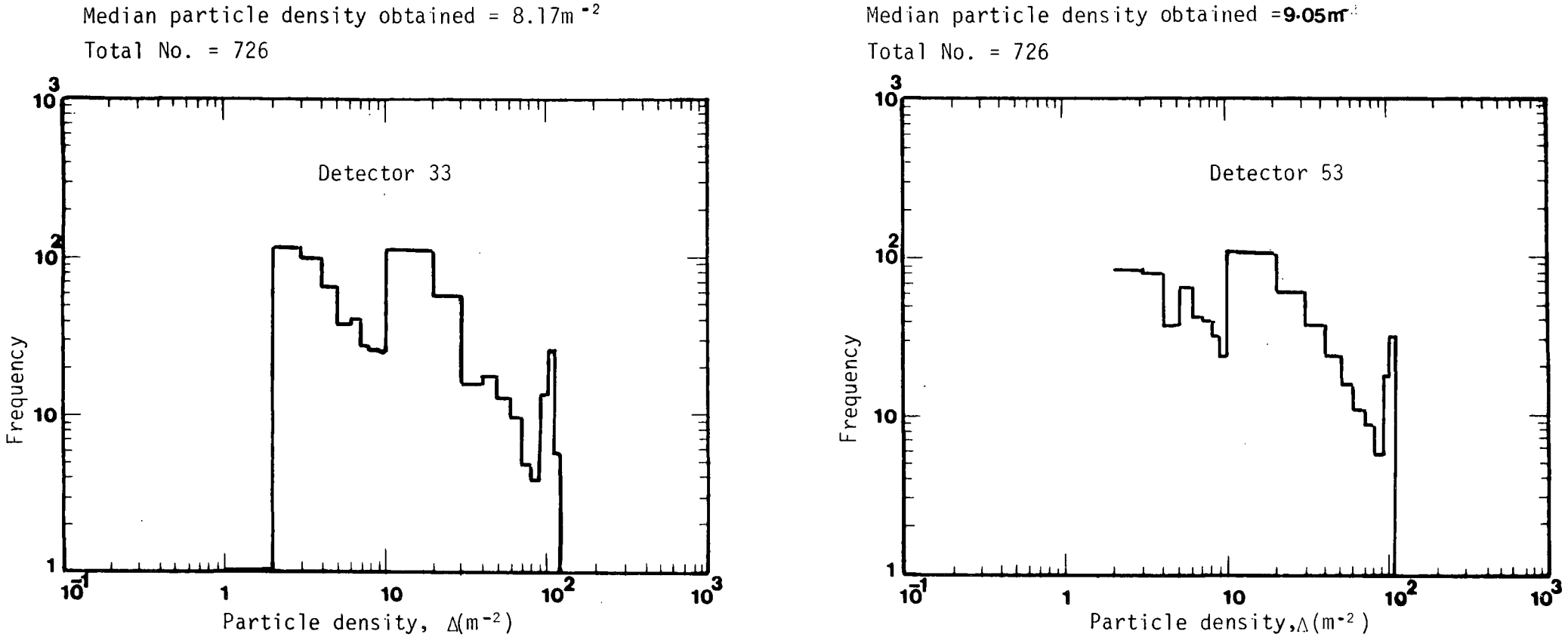

Fig. 2.16 Continued. Differential frequency distribution of particle density from detectors 33 and 53 from a sample of 726 shower triggers obtained using outer ring trigger $\Delta_C(\geq 4m^{-2}).\Delta_{13}(\geq 2m^{-2}).\Delta_{33}(\geq 2m^{-2}).\Delta_{53}(\geq 2m^{-2})$

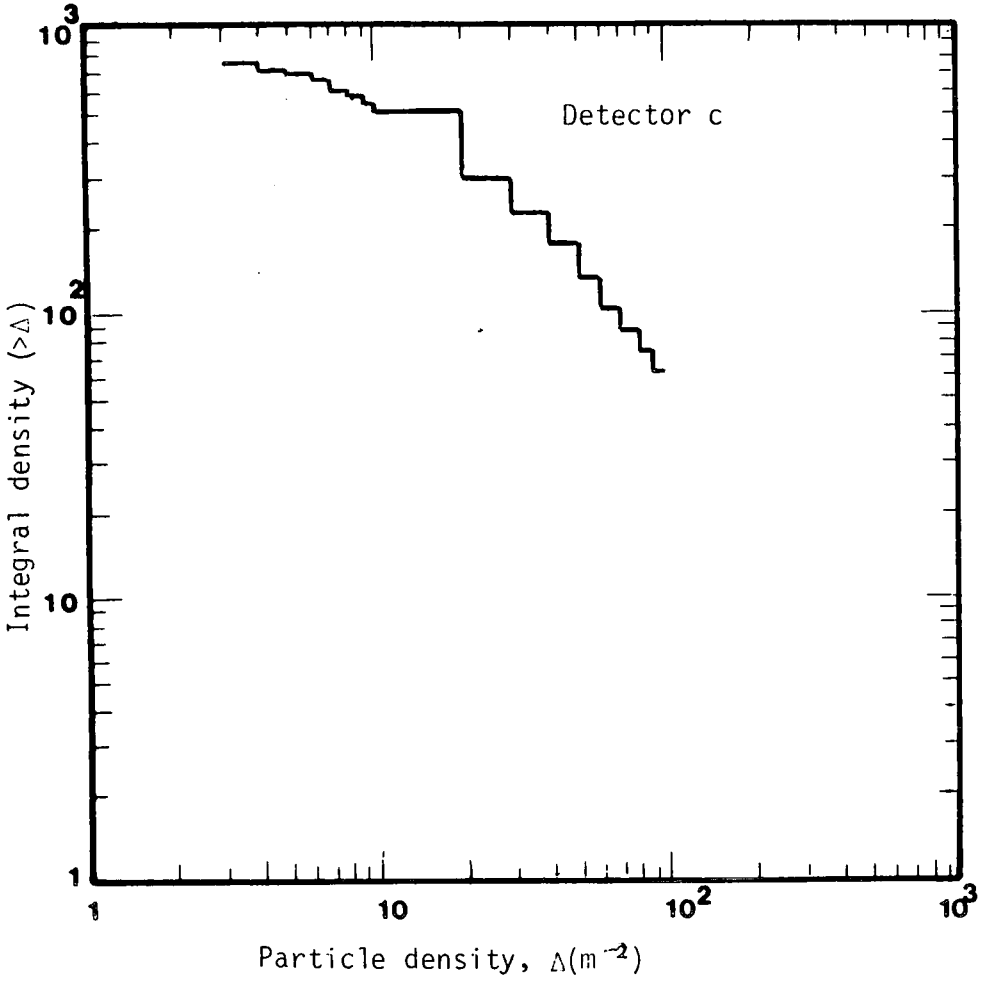

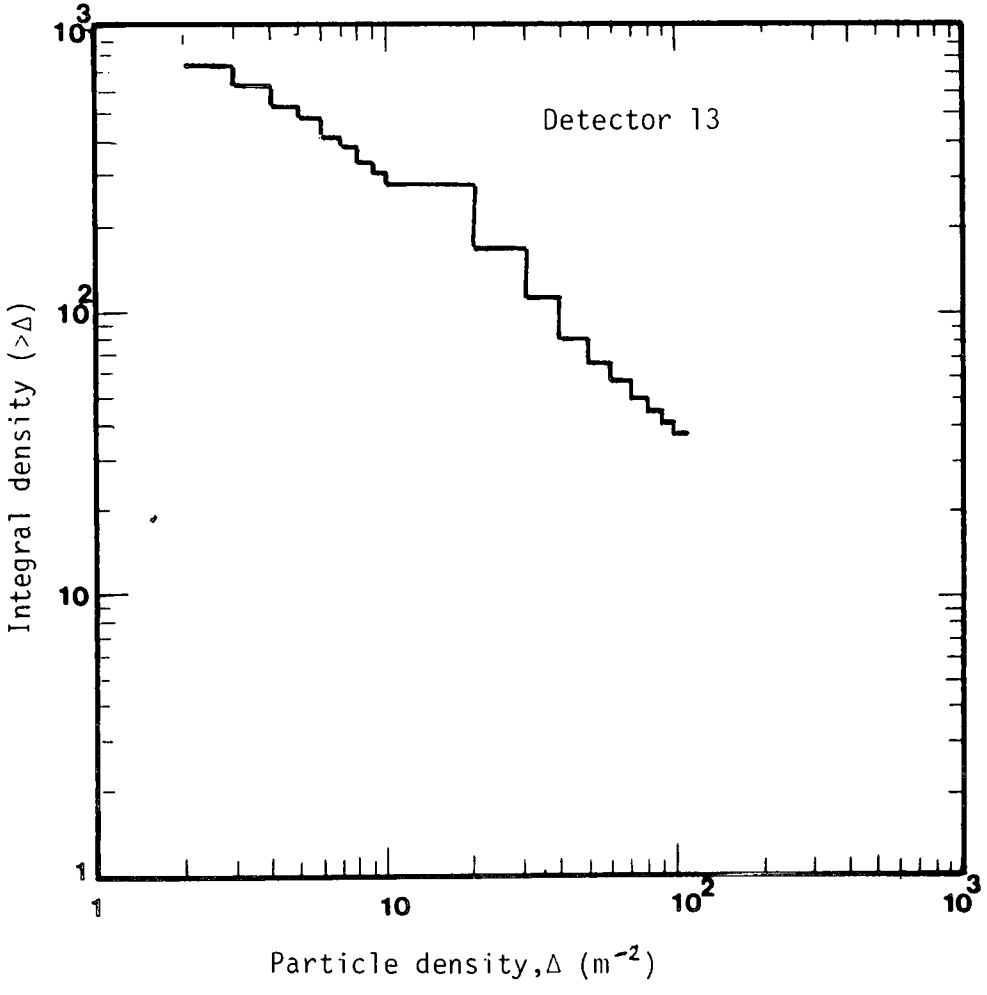

Figure 2.17 Integral distribution of particle density from detectors c and 13, using the outer ring trigger $\Delta_C(\geq 4m^{-2})$. $\Delta_{13}(\geq 2m^{-2})$. $\Delta_{33}(\geq 2m^{-2})$. $\Delta_{53}(\geq 2m^{-2})$.

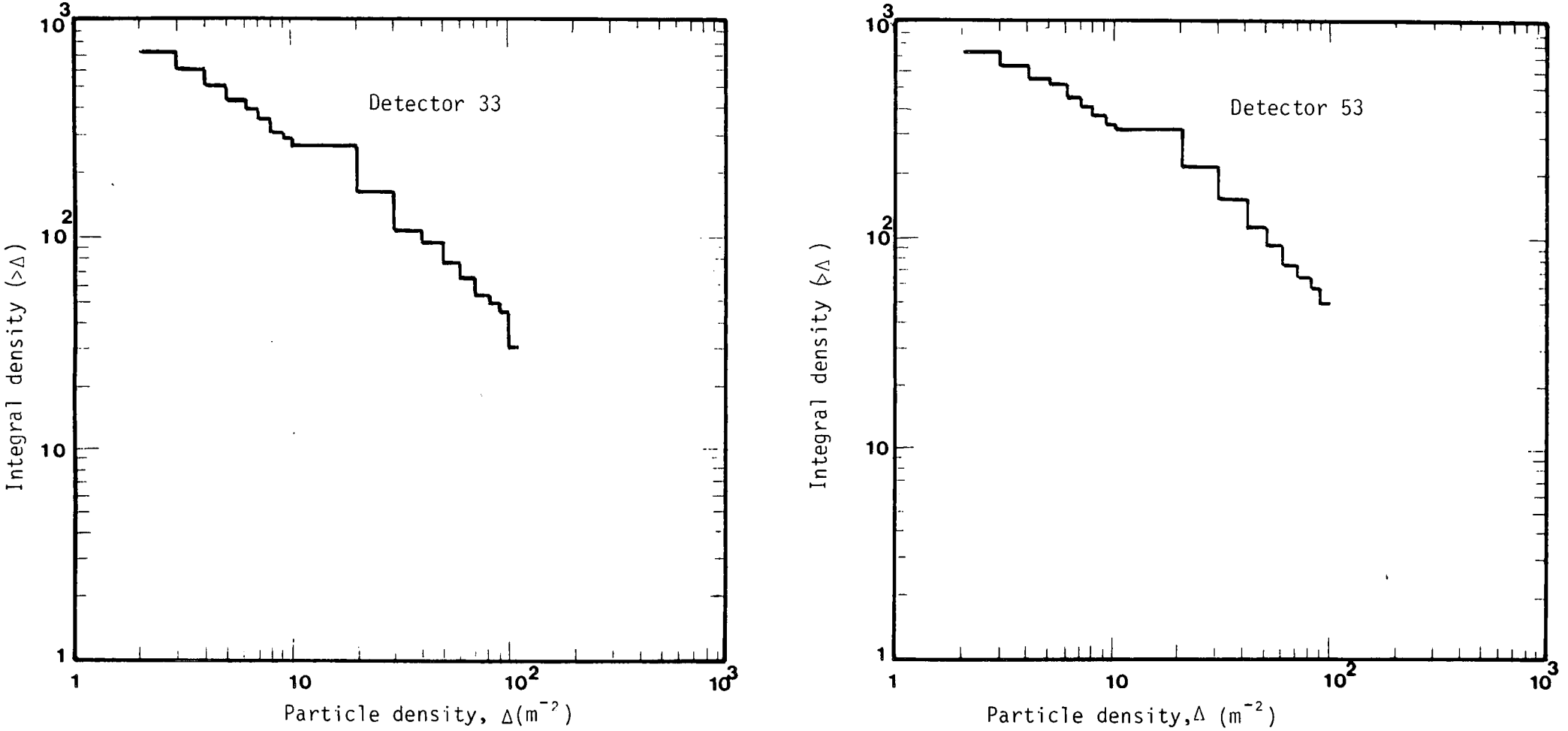

Figure 2.17 Continued. Integral distribution of density from detectors 33, 53, using the outer ring trigger $\Delta_C(\geq 4m^{-2})$. $\Delta_{13}(\geq 2m^{-2})$. $\Delta_{33}(\geq 2m^{-2})$. $\Delta_{53}(\geq 2, ^{-2})$.

Detector	Median density for outer ring trigger	Median density for inner ring trigger
	No. of showers = 632	No. of showers = 726
C	17.10 m^{-2}	8·25 m^{-2}
11	19.12 m^{-2}	9.25 m^{-2}
31	25·80 m^{-2}	9.29 m^{-2}
51	16.95 m^{-2}	6·81 m^{-2}
13	8·08 m^{-2}	2.39 m^{-2}
33	8·17 m^{-2}	2.01 m^{-2}
53	9·05 m^{-2}	1·50 m^{-2}
12	9·58 m^{-2}	2·21 m^{-2}
32	11.10 m^{-2}	2.07 m^{-2}
61	14·40 m^{-2}	7·16 m^{-2}
62	7·90 m^{-2}	1·97 m^{-2}
52	11·82 m^{-2}	5·25 m^{-2}
41	13·25 m^{-2}	2·10 m^{-2}
42	7·91 m^{-2}	1·91 m^{-2}

Table 2.3 : Comparison of median particle densities for each detector using outer ring and inner ring triggering.

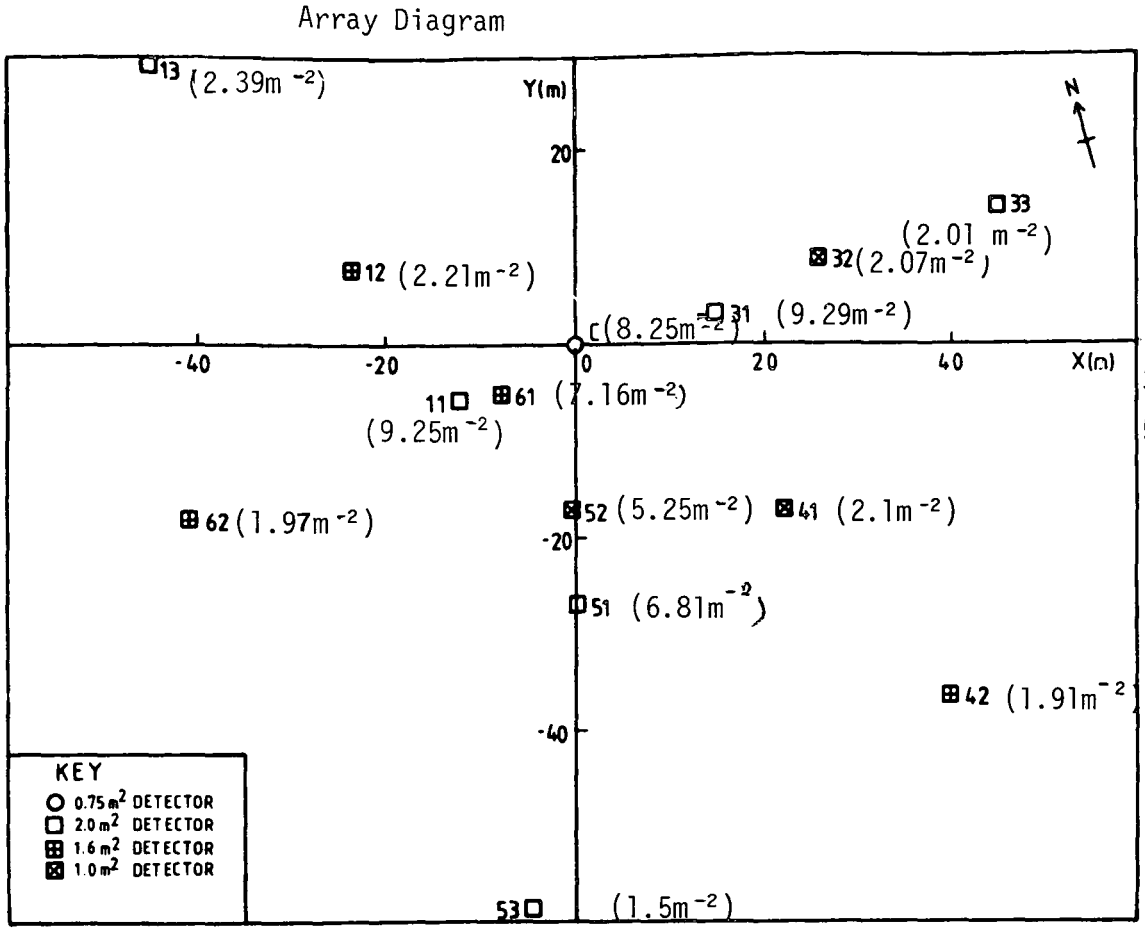

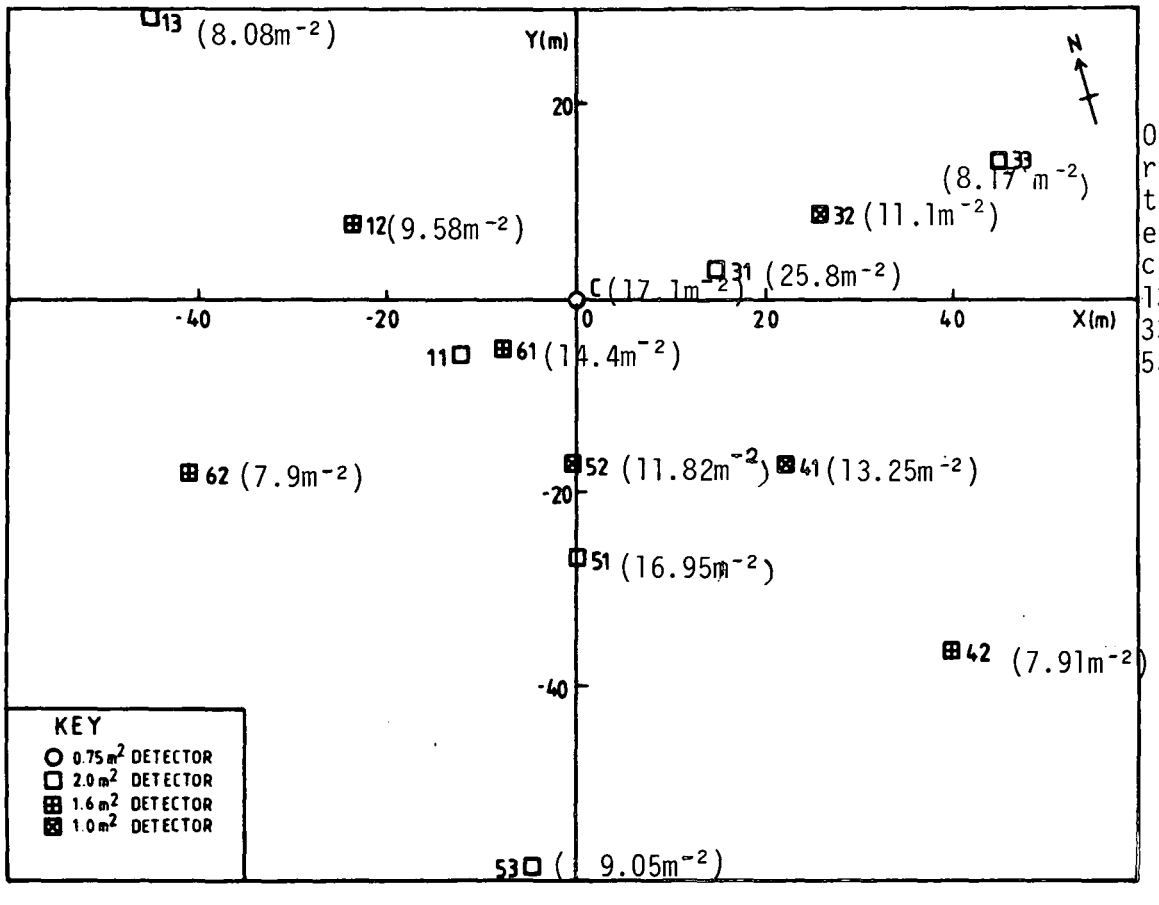

Fig.2.18 Durham EAS Array with median particle density recorded for each detector for outer ring and inner ring triggers

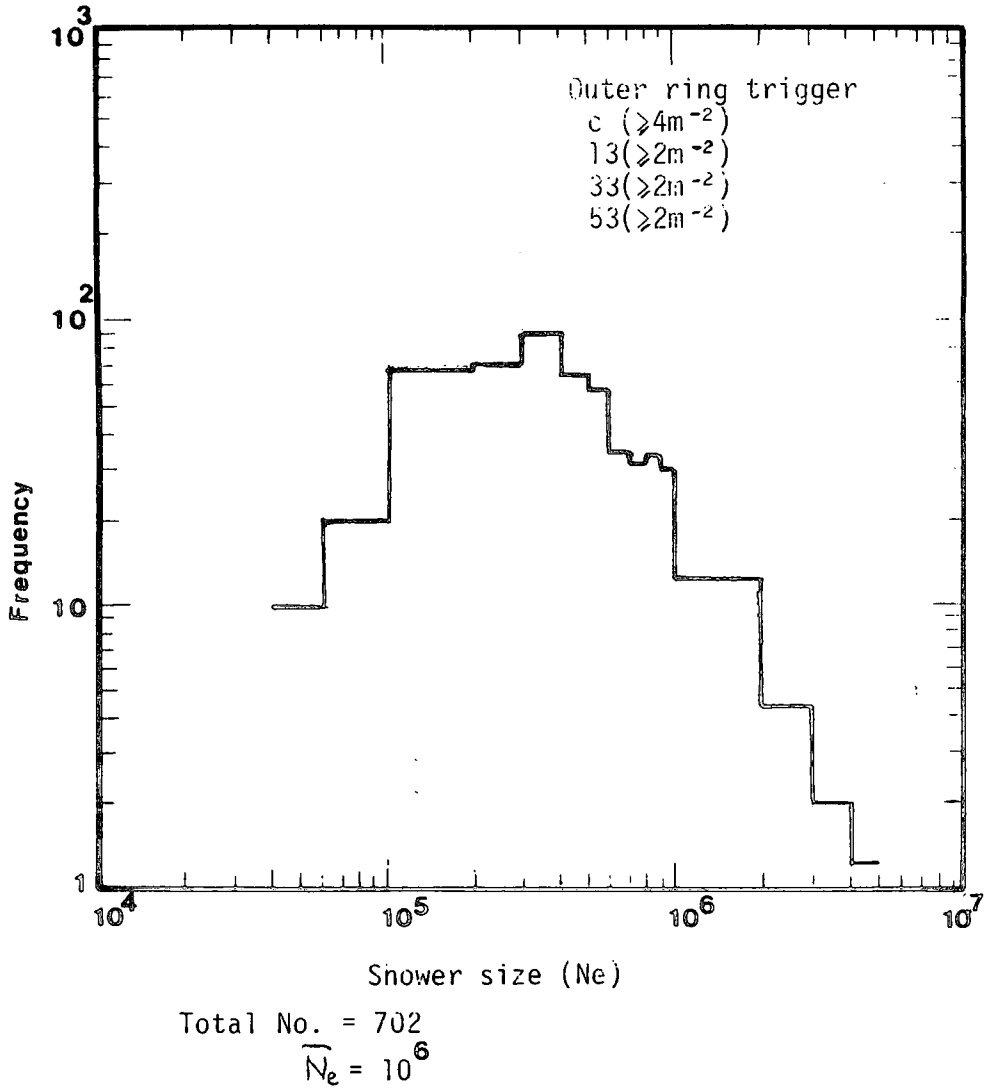

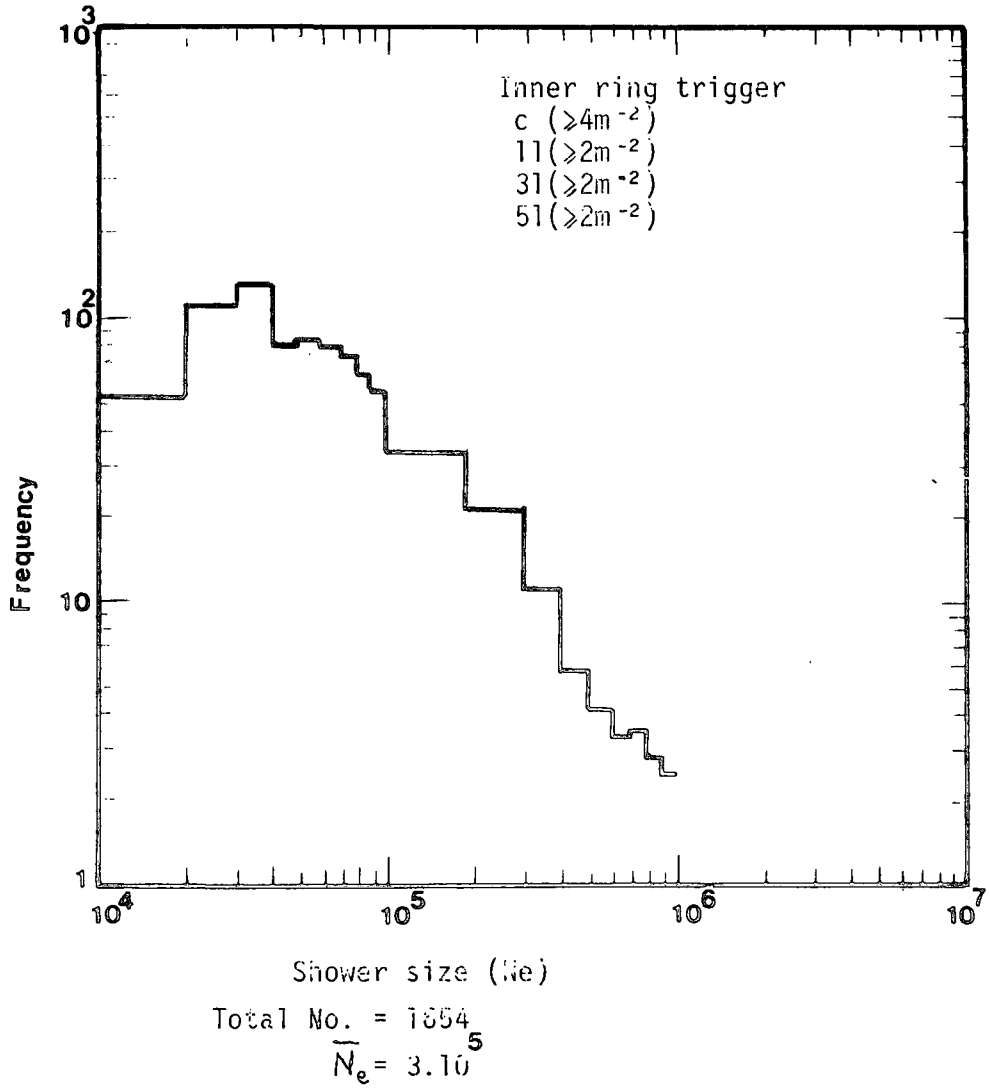

Figure 2.19 Size distribution of measured EAS using outer ring and inner ring trigger

2.7.3 Timing information

Each pulse from the Phillips 56 AVP P.M.T is first amplified by a NE 4634 fast amplifier and then is passed to a NE 4635 fast discriminator. It is essential that the pulse from C arrives first and for detectors 11, 31, 51 a large coil of coaxial cable is used in the line to delay the arrival of pulses relative to the arrival of the pulse from C. For the other three detectors 13, 33, 53 their distance from the laboratory is enough to ensure this. The time signal from detector C is used to trigger each of six NE 4645 (time to amplitude convertors (TACs)). The TACs generate a rectangular output pulse of height proportional to the time difference between the start and stop pulses with width 5 μs. The output pulses from the individual timing detectors stop the TACs so the output of the TAC is proportional to the time difference that a shower front passes through the detector relative to the time it passes through C plus electronic delays and differences in the cable delays. In analysing the basic data the fast timing information is first used to find the zenith angle and azimuthal angle of the shower axis direction. Subsequently the core position of the shower is found and then the shower size determined (Smith and Thompson 1977, Ashton et al 1977). All these calculations are carried out by computer.

CHAPTER 3

THE ZENITH ANGLE DISTRIBUTION OF EAS AND ITS MEASUREMENT AS A FUNCTION OF SHOWER SIZE

3.1 DETERMINING THE ARRIVAL DIRECTION OF EXTENSIVE AIR SHOWERS FROM FAST TIMING MEASUREMENTS

3.1.1 Introduction

Fast timing between scintillation counter detectors was first used by Bassi et al. (1953) to determine the zenith angle and azimuthal angle of arrival of EAS. These authors also showed that the thickness of the electron shower front is ~1.5 m with a radius of curvature of ~2.6 Km for showers of size 10^5-10^6 particles at sea level. The problem of determining the exact shower front thickness and curvature for electrons, muons and hadrons as a function of core distance and shower size is a problem of continuing study, although some progress has been made by Linsley and Scarsi (1962), Waidneck and Bohm (1975). Crouch et al (1977) have briefly discussed a procedure for determining the error in the measured zenith angle obtained from fast timing measurements for the special case of all the detectors being situated in one plane.

3.1.2 Design of a fast timing array

Consider a central timing detector C placed at the origin of a right hand set of cartesian co-ordinates and a single detector X placed at point (α,β,γ) as shown in Figure 3.1. In the following analysis it will be assumed that the fast timing detectors are all at distance $\lesssim$ 50 m from the shower axis so that the shower front can be considered plane to a good approximation. If the normal to the shower front has zenith angle θ and azimuthal angle ϕ then as the shower front passes through X it is defined by a plane containing XS which is normal to CS. To calculate the time at which the shower front sweeps through C

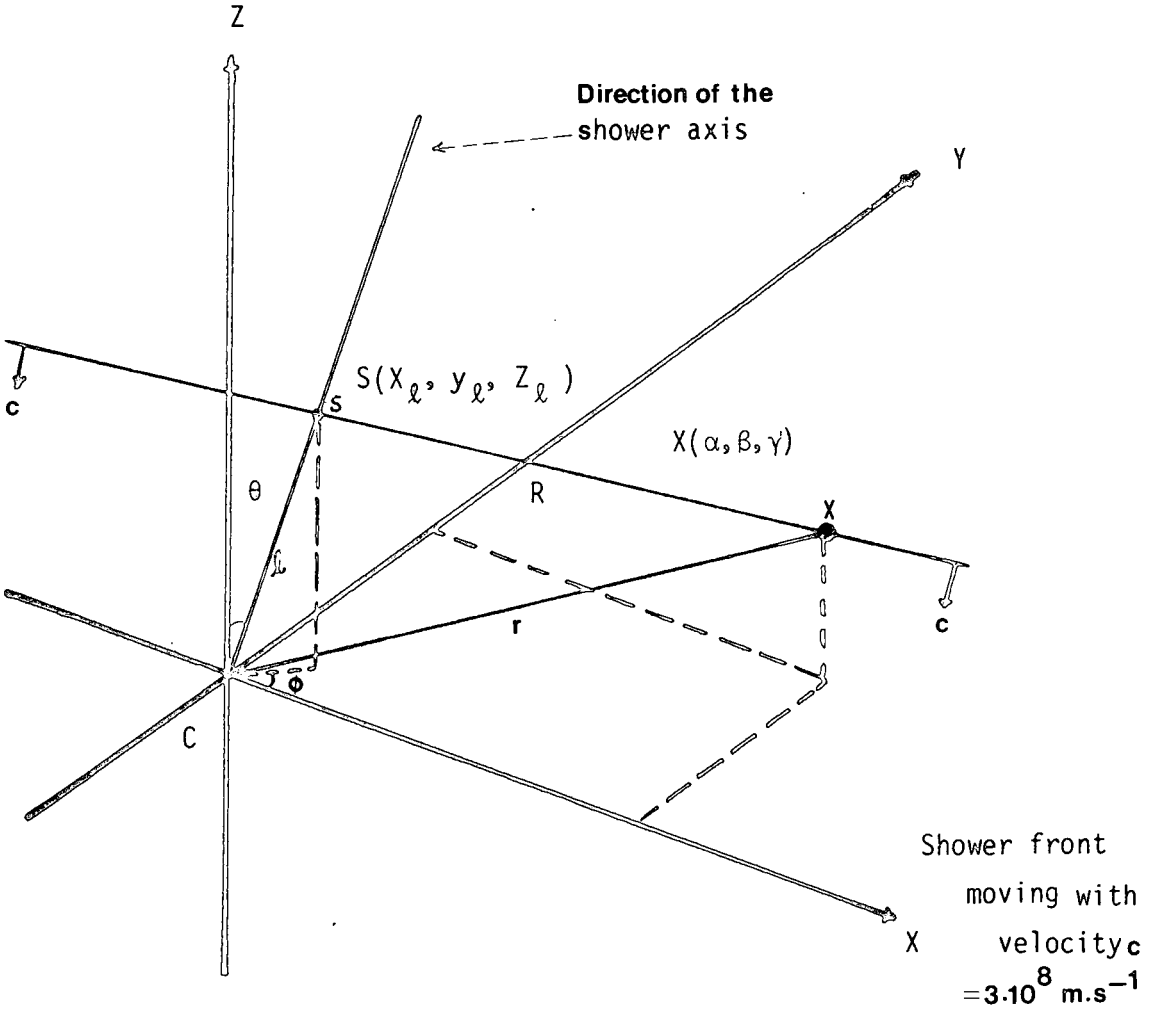

Figure 3.1 : Diagram showing a shower whose axis has zenith angle θ and azimuthal angle ϕ The shower front is a plane containing XS which is normal to the shower axis direction CS. CS = ℓ, SX = R and CX = r.

after being at XS it is necessary to calculate the distance CS = ℓ. For any position of the point S on the line CS

$$R = [\,(x_\ell - \alpha)^2 + (y_\ell - \beta)^2 + (Z_\ell - \gamma)^2\,]^{\frac{1}{2}}$$

$$= [\,(\ell \sin\theta \cos\phi - \alpha)^2 + (\ell \sin\theta \sin\phi - \beta)^2 + (\ell \cos\theta - \gamma)^2\,]^{\frac{1}{2}}$$

As ℓ varies in magnitude XS will be orthogonal to CS when R is a minimum. Evaluating $\frac{dR}{d\ell}$ and equating to zero shows that R is a minimum when

$$\ell = \alpha \sin\theta \cos\phi + \beta \sin\theta \sin\phi + \gamma \cos\theta \qquad (3.1)$$

in which case

$$R = [(\alpha^2 + \beta^2 + \gamma^2) - (\alpha \sin\theta \cos\phi + \beta \sin\theta \sin\phi + \gamma \cos\theta)^2]^{\frac{1}{2}} \qquad (3.2)$$

Equation 3.2 is useful in determining the orthogonal shower axis distance from a subsidiary detector (e.g. a muon detector in an EAS array). Suppose a shower axis having zenith angle θ and azimuthal angle ϕ crosses the XY plane of the array co-ordinate system at the point (x_1, y_1, o) and that a muon detector is located at the point (x_2, y_2, z_2). The orthogonal core distance R from the muon detector to the shower axis is given by

$$R^2 = [\,(x_2 - x_1)^2 + (y_2 - y_1)^2 + z^2\,] - [\,(x_2 - x_1) \sin\theta \cos\phi + (y_2 - y_1) \sin\theta \sin\phi + z_2 \cos\theta\,]^2$$

The co-ordinates of the fast timing detectors of the Durham EAS array are shown in Table 3.1.

Detector	C	13	33	53	11	31	51
X	0	-41.8	45.1	- 3.6	-12.1	13.2	1.0
Y	0	26.3	14.9	-57.3	- 6.0	4.0	-27.1
Z	0	-13.3	0.2	- 9.3	- 4.9	0.2	0.2

Table 3.1 : Co-ordinates (in metres) of the centres of the fast timing detectors in the Durham EAS array.

Using equation 3.1 the time difference t between an EAS shower front traversing a given detector and detector C is given by

$$ct = \alpha \sin\theta \cos\phi + \beta \sin\theta \sin\phi + \gamma \cos\theta$$

where $c = 3.0.10^8$ ms^{-1} is the velocity of light. How t depends on θ and ϕ for detectors C and 13 is shown in Figure 3.2. It is seen that the maximum value of t = +180ns (corresponding to a shower with $\theta = 90°$, $\phi = 330°$ which sweeps through C before 13) and the minimum value of t = -180ns (corresponding to a shower with $\theta = 90°$, $\phi = 150°$ which sweeps through 13 before C). Curves similar to those shown in Figure 3.2 have been evaluated for detector C and each timing detector. In each case it is found that the maximum and minimum values of t occur for $\theta = 90°$ and that if the maximum occurs for an azimuthal angle ϕ then the minimum value occurs for $\phi + 180°$. In the Durham array fast timing is achieved using time to amplitude converters which are started when a pulse arrives from detector C and stopped when pulses arrive from the 6 surrounding timing detectors. For this to work, known cable delays must be inserted in the timing channels 13, 33, 53, 11, 31, 51 to ensure that the pulse from C always arrives at the time to amplitude converters before the pulses from the 6 outer timing detectors. The cable delays used in the different channels as well as the maximum time differences at which shower fronts can traverse a given detector before C are shown in Table 3.2. It is seen that in all cases the cable delays used are ample to efficiently record all showers with zenith angles in the range 0 to 90°.

3.1.3 The inverse problem.

In practice the values of t are measured and the problem is to find θ and ϕ. Suppose the shower front passes through two timing detectors D1 and D2 located at (x_1, y_1, z_1) at time differences t_1 and

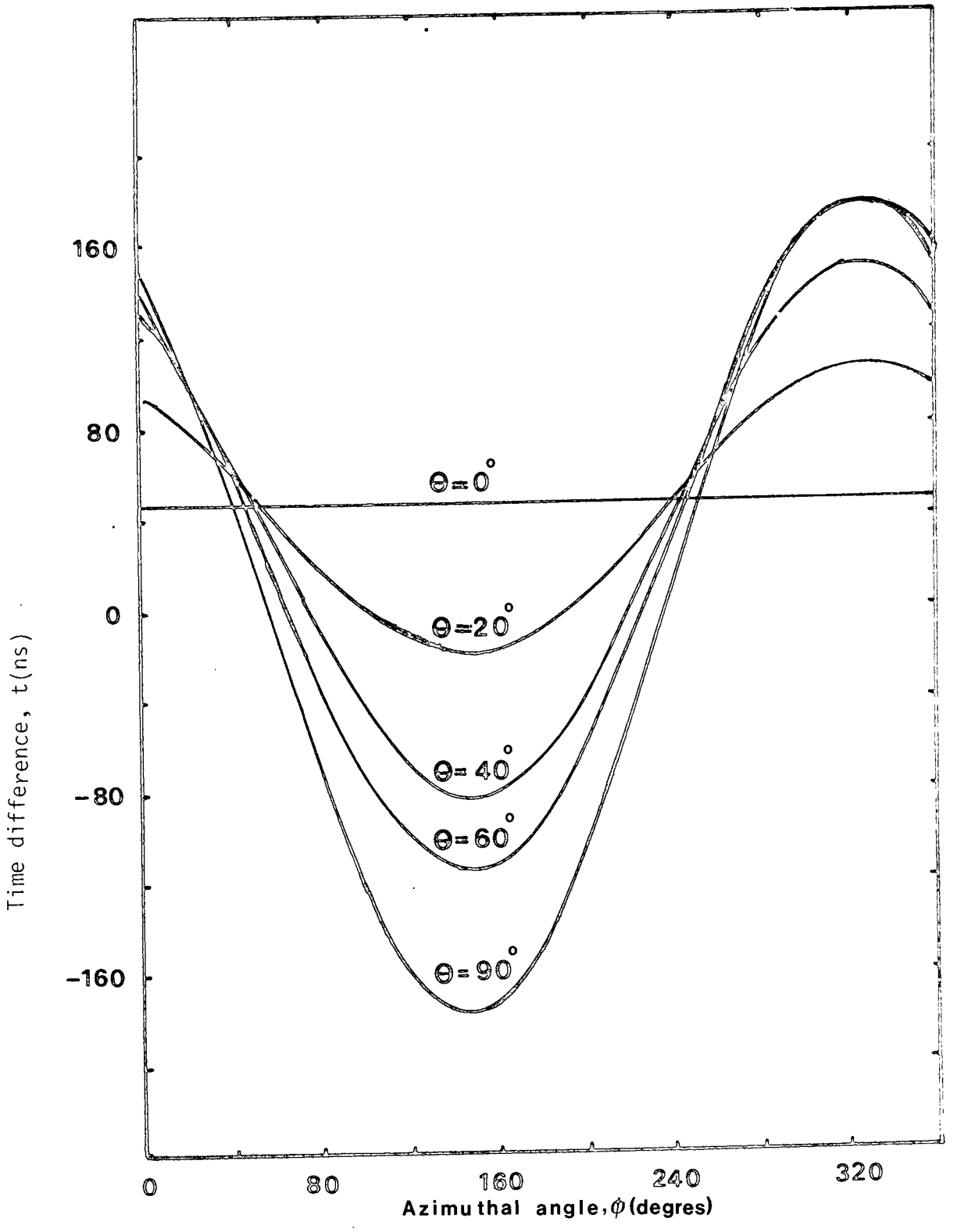

Figure 3.2 : Time difference t(ns) between a shower front traversing detectors C & 13 as a function of the azimuthal angle ϕ for different zenith angles θ of the E.A.S. t is counted +t if the shower front traverses C before 13 and -t if it traverses 13 before C.

Detector	Cable delay	Cable delay relative to C	Maximum value of time difference $\|t\|$ for a shower front which traverses the indicated detector before C
C	210ns	0	-
13	520	310	180ns
33	511	30	155
53	575	365	195
11	517	307	46
31	512	302	47
51	589	379	90

Table 3.2 Cable delays used for pulses between the detector indicated and the recording electronics. Maximum values of the time difference $|t|$ for a shower front which traverses the indicated detector before C are also shown. Maximum values of $|t|$ correspond to showers with $\theta = 90°$ (but different azimuthal angles ϕ) in all cases.

t_2 relative to the time it passes through C which is situated at the origin. t_1 and t_2 are counted positive if the shower front traverses C first and negative if it traverses them before it traverses C.

Using equation (3.1)

$$ct_1 = x_1 \sin\theta \cos\phi + y_1 \sin\theta \sin\phi + z_1 \cos\theta \tag{3.3a}$$

$$ct_2 = x_2 \sin\theta \cos\phi + y_2 \sin\theta \sin\phi + z_2 \cos\theta \tag{3.3b}$$

Writing $\ell = \sin\theta \cos\phi$, $m = \sin\theta \sin\phi$, $n = \cos\theta$, $ct_1 = T_1$, $ct_2 = T_2$ these equations become

$$T_1 = \ell x_1 + m y_1 + n z_1 \tag{3.4a}$$

$$T_2 = \ell x_2 + m y_2 + n z_2 \tag{3.4b}$$

Multiplying (3.4a) by y_2 and (3.4b) by y_1

$$y_2 T_1 = y_2 \ell x_1 + y_2 m y_1 + y_2 n z_1 \tag{3.5a}$$

$$y_1 T_2 = y_1 \ell x_2 + y_1 m y_2 + y_1 n z_2 \tag{3.5b}$$

Subtracting gives

$$y_2 T_1 - y_1 T_2 = \ell(y_2 x_1 - y_1 x_2) + n(y_2 z_1 - y_1 z_2)$$

$$\ell = \frac{y_2 T_1 - y_1 T_2}{y_2 x_1 - y_1 x_2} + \frac{y_1 z_2 - y_2 z_1}{y_2 x_1 - y_1 x_2} n$$

$$= A + Bn \tag{3.6a}$$

where $A = \dfrac{y_2 T_1 - y_1 T_2}{y_2 x_1 - y_1 x_2}$ (3.6b)

and $B = \dfrac{y_1 z_2 - y_2 z_1}{y_2 x_1 - y_1 x_2}$ (3.6c)

Similarly by multiplying (3.4a) by x_2 and (3.4b) by x_1 and eliminating ℓ one finds

$$m = C + Dn \tag{3.7a}$$

where $$C = \frac{x_1T_2 - x_2T_1}{x_1y_2 - x_2y_1} \tag{3.7b}$$

and $$D = \frac{x_2z_1 - x_1z_2}{x_1y_2 - x_2y_1} \tag{3.7c}$$

Since ℓ, m, n are the components of a unit vector in polar co-ordinates

$$\ell^2 + m^2 + n^2 = 1 \tag{3.8}$$

Substituting for ℓ and m in 3.8 from 3.6a and 3.7a

$$A^2 + B^2n^2 + 2ABn + C^2 + D^2 + 2CDn + n^2 = 1$$

$$n^2(B^2 + D^2 + 1) + 2(AB + CD)n + (A^2 + C^2 - 1) = 0$$

$$n = \cos\theta = \frac{-(AB + CD) \pm \sqrt{(AB + CD)^2 - (B^2 + D^2 + 1)(A^2 + C^2 - 1)}}{(B^2 + D^2 + 1)} \tag{3.9}$$

Recalling that A,B,C,D are given in terms of detector co-ordinates, time differences and the velocity of light, equation (3.9) enables the zenith angle of the shower axis to be calculated. The required solution requires $\cos\theta$ to be positive as θ must lie in the range 0 - 90°. Using (3.6a) and (3.7a) the azimuthal angle of the shower axis is given by

$$\frac{m}{\ell} = \frac{\sin\theta\sin\phi}{\sin\theta\cos\phi} = \tan\phi = \frac{C + Dn}{A + Bn} \tag{3.10}$$

Thus, in principle, the arrival direction of an air shower can be determined with a minimum of 3 timing detectors. In practice at least 4 detectors are required so that the extra information can be used to check that the result obtained from all possible pairs are consistent.

If a large number of timing detectors are used then a numerical minimising procedure can be used to find θ and ϕ. To solve (3.3a) and (3.3b) numerically suppose arbitrary values of θ, ϕ are assumed. Substituting in (3.3a) and (3.3b) gives predicted values of the time differences t_1 and t_2. Calculating (3.3b)

$$\chi^2 = (t_1 \text{ measured} - t_1 \text{ predicted})^2 + (t_2 \text{ measured} - t_2 \text{ predicted})^2$$

gives a measure of the goodness of fit. Using a lattice of points in θ, ϕ space it is possible to zero in on the best θ, ϕ (corresponding to minimum χ^2) using the information available from how the gradient of χ^2 varies at four or more points surrounding the assumed θ, ϕ. Computer programmes (eg. MINUIT) are available for carrying out such a procedure.

3.1.4 Conclusion

Using a central timing detector surrounded by outer timing detectors, the problem of how much cable delay must be introduced into the outer channels, so that the pulse from the central detector always arrives at the recording station before the pulses from the other detectors, is solved. Two methods for determining the zenith and azimuthal angles of EAS from fast timing measurements are described.

3.2 THE SIZE DEPENDENCE OF THE ZENITH ANGLE DISTRIBUTION OF EXTENSIVE AIR SHOWERS AT SEA LEVEL

3.2.1 Introduction

The size dependence of the zenith angle distribution of extensive air showers at sea level is a fundamental constant of the cosmic radiation. Also the exact form of the zenith angle distribution is sensitive to the characteristics of high energy interactions (Kalmykov et al, 1973). Previous measurements see Galbraith (1958) pg. 129, Hayakawa (1969) pgs. 459 and 466, Ashton et al (1975) related to a wide range of shower size and no systematic studies using a single EAS array have been made.

In the present work preliminary measurements obtained using the Durham EAS array covering the size range 10^4 - $1.4.10^6$ particles at sea level are described.

3.2.2 Results

Using both an inner ring trigger $\Delta_c(\geq 4\ m^{-2}).\Delta_{11}(\geq 2\ m^{-2}).\Delta_{31}(\geq 2\ m^{-2}).\Delta_{51}(\geq 2\ m^{-2})$ and an outer ring trigger $\Delta c(\geq 4\ m^{-2}).\Delta_{13}(\geq 2\ m^{-2}).\Delta_{33}(\geq 2\ m^{-2}).\Delta_{53}(\geq 2\ m^{-2})$ of the Durham EAS array the zenith angle θ and azimuthal angle ϕ of each EAS trigger has been determined using fast timing. Also, a flash tube chamber was operational at the time that the measurements were made and a large fraction of the triggers showed at least one muon with E >1 Gev traversing the chamber. A comparison of the measured projected zenith angle of the muon track in the front view of the chamber with the value expected from the fast timing measurements provides a useful check on the fast timing measurements. As the height of origin of 1 Gev muons in EAS at small core distances (<100m) is $\sim$ 2 Km above sea level (Earnshaw et al, 1973;

Turver, 1973) and a 1 Gev muon track observed at 100 m from the core should be parallel to the shower axis direction to a precision of $\pm 3°$. On the average, the core distances involved in the present work are <100m so the precision should be better than this. As all the flash tubes in the flash tube chamber were mounted parallel to one another only the projected zenith angle that the muon track makes in the front plane of the chamber could be measured. The front plane of the chamber is parallel to the X axis of the cartesian coordinate system used to locate the detectors in the EAS array, so the expected muon projected zenith angle can be readily calculated, knowing the spatial zenith angle and azimuthal angle from the fast timing measurements as shown in Figure 3.3. It is found that $\tan\alpha = \tan\theta \cos\phi$ where α is the muon track projected zenith angle and θ, ϕ are the spatial zenith angle and azimuthal angle determined from the fast timing measurements. Figure 3.4 shows the frequency distribution of α (measured) - α (calculated) where α (measured) is the measured projected zenith angle of the muon tracks in the flash tube chamber and α(calculated) is their calculated value for showers in two different size ranges. In the small size range (10^4 - 5.10^5) the standard deviation of the distribution is (9.1 ± 0.4) degrees and in the larger size range (5.10^5 - $\sim 4.10^6$) the standard deviation is (7.6 ± 0.5) degrees. The distribution in shower size to which these data refer is also shown in Figure 3.4. The data presented in Figure 3.4 gives confidence in the reliability of the zenith and azimuthal angle results obtained from the fast timing measurements. In obtaining θ and ϕ for the EAS shown in Figures 3.4a and 3.4b a total of 6 fast timing detectors were functioning (detectors C,11,13,31,33,53 of the Durham EAS array). Similar plots to Figures 3.4a and 3.4b covering the same size ranges where only 4 fast timing detectors were functioning (C,13,33,53) showed the standard deviations of the

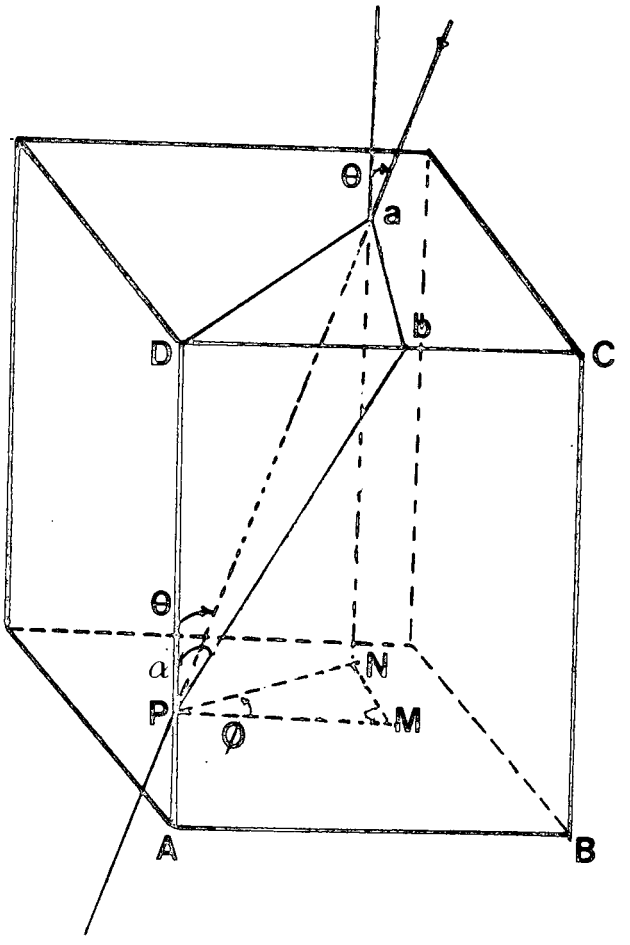

$Db = \ell_a$

$Dp = \ell_1$

$$\tan\alpha = \frac{\ell_2}{\ell_1} \qquad (1)$$

$$\tan\theta = \frac{PN}{\ell_1} \text{ where } PN\cos\phi = PM$$

$$= \frac{\ell_2}{\ell_1} \cdot \frac{1}{\cos\phi}$$

$$= \frac{\tan\alpha}{\cos\phi} \text{ using (1)}$$

i.e. $\tan\alpha = \tan\theta\cos\phi$

Figure 3.3 : ABCD is the front plane of the flash tube chamber and all the flash tubes are mounted with their axes perpendicular to it. Pa is the spatial direction of a muon track and Pb is its projected spatial direction as measured from the flash tube photograph.

Figs. 3.4a, 3.4b, 3.4c.

3.2a and 3.2b show the frequency distributions of α measured $-\alpha$ calculated where α measured is the measured projected zenith angle of a muon track in the flash tube chamber and α calculated is the calculated muon projected zenith angle. α calculated is determined from the zenith and azimuthal angles of the EAS as found from fast timing measurements. The dash histograms are fitted Gaussian distributions.

3.4.c shows the size distribution of the showers used in 3.4a and 3.4b.

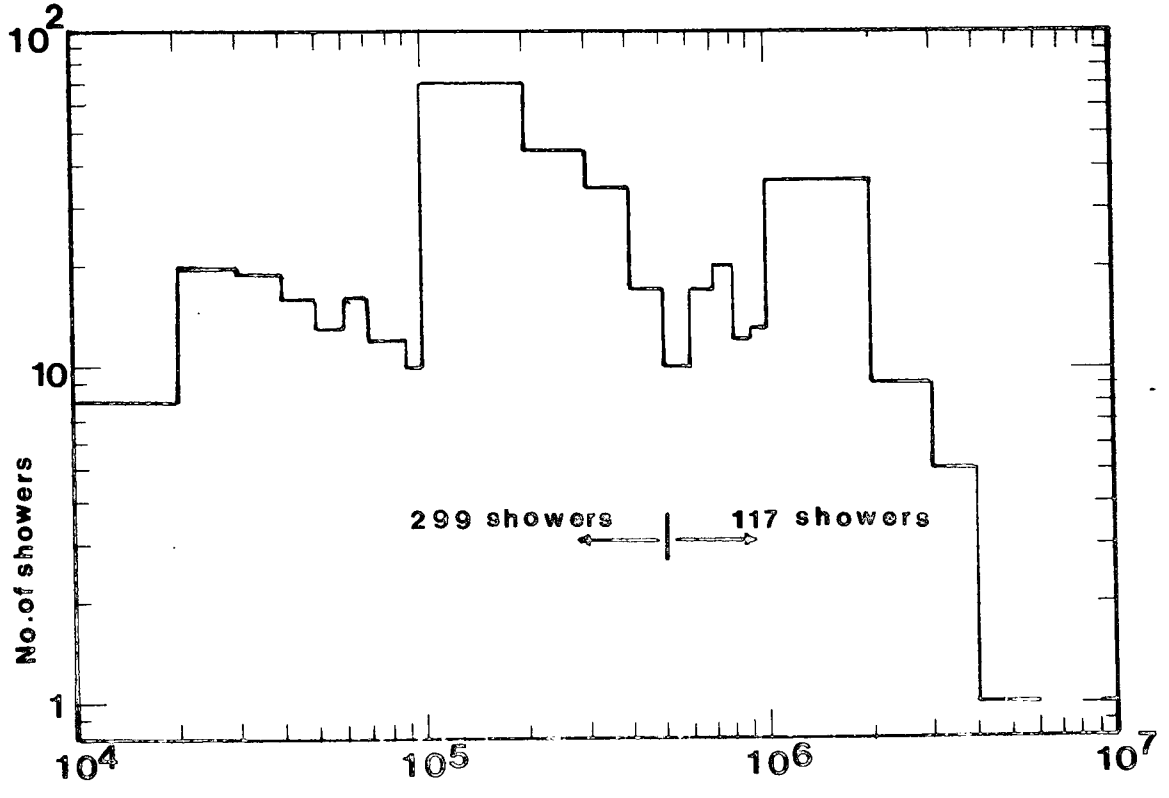

Figure 3.4c

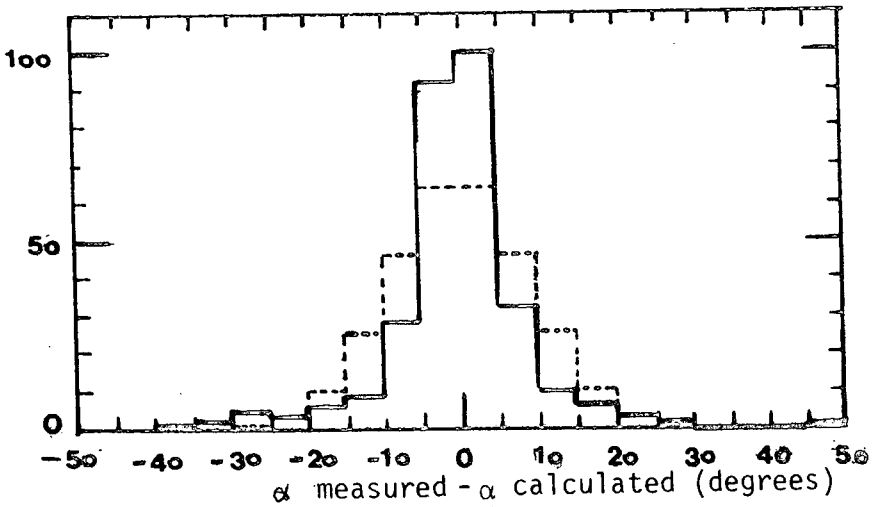

Figure 3.4a
$10^4 < N < 5.10^5$
$\sigma = 9.06° \pm .37°$
299 showers

Figure 3.4b
$N > 5.10^5$
$\sigma = 7.6° \pm .5°$
117 showers

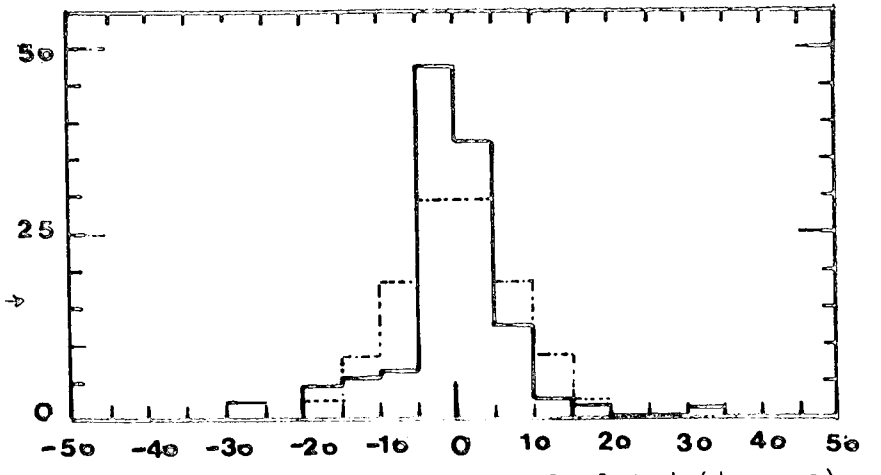

distributions were (12.3 $\pm$ 0.8) degrees and (8.0 $\pm$ 0.6) degrees. This shows that the precision of determining θ and ϕ increases as the number of fast timing detectors used increases as expected.

To find the best value of n that describes the zenith angle distribution of showers in $I(\theta) = I(o) \cos^n\theta$/unit area/unit time/unit solid angle two different methods have been used.

(a) Log $I(\theta)$ - log $\cos\theta$ plot If $I(\theta) = I(0)\cos^n\theta$ then a plot of log $I(\theta)$ versus log $\cos\theta$ will be a straight line of slope n. To find $I(\theta)$ from a set of experimental data suppose N showers with zenith angles between θ and $\theta + d\theta$ are observed to cross a horizontal area A in time t. Suppose the θ range is from θ_1 to θ_2 i.e. $d\theta = \theta_2 - \theta_1$ and $\bar{\theta} = \frac{\theta_1 + \theta_2}{2}$. The intensity of showers is given by

$$I(\bar{\theta}) = \frac{N}{t.\ A \cos\bar{\theta}.\ \int_{\theta_1}^{\theta_2} 2\pi \sin\theta d\theta}$$

$$= \frac{N}{t.\ A \cos\bar{\theta}.\quad 2\pi\,(\cos\theta_1 - \cos\theta_2)}$$

Assuming that it can be verified experimentally that A is not θ dependent (or A can be determined for each range of θ), $I(\bar{\theta})$ can be calculated and n found in the above way. Figure 3.5 shows the distribution in core distance (measured in the horizontal plane) from the central detector C of the Durham EAS array for different ranges of zenith angle for a sample of 452 showers with sizes in the range 3.10^5 - 7.10^5 particles. It is seen that all showers have a core distance < 80 m from C and accordingly the collecting area A is taken to be of constant area irrespective of zenith angle in evaluating $I(\bar{\theta})$. Figure 3.6 shows a plot of log $I(\bar{\theta})$ versus log $\cos\bar{\theta}$ for this size range which gives $n = 8.9 \pm 1.1$. Similar plots have been made

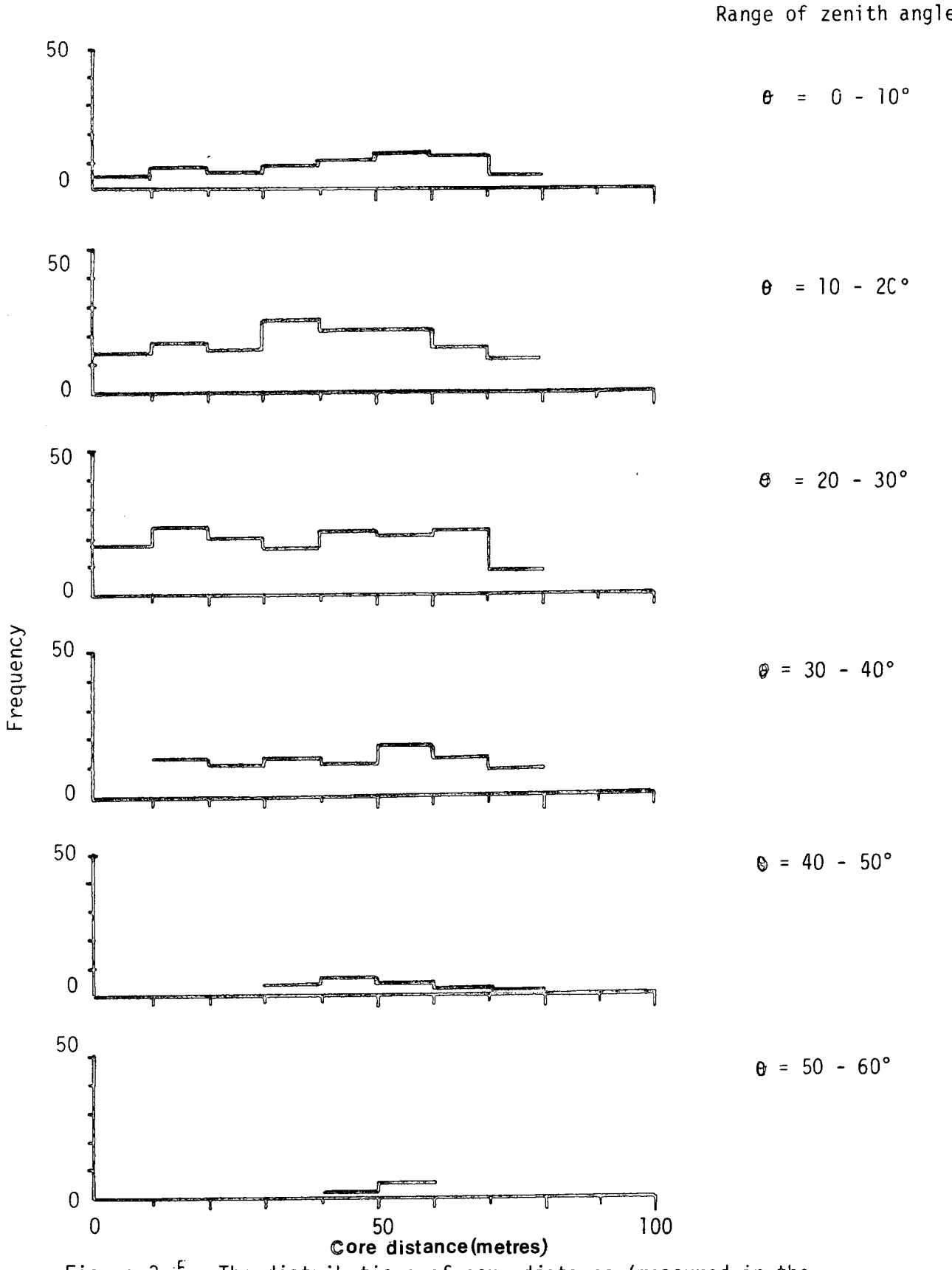

Figure 3.5 : The distributions of core distance (measured in the horizontal plane) from the central detector C of the Durham EAS array, for different ranges of zenith angle, for a sample of 452 showers with N in the range 3.10^5 - 7.10^5.

for other size ranges and the results are summarised in Table 3.3.

(b) χ^2 - n plot If $I(\theta) = I(0) \cos^n\theta$ then the number of showers observed to cross a horizontal collecting area A in time t with zenith angle in the range θ to $\theta + d\theta$ is given by

$$N(\theta)d\theta = I(0) \cos^n\theta . \; A \cos\theta . \; t . \; 2\pi \sin\theta d\theta .$$

For A and t fixed the proability that a given shower has zenith angle in the range θ to $\theta + d\theta$ is given by

$$P(\theta)d\theta \propto \cos^{n+1}\theta . \; \sin\theta d\theta$$

$$= (n+2) \cos^{n+1}\theta \sin\theta d\theta$$

using the fact that $\int_0^{\pi/2} P(\theta)d\theta = 1$. Thus for a sample of N_0 showers the expected number with zenith angle in the range θ_1 to θ_2 is

$$N(\theta_1 \to \theta_2) = N_0(n+2) \int_{\theta_1}^{\theta_2} \cos^{n+1}\theta . \; \sin\theta d\theta$$

$$= N_0 [\cos^{n+2}\theta_1 - \cos^{n+2}\theta_2]$$

To find the best n that fits a set of measurements by this approach, a trial and error procedure is adopted. A value of n is assumed and the expected number of showers in the zenith angle ranges 0° - 10°, 10° - 20°, etc. is calculated. The goodness of fit is found using a χ^2 test and when χ^2 is available for a range of values of n, the value of n that gives the minimum χ^2 can be found from a χ^2-n plot. This procedure has been used to find the best n for the ranges of shower size used in the present analysis, and the results are given in Table 3.3 where they are also compared with the values of n found by log $I(\bar{\theta})$ - log $\cos\bar{\theta}$ plots.

Size range	No. of showers	Median shower size	n from $\log I(\bar{\theta})$ - log $\cos\bar{\theta}$ plot	n from χ^2 - n plot
$10^4<N<5.10^4$	326	$3.2.10^4$	5.1 ± 1.3	5.4±1.0
$5.10^4<N<10^5$	325	$7.1.10^4$	8.4 ± 1.1	8.2±0.6
$10^5<N<3.10^5$	602	$1.9.10^5$	8.6 ± 1.3	8.7±0.7
$3.10^5<N<7.10^5$	452	$4.3.10^5$	8.9 ± 1.1	8.7±1.2
$N<7.10^5$	512	$1.4.10^6$	7.6 ± 1.1	8.6±1.1

Table 3.3 Comparison of the best values of n in $I(\theta) = \bar{I}(o) \cos^n\theta$ found from $\log I(\bar{\theta})$ - log $\cos\bar{\theta}$ plots and the χ^2 - n method. The measurements are consistent with a constant value of $n = 8.4 \pm 0.3$ over the size range 5.10^4 - $1.4.10^6$ particles

3.2.3 CONCLUSION

Using the expression $I(\theta) = I(o) \cos^{n}\theta$ to fit the measured zenith angle distribution of EAS it is found that over the size range 5.10^4 to $1.4.10^6$ the measurements are consistent with a constant value of $n = 8.4 \pm 0.3$ For the smallest size range studied (10^4 - 5.10^4) the present results suggest a smaller value of $n = 5.3 \pm 0.8$

CHAPTER 4

DESIGN AND PERFORMANCE OF MORE EFFICIENT PLASTIC SCINTILLATORS FOR USE IN THE EAS ARRAY

4.1 INTRODUCTION

None of the scintillation counters originally used in the EAS array (see Chapter 2) gave a single particle peak due to the passage of the global cosmic ray flux when their outputs were fed into a pulse height analyser. The reason for this is that only relatively few of the scintillation photons produced by the passage of single relativistic charged particles were collected by the photomultipliers observing the phosphor. The result of this was that the position of the single particle peak was lost in the noise of pulses generated by single thermionic electrons leaving the cathodes of the photomultipliers. Accordingly, the average pulse height produced by single particles traversing the phosphor at normal incidence had to be found using a subsidiary cosmic ray telescope. As the detectors in the array are situated outside the physics department building in small weatherproof containers the calibration of the detectors was a time consuming and awkward job to carry out. It was therefore decided to construct detectors with a more efficient light collection efficiency, such that their outputs would show a clearly resolved cosmic ray peak when displayed on a pulse height analyser. The design of detector investigated is shown in Figure 4.1 and subsequently 9 such detectors have been constructed.

4.2 DETERMINING THE RELATIVE SENSITIVITIES OF PHOTOMULTIPLIERS

If the output from a single photomultiplier shown in Figure 4.1 is displayed on a pulse height analyser (PHA) then a clearly resolved peak on the PHA is not observed. However, if both photomultipliers

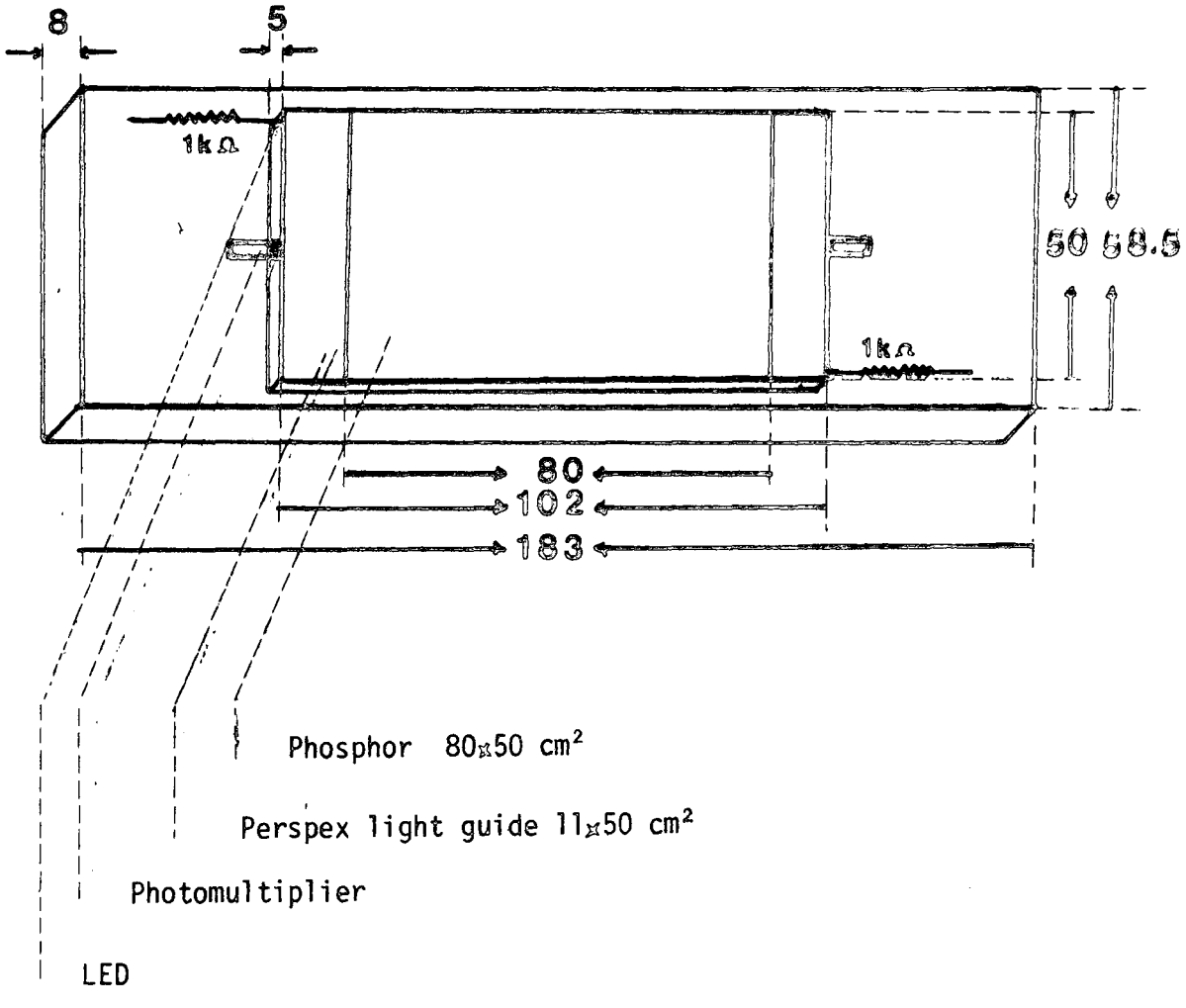

Figure 4.1 : Design of plastic scintillation counter.
All dimensions are in centimetres.

are adjusted to have the same sensitivity and the pulses added then a clearly resolved peak is observed. The problem in constructing such a detector is thus to determine the operating voltages of both photomultipliers such that they have the same sensitivity. This was achieved in a subsidiary experiment using the arrangement shown in Figure 4.2. The variation of output pulse height with applied voltage for a large number of photomultipliers was measured using standard light pulses from a light emitting diode. A typical result is shown in Figure 4.3 and Table 4.1 summarises the results obtained for the relative sensitivities of 18 photomultipliers studied in this way. Table 4.2 shows the pairs of photo tubes that have been used in the 9 scintillation counters that have been constructed. Figure 4.4 shows the values of the resistors used in the Mullard 53 AVP photomultipliers employed.

Some properties of the light emitting diode which was driven with voltage pulses from a pulse generator via a 1K Ω series resistor are shown in Figures 4.5a and 4.5b. Figure 4.5a shows the dependence of photomultiplier output pulse height on the width in microseconds of the driving pulse. Figure 4.5b shows the variation of photomultiplier output pulse height with the voltage applied to the LED for pulses of width 1 μs, 2 μs and 5μs applied to the light emitting diode. In the measurements previously described and shown in Figure 4.3 and Table 4.1 pulses of width 1μs were applied to the light emitting diode.

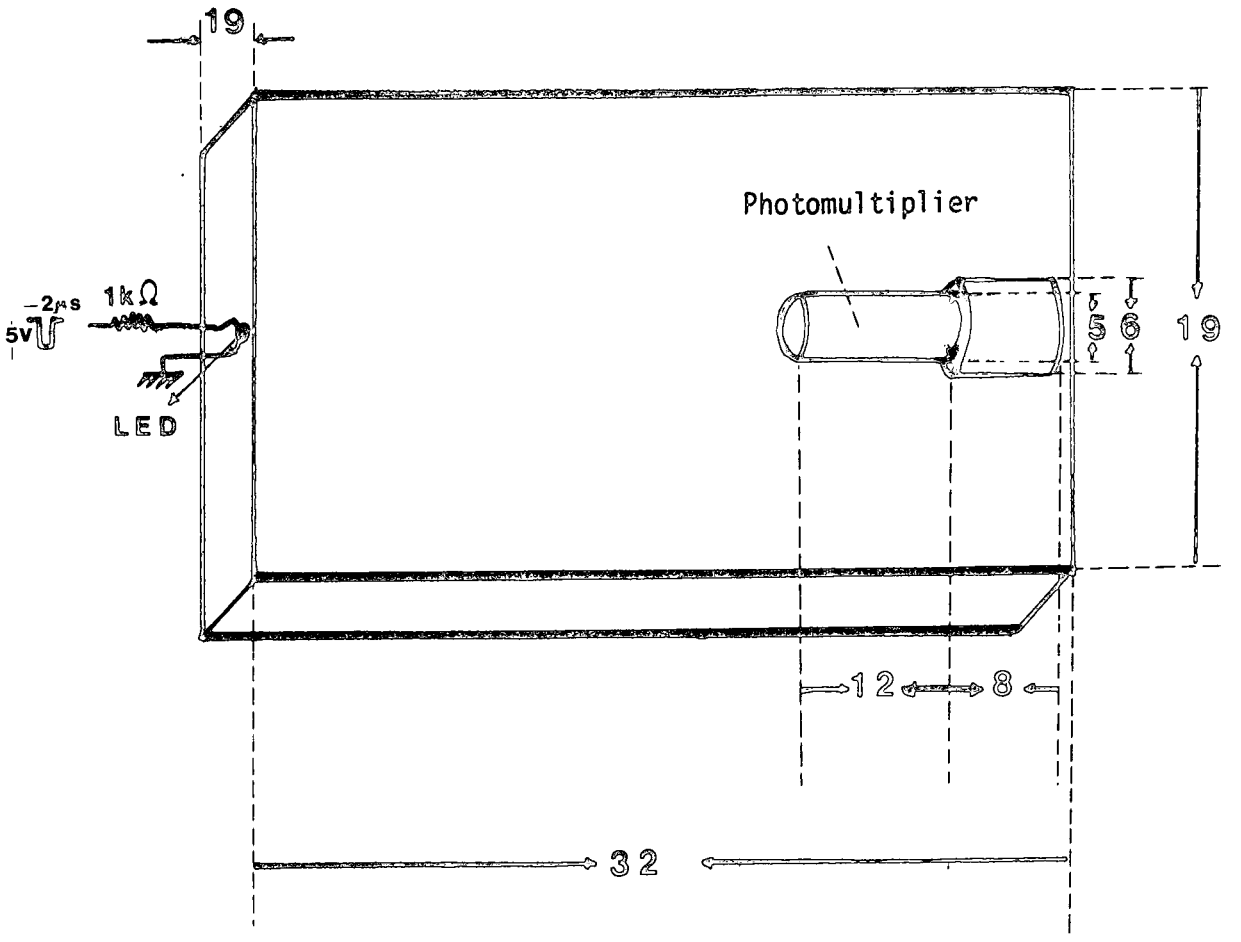

Figure 4.2 : Arrangement used for measuring the relative sensitivities of photomultipliers as a function of the voltage applied to the photomultiplier. All dimensions are in centimetres.

Phototube No.	Equation
1	$v = 3.63 \times 10^{-28} V^{8.49 \pm 0.3}$
2	$v = 2.45 \times 10^{-28} V^{8.3 \pm 0.1}$
3	$v = 9.6 \times 10^{-29} V^{8.37 \pm 0.06}$
4	$v = 5.69 \times 10^{-29} V^{8.4 \pm 0.06}$
5	$v = 1.1 \times 10^{-30} V^{9.07 \pm 0.06}$
6	$v = 5.56 \times 10^{-35} V^{10.34 \pm 0.1}$
7	$v = 5.9 \times 10^{-29} V^{9.0 \pm 0.05}$
8	$v = 5.6 \times 10^{-31} V^{9.27 \pm 0.24}$
9	$v = 5.09 \times 10^{-29} V^{8.76 \pm 0.09}$
10	$v = 1.51 \times 10^{-29} V^{8.73 \pm 0.04}$
11	$v = 1.04 \times 10^{-28} V^{8.4 \pm 0.04}$
12	$v = 1.64 \times 10^{-27} V^{8.7 \pm 0.06}$
13	$v = 8.72 \times 10^{-29} V^{8.48 \pm 0.04}$
14	$v = 10^{-27} V^{8.1 \pm 0.06}$
15	$v = 3.08 \times 10^{-28} V^{8.25 \pm 0.12}$
16	$v = 2.84 \times 10^{-28} V^{8.22 \pm 0.05}$
17	$v = 3.2 \times 10^{-27} V^{8.11 \pm 0.01}$
18	$v = 5.59 \times 10^{-30} V^{8.7 \pm 0.05}$

Table 4.1 : Variation of output pulse height (v in volts) with the EHT voltage (V in volts) applied to a sample of 18 photomultiplier tubes. The same standard light pulse from a pulsed light emitting diode was applied to all the tubes.

Number of scintillation counter	Phototube numbers (see Table 4.1) used
1	6 and 15
2	9 and 5
3	8 and 17
4	13 and 10
5	14 and 3
6	1 and 4
7	11 and 2
8	18 and 16
9	7 and 12

Table 4.2 : The pairs of phototubes that have been used in the 9 scintillation counters that have been constructed.

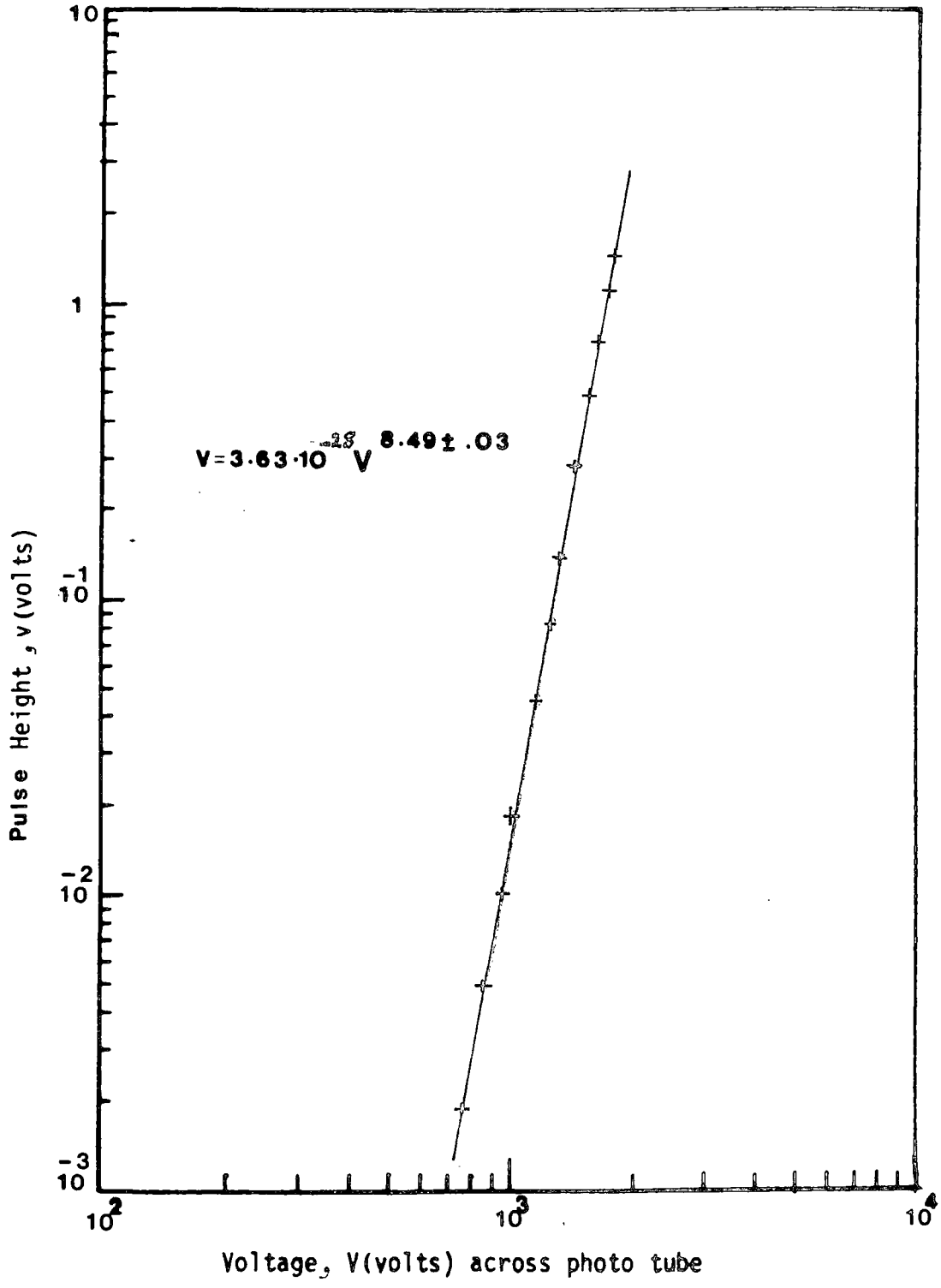

Figure 4.3 : Variation of output pulse height with applied EHT voltage for phototube number 1. Standard light pulses from a light emitting diode were applied to the tube.

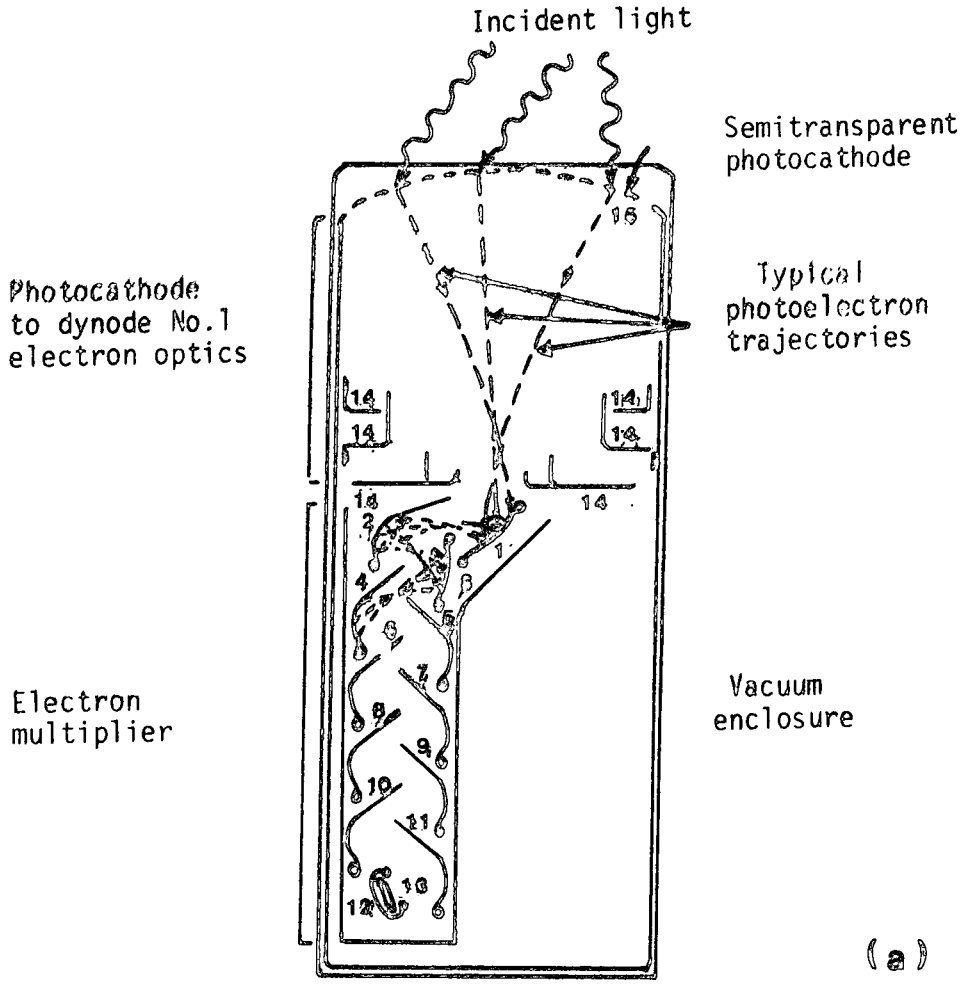

Figure 4.4a : Basic elements of a photomultiplier tube

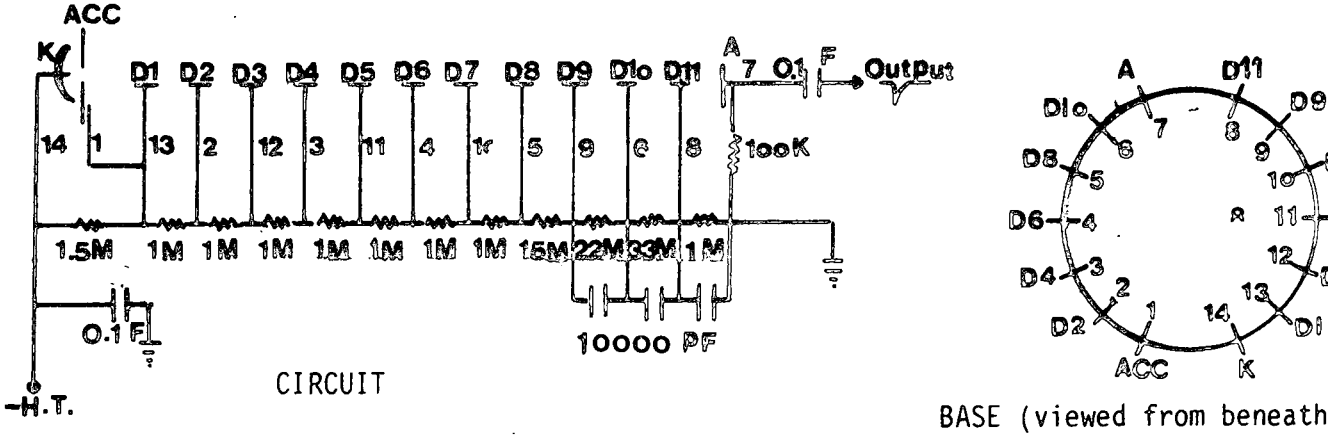

Figure 4.4b : Base circuit for Philips 53AVP photomultiplier

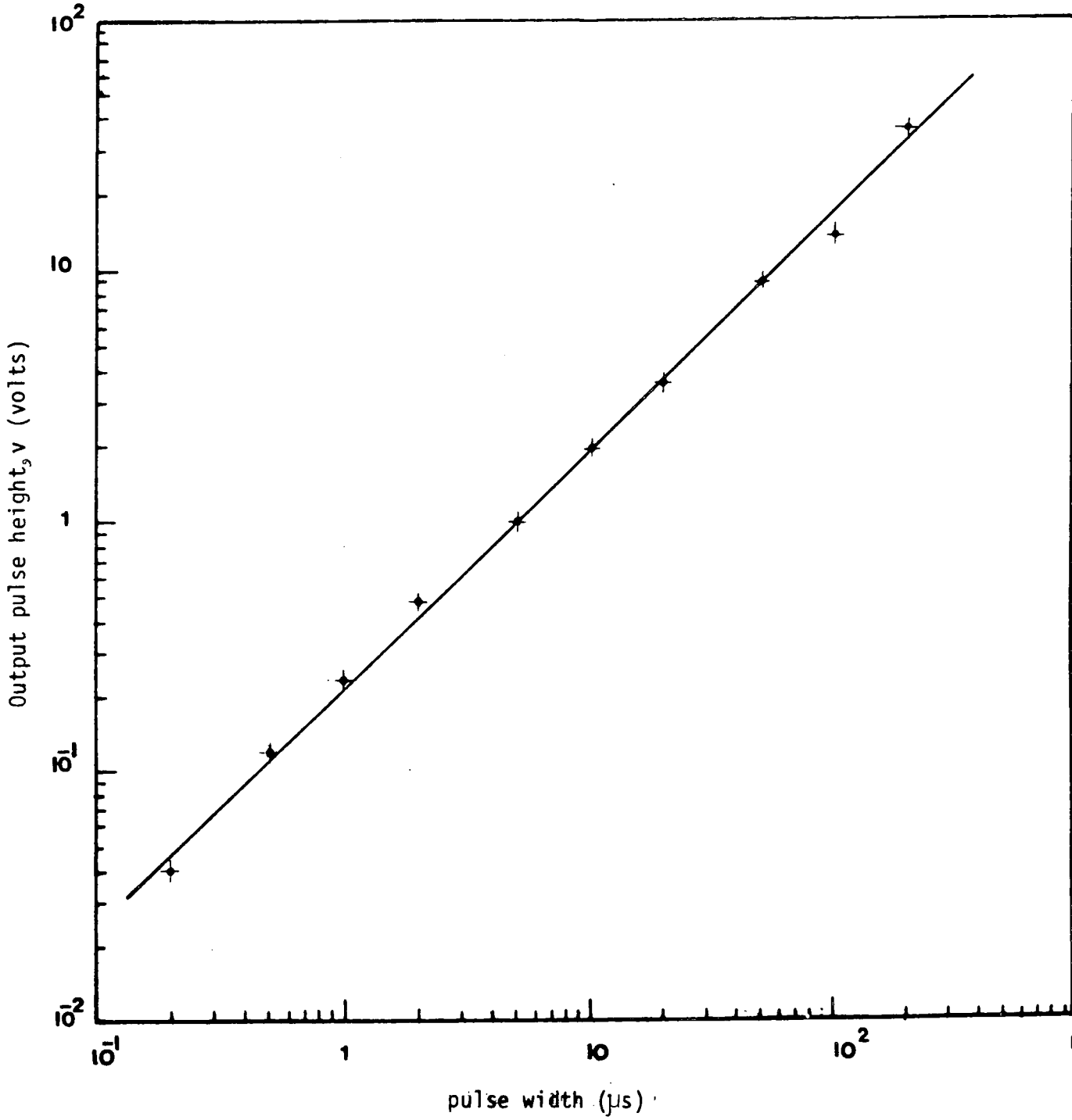

Figure 4.5a : Dependence of photo tube output pulse height v on the width T of the voltage pulse applied to the light emitting diode. The phototube EHT was held constant at -1.5kv. The measurements are fitted by $v = 22\ T^{0.97}$ with v in volts and T in μs.

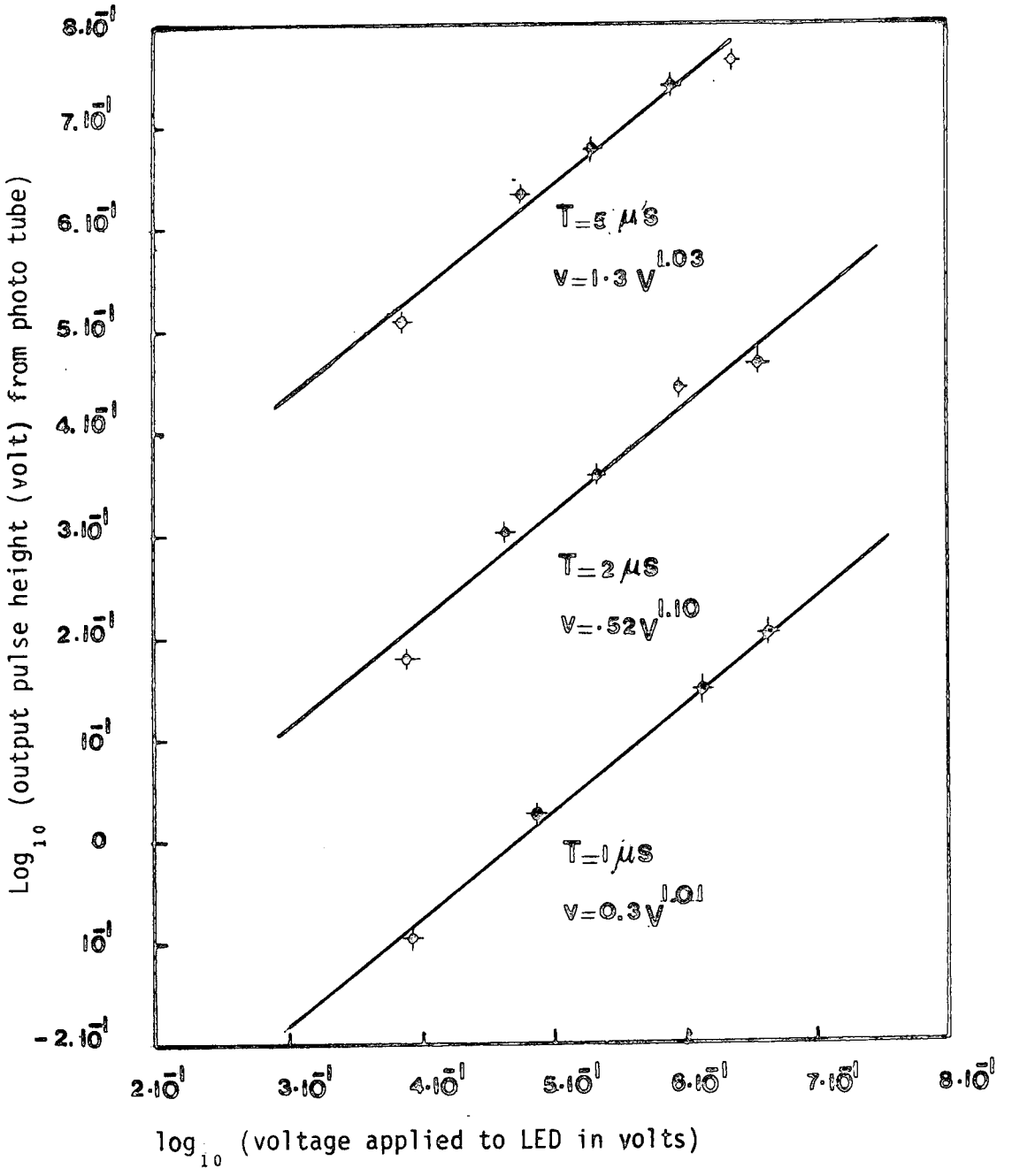

Figure 4.5b : Variation of output pulse height v from phototube with voltage V applied to the light emitting diode for different pulse widths, T. The data is represented by the expressions indicated with both v and V in volts. The phototube EHT was fixed at -1.5kv.

4.3 SUPPLYING THE PHOTOMULTIPLIER OPERATING VOLTAGES AND THE COUNTER HEAD UNITS

The correct operating voltage for each photomultiplier was obtained using a distribution box as shown in Figure 4.6, the main E.H.T power supply being set at -2.0 KV. The head unit used with each counter was a simple emitter follower, the circuit diagram being shown in Figure 4.7. The outputs from the two photomultipliers (see Figure 4.4b) were connected to the same emitter follower input using short lengths of coaxial cable so that the arrangement acted both as a charge pulse adder and a device with a low output impedence for driving the resulting pulse to the main electronics.

To test the performance of the photomultipliers when glued in position in a counter, two matched light emitting diodes were mounted close to one side of the light guide at either end of the counter (see Figure 4.1). Figure 4.8 shows the variation of photo-tube output pulse height with EHT when the two photomultiplier tubes in a counter were individually excited with matched light pulses from the LED situated on the opposite side of the phosphor to them.

4.4 CALIBRATION OF THE PULSE HEIGHT ANALYSER AND ITS USE TO STUDY THE COUNTER RESPONSE TO THE GLOBAL COSMIC RAY FLUX

Using the pulse height analyser (PHA) 1 μs wide pulses from a pulse generator were applied at its input and the relation between input pulses height and the channel number in which the pulses were recorded was measured. This was done for different available values for the gain of the internal PHA amplifier and the result is shown in Figure 4.9. Also the relationship between the vertical displacement per channel in terms of the number of pulses injected into a channel was studied and the result is shown in Figure 4.10.

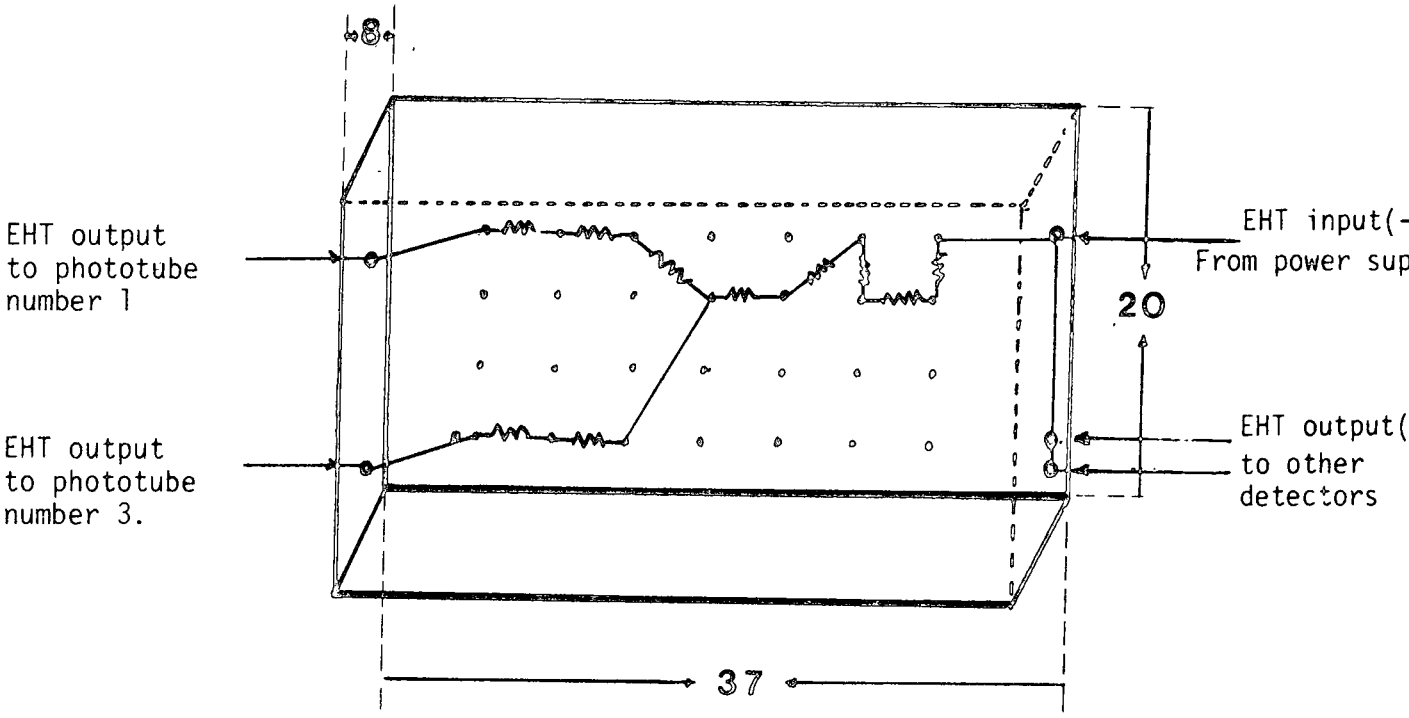

Figure 4.6 : The EHT distribution box used with each scintillation counter. Dimensions indicated are in cemtimetres.

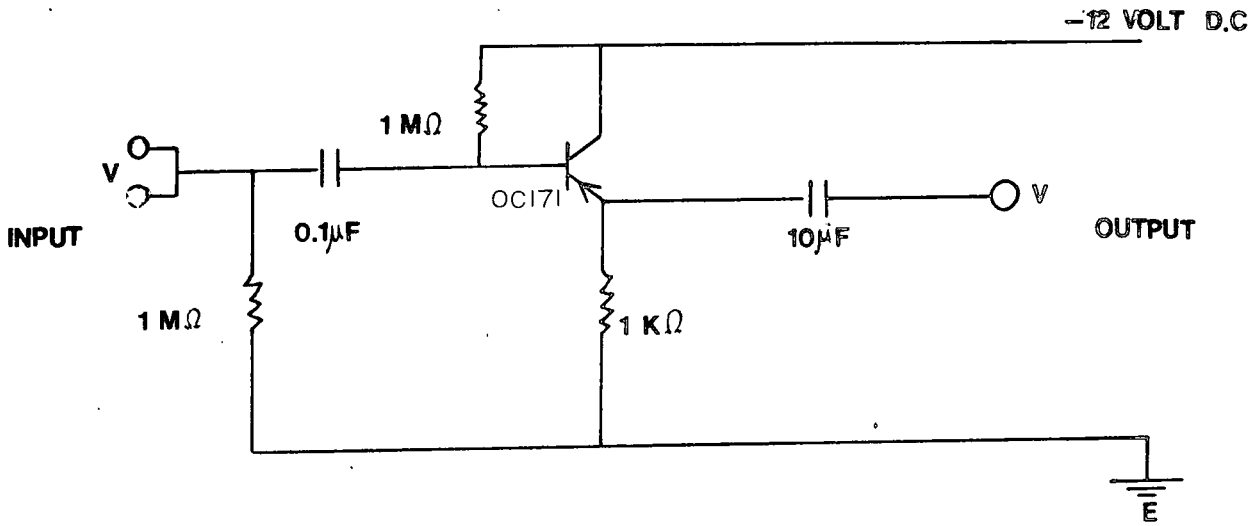

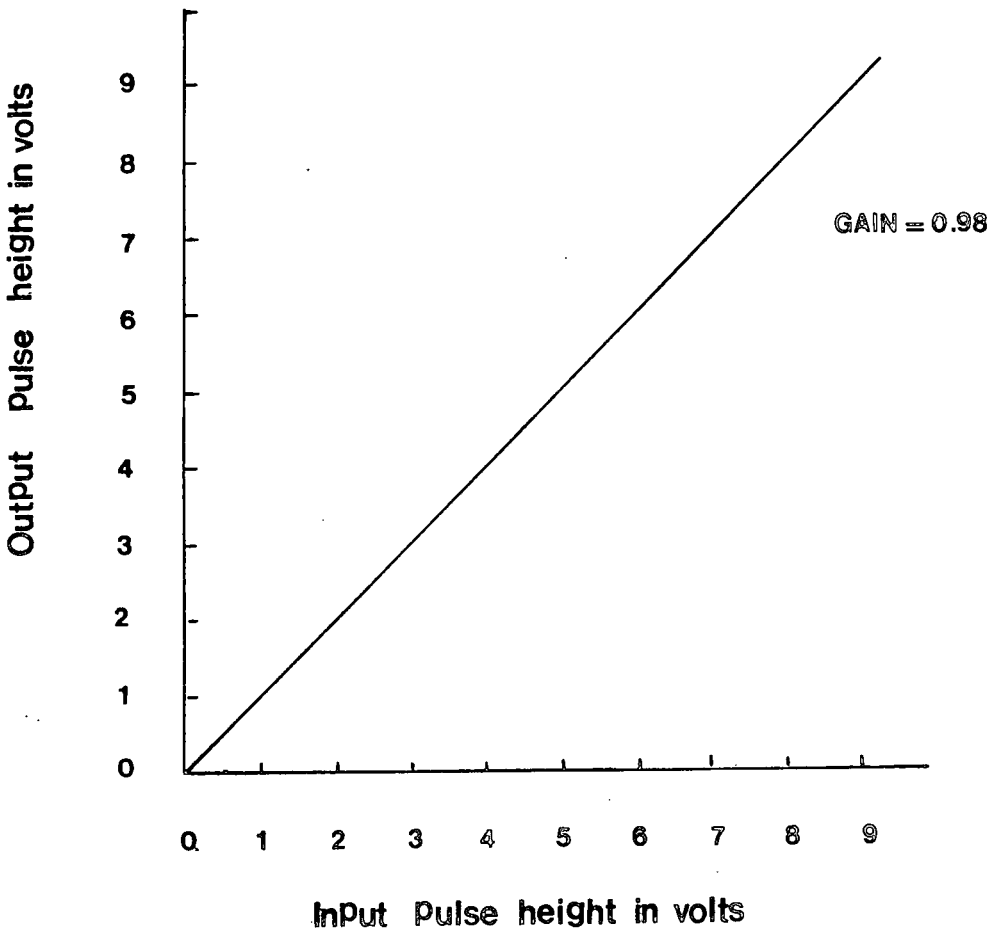

Figure 4.7 : Circuit diagram and response of emitter follower.

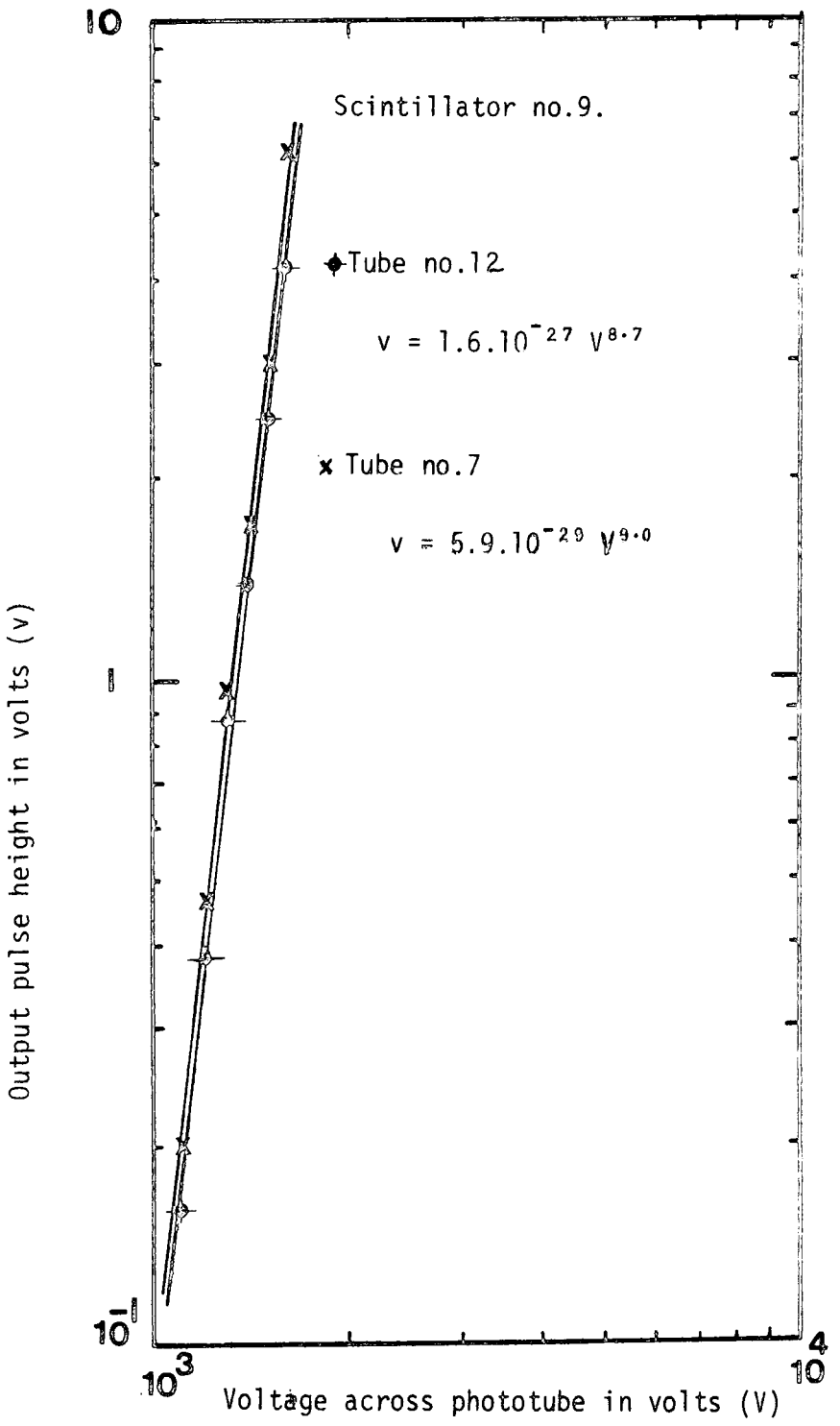

Figure 4.8 : Variation of phototube output pulse height with EHT when the two photomultipliers in a counter were individually excited with matched LED light pulses from the LED situated on the opposite side of the phosphor to them (see figure 4.1). The outputs from the tubes are shown by ⊕ (tube number 12) and x (tube number 7).

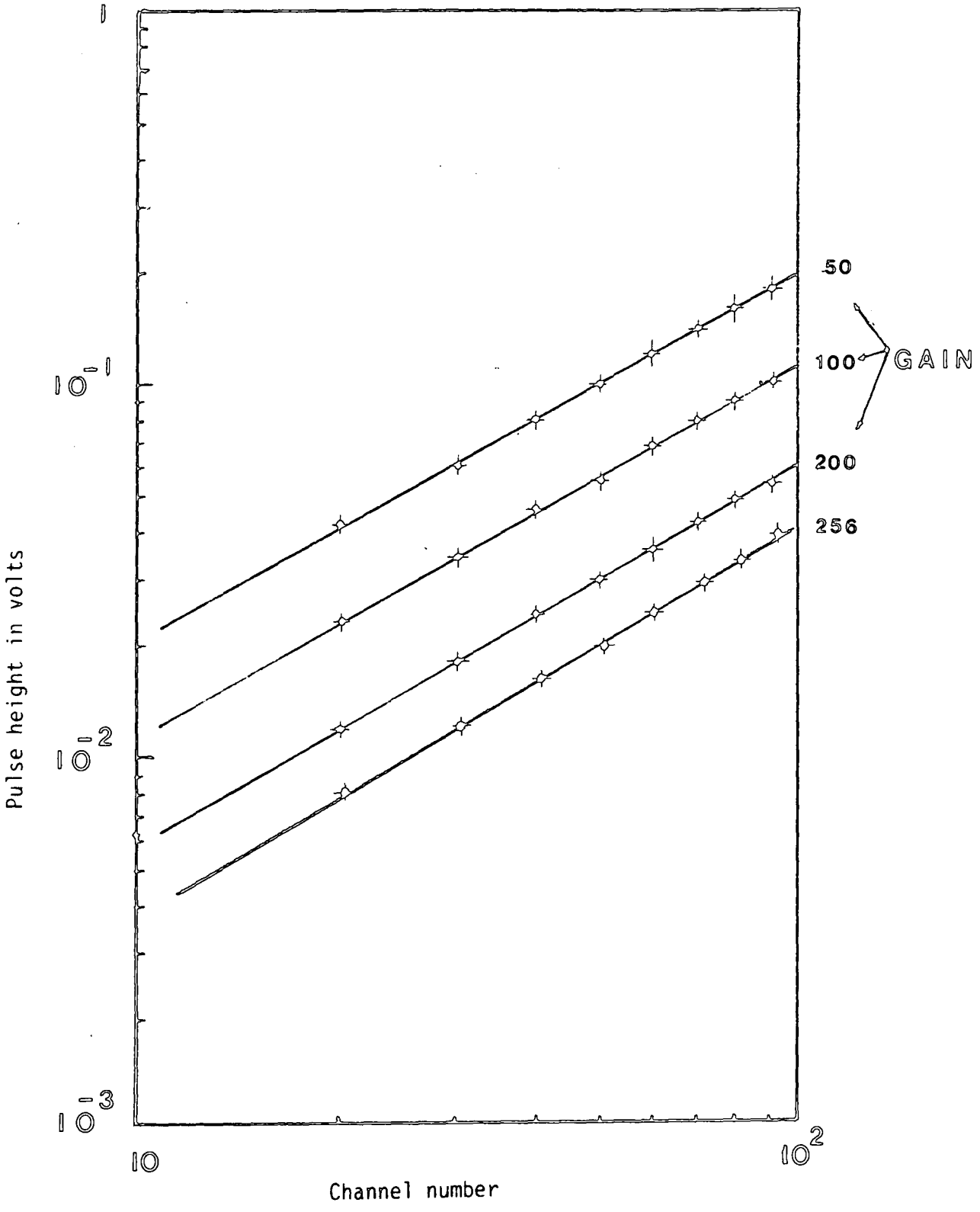

Figure 4.9 : Calibration of the pulse height analyser using 1 μs width input pulses.

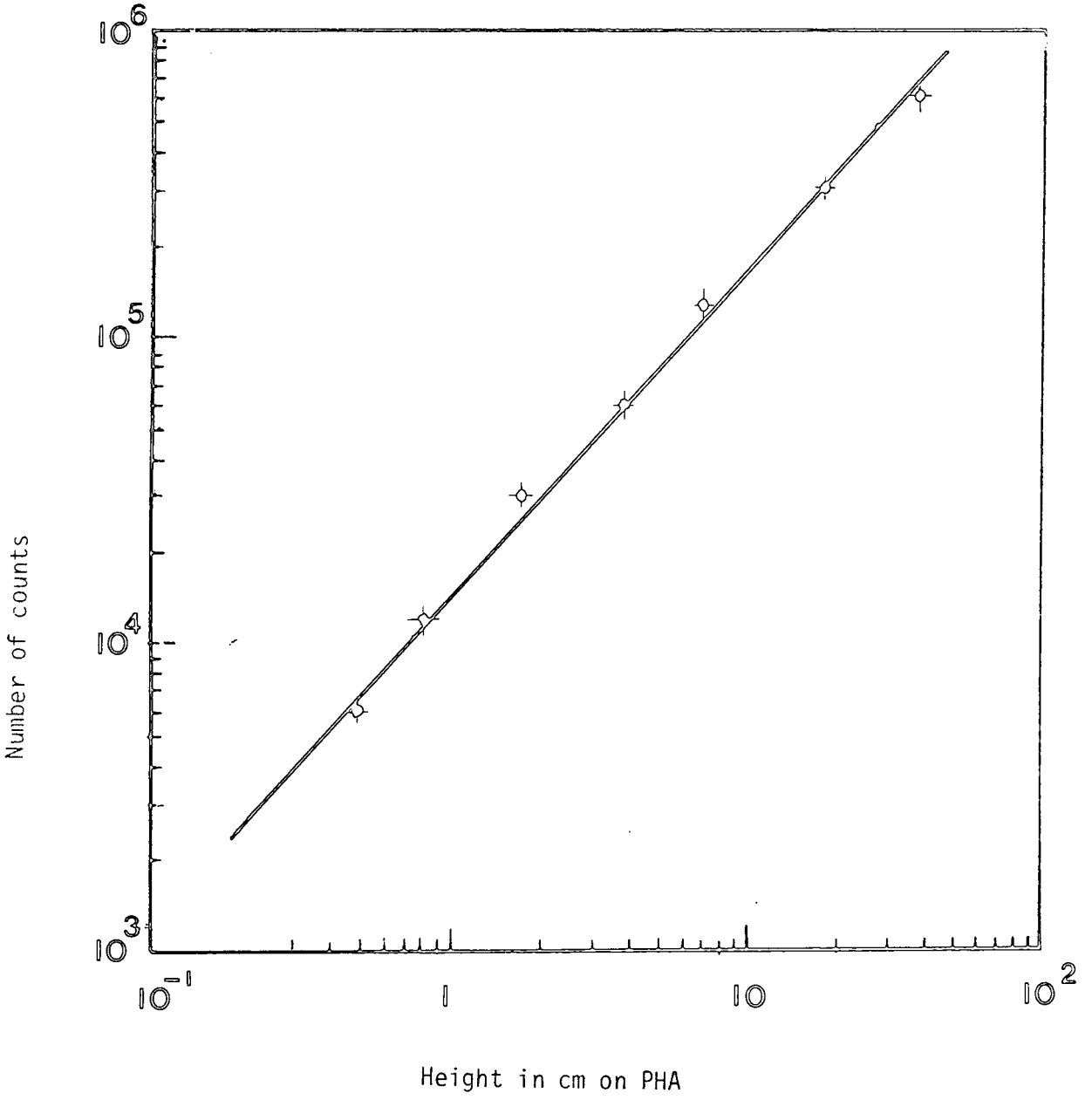

Figure 4.10 : Calibration of the pulse height analyser vertical displacement per channel in terms of the number of pulses injected into that channel.

Figure 4.11 shows the response of scintillator number 9 to the global cosmic ray flux as recorded by the pulse height analyser. It is seen that a well resolved peak due to the passage of single relativistic cosmic ray particles through the counter is observed. Using the calibration data shown in Figures 4.9 and 4.10 the number of counts in a given channel was found and then the rate of pulses of size >V as a function of γ was calculated, the result being shown in Figure 4.12. Figure 4.13 shows the variation of the pulse height of the cosmic ray peak as a function of the EHT voltage applied to the photomultipliers. This observed variation is consistent with the dependence found using LED light pulses to excite the photomultipliers.

4.5 RESPONSE OF THE COUNTER MEASURED WITH AN AMPLIFIER AND DISCRIMINATOR

The pulse height analyser gives detailed information concerning the response of the counter in the region of pulse heights close to the cosmic ray peak. To study the response over a much larger range of pulse heights it is more convenient to use an amplifier and scaler to make the measurements. The results of such a study are shown in Figure 4.14a. The position of the cosmic ray peak can be found by differentiating this curve and the result is indicated by the arrow in the figure. Figure 4.14b is the same as Figure 4.14a except that the units of the abscissa have been changed to equivalent particles per square metre. A comparison of this plot with what is known about the density spectrum of electrons over the range 3 - 100 particles/m^2 shows that the large pulses generated from a single detector are not due to the passage of several electrons but are more likely caused by nuclear interactions of neutrons in the phosphor.

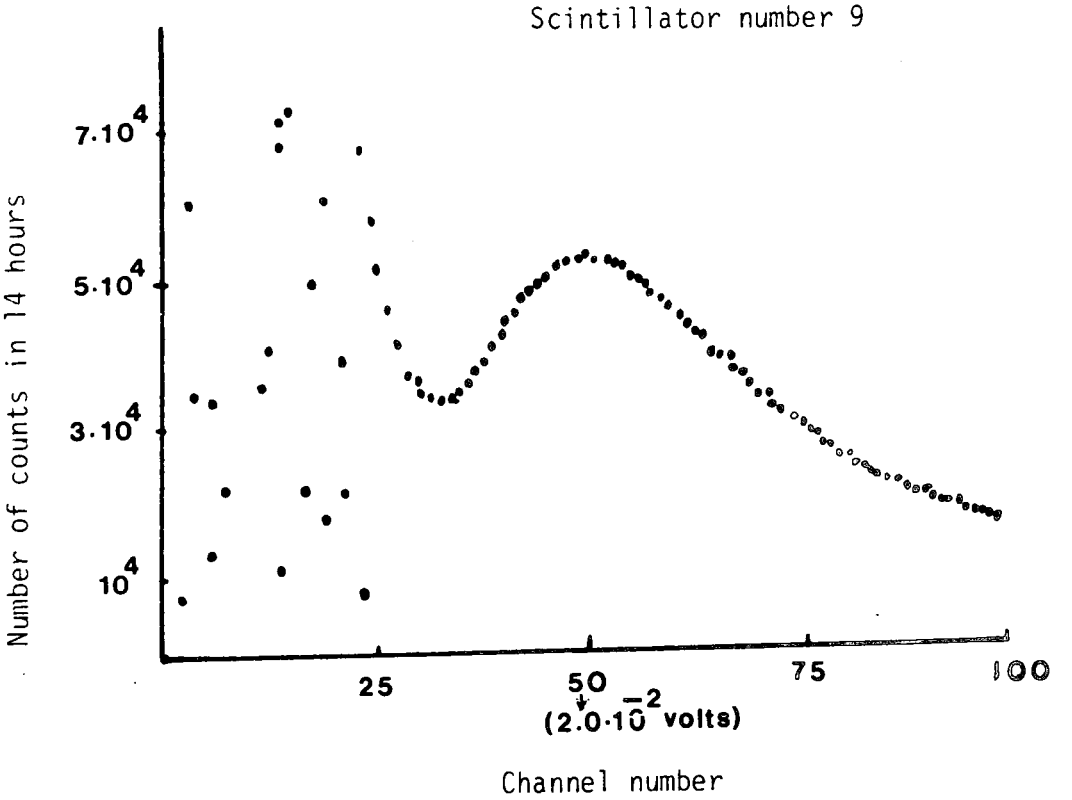

Figure 4.11 : Typical single particle cosmic ray peak as displayed on the pulse height analyser.
Gain=256

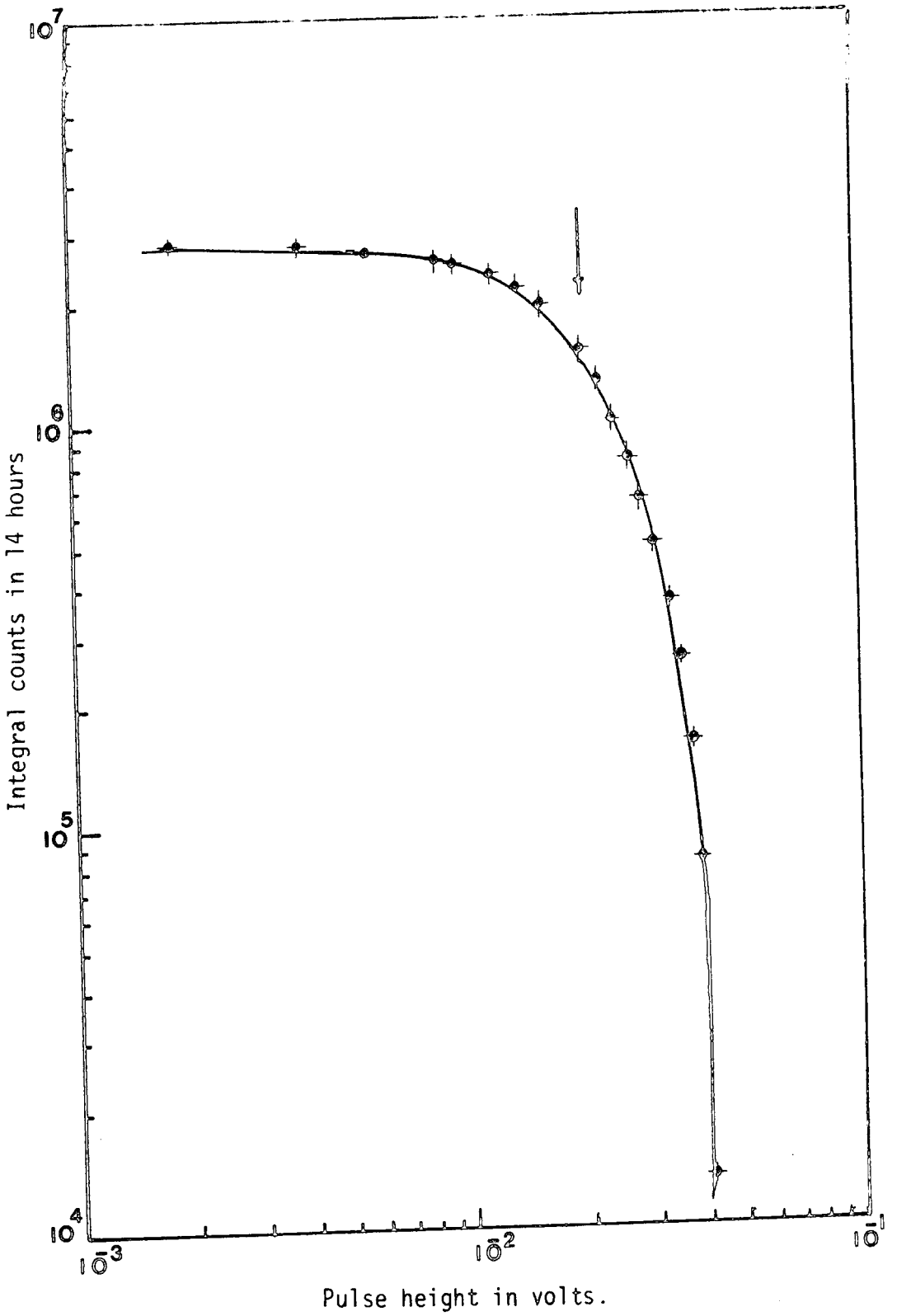

Figure 4.12 : Rate of pulses of height >v versus pulse height v as calculated from the pulse height analyser display shown in figure 4.11. for scintillator number 9. The position of the cosmic ray single particle peak is shown by the arrow.

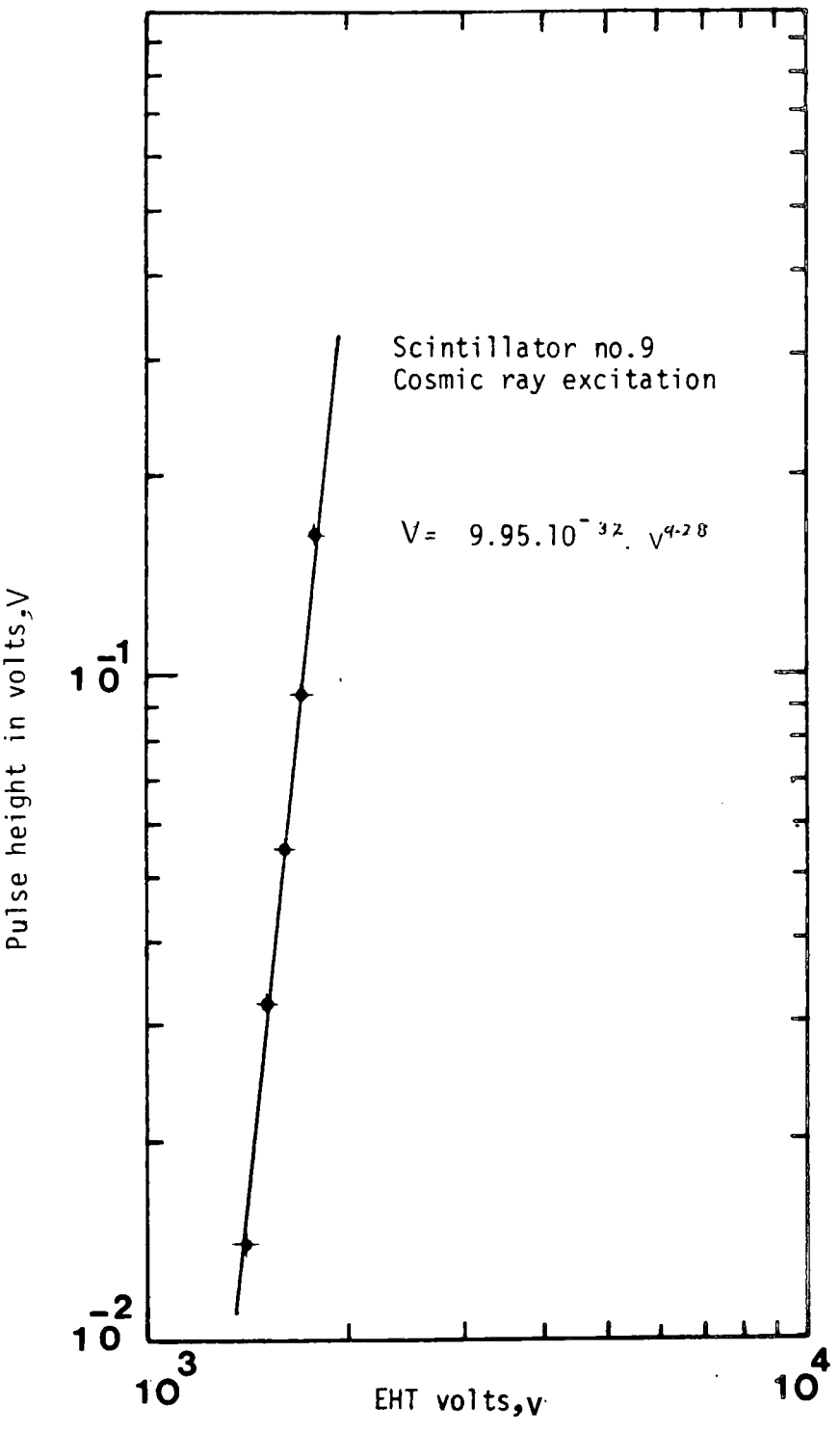

Figure 4.13 : Variation of the peak pulse height produced by the global cosmic ray flux traversing the counter as a function of the voltage applied to the photomultiplier tube. The measurements are fitted by $V = 9.95.10^{-32} . V^{9.28}$ This result is consistent with the results obtained when individual phototubes are excited with light pulses from an LED.

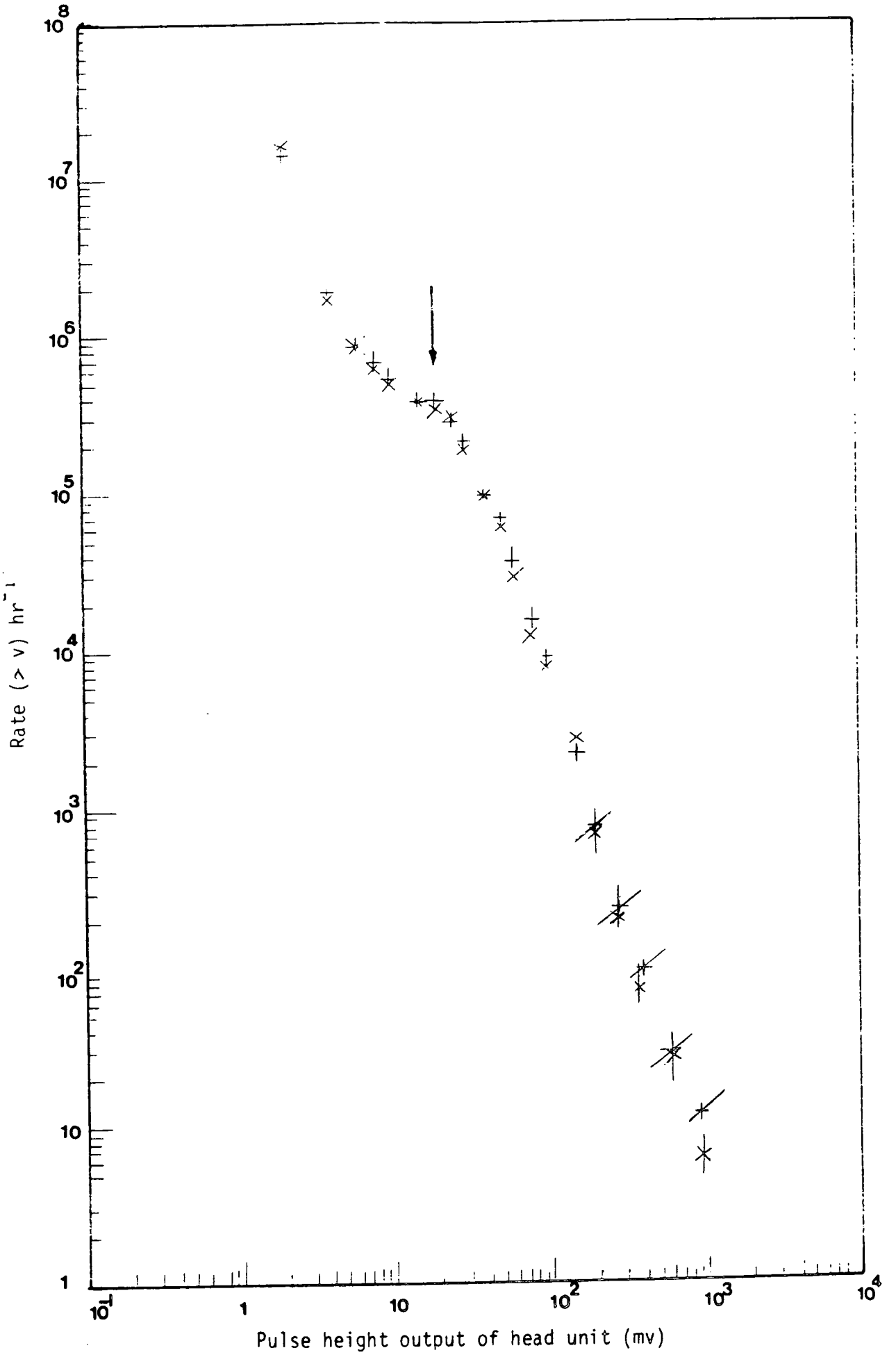

Figure 4.14a. Integral rate of pulses of height > v versus pulse height as measured at the output of the head unit. When the counter is exposed to the global cosmic ray flux the most probable pulse height produced by single relativistic cosmic ray particles traversing the counter is indicated by the arrow.

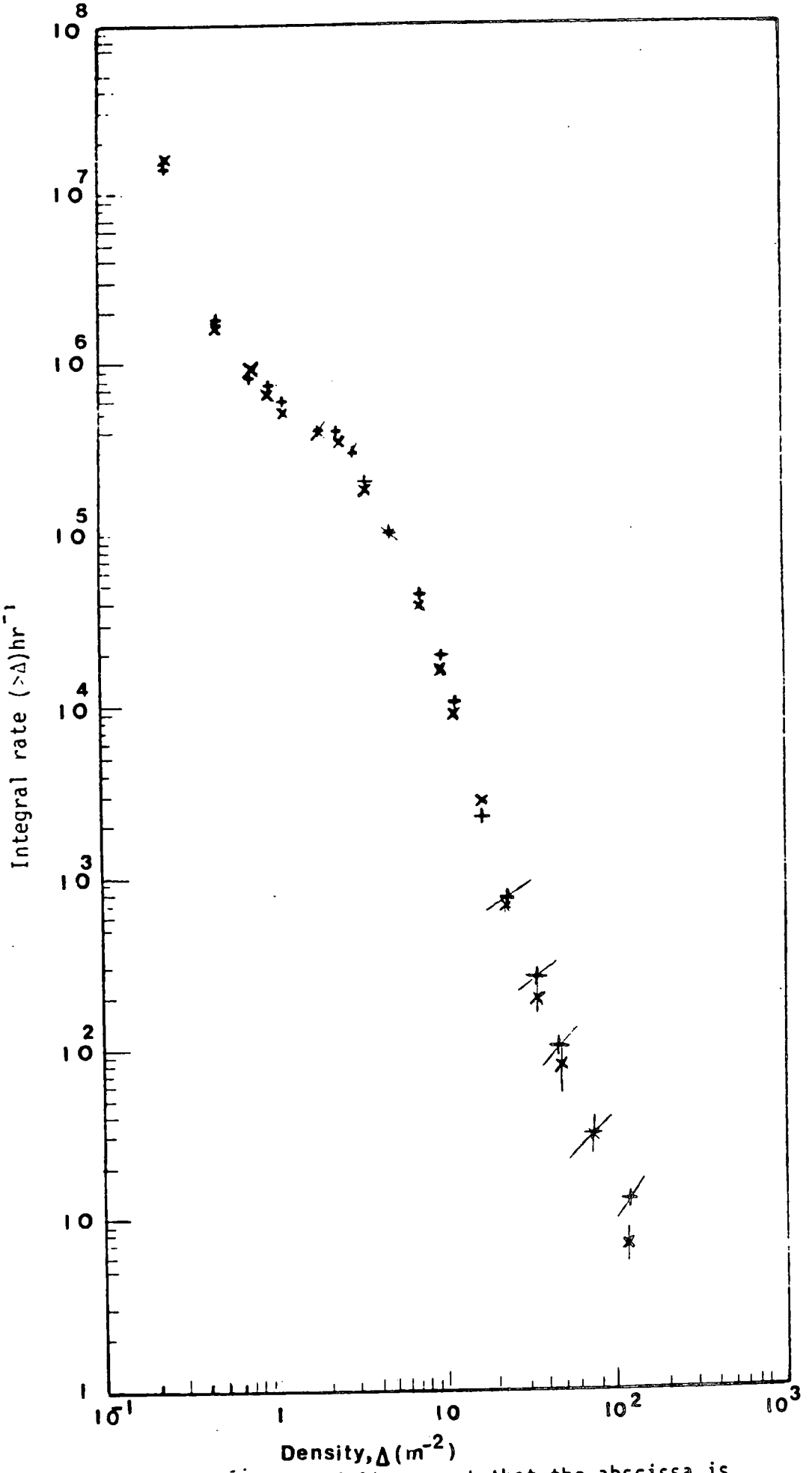

Figure 4.14b : Same as figure 4.14a except that the abscissa is plotted in terms of the apparent density of particles traversing the scintillation which has area $0.4m^2$. Single relativistic particles traversing the scintillator correspond to a density of $2.5m^{-2}$

4.6 DISCUSSION

When used in an experiment as a proportional detector it is useful to be able to determine the average height produced by relativistic particles traversing the phosphor at normal incidence from the measured response to the global cosmic ray flux as it is not always convenient or possible to use a subsidiary narrow angle vertical telescope for calibration purposes.

At sea level the cosmic radiation consists predominantly of muons and electrons, the rate at zenith angle θ, $I(\theta)$ being well represented by $I(\theta) = I(0) \cos^{n}\theta$. For muons $I(0) = 0.8.10^{-2}cm^{-2}$ $sec^{-1}st^{-1}$, $n = 2.1$ and for electrons $I(0) = 0.3.10^{-2}cm^{-2}sec^{-1}st^{-1}$, $n = 3.6$ (Aquilar-Benitez et al. 1982; Greisen, 1942; Pathak et al.1981). For radiation with the above zenith angle distribution the track length distribution $P(\ell)d\ell$ in traversing a thin phosphor of vertical thickness Z can be found by noting that $P(\ell)d\ell = P(\theta)d\theta$ where $\ell = Z/\cos\theta$. For a detector of area A with an "on time" t the number of cosmic rays traversing it with zenith angle in the range θ to $\theta + d\theta$ is given by $N(\theta)d\theta = I(0) \cos^{n}\theta .A \cos\theta. 2\pi \sin\theta d\theta.t.$ which is proportional to $\cos^{n+1}\theta.\sin\theta d\theta$. Thus the probability of a particle traversing the phosphor with θ in the range θ to $\theta + d\theta$ is given by $P(\theta)d\theta = B \cos^{n+1}\theta.\sin\theta d\theta = (n+2) \cos^{n+1}\theta.\sin\theta d\theta$ where B is found using $B \int_0^1 \cos^{n+1}\theta d(\cos\theta)=1$. Thus the probability that a cosmic ray particle has a track length in the phosphor in the range ℓ to $\ell + d\ell$ is given by $P(\ell)d\ell = -(n+2) \cos^{n+1}\theta d(\cos\theta)$ where $\ell = Z/\cos\theta$.

$$= -(n+2)\left(\frac{Z}{\ell}\right)^{n+1}.\left(-\frac{Z.d\ell}{\ell^2}\right) = (n+2)\cdot\frac{Z^{n+2}}{\ell^{n+3}}.d\ell$$

For a counter of uniform response over its area and with an output pulse height directly proportional to particle track length (i.e. sufficient light produced along the track that fluctuations in the average number of photons collected by and photoelectrons produced by the photomultiplier photocathodes is negligible) then the expected output pulse height distribution is $N(v)dv = c/v^{n+3} dv$ for $v > vo$ where vo is the pulse height produced by particles traversing the counter at normal incidence. It is seen from Figure 4.11 that the response of the present counter is not precisely of this form even after subtracting off the contribution of thermal electrons in the channels at the left hand side of the peak. Different processes that convert the expected distribution to the observed distribution are Landau ionisation loss fluctuations that are reflected in the number of scintillation photons that arrive at the photomultiplier photocathodes, fluctuations in the number of photoelectrons produced and the non uniformity of response of the phosphor over its area.

For a perfect counter the expected most probable value of the observed distribution corresponds to particles traversing the counter at normal incidence. The effect of photon fluctuations is to broaden this distribution but the most probable value of the observed distribution (Figure 4.11) is expected to correspond closely to the average pulse height produced by cosmic ray particles traversing the phosphor at normal incidence. Thus this latter quantity can be determined from the response of the detector to the global cosmic ray flux without resorting to the use of a narrow angle vertical calibration telescope. The relative height of voltage pulses produced by muons traversing the phosphor (which produce scintillation light) compared to muons traversing the perspex light guide (which produce Cerenkov radiation) can be estimated by calculating the number of primary photons produced

by each process which are detected by photomultipliers with a typical Cs-Sb photocathode response. Assume relativistic charge e particles lose 2 Mev/g cm^{-2} and that on the average an energy loss of 212 ev is required to produce a scintillation photon (Ashton et al. 1965) **then** the number of scintillation photons produced by a particle traversing the phosphor at normal incidence is $\frac{2.10^6.5}{212} = 4.7\times10^4$. For the same thickness of perspex the comparable number of Cerenkov photons produced is 1.3×10^3 (Jelley, 1958, p. 279). Thus the ratio of the number of produced scintillation photons to Cerenkov photons is 36/1. Allowing for the absorption of scintillation light in the phosphor (estimated to be a factor of 2.2 at the worst position of particle passage) and assuming that the fraction of produced photons that arrive at a photocathode is the area of the photocathode divided by the cross sectional area of the light guide to which the photomultiplier is attached for both scintillation and Cerenkov light, then the ratio of the number of produced photons that are collected is estimated to be $36/2.2:1 \simeq 16/1$. Thus on the average, pulses produced by Cerenkov radiation in the perspex light guides of the present detector are estimated to be at least sixteen times smaller than pulses produced by particles traversing the phosphor.

4.7 CONCLUSION

A plastic scintillation counter detector of area $0.4m^2$ and 5 cm thick that is suitable for making electron density samples in extensive air showers has been developed, The counter is relatively light and can be transported from place to place by **two** people. In all, 9 such counters have been constructed and eventually it is intended to use them in the EAS array described in Chapter 2. In the present work 2 of the counters have been used to obtain a local electron density EAS trigger and this work is described in Chapter 6.

CHAPTER 5

TACHYON THEORY AND PREVIOUS TACHYON SEARCHES

5.1 INTRODUCTION

In recent years, there has been some discussion of particles (tachyons) that move with velocities greater than the speed of light, particularly in relation to the special theory of relativity. The first point in any account of tachyon theory is that of its acceptability in the framework of relativity. Since the publication in 1905 of Einstein's original paper, objections to superluminal particles have been based on the fact that particles cannot be accelerated to velocities greater than c, the velocity of the light in a vacuum $c = 3 \times 10^8$ m Sec^{-1}. However, several workers have investigated the possibility that the velocity of light does not represent a barrier but a limit approachable from below and above. Bilaniuk and Sudarshan (1962) point out that, although the theory disallowed acceleration of subluminal particles to superluminal velocities, in principle it permits the existence of particles that have velocities always greater than the velocity of light. Such particles would seepd up as they lose energy and would never be observed with velocity equal to or less than c. More recently, Feinberg (1967) has proposed a quantum field theory of non interacting, spinless, faster than light particles. Many experiments were carried out to detect such particles not only through their ionization in conventional particle detectors, but also through their production of Cerenkov radiation in vacuum.

The existence of superluminal velocities would therefore introduce a new class of particle to physics in addition to "normal" subluminal particles and luminal particles, e.g. photons and neutrinos. Particles of these groups can only exist in their respective domains.

5 .2 THE SPECIAL THEORY OF RELATIVITY

The special theory of relativity is founded on two distinct postulates:

(i) Any law of physics which holds in one coordinate system also holds in identical form in any other coordinate system moving uniformly with respect to the first and (ii) the velocity of electromagnetic radiation is independent of the velocity of the source.

The basic relations between energy, momentum and speed that must be satisfied by any object obeying the special theory of relativity is given by the following equations:

$$E = \frac{mo c^2}{\sqrt{(1 - \frac{v^2}{c^2})}} = \gamma mo c^2 \qquad 5.1$$

$$|P| = \frac{mo v}{\sqrt{(1 - \frac{v^2}{c^2})}} = \gamma mo v \qquad 5.2$$

where $\beta = \frac{v}{c}$, $\gamma = (1 - \frac{v^2}{c^2})^{-\frac{1}{2}}$ and mo is the rest mass.

For v less than c as γ is real and positive the energy would be real and it also holds for v equal to c, provided mo is set to zero which is shown to be true by the existence of photons and neutrinos. It is obvious from the equations 5.1 and 5.2 that the energy and momentum of such a particle becomes infinite when its velocity approaches the velocity of light, $v \to c$. Since the energy must be supplied by whatever is accelerating the particle, an infinite source of energy would be needed to speed up a particle to the speed of light from any lower speed. Surely no such infinite energy source is available, and so it is impossible to make a particle go from less than c to $\geq c$.

5.3 THE TACHYON AND ITS BASIC PROPERTIES

As mentioned before there is no possibility to accelerate a particle to go from less than c to $\geq$ c, but it doesn't mean that particles that always travel faster than light do not exist (called tachyons). Tachyons avoid the need for being accelerated through the light barrier with the attendant expenditure of infinite energy. For tachyons $\frac{v}{c} = \beta > 1$ and in order for the energy E to be given by a real number, because $\sqrt{1 - \frac{v^2}{c^2}}$ becomes negative, the expression for proper mass m_0 must be imaginary; so it is expressed as some real number μ_0 times the square root of minus one, $m_0 = \sqrt{-1}\mu_0$. Thus equation 5.1 and 5.2 would be rewritten as follows

$$E = \frac{\mu_0 c^2}{\sqrt{(\frac{v^2}{c^2} - 1)}} \qquad 5.3$$

$$P = \frac{\mu_0 v}{\sqrt{(\frac{v^2}{c^2} - 1)}} \qquad 5.4$$

To deal with the imaginary mass, it is noted that the quantity m, or the rest mass, that appears in equations 5.1, 5.2 is not a directly measurable quantity, unless the particle can be brought to rest. We are therefore free to hypothesize a particle for which $v > c$ always, and m is an imaginary quantity.

From the energy and momentum equations, one can write

$$c^2p^2 - E^2 = \mu_0^2 c^4 \qquad 5.5$$

and the range of the energy and momentum are given by

$$0 \leq E \leq \infty \ , \ \mu_0 c \leq p \leq \infty \qquad 5.6$$

Also these equations imply that both the energy and momentum are monotonic decreasing junctions of the velocity, so that tachyons would speed up as they lose energy. A tachyon with $v \to \infty$ carries no energy, $E \to 0$ and $p \to \mu_0 c$ but with reference to the usual velocity transformation law tachyons with infinite speed in one frame have almost a finite velocity in another frame and in both frames the velocity is greater than the velocity of light

Figure 5.1 shows the solutions of the energy momentum vector ($E^2 = P^2c^2 + m_0^2 c^4$) in E - P space. The upper branch only describes the particles with $v < c$ (known as bradyons) and v_x is given by $v_x = \frac{dE}{dp_x}$ It is noted that the velocity of bradyons never reaches c even when the energy is very large.

For the particles with $m_0 = o$ (luxons) there are straight lines above the X axis, which shows that everywhere on this line the velocity is c

The left and right branches, above the X - axis for particles with $v > c$ describe tachyons and show that their existence would complete the symmetry of the solutions.

The branches below the X-axis (of all three types) can be associated with anti-particles which have "negative energy".

5.4 CAUSALITY AND THE REINTERPRETATION PRINCIPLE

The existence of tachyons with $v > c$ leads to a number of different problems. The first is that tachyons cannot be reduced in velocity to $v < c$ since an infinite amount of energy would be required to traverse the light barrier. The second is that the sign of the energy can be changed by an ordinary Lorentz transformation. Hence, a particle which is seen by one observer to have positive energy will have negative energy to another observer.

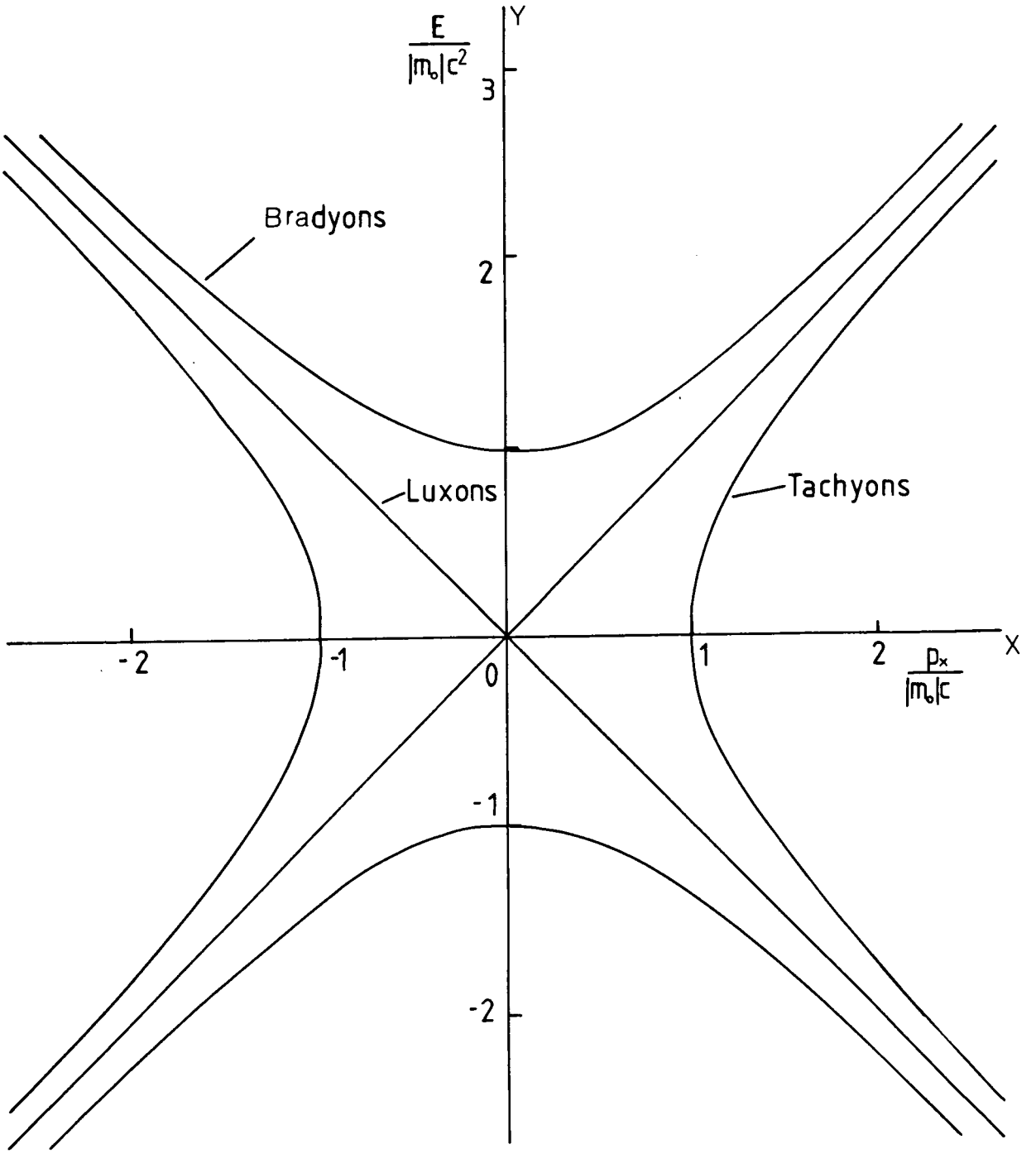

FIGURE 5.1 : Plot of the energy-momentum vector invariant, showing the solutions for particles in each of the three velocity domains

Before any further discussion, consider the Minkowski-time-space diagram, in one dimension, figures 5.2a, 5.2b.

Suppose a reference frame A is moving with uniform velocity parameter β in the x-direction with respect to a reference frame B, then

$$\begin{aligned} x' &= \gamma(x - \beta ct) \\ y' &= y \\ z' &= z \\ t' &= \gamma\left(t - \beta x/c\right) \end{aligned} \qquad 5.7$$

(x', y', z', t') is the four-vector of an event as measured in A, (x, y, z, t) is the four-vector of the same event measured from the same origin in B. Figure 5.2a shows the x,t axes of reference frame A are rotated into the positive quadrant of reference frame B by θ degrees where $\theta = \tan^{-1}(\beta)$,

If two events in reference frame A have (x_1', t_1') and (x_2', t_2'), and all quantities in reference from B are similarly represented by unprimed parameters then we have

$$t_2 - t_1 = (t_2' - t_1')\gamma \qquad 5.8$$

$$x_2 - x_1 = (x_2' - x_1')\gamma \qquad 5.9$$

For $\beta < 1$, equation 5.8 implies that the time interval in a moving reference frame is always smaller than in a stationary reference frame. This phenomenon is called "time dilation"

Similarly equation 5.9 implies that the spatial extent in the direction of the moving reference frame is always smaller in the

Minkowski space - time diagram (subluminal)

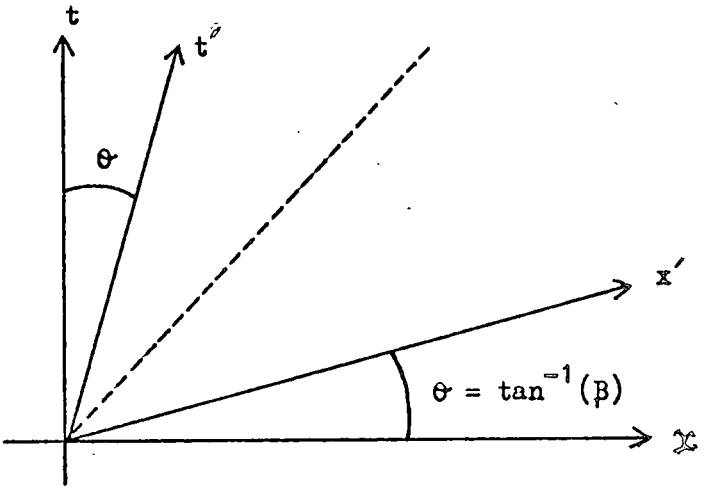

Figure 5.2a

Minkowski space - time diagram (superluminal)

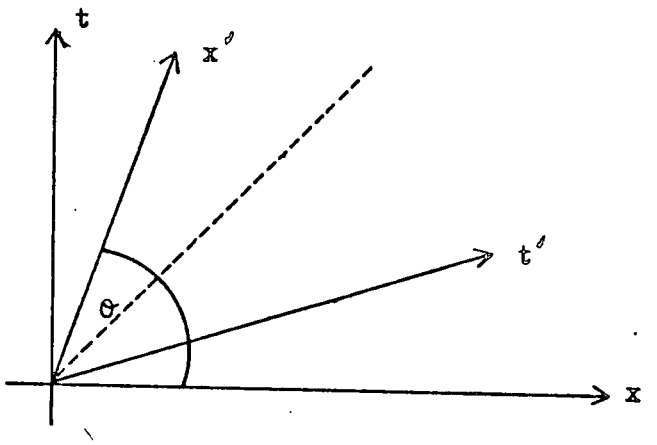

Figure 5.2b

moving reference frame than in a stationary reference frame. This phenomenon is the Lorentz-Fitzgerald Contraction,
It is obvious that no reference frame could travel at the speed of light, $\theta = 45°$ in the Minkowski diagram.

It is possible to replace the four vector (P_x, P_y, P_z, E) in momentum-energy space in place of the four vectors of position-time space and these imply that the expressions for momentum P and energy E in a stationary reference frame of an object moving with velocity parameter β in the direction in which momentum is being measured are:

$$P = \gamma M_o \beta c \qquad 5.10$$

$$E = \gamma M_o c^2 \qquad 5.11$$

where Mo is the rest mass of an object in the reference frame in which the object is stationary. The above synopsis of subluminal special relativity rests on two postulates which were first introduced by Einstein (1905) which were mentioned before.

For superluminal particles Figure 5.2b shows the Minkowski space-time diagram for $\theta > 45°$ which corresponds to a velocity parameter $\beta > 1$ in all reference frames. This suggests that tachyons which travel faster than light are a new class of particles. With the introduction of imaginary mass and considering the case $\beta > 1$ the energy and momentum of a tachyon would be

$$P = \frac{\mu_o \beta c}{\sqrt{\beta^2 - 1}} \quad , \quad E = \frac{\mu_o c^2}{\sqrt{\beta^2 - 1}} \qquad 5.12$$

With consideration of transformation equation 5.7 in momentum-energy space these have the form

$$P_x' = \gamma(P_x - \frac{\beta_1 E}{c}) \quad ; \quad P_y' = P_y$$
$$P_z' = P_z \qquad 5.13$$
$$E' = \gamma(E - \beta_1 P_x c)$$

where E and P are the energy and momentum of a tachyon in its rest frame. β_1 is the velocity parameter in the x-direction which the primed quantities refer to measurements made in.

Since the velocity parameter $\beta = \frac{Pc}{E}$ of tachyons is greater than unity one can always choose β_1 so that the energy of the tachyon is negative which is one of the more serious objections to the existence of tachyons.

The occurrence of negative energy implies the existence of reference frames in which tachyons could be copiously produced, since the system could not be stable against their spontaneous emission.

However, it is useful to cite another objection, as the two are really part of the same problem. When the velocity of an object is greater than c, it is possible to change the sense of the propogation in time by an ordinary Lorentz transformation. Suppose that for one observer, a particle moves through two points x_1, x_2 at times t_1, t_2

$$\frac{\Delta x}{\Delta t} = \frac{x_2 - x_1}{t_2 - t_1} > c \quad \text{and} \quad t_2 - t_1 = \Delta t > 0 \qquad 5.14$$

For the second observer moving along the x direction with velocity parameter β_1 where $\beta_1 = \frac{\Delta x}{\Delta t} \times \frac{1}{c}$ is the velocity parameter of

a tachyon

$$\Delta x' = \gamma(\Delta x - \beta_1 c\Delta t) \; ; \quad \Delta y' = \Delta y \; ; \quad \Delta z' = \Delta z \; ;$$

5.15

$$\Delta t' = \gamma(\Delta t - \beta_1 \frac{\Delta x}{c}) = \gamma . \Delta t.(1- \beta_1\beta)$$

The value for β_1 can be chosen such that $\Delta t'$ is negative when Δt is positive. This implies that we can find reference frames in which the time ordering of events is reversed, which contradicts intuitive notions of causality.

From (5.13) and (5.14) we have

$$\frac{E'}{E} = \frac{t'}{t} = \gamma(1-\beta\beta_1) \qquad 5.16$$

When $\beta_1 \beta > 1$, E' and $\Delta t'$ are negative for positive value of E and Δt. This is, apparently, an untenable state of affairs. Bilanuk and Sudarshan have noted that this time reversal also occurs at the point where the energy becomes negative and they produced a principle which allowed a consistent theory of tachyons to be developed which is known as the reinterpretation principle (R.I.P). The RIP assumes that a negative energy particle which is observed first and later emitted is equivalent to a positive energy particle which is absorbed after emission. It is related to the ideas of Dirac on positrons as electrons going backwards in time. However, the idea of the RIP is similar to the idea of anti-particles and the Stuckelberg-Feynman interpretation of positrons as negative energy electrons running backwards in time (Feynman, 1949).

5.5 THE ENERGY OF A TACHYON

Plotting energy as a function of $\beta(=\frac{v}{c})$ as shown in Figure 5.3 clearly illustrates the following points:

a) As velocities are increased the behaviour of the energy and momentum of particles obey the special theory of relativity. Since the E - β and P - β relationships are asympototic in the region β = 1, a particle moving slower than light, and faster than light can never travel with the speed of light. It means that the speed of light c acts as a limiting speed, which for a tachyon is a lower limit, just as it is an upper limit for ordinary objects.

b) For ordinary particles (bradyons) as their speed increases, their energy also increases. However for tachyons, in contrast both the energy and momentum are monotonic decreasing functions of the velocity. Therefore the minimum energy for a tachyon will be zero when its velocity is infinite but its momentum would remain finite. For an ordinary particle with non zero rest mass the total energy can never vanish. Also from the figure it is concluded that the energy of a tachyon is always less than its momentum multiplied by c. This ambivalence does not apply to ordinary particles.

5.6 PREVIOUS SEARCHES FOR TACHYONS

As far as there is no consensus on the properties of tachyons, the question is how to conduct the search. It is apparent that the most 'reliable' method is to measure time of flight between detectors of known separation as this is fundamental to the particle's definition. More contentious methods are the search for Cerenkov radiation produced by tachyons traversing a vacuum and the observation

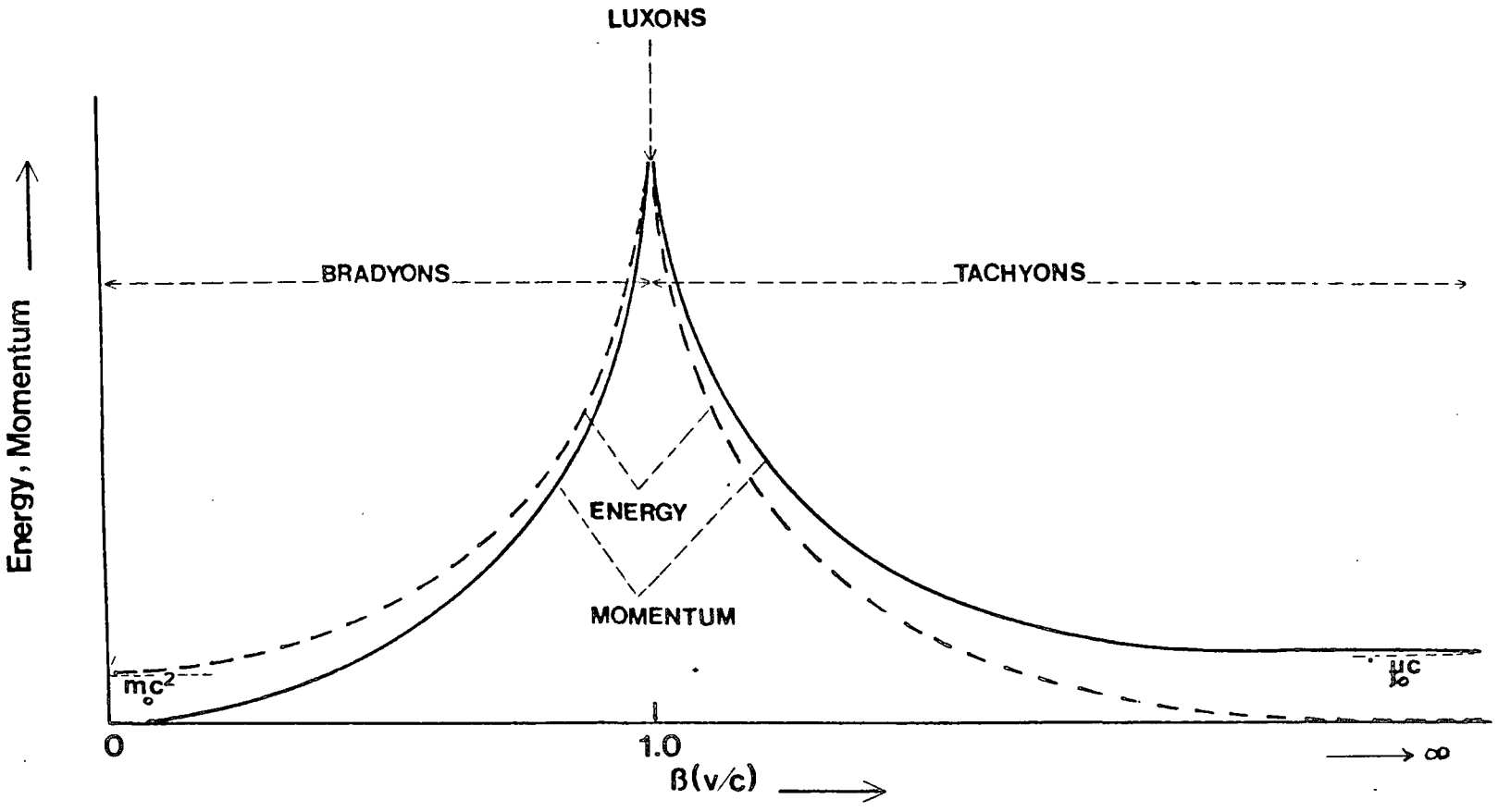

Figure 5.3 : Energy-momentum dependence as a function of velocity $\beta(v/c)$ for three classes of particles, where v is the velocity of the particle and c is the velocity of light.

of particle production in bubble chambers. The most popular method, though, has been to search for tachyons produced by Cosmic ray interactions in the upper atmosphere. In what follows the experiments that have previously been carried out will be briefly reviewed.

A search for Cerenkov radiation emitted by a tachyon traversing a vacuum has been carried out by Alvager and Kreisler (1968). The experiment attempted to detect tachyons travelling through an evacuated chamber in which an electrostatic field of 3kv/cm was maintained. In this experiment tachyons were hoped to be produced by pair production from γ-photons in a cylindrical lead shield surrounding a 5-mci ceasium-134 source. The tachyons would pass into the detector which consisted of two parallel plates between which an electric field was maintained. A photomultiplier was located to view the area between the plates which were in a vacuum of $\sim 10^{-6}$ torr. It was expected that the tachyons would produce a peak in the pulse height spectrum obtained from the photomultiplier. No peak was observed. The authors thus estimated an upper limit to the cross-section for the production of tachyons by 0.8 kev photons in lead as $3.10^{-30} cm^2$.

A similar experiment to that described above but using a 129 mci cobalt 60 source of energy ~ 1.2 Mev and two detection photomultipliers in coincidence was conducted by Davis et al (1969). The result again was negative. Bartlett and Lahara (1972) changed the electric field to a magnetic field on the supposition that a tachyon should act as a magnetic monopole. Again the result was negative and it was found that the upper limit to the cross-section for tachyon production by 1 Mev γ-rays in lead and water were $0.6\ 10^{-36} cm^2$ and $2.10^{-36}\ cm^2$ respectively.

Baltay et al (1970) searched for (neutral) tachyons produced by

negative kaons and anti-protons interacting with protons in a bubble chamber. The reactions searched for were as follows:

$$k^- + p \rightarrow \Lambda^0 + t^0 \rightarrow p + \pi^- + t^0 \qquad \text{I}$$

$$k^- + p \rightarrow \Lambda^0 + t^0 + \bar{t}^0 \rightarrow p + \pi^- + t^0 + \bar{t}^0 \qquad \text{II}$$

$$\bar{p} + p \rightarrow \pi^+ + \pi^- + t^0 \qquad \text{III}$$

$$\bar{p} + p \rightarrow \pi^+ + \pi^- + t^0 + \bar{t}^0 \qquad \text{IV}$$

(t^0 and $\bar{t}^0$ are a neutral tachyon and antitachyon)

In reaction I and III the missing mass technique was used. The four momenta of the charged particles involved in these reactions can be measured. Both the k^- and the $\bar{p}$ were captured at rest in hydrogen. The incoming energy and momentum (zero) were known, the energy and momentum of the resultant ordinary particles (Λ^0, π^- pairs) were measured. The energy E and momentum p of the remaining neutrals can be calculated using energy and momentum conservation. $E^2 - p^2 > 0$ if these neutrals were made up of ordinary particles with velocity less than c.

The presence of a tachyon or tachyon pair would have been indicated by $E^2 - p^2 < 0$ a negative missing mass squared, where $m^2 = E^2 - p^2$. Since the rest mass of a tachyon is imaginary these measurements of missing mass squared would show up as a spike in the frequency histogram of observed missing mass squared. From theoretical considerations (Feinberg 1972) pair production of tachyons seems more likely (reactions II and IV).

Out of 2348 events where the products were produced from

K^- and $\bar{p}$ at rest no events with a negative missing mass squared were found. The resulting production rates are given as:

$$\frac{K^- + p \to \Lambda^0 + t^0}{K^- + p \to \Lambda^0 + \pi^0} \leq 2.10^{-3}$$

$$\frac{K^- + p \to \Lambda^0 + t^0 + \bar{t}^0}{K^- + p \to \Lambda^0 + \pi^0} \leq 2.5 \ 10^{-3}$$

$$\frac{\bar{p} + p \to \pi^+ + \pi^- + t^0}{\bar{p} + p \longrightarrow 3\pi} \leq 2.10^{-3}$$

$$\frac{\bar{p} + p \to \pi^+ + \pi^- + t^0 + \bar{t}^0}{\bar{p} + p \to 4\pi} \leq 1.10^{-3}$$

It is concluded that if tachyons exist then they must be very weakly interacting with ordinary matter.

The advantage of a search such as this is that no assumption regarding the behaviour and/or properties of the tachyons need to be made. But the main experimental problem is a background of events in which the missing neutral is one or more π^0's.

Another type of experiment to detect tachyons was performed by Murth y (1971) using cosmic ray extensive air showers.
This type of search assumes three properties of tachyons to be true:

a) they travel faster than light

b) they are detectable (i.e. they should give up energy to a scintillator)

c) they are produced in the interaction of very high energy cosmic ray primary particles at the top of the atmosphere,

and are not absorbed by the atmosphere - the "shower front" travels through the atmosphere nearly at the speed of light. Tachyons on the other hand, would precede this shower front since they travel faster than light.

Ramana Murthy (1971) conducted his tachyon search at mountain altitude such that the average height of initiation of an air shower above the apparatus is $\sim$2km and he estimated $\frac{v_t}{c} \sim 1.4$. These assumptions give an estimated 20 μs interval between the arrival of the tachyon and the extensive air shower. Murthy used two types of tachyon detector. The first was a liquid scintillator (75 x 75 x 22cm^3) which could detect either charged or neutral tachyons from the secondary electrons produced by a tachyon interaction with the material of the scintillator (mode I).

The second detector was based on the same principle as that used by Alvager and Kreisler (1968) (mode II). Two photomultipliers viewed an air gap normal to the direction of an electrostatic field of 2.1 kv/cm. Under these conditions the Cerenkov light produced by an ordinary charged particle, would be negligible. The idea of using an electric field was to supply energy to any charged tachyon entering the detector so that it could emit Cerenkov light even if it lost all of its energy in the first fraction of a centimeter of the detector region. Any coincidence between pulses from both photomultipliers were expected to be due to chance or to Cerenkov light produced by a charged tachyon traversing the near vacuum of the detector region. The equilibrium energy of a singly charged tachyon emitting Cerenkov radiation in such an electric field was calculated to be 3.4 ev. The photomultipliers were sensitive to photons in the range 2.3 ev. to 3.4 ev. To detect the associated extensive air

shower, Murthy used 4 x 0.26m^2 scintillators arranged in a square array of side 10m and placed symmetrically about the tachyon detector. A coincidence of >1 particle m^{-2} in each scintillator provided the trigger. Each coincidence triggered an oscilloscope on which the times of occurrence of the potential tachyon signal and the extensive air shower were recorded. The experiment was run for 5079 hr in mode I and 2597 hr in mode II with a trigger rate of 20 min^{-1} . In both cases the number of observed coincidences fell within one standard deviation of the expected number of chance coincidences. The frequency distribution of the time separation showed that they were randomly distributed in the region 0-20μs. He concluded that the frequency of occurrence of tachyons (T^0, T^+, T^-) in extensive air shower was less than 3.10^{-4} to 10^{-5} relative to that of electrons.

Ashton et. al (1970) searched for tachyons by measuring time of flight over a known distance and looked for values exceeding the speed of light. Two large scintillators ($1m^2$) viewed by single photomultiplier tubes and separated by 5.3 m were used. No evidence for the presence of particles travelling with velocity >1.6c in cosmic rays at sea level were found. They were able to place an upper limit of less than 2.2 x $10^{-5} cm^{-2} s^{-1}$. st^{-1} at the 90% confidence level on the flux of tachyons in the incoherent sea level cosmic radiation.

Clay and Crouch(1974) set up an experiment similar in many ways to that of Murthy. A plastic scintillator was used as a tachyon detector ($1m^2$ x 5cm) and fed the pulses recorded by this into a digital transient recorder which at any instant held a record of pulses occurring in the previous 128 μs. This was then output to a chart recorder which reduced the effective delay to 114 μs.

The extensive air shower trigger was obtained from five $(1 \times 1 \times 0.005) m^3$ plastic scintillators, arranged in a square array of side 30m, one at each corner and one at the centre. A coincidence between the central detector and any three of the others produced a trigger which was then used to trigger the transient recorder. The trigger rate of showers of 7.2 hr^{-1} corresponded to showers of energy $>2 \times 10^{15}$ ev. The method of analysis was to record the time of arrival of pulses in the 97.5 μs. time interval preceding the arrival of the air shower front. Comparison of the time of the "largest pulse" in the 97.5 μs previous to the arrival of 1307 air showers with a randomly generated set of arrival times gave a χ^2 probability of 10^{-4} that the test data and extensive air shower data were from the same distribution. They concluded that they had observed non-random events preceding the arrival of an extensive air shower, and it was suggested that this was a result of particles travelling with an apparent velocity greater than c.

After Clay and Crouch's article was published several similar experiments have been performed. Prescott (1975) pointed out two criticisms of the Clay and Crouch results which raise doubts as to their validity.

Prescott (1975) essentially repeated the Clay and Crouch experiments with the original apparatus. His re-analysis consisted of comparing the number of pulses in the 0 to 105 μs. previous time to the shower front with that in the 105 to 210 μs. region after the arrival of the shower front. No excess of pulses appears in the former interval, thus contradicting the previous results. He also discussed what might have been the reason for the non random distribution initially found by Clay and Crouch. Apparently any pulses in the first and second bins

would be substantially lowered if a large pulse arrived just prior to them. This led to a deficiency in 'largest pulse' counts in these bins and hence an erroneous χ^2. In fact Prescott found such a systematic effect because of the method of analysis used by Clay and Crouch i.e. selecting the largest pulse in the 105 μs previous to the arrival of an air shower. The pulses observed by Clay and Crouch were ~10% the height of the pulse produced by a relativistic (subluminal) muon traversing the tachyon detector.

Also an independent search for tachyons was devised by Prescot. Using a (50 x 50 x 10) cm^3 plastic scintillator, viewed by a two inch photomultiplier, located 17.5 m from the centre of the Buckland Park array. The output signal was amplified and delivered to a transient recorder with output to a chart recorder. Signal to noise was improved by two orders of magnitude, from ~0.1 of the mean single particle energy release in the scintillator to 5×10^{-4}. Overshoot was reduced to less than 0.5% and he compared the distribution in time of arrival of pulses preceding 4315 showers of size greater than 10^5 particles with the time of arrival of 5715 randomly triggered events. In both sets of events the time distribution of signals has a uniform distribution. Moreover, the frequency of events in which zero, one, two, etc. pulses were recorded had a poisson distribution, indicating no tendency for pulses to be associated in time. An upper limit on the tachyon/electron flux, at the 90% confidence limit, was determined as 5×10^{-5}.

Fegan (1975) used a 2.5 m^2 x 5cm plastic scintillator as a tachyon detector which was placed at the centre of a triangular array of three plastic detectors which provided the air shower trigger. The output of the two, five inch, photomultipliers, viewing the detector in coincidence, was fed to a 200 bit static shift register which

produced an 800 μs record of the time distribution of detector events. Two sets of data were obtained. The first, mode A, demanded coincidence between the two photomultipliers and corresponded to an energy deposit in the scintillator of ≥1 Mev. The second, mode B, demanded a single pulse from a single photomultiplier corresponding to a deposit of ≥0.5 Mev. A master pulse inhibited the register 380 μs after an air shower arrival was obtained. The register now contains the profile in time of detected events for the interval 420 μs before the shower front.

A statistical analysis based on a χ^2 test of the interval 12 μs to 408 μs before the air shower front arrival produced no evidence for a deviation from a random distribution. Mean calculated shower energies are 2×10^{15}ev. Comparing the observed number of pulses in the 108μs to 12μs before the air shower arrival with the number expected in a random 96 μs time interval, the upper limits for the tachyon flux, at the 3σ level, were determined as 2.06×10^{-2} per shower per m^2 in mode A and 6.58×10^{-2} per shower per m^2 in mode B, at the mean shower energy.

Another group conducted two searches for tachyons associated with air showers were workers at the University of Tasmania (Emery et al, 1975). They used the same technique as used by Clay and Crouch but using Geiger Muller (G-M) counters and liquid scintillators. The first search demanded that a tachyon produce a pulse in one of 96 G-M tubes in four 1m x 1m trays evenly spaced around a circle of radius 21.2m in the 108 μs before the arrival of an air shower as detected by these trays of G-M tubes. The air shower trigger was such as to produce a rate of 357 per day with energy of about 10^{15}ev.

After analysing 27449 showers and observing 3512 pulses which preceded these showers by up to 108 μs they found a 0.9 probability

that the time distribution was flat, based on a χ^2 test. They conducted a second search using a 75 cm diameter, 2.5 cm deep, liquid scintillator at the centre of the array as a tachyon detector. The system could register pulses greater than 0.1 times the pulse height due to a single muon. 3766 precursor pulses were seen in the 108 μs before 9521 showers. The probability of the distribution being uniform was 0.15. They concluded from their results that there was no positive evidence for tachyons in association with air showers.

Smith and Standil (1977) used a cosmic ray telescope, consisting of 5 scintillators of area 0.7 m^2 as elements. Each element of the telescope registered the occurrence of events depositing more energy than $\frac{Eo}{5}$ where Eo is the energy corresponding to the 'through peak' of the muon pulse height distribution and the detector registered charged particles at a rate of 27.5 s^{-1}. Air showers were detected by an array of three detectors which was sensitive to showers of energy greater than 6 x 10^{14}ev at a rate of $10^{-2}sec^{-1}$. Tachyon detection by the large telescope initiated a data readout cycle by starting a TAC time scan and caused three independent measurements of the ionization of the initiating event to be digitized and stored. If an air shower arrived within 290μs of this event, the data, along with the pulse heights from the array detectors and the time, would be saved and stored. They carried out numerous checks on the stability of the detecting system and 204702 showers were recorded, along with 1519 ± 39 tachyon candidates. When the number of expected coincidences were subtracted, an excess of 46 ± 40 events were found. It was concluded that these could be as random coincidences between the start and stop signals at the time to amplitude converter.

Ashton et al (1977) used the air shower triggers provided by

the Durham array outer ring trigger (Detectors 13, 33, 53 and c in operation) (see Chapter II). With a minimum shower size of about 8×10^4 particles and a rate of $(8.53 \pm 0.46)hr^{-1}$ the equipment used consisted of, from top to bottom, 15 cm. of lead, 8 layers of neon flash tubes, 15 cm. of iron, the tachyon detector with total sensitive area of 2.1 m^2 and thickness 5 cm. and 108 layers of flash tubes. The summed outputs from the 6 photomultipliers viewing the scintillator passed through a 240 μs delay line and were displayed on an oscilloscope, the screen of which was photographed. The flash tubes allowed the track of tachyon candidates to be recorded. In 341 showers, six precursors were observed with pulse heights greater than three times the height of that due to a relativistic muon which all occurred in the time interval of 0-120 μs preceding the shower front. A χ^2 test gave a probability of 4.5×10^{-6} that 6 events would occur in this region and none in the 120 to 220 μs region. The expected number of chance events has been estimated as 0.81. It was concluded that the possibility of a tachyon flux existed but that better statistics were required.

Later Ashton et al (1979) devised another search for tachyons. They used an unshielded plastic scintillator of area $2m^2$ as a tachyon detector. The Durham array outer ring trigger gave a shower arrival signal at sea level generated by primary cosmic rays of energy $\geq 2.5 \times 10^{15}$ ev. with a rate of 4.3 hr^{-1} corresponding to a minimum shower size of 2.5×10^5 particles. The electronic system used to display pre-shower front pulses consisted of a delay line giving an overall delay of 264 μs. Tachyon pulses were expected to occur in the 120 μs time domain preceding the extensive air shower front pulse. Results for the time distribution of pulses corresponding to different threshold energy losses in the tachyon detector obtained from a sample of 1107 shower

triggers were obtained. The distributions are expected to be flat over the range 20 - 260 μs. Using a χ^2 test to determine whether the measured time distributions are really flat it was concluded that in all cases there is no evidence for a significant number of events being produced by tachyons.

Bhat, P.N. et al (1979) conducted a search for tachyons using a tachyon detector consisting of two plastic scintillators each $(80 \times 80 \times 1)\,cm^3$, located in a stack of 14 g cm^{-2} iron plates which form the multi-plate assembly of a large cloud chamber. The chamber was shielded by a 48 g cm^{-2} layer of lead from low energy particles. The output of the detector was discriminated at the three muon level. The tachyon detector is located about 10 m from the centre of an array of 24 detectors. The apparatus was operated in two modes. In the mode A two scintillators were operated in coincidence and following each potential tachyon signal a time interval of 1-401μs after a tachyon candidate was scanned for the arrival of an air shower. If any air shower arrived in this time interval then the delay time and the air shower data were recorded. The rate of air shower triggers was observed to be 12 hr^{-1} and the estimated minimum size of the shower, was 2×10^5, corresponding to a primary energy of about 6×10^{14} ev. In 1749 hr 20988 showers were observed and only four events have been observed. Since the number expected due to background was seven, there was no excess of events. In the second mode only one detector was used. The trigger was adjusted and gave a rate of 42 hr^{-1} with a minimum shower size of around 10^5 and primary energy of about 3×10^{14} ev. In 1872 hours 78624 showers were detected and 27 events observed. The expected number of chance events in this period is 31, the events being also uniformly distributed over the time interval.

They concluded there is no evidence for any finite flux of tachyons from this experiment. The upper limit on the tachyon flux, at the 95% confidence level, is $2.3 \times 10^{-10} cm^{-2} . s^{-1} . st^{-1}$.

A recent experiment searching for tachyons associated with extensive air showers at energies $E > 3 \times 10^{16}$ ev. is D.J. Fegan 1981. He used an 0.5 m^2 area plastic scintillator of thickness 0.025m as a tachyon detector, the top surface of the plastic scintillator being viewed by two photomultiplier tubes of 12.5 cm diameter. The detector was located at the centre of an equilateral triangle with sides of length 20m and three circular plastic scintillators of 0.05 m^2 area located at the vertices constituted the air shower selector, the minimum shower energy which could produce a trigger was 10^{16} ev. which corresponded to a rate of 0.17 hr^{-1}. The tachyon detector was shielded by 25 cm of concrete and by an additional 15 cm of lead over burden. The signal from both photomultiplier tubes of the tachyon detector were linearly summed and fed to a transient recorder. This allowed a period of 480 μs before the shower front and 24 μs after to be recorded.

Fegan in his experiment used two different approaches. (a) The trigger threshold energy was increased above that previously used so as to reduce the dilution effect of a large number of background pulses. (b) The exposure time was made longer than previous experiments which gives a reasonably large statistical sample at the higher threshold. Amplitude integrated histograms were produced, both for the real data and the random data, which was from triggers injected throughout the experiment as a system check. The resulting histogram showed "an excess of events in the 48 to 60 μs region prior to the arrival of the air shower front." Fegan suggested that the excess is not inconsistent with tachyons, but the observed deviation of 5.33 σ from the mean at

57 μs could be caused by the disintegration of cosmic ray nuclei in the field of solar photons leading to the production of correlated showers in the earth's atmosphere, (Gerasimova et al 1960). However, Gerasimova et al determine the cores of associated showers to be separated by a distance of about 1 km which makes this explanation unlikely.

5.7 Conclusion

Although only the results of Fegan (1981) have yielded a possible tachyon signal it is realised that there are considerable experimental difficulties in searching for particles that precede an extensive air shower in the time domain 0-150μs preceding the arrival of the air shower front. This is particularly true of digitised detectors and for this reason the experiment described by the author in the next chapter used 1 μs/foot delay lines to store information which was then displayed on a dual beam oscilloscope. In this way a clear picture of what is happening in the time domain of interest to detecting a possible tachyon flux is obtained.

CHAPTER 6

EXPERIMENTAL ARRANGEMENT USED FOR THE TACHYON EXPERIMENT

6.1 INTRODUCTION

The principle of the experiment which is now described is to search for tachyons associated with cosmic ray showers of primary energy of $\gtrsim 10^{15}$ ev. The method used for the search is that first used by Ramana Murthy (1971) and since used by others.

Consider a primary cosmic ray proton incident from the zenith and making its first interaction at an atmospheric depth of 80 g/cm^2 of air corresponding to an altitude of 17.7 km above sea level (van Allen et al 1950) as shown in figures 6.1 a and 6.1 b . It is assumed that tachyons are produced as particle antiparticle pairs in interactions of the sort that occur when a high energy cosmic ray primary proton collides with a nucleus in the upper atmosphere, i.e. a reaction of the type: $P + N \rightarrow N + N + t + \bar{t}$ + pions etc., Another assumption held is that at least some of any produced tachyons with $v > c$ should survive for long enough to reach sea level and then either loose energy in a scintillator and give rise to photons or be detectable by the production of secondary particles which can be detected.

A primary proton if it has sufficiently high energy ($\geq 10^6$ Gev) will then produce an extensive air shower. At such high energies the main electron photon shower front velocity is approximately the speed of light. The most likely kinetic energy of a tachyon is approaching zero if it is created at the production threshold

energy and its velocity will then approach infinity. Also if the initial kinetic energy is greater than zero, any interaction with the atmosphere will lower its kinetic energy and its velocity will increase. Hence, a tachyon will reach sea level at sometime in the 59 μs time period before the arrival of the main electron-photon shower front for a vertically incident shower. Such a situation is illustrated schematically in figure 6.1b. For a shower incident at a zenith angle of 60° the relevant time interval is 150 μs. As <1% of showers have zenith angle >60° it is necessary for a tachyon detector to be able to record the occurrence of preshower front pulses in at most the 150 μs time domain preceding the shower front arrival time.

For finite velocity tachyons or for tachyons produced in secondary hadron interactions, low in the atmosphere, the delay time would be smaller. Any heavy particles produced in the extensive air shower hadron cascade are expected to trail the shower front.

One major difference between the present search and previous searches is the fact that the tachyon detection scintillator is shielded by 20cm of lead and 20 cm of iron. This allows the possibility that the experiment is sensitive to both penetrating tachyons and also to tachyons that interact in the absorber with their secondaries being detected by the tachyon detection scintillation counter.

6.2 EXPERIMENTAL ARRANGEMENT

A scale diagram of the experimental arrangement used is shown in figure 6.2. Briefly a twofold coincidence between scintillators A and B is used to detect the arrival of an air shower front and in such an occurrence the pulses detected by scintillator C (the tachyon detector) are recorded in the 265μs time domain preceding the shower front and also in the 235μs time domain after the arrival

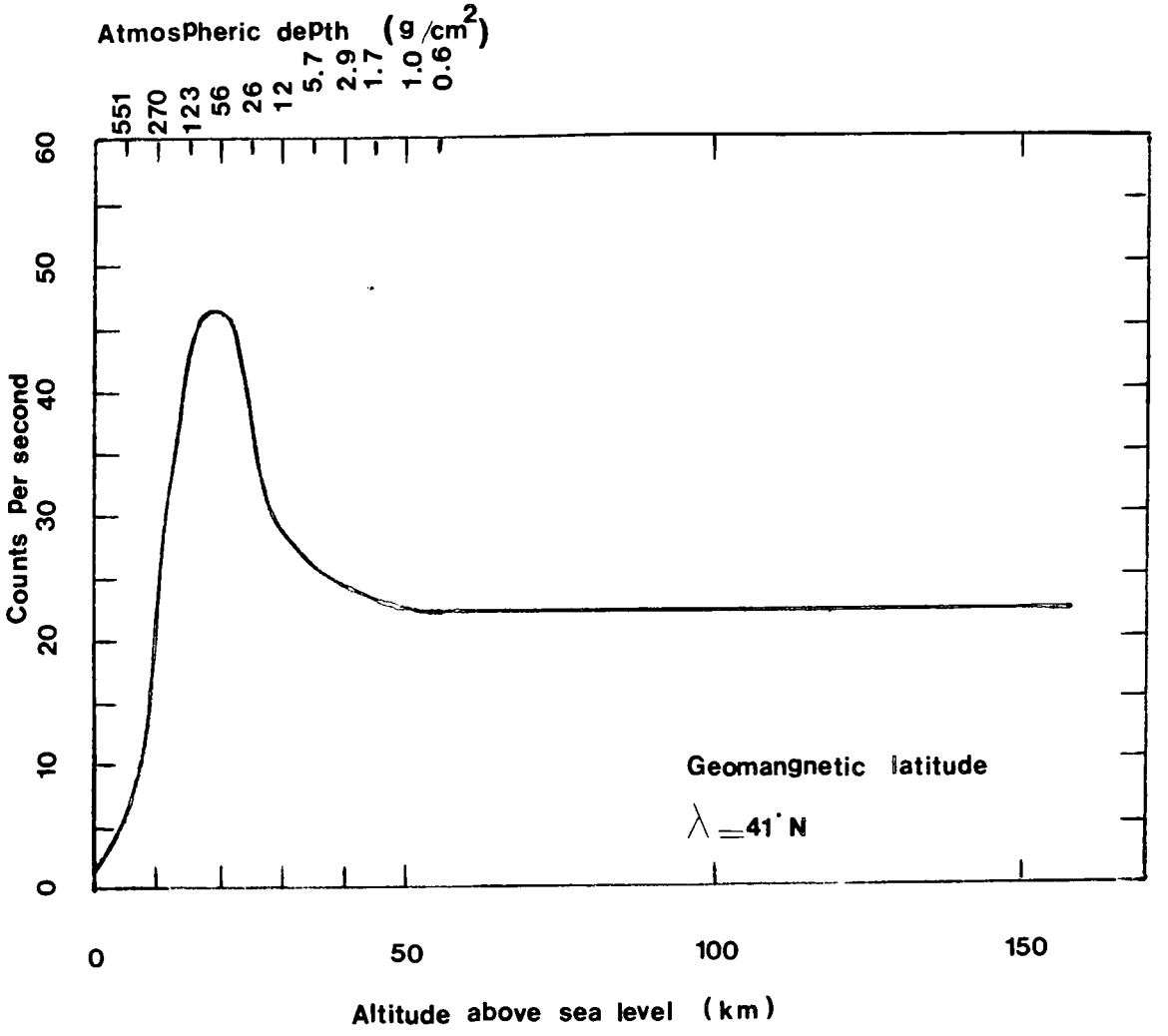

Figure 6.1a Variation of counting rate of single Geiger counter with altitude (after Van Allen et al 1950)

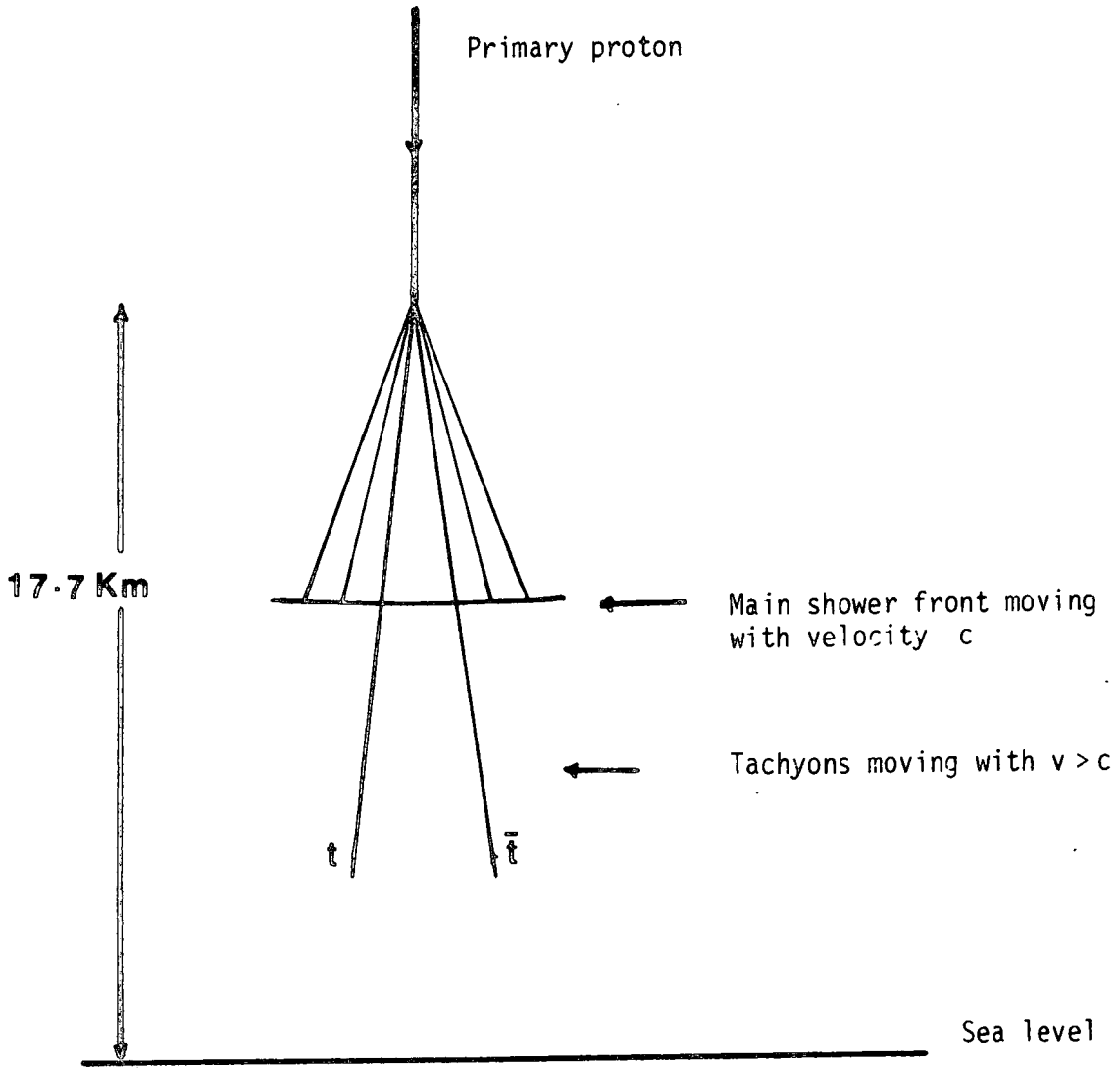

Figure 6.1b: Diagram illustrating the possible production of $t\bar{t}$ pairs in the interactions of a primary proton with an air nucleus at an atmospheric depth of 80 gcm^{-2} (λ mean free path) corresponding to an altitude of 17.7 km above sea level.

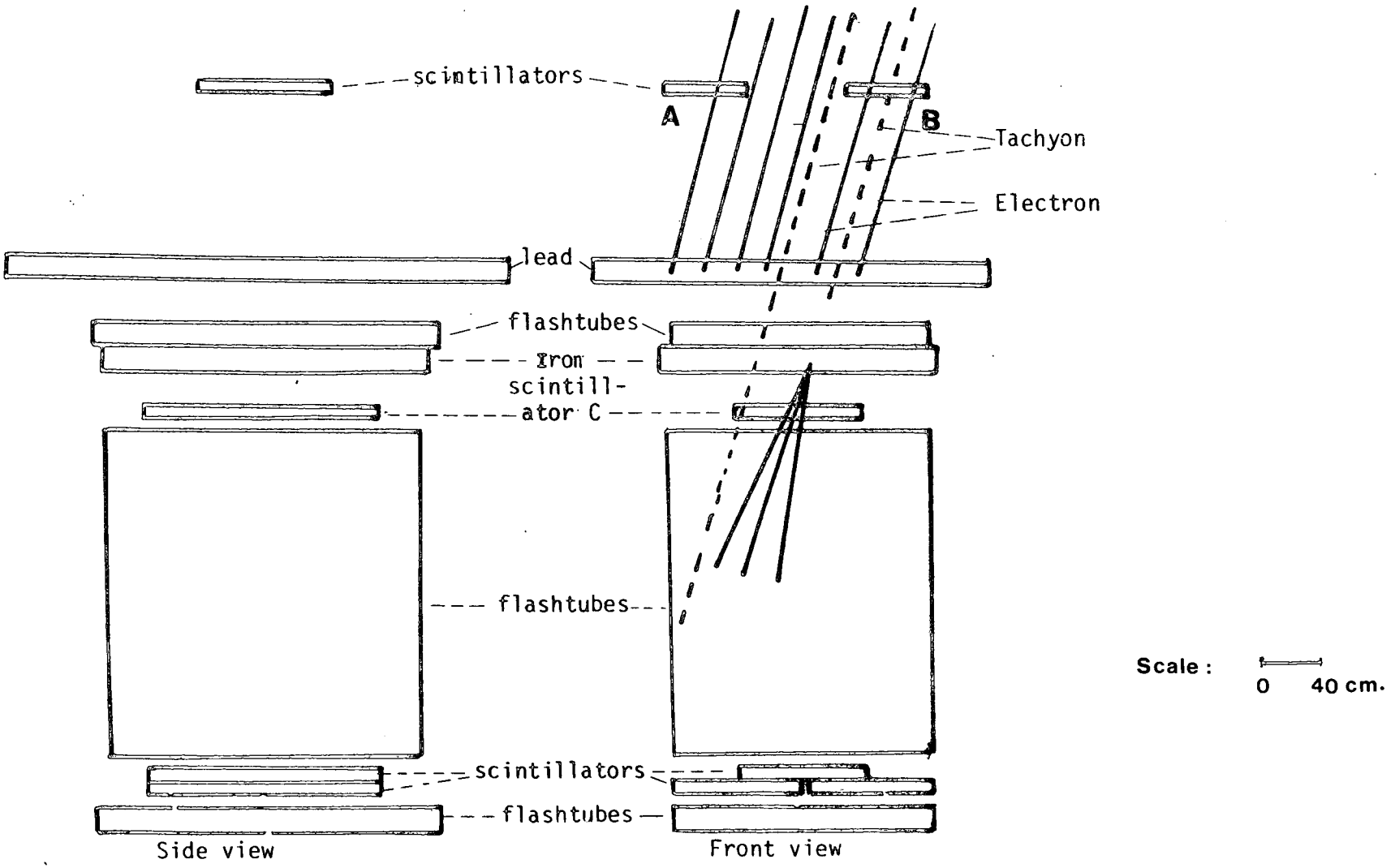

Figure **6.2** : Experimental arrangement used in the tachyon experiment. A twofold coincidence between scintiallators **A** and B was used to detect EAS of local electron density $>25m^{-2}$. Scintillator C was used as the tachyon detector **and** could register either penetrating tachyons or the effects of tachyon interactions in the iron or lead absorbers as illustrated. The flash tubes were not operational in the present work nor were the 3 scintillators shown at the bottom of the detector. Phosphor areas of scintillators A,B are 80 x 50 cm^2 ($0.4m^2$) and C is 140 x 75cm ($1.05m^2$).

of the shower front. The equipment is mounted as an integral part of a large flash tube chamber (see Appendix A for details) but the chamber was not operated in the present work. It is noted that tachyons could be detected either by their direct interaction with the phosphor material of scintillator C or via their production of normal secondary particles by their interaction in the lead or iron shielding layers each of which is 20 cm thick.

6.3 EAS SELECTION

A block diagram of all the electronics used in the experiment is shown in figure 6.3. EAS were selected by a twofold coincidence between scintillators A and B each of area 0.4 m^2. Both scintillators and the head units used are of the type described in chapter 4. Figure 6.4 shows the integral response of each scintillator to the global cosmic ray flux where pulse heights are measured at the output of each scintillator head unit. Both scintillators were adjusted so that the average pulse height produced by relativistic muons traversing their areas at normal incidence produced an average pulse height of 20 mv at the head unit outputs. Also shown in figure 6.4 is the coincidence rate between A and B as a function of the minimum selected head unit output pulse height imposed separately on the A and B outputs. In figure 6.5 these coincidence rate measurements have been converted to an electron density spectrum and it is seen that the results obtained are in reasonable agreement with the summary of such measurements made by Greisen (1960).

To select EAS for the tachyon experiment the threshold electron densities required to be recorded by both scintillators A and B was set to 25 m^{-2}. During a running time of 114hr 21min 56sec a total of 1443 EAS triggers were recorded. During this time a record was

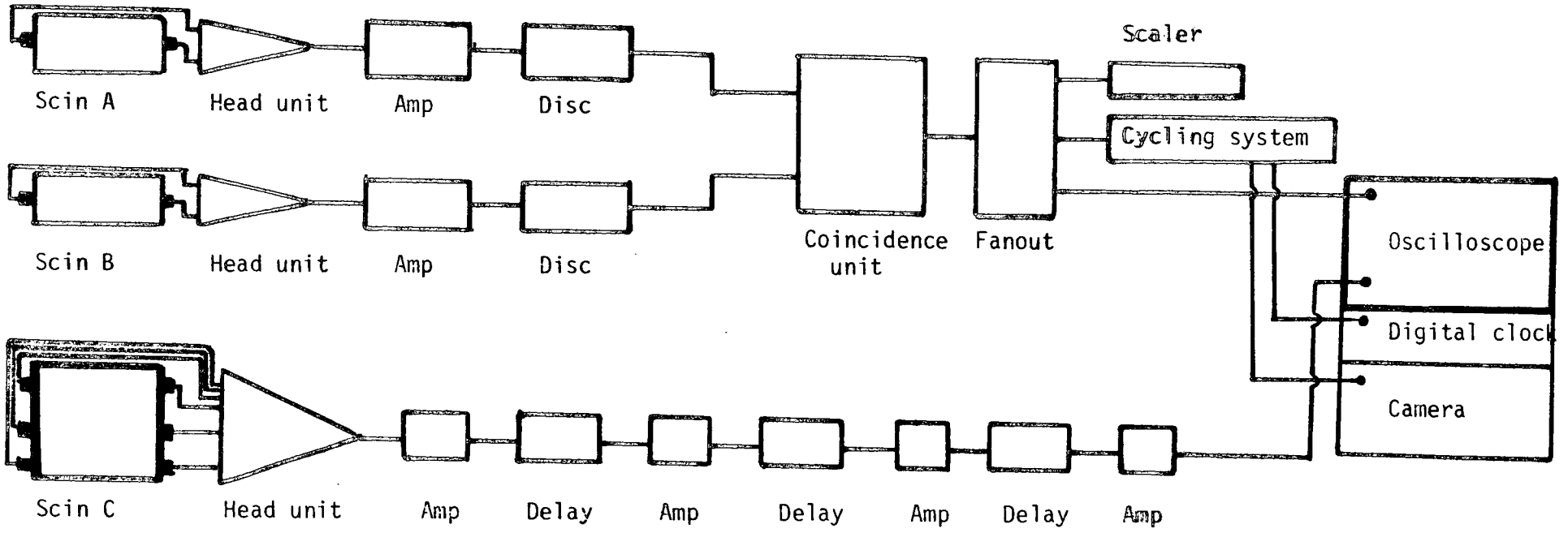

Tachyon detector

Figure 6.3 : Block diagram of the electronics used in the tachyon experiment.
Scintillator A and B are used for detecting EAS of local electron density $\geq 25\ m^{-2}$

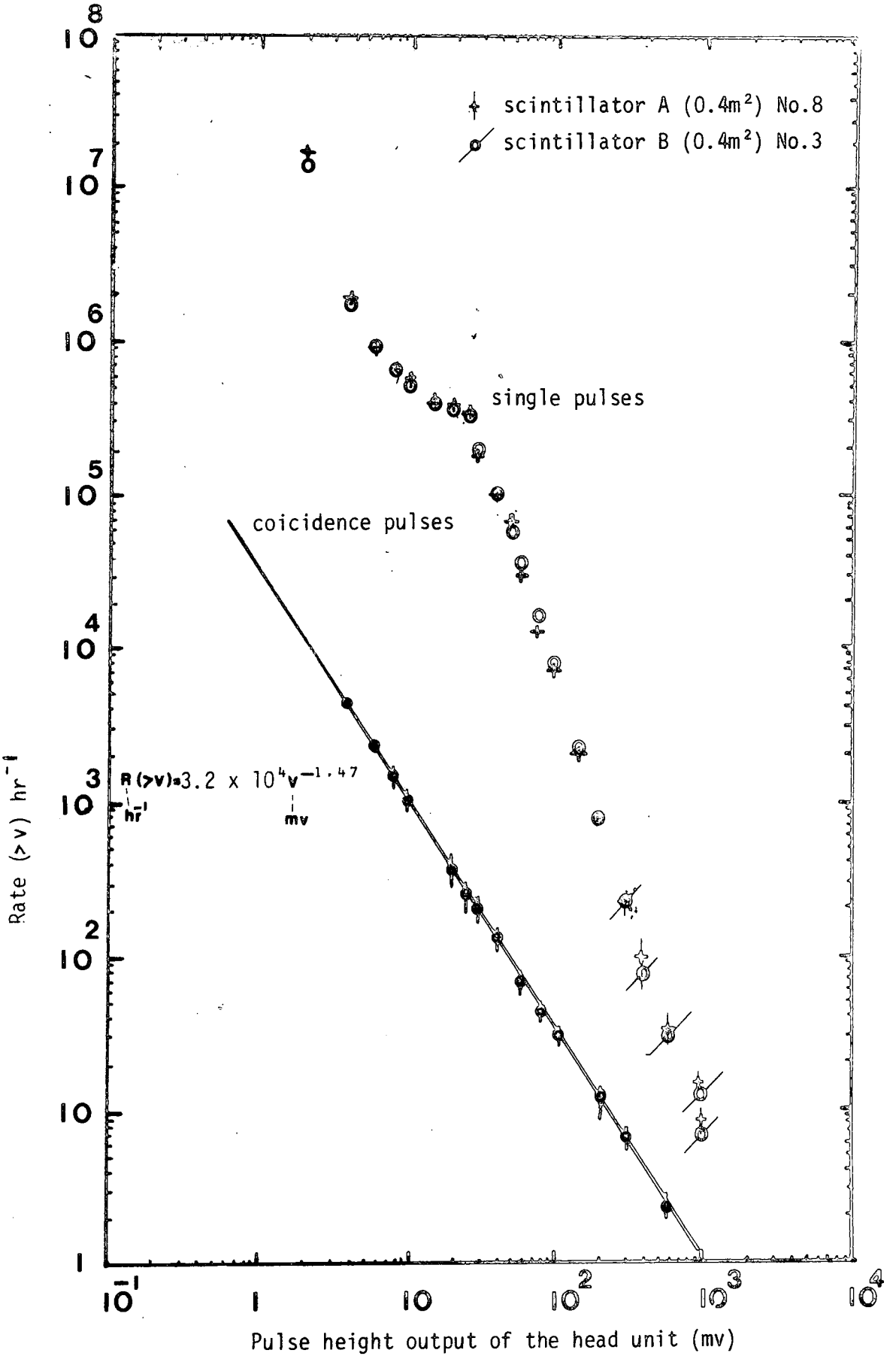

Figure 6.4 : The integral rate of pulses R(>v) measured at the output of the head units of scintillators A and B measured as a function of the threshold pulse height v. Also shown is the measured coincidence rate between A and B as a function of v. For both A and B the average pulse height produced by relativistic particles traversing their area at normal incidence is 20mv. The areas of both A and B are 0.4m².

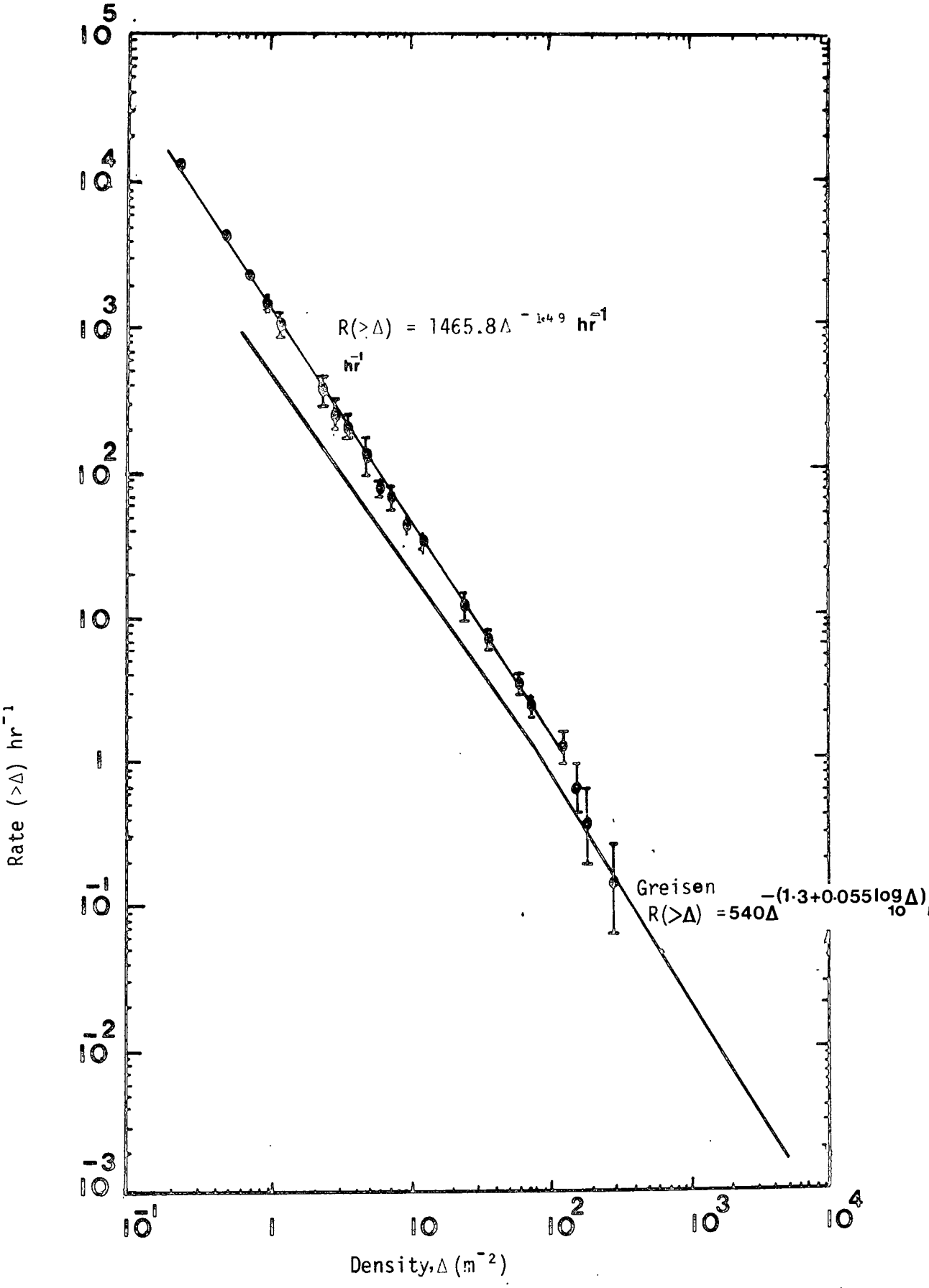

Figure 6.5 : The measured integral density spectrum of electrons at sea level compared with the result given by Greisen(1960)

made of the barometric pressure and figure 6.6 shows how the twofold coincidence rate $\Delta_A(\geq 25m^{-2})$. $\Delta_B(\geq 25m^{-2})$ was found to vary with atmospheric pressure. The straight line shows the best least squares fit to the data assuming it can be represented by $R = R_o \exp -\beta P$. The mean pressure at which events were recorded was 75.4 cm Hg and the best fit line shows that the pressure variation of the rate due to pressure changes from the mean value is $(11 \pm 1)\%$ per cm Hg.

6.4 THE TACHYON DETECTOR SCINTILLATOR (SCINTILLATOR C)

The design of the tachyon detector scintillator with phosphor dimensions 140 x 75 x 5 cm (area 1.05 m^2) is shown in figure 6.7. In order to achieve a large signal to noise ratio (noise pulses being produced by single thermionic electrons emitted by the photomultiplier photocathodes) the phosphor was viewed through rectangular perspex light guides by a total of 6 photomultipliers. To adjust each photomultiplier operating voltage so that the photomultipliers all had equal sensitivity a pulsed light emitting diode was used which was mounted successively at the points α and β shown in figure 6.7 in order to illuminate the photomultipliers on the opposite side of the counter. To keep the electronics as simple as possible the outputs from all 6 photomultipliers were connected together using short lengths of coaxial cable and the common connection was used as the input to a simple emitter follower of exactly the same type already described in chapter 4. Figure 6.8 shows the response of the counter to the global cosmic ray flux and it is seen that the single particle peak is well resolved from the noise. Figures 6.9, 6.10, 6.11, 6.12 and 6.13 display various other measurements relevant to the performance of scintillator C and the relevant details are apparent from the figure captions.

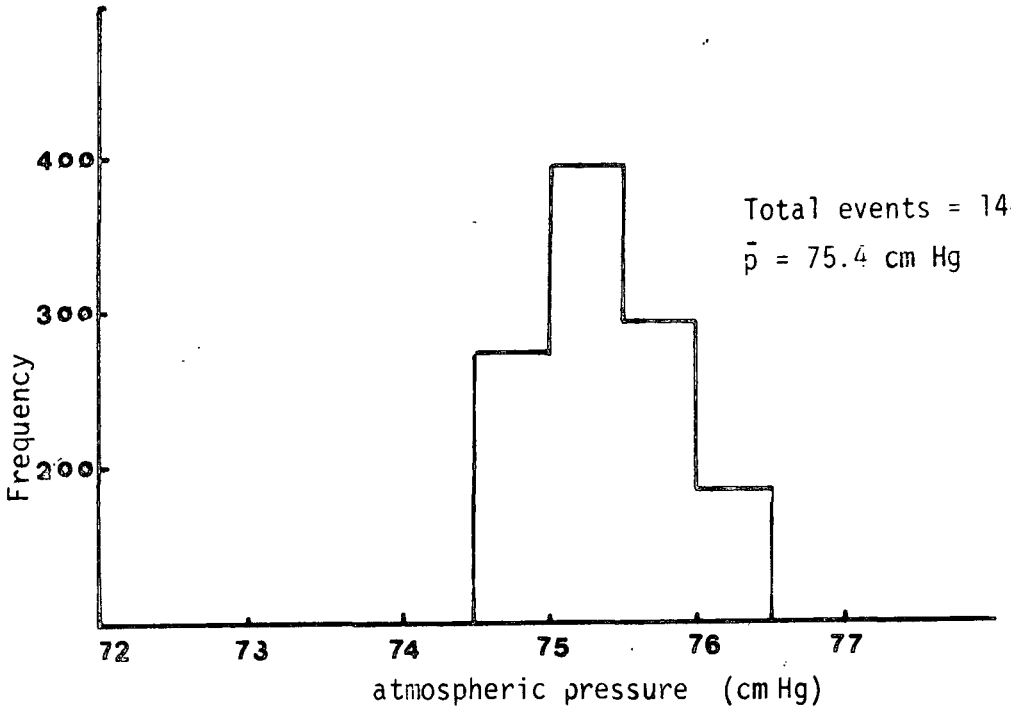

Distribution of atmospheric pressure recorded at the time that each EAS event was detected.

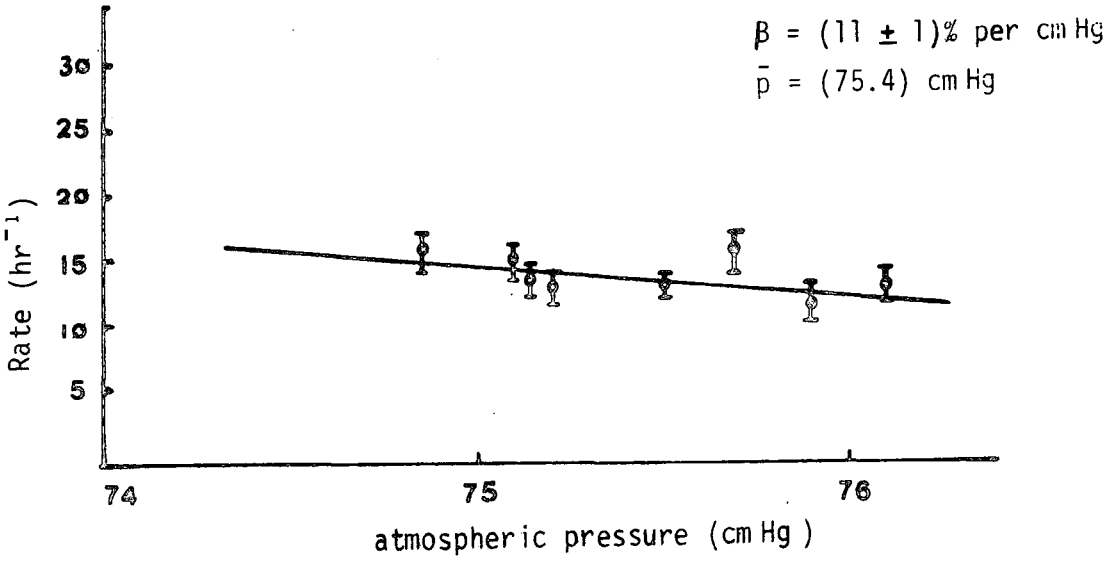

Figure 6.6 : The variation of trigger rate of observed showers with atmospheric pressure.

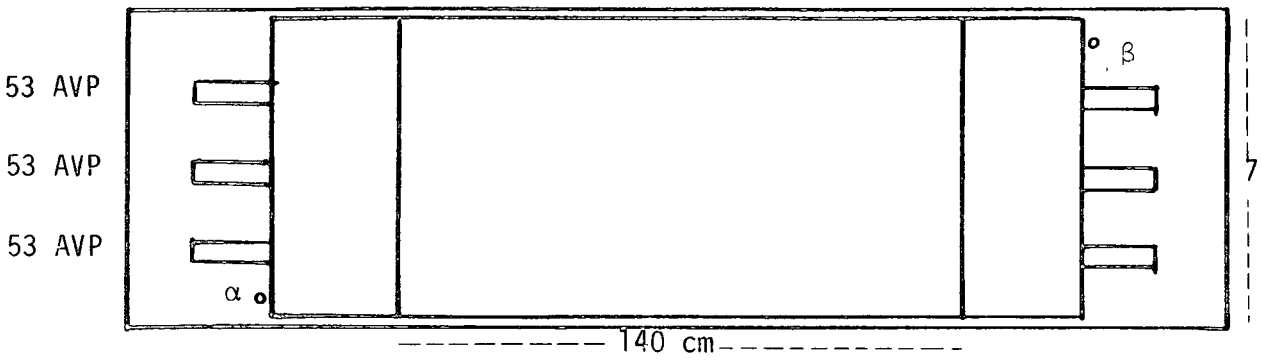

Scale diagram of the top view of the plastic scintillator C used as the tachyon detector with dimension 140 x 75 x 5 cm^3

Figure 6.7 : Details of the tachyon detector, scintillator C. α and β are the successive locations for a pulsed photodiode which is used to adjust the photomultipliers on the opposite side of the counter to have equal sensitivities.

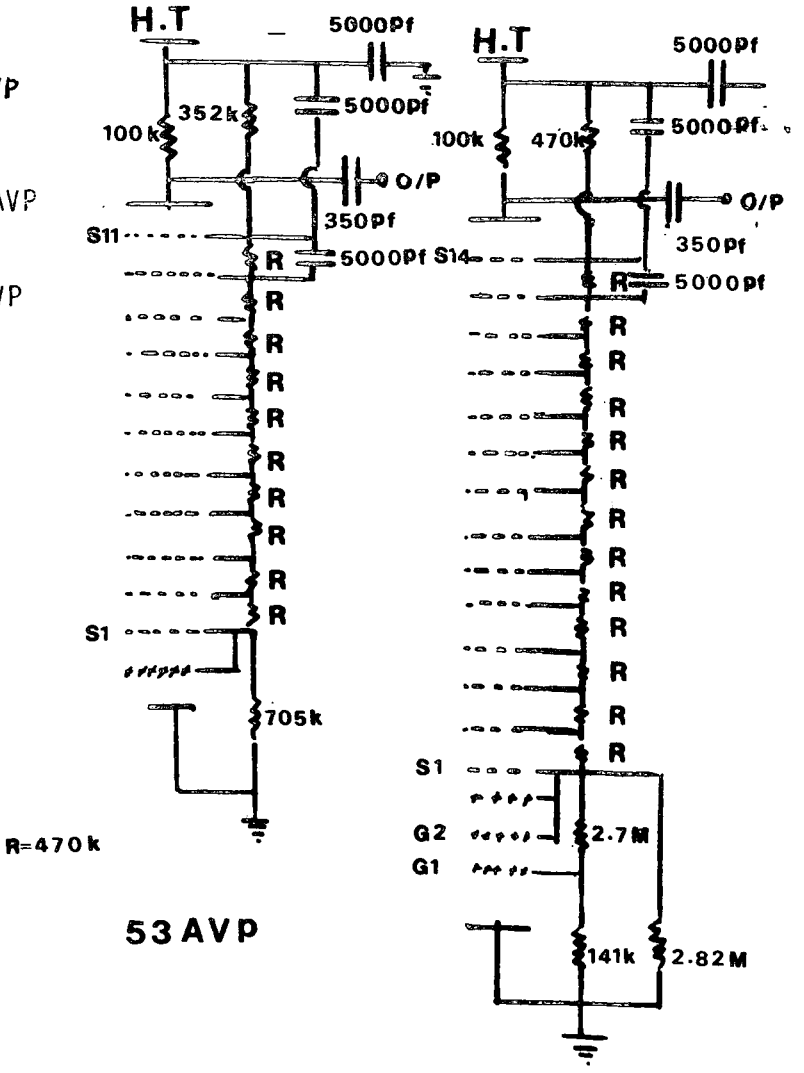

Resistance chains for the two types of photomultiplier used in scintillator C.

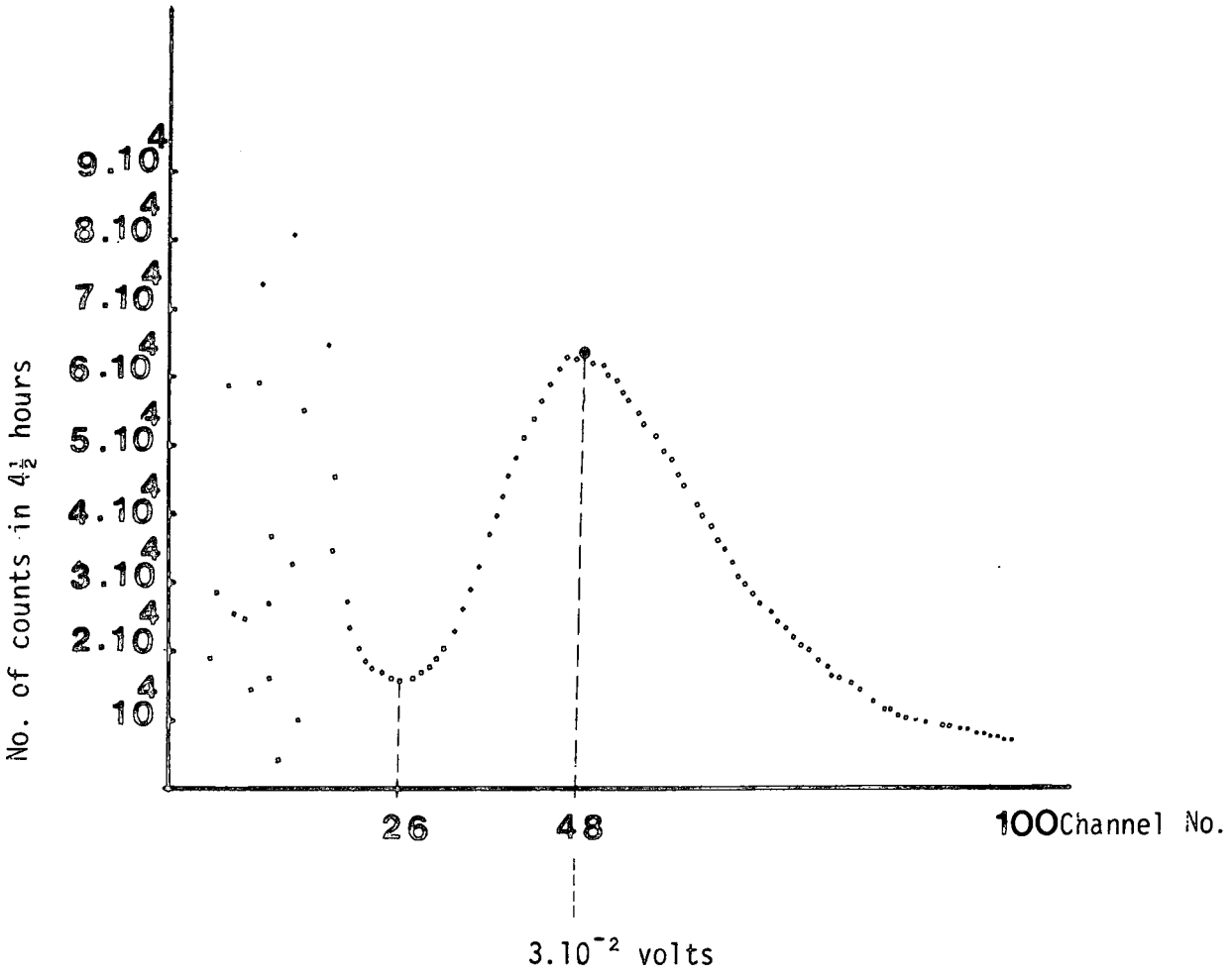

Figure 6.8 : Typical single particle cosmic ray peak as displayed on the pulse height analyser for scintillator C.
P.H.A. Gain = 200

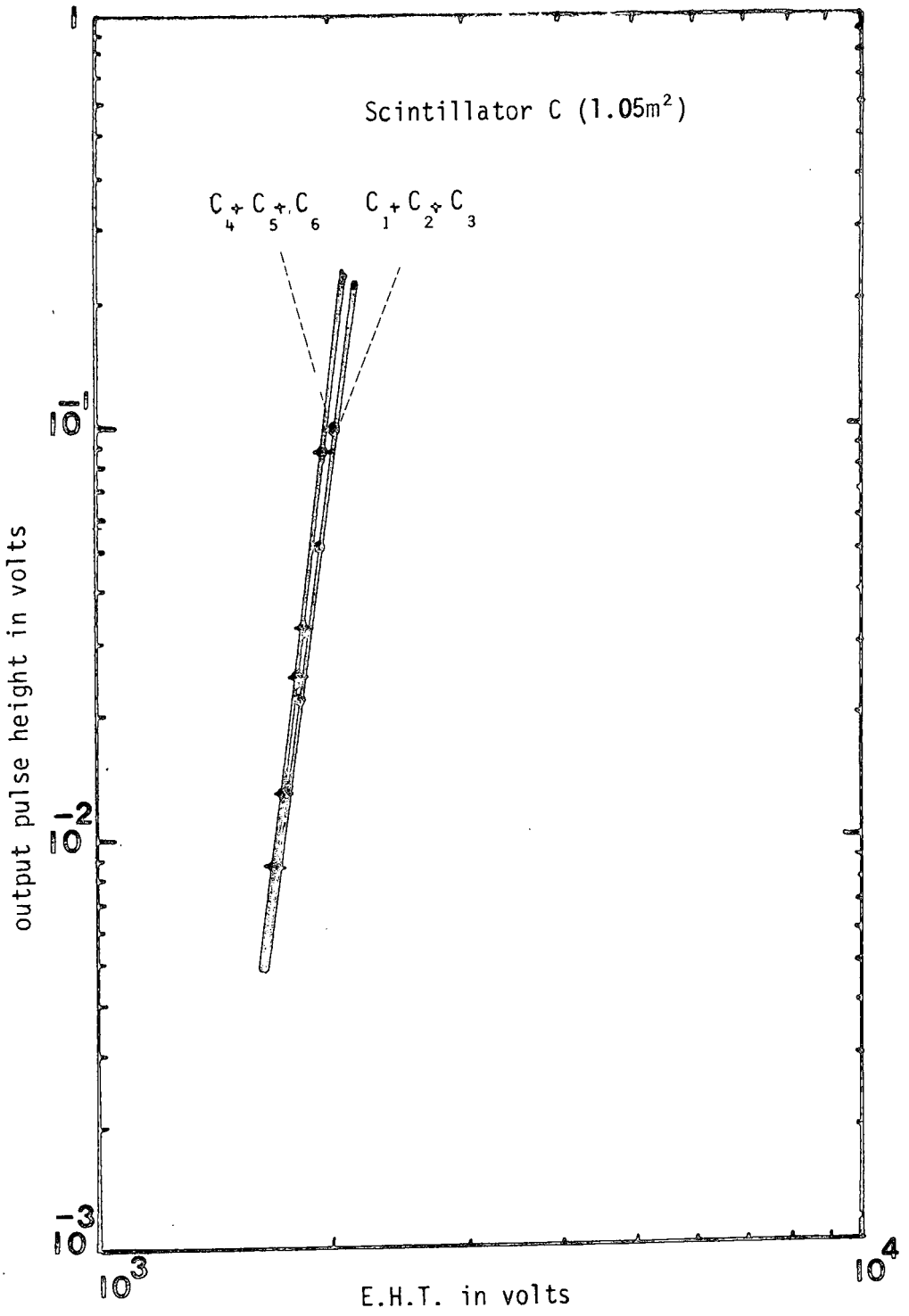

Figure 6.9 : Variation of the peak pulse height from each side of scintillator C (3 matched phototubes operational, $C_1+C_2+C_3$ & $C_4+C_5+C_6$) separately produced by the global cosmic ray flux traversing the scintillator as a function of the voltage applied to the phototubes

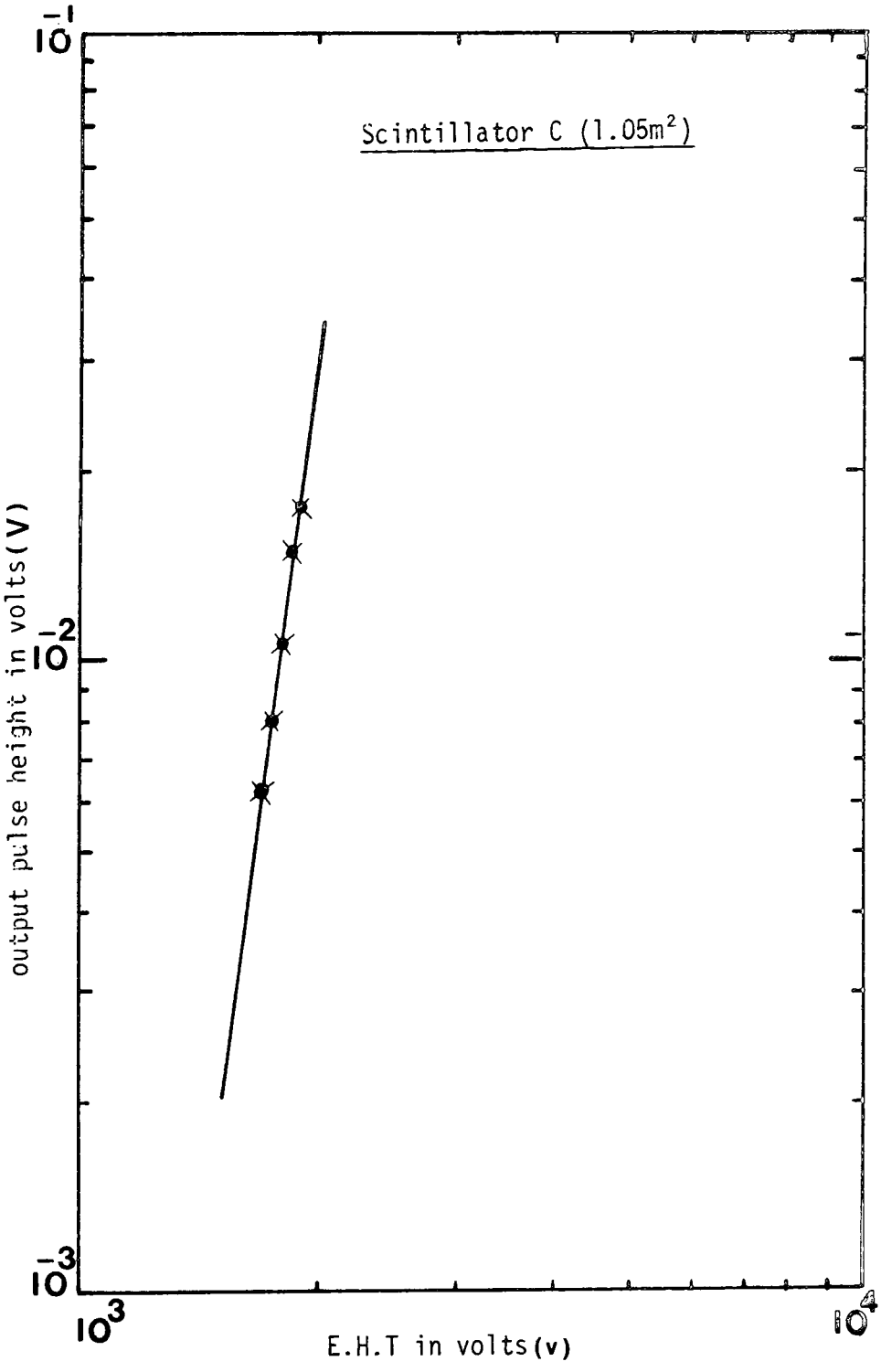

Figure 6.10 : Variation of the peak pulse height produced by the global cosmic ray flux traversing scintillator C as a function of the voltage applied to the matched photomultiplier tubes. The measurements are fitted by $V=1.5\times10^{-36}v^{9.79}$
This result is consistent with the results obtained when individual phototubes are excited with light pulses from an LED

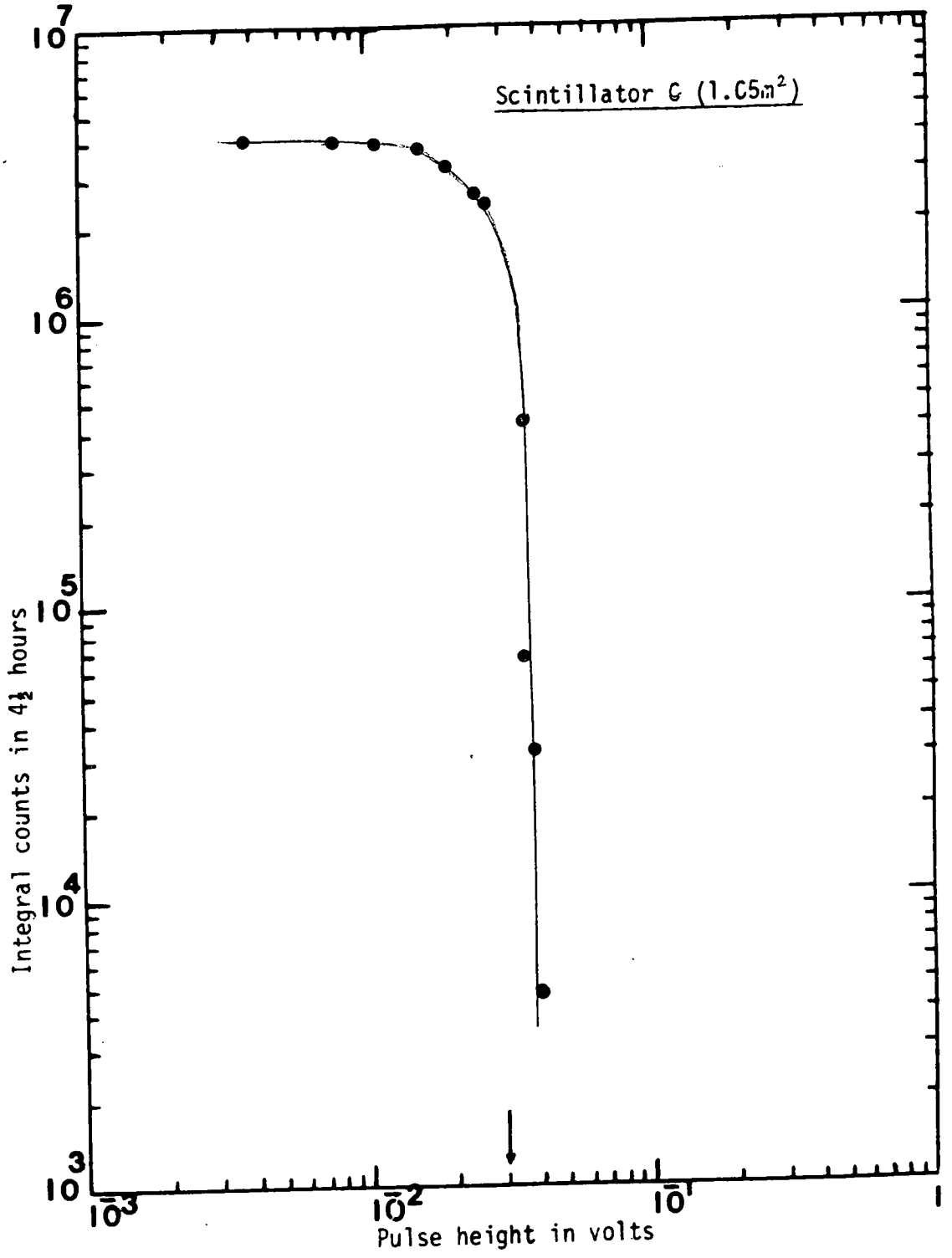

Figure 6.11 : Rate of the pulses >v versus pulses height v as calculated from the pulse height analyser display shown in fig.6.8 The position of the cosmic ray single particle peak is shown by the arrow.

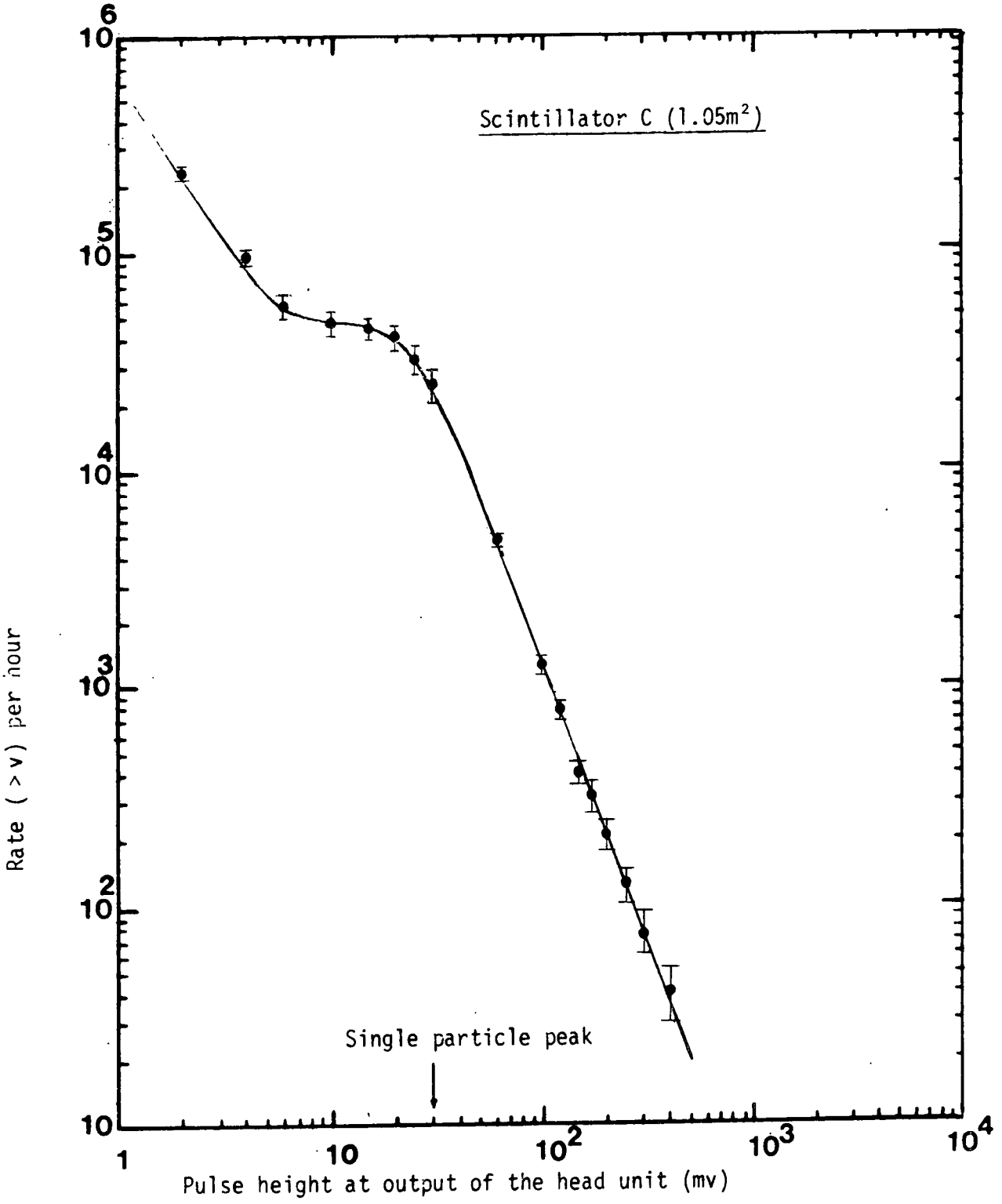

Figure 6.12 : The integral pulse height distribution produced by the global cosmic ray flux measured using an amplifier and discriminator for scintillator C. The corresponding pulse height analyser display shows that the most probable pulse height produced by cosmic ray particles corresponds to a pulse height of 30 mv.

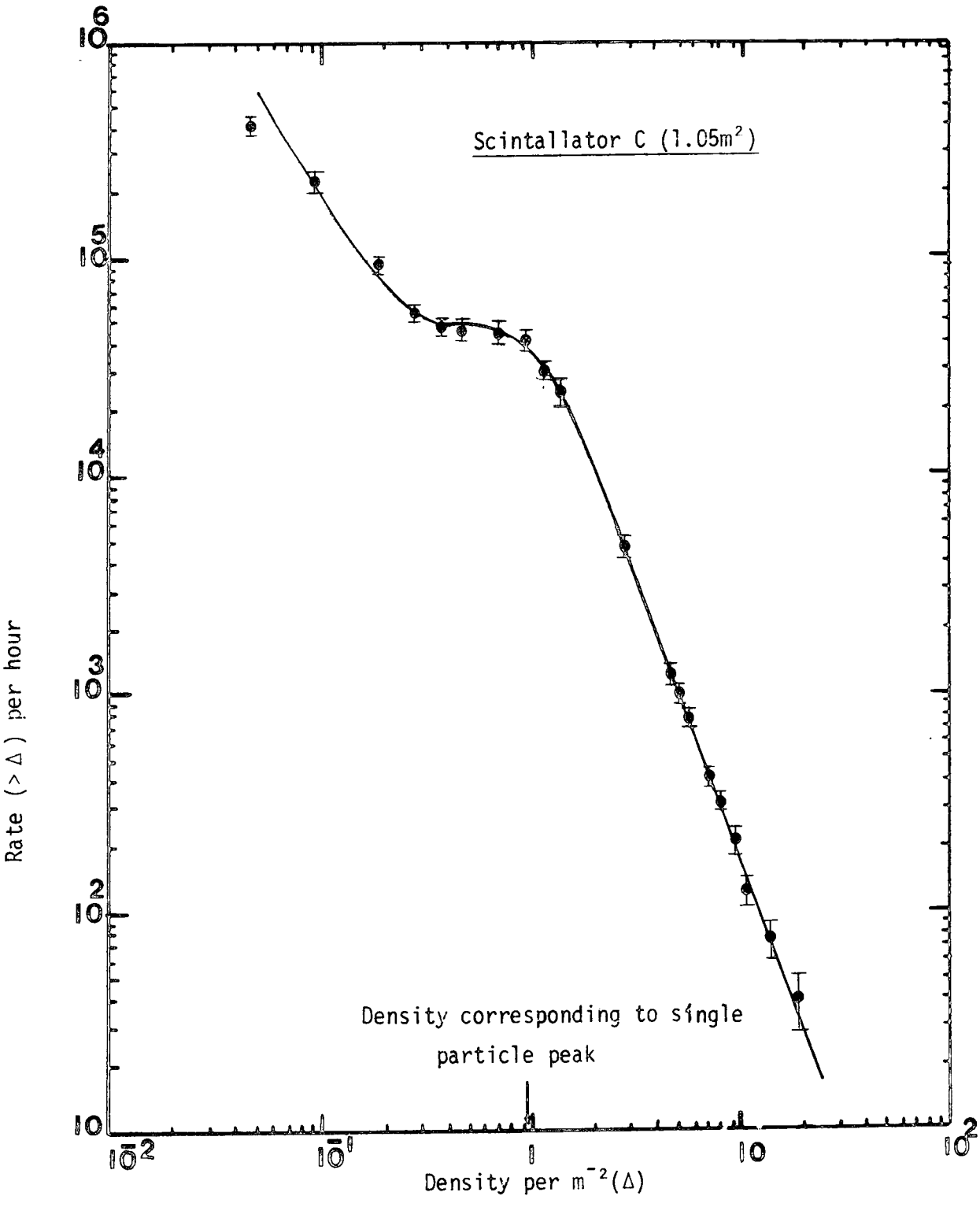

Figure 6.13 : The integral response of scintillator C expressed in terms of the density of particles traversing the phosphor which has area $1.05m^2$. Single relativistic particles traversing the phosphor at normal incidence correspond to a density of $0.95\ m^{-2}$.

In order to measure the occurrence of ionising events occurring in scintillator C before the arrival of the main air shower front some method must be used to store the relevant information. In the present work lengths of Hackethall delay cable (delay 1μs per foot) are used. Figure 6.14 shows that the attenuation suffered by 2μs square pulses in traversing an 80μs length of this cable is a factor of 5. In the actual experimental arrangement used (see figure 6.3) three successive lengths of cable, each followed by an amplifier and giving a total delay of 265μs was used. The final output was displayed on a dual beam oscilloscope with a total sweep time of 500μs so that both the 265μs time domain before the arrival of the shower front pulse and the 235μs afterwards could be investigated. To achieve as large a dynamic range as possible for pulse height measurement one channel of the oscilloscope was operated on a sensitivity of 5 mv/cm with a maximum possible deflection of 7 cm and the other channel was operated on a sensitivity of 200 mv/cm with a maximum possible deflection of 8 cm. Figure 6.15 shows the relation between the pulse height at the output of the head unit and the pulse height recorded on the oscilloscope. In practice the oscilloscope was viewed by a camera with an open shutter and on the occurrence of an EAS event the time base was triggered and the details recorded on 35 mm film. Also recorded on the same film was the time of occurrence of the event. This was achieved using a pulsed display digital clock. Figure 6.16 shows the appearance of an idealised event as photographed on the dual beam oscilloscope in one of its sensitivity channels. Figures 6.17, 6.18, 6.19, 6.20 and 6.21 give details of the amplifier, discriminator, coincidence unit, fan out and cycling system trigger units shown in the block diagram of the electronics used (figure 6.3).

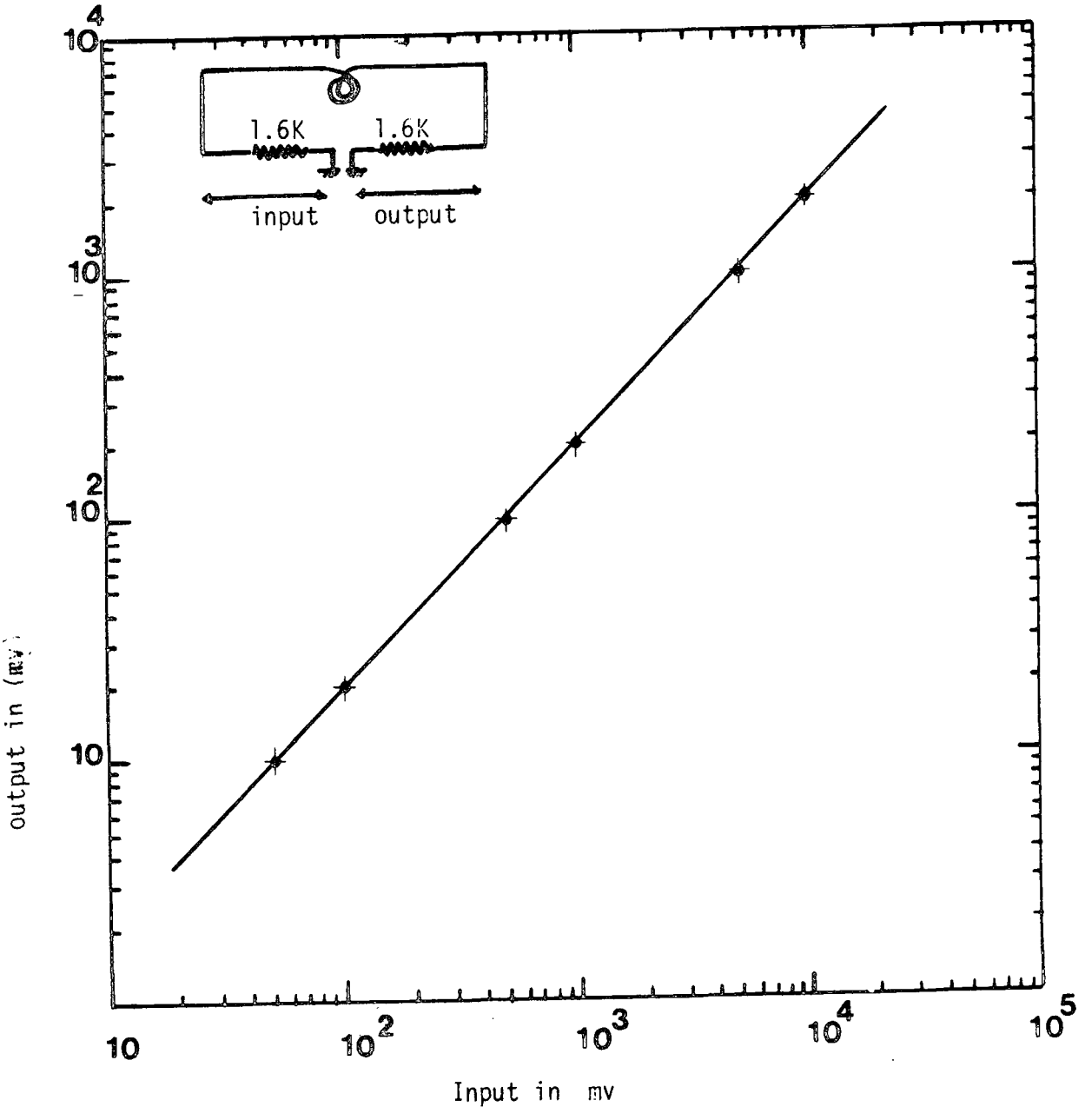

Figure 6.14 : The attenuation of a 2 μs square pulse after transmission down 80 μs of Hackethall HH 1600 delay line.

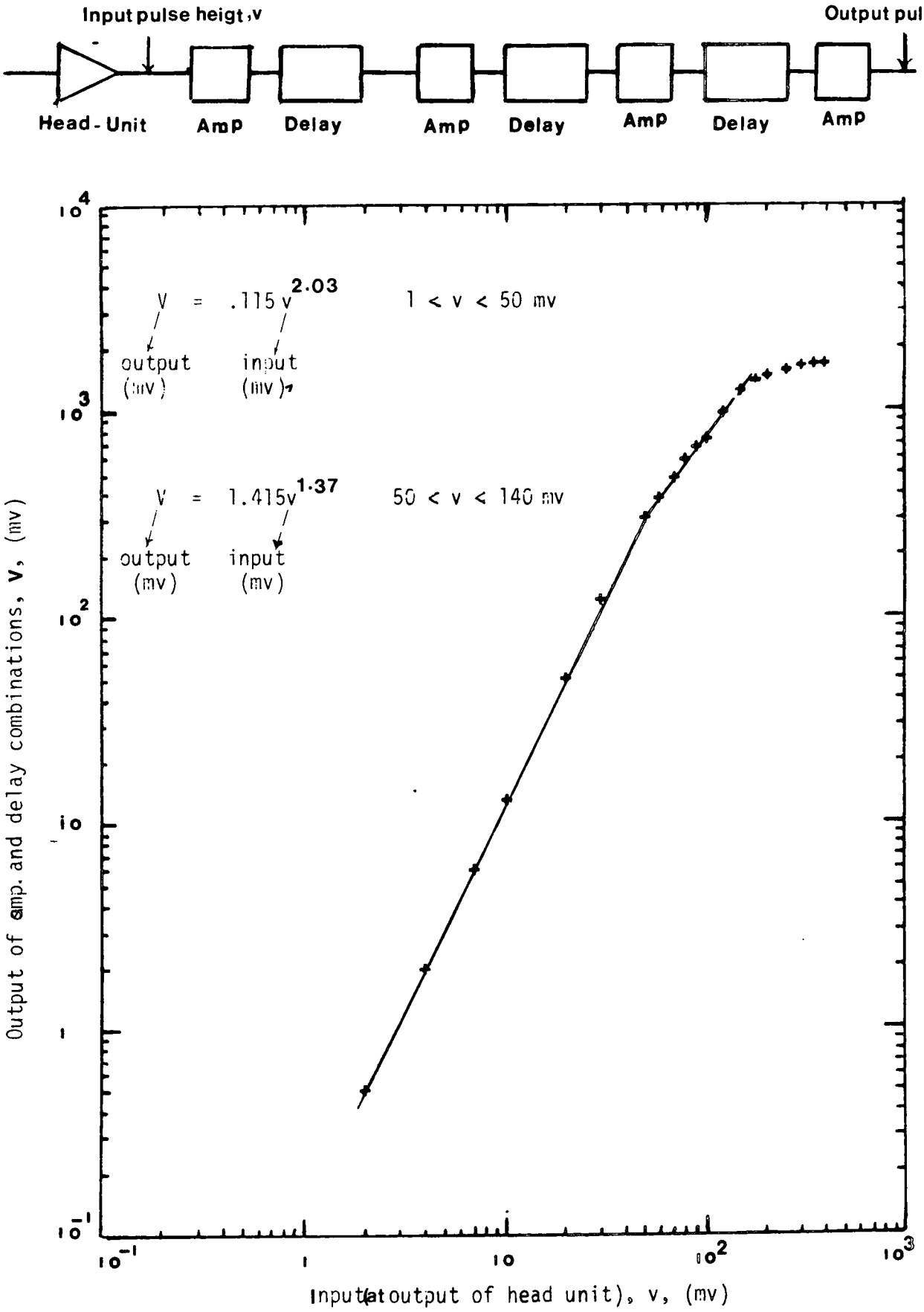

Figure 6.15 : Input/output calibration curve used in the tachyon experiment .

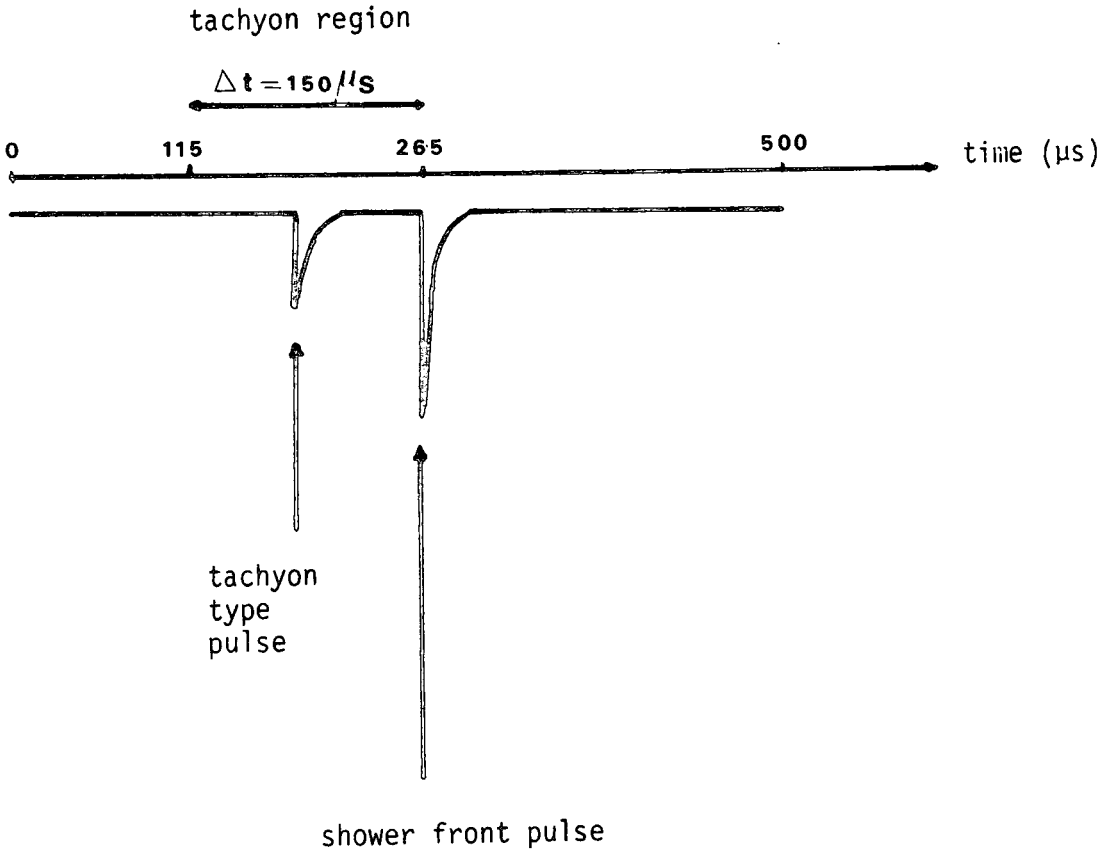

Figure 6.16 : The appearance of an idealised event as photographed on the dual beam oscilloscope in one of its sensitivity channels.

Circuit diagrams for the electronics units used for the experiments described are shown. Unless otherwise stated all values of resistance are quoted in $K\Omega(10^3\Omega)$, all values of capacitance are quoted in $\mu f(10^{-6}F)$, and all transistors used were of the type OC171.

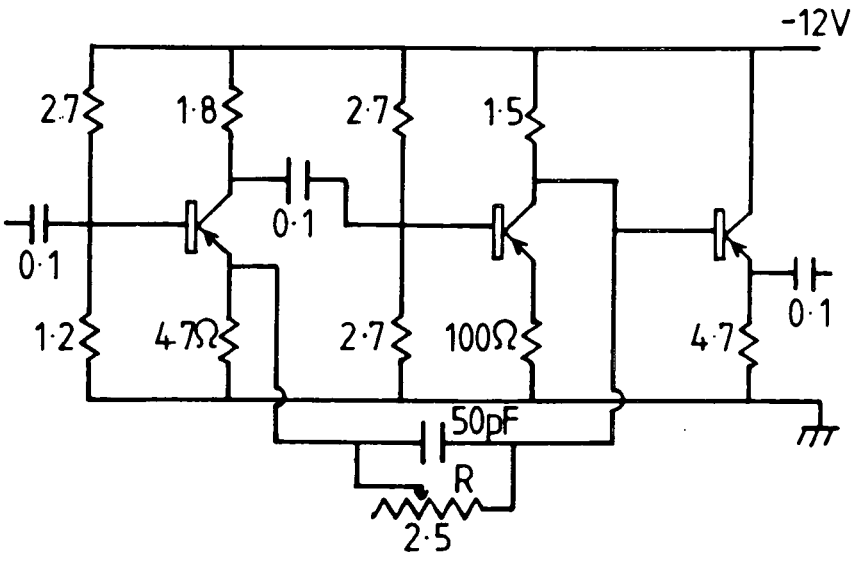

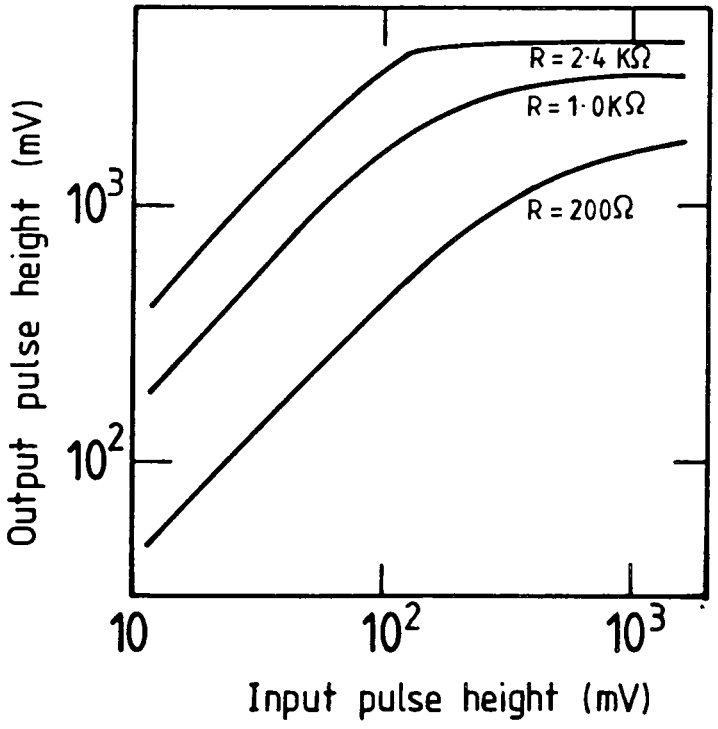

Figure 6.17 : The voltage amplifier and its characteristics for various values of feedback resistance R.
Measurement made using 1 μsecond wide-ve input pulses, from a pulse generator.

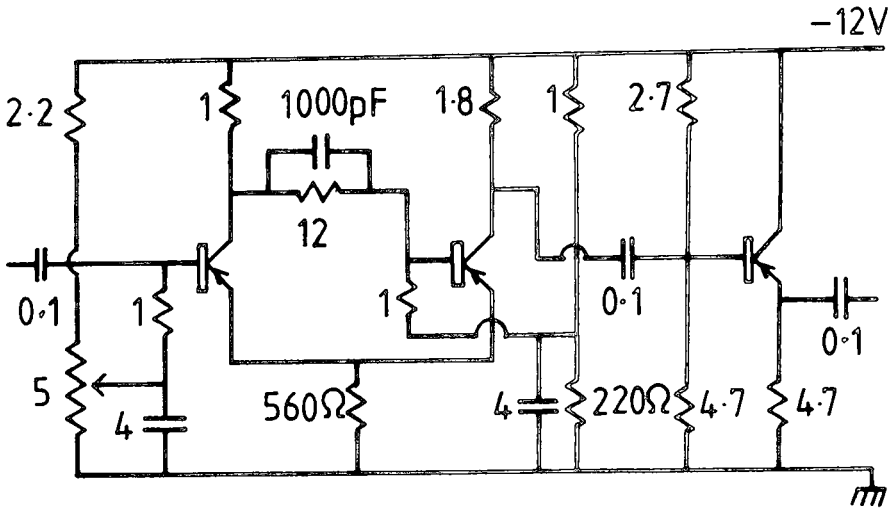

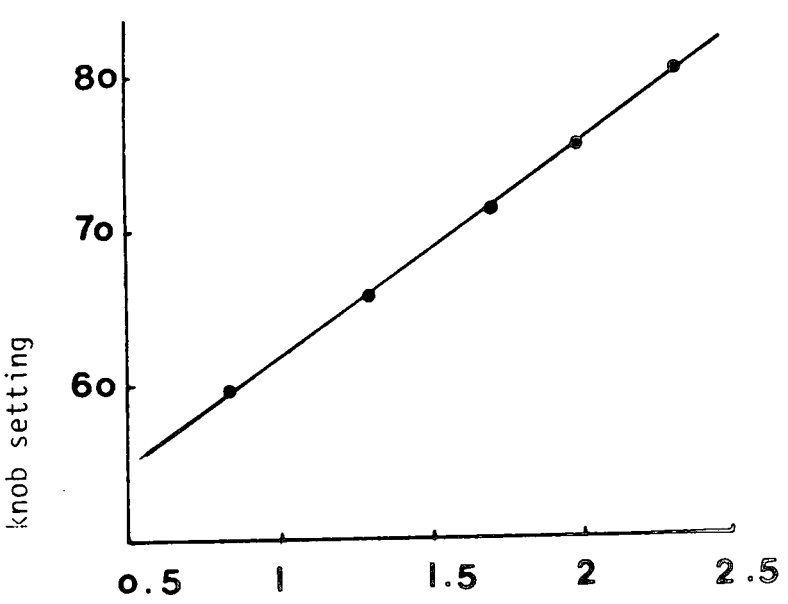

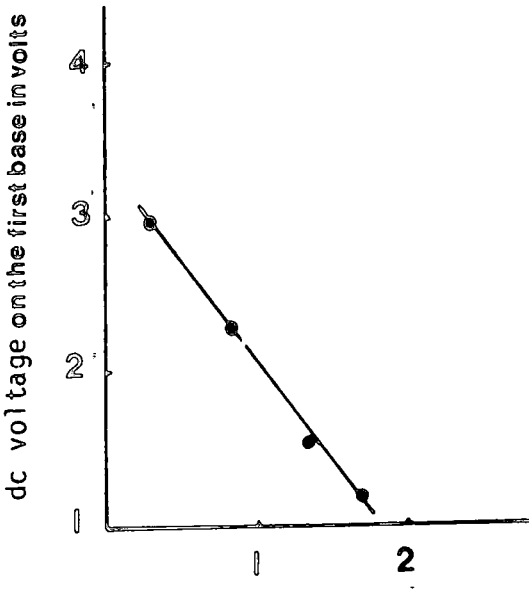

Figure 6.18 : The discriminator circuit and the relationship between the d.c. level on the base of the first transister and the minimum input pulse height required to trigger the circuit and also the relationship between knob setting and minimum input pulse height.
Measurements made using 1 μ second wide - ve input pulses from a pulse generator. For input pulse heights above threshold the output pulse height has the constant value of 5.2 volts independent of input pulse height.

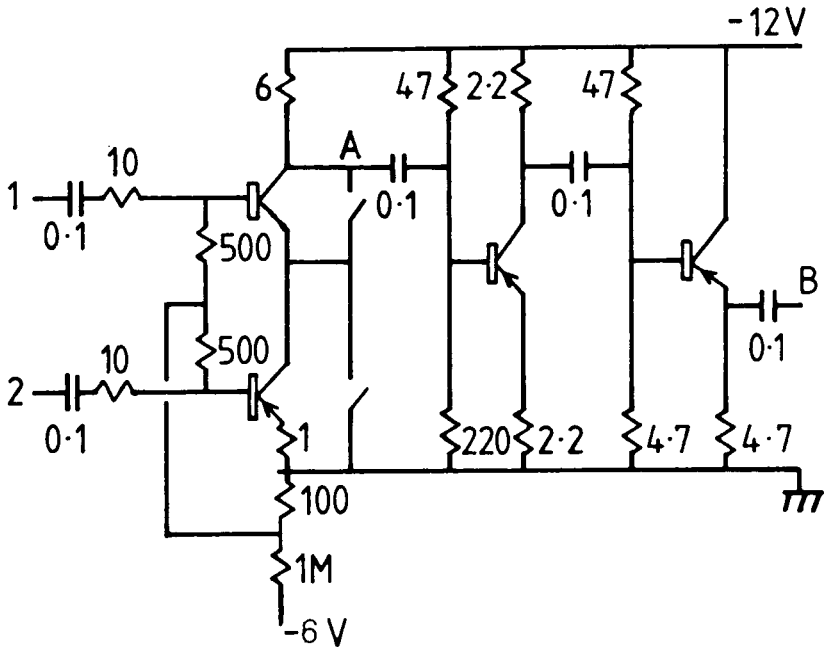

	input from pulse generator	output at **A**		output at **B**		
		1 fold	2 fold	1 fold	2 fold	pulse width
Channel 1	-3 volts	0.0044 volts	+6 volts	-0.03 volts	-4 volts	1μsecond
Channel 2	-3 volts	0.008 volts		-0.015 volts		1μsecond

Figure 6.19 : A two-fold coincidence unit
Table produced by tests using 1 μs wide - 3 volts input pulses using the pulse generator.

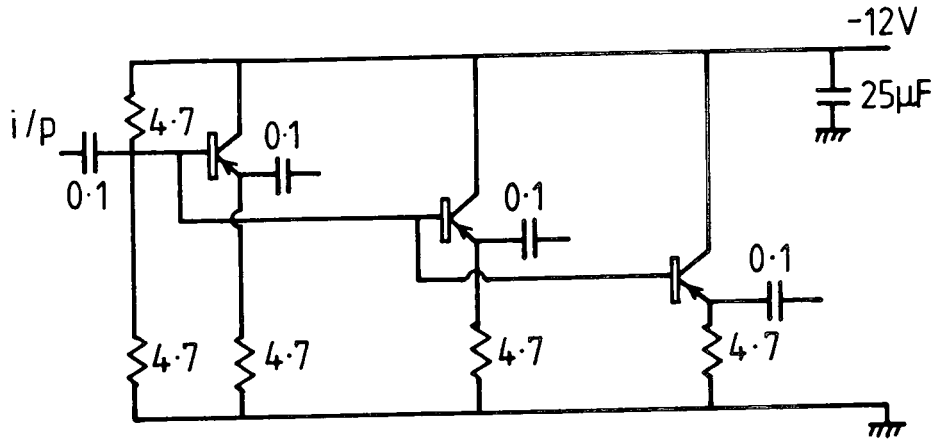

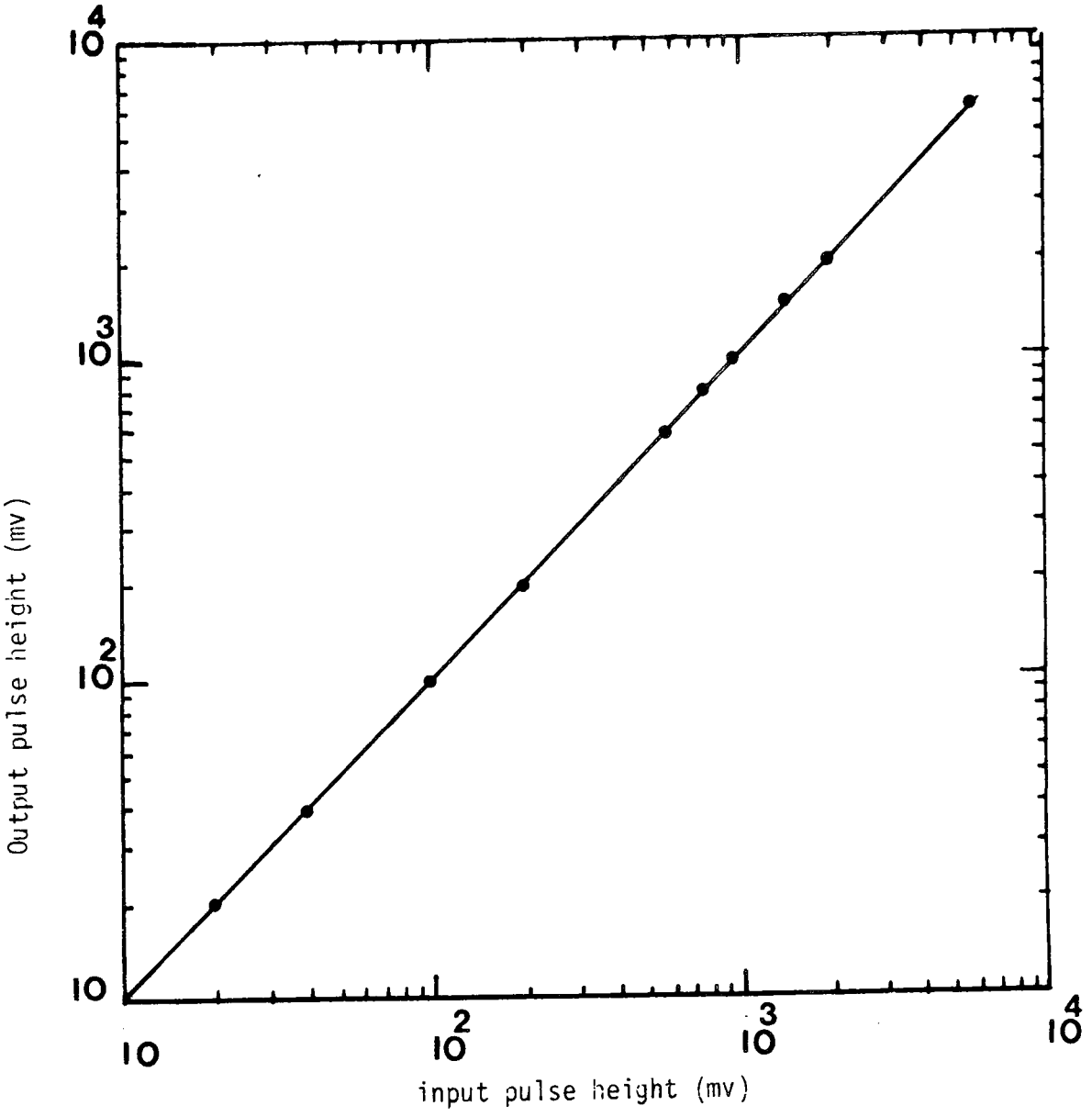

Figure 6.20 : The fan out and its input-output characteristics. Test using 1 μsecond wide - ve input pulses from a pulse generator.

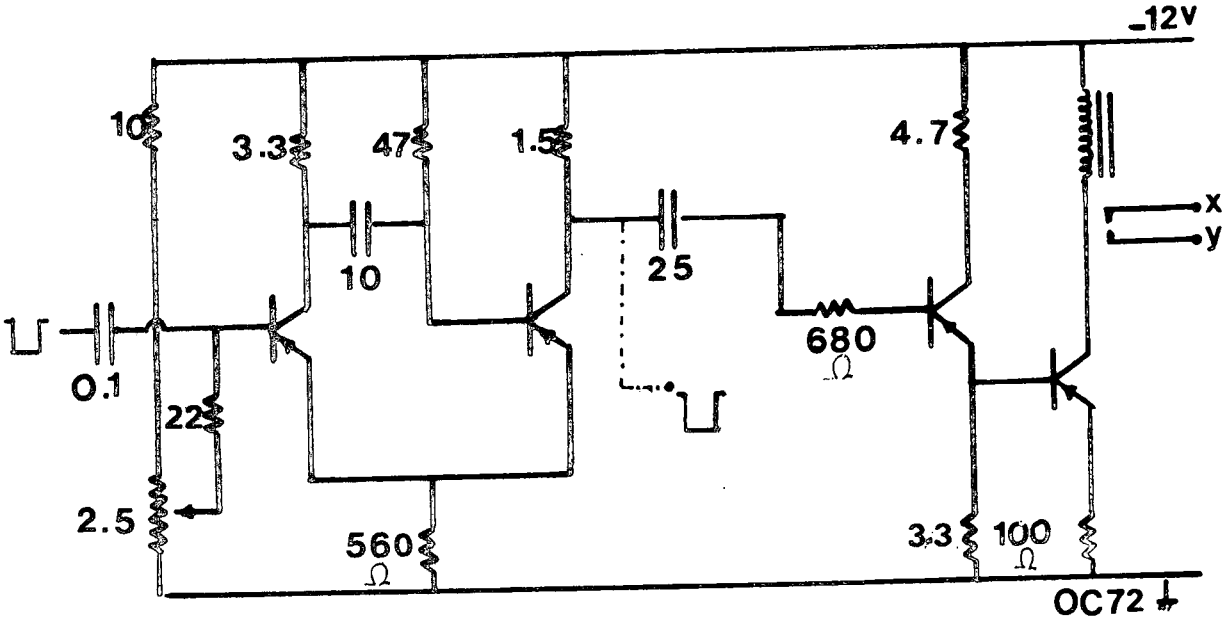

Figure 6.21 : The cycling system trigger.
A -5 volt, 1 μsecond, pulse at the input will close the relay and start the cycling system.
Test using 1μs wide - 3 volt pulses from a pulse generator.
A single short pulse causes x,y to be connected for about 1 second

CHAPTER 7

RESULTS OF THE TACHYON EXPERIMENTS

7.1 INTRODUCTION

As explained in the last chapter any tachyons produced in the interactions of primary cosmic ray protons are expected to arrive at sea level in the 59μs time domain before the arrival of the main shower front for showers incident from the zenith and some time in the preceding 150μs for showers incident at an angle of 60° to the zenith. Unfortunately pulses can also be observed in these time domains due to (a) random thermal noise pulses originating from thermionic emission from the photomultiplier photocathodes (b) background radioactivity (presumably mainly γ rays) from the environment (c) the chance passage of cosmic rays through the detector which are not associated with the detected air shower trigger. The thickness of the tachyon detector phosphor used in the present work is 5 cm so that a relativistic muon traversing the detector at normal incidence will deposit ∿10 MeV energy in the phosphor. In general (a) and (b) are expected to produce very much smaller detected pulse heights than (c).

The types of detected pulse expected from the present detector are shown in figures 7.1a and 7.1b. In all a sample of 1,443 EAS triggers were recorded. Analysis of the oscilloscope photographs showed a significant number of background pulses so a sample of 1,010 photographs were taken in which the oscilloscope time base was triggered at random rather than by the arrival of an EAS so as to have a sample of data from which the true random background could be established. A summary of the basic data used in the present work is shown in table 7.1.

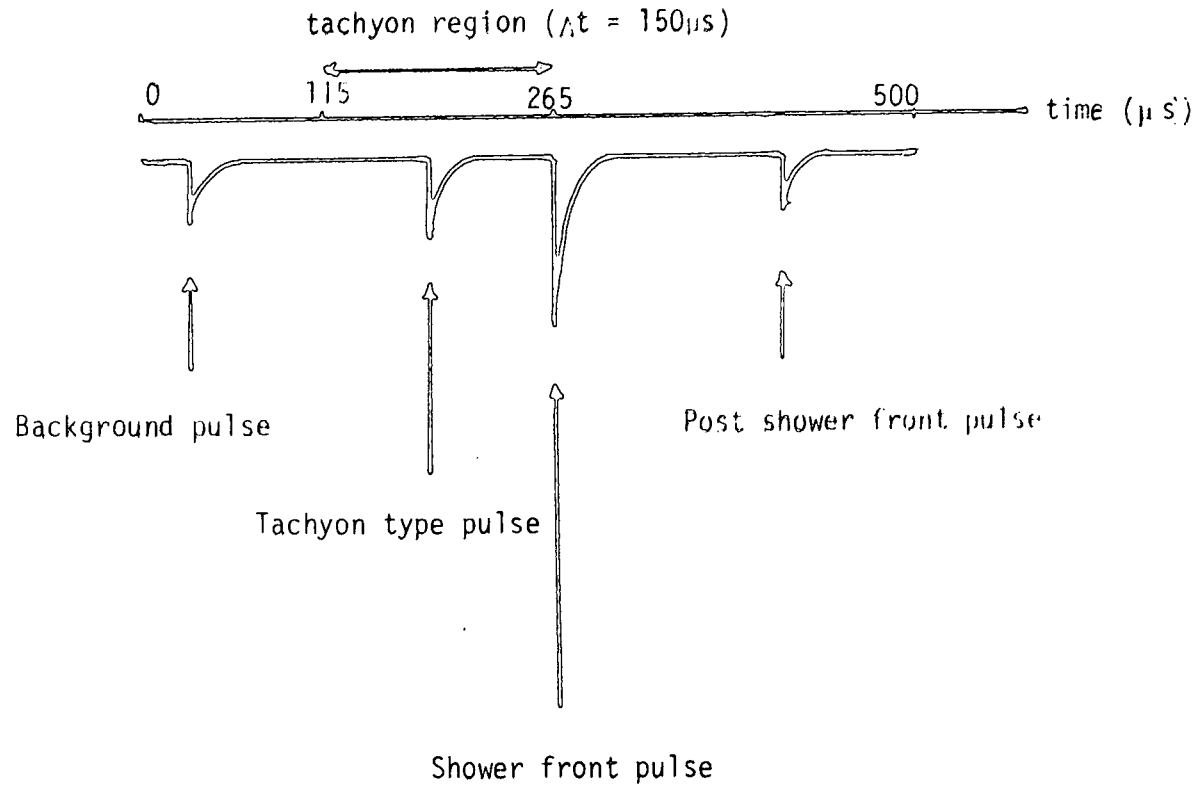

Figure 7.1a: Types of pulse expected to be observed in the present experiment

Figure 7.1b

a) Trace showing two precursor pulses, occurring at 50μs and 140μs prior to the shower front, and one after shower front occurring at 325 μs. Times are measured from the start of the oscilloscope sweep, the shower front pulse occurring at 265 μs as shown in figure 7.1a.

b) Trace showing two precursor pulses, occurring at 25 μs and 180 μs prior to the shower front.

The time between the start of the time base and the arrival of the shower front is 265 μs. The vertical scale is 1 cm : 5 mv.

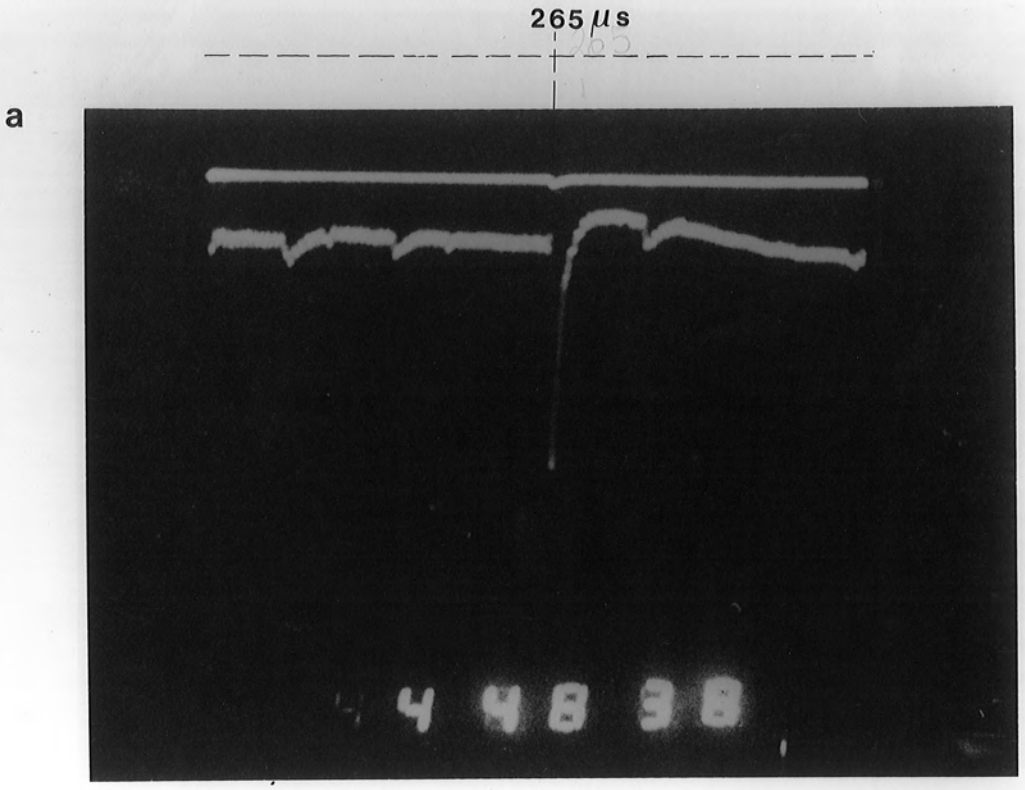
265 μs
a
4 4 8 3 8

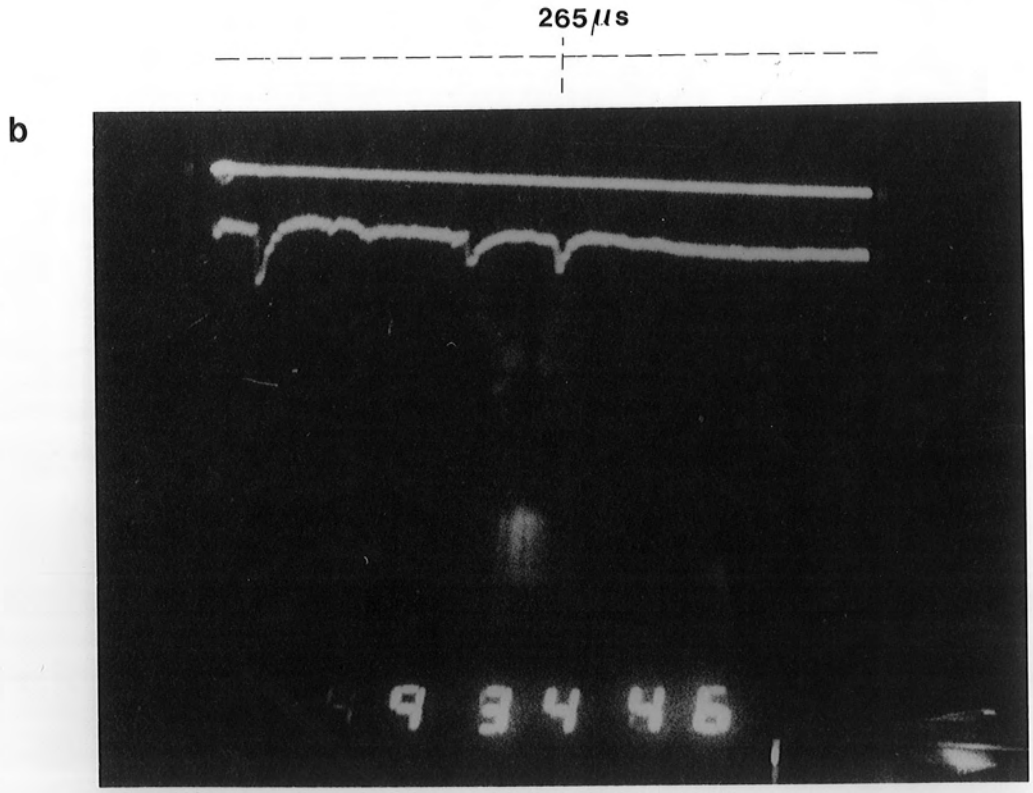
265 μs
b
9 3 4 4 6

Total number of EAS triggers $\Delta_A(\geq 25m^{-2})$. $\Delta_B(\geq 25m^{-2})$	1,443
Running time	114hr 21min 56sec
EAS trigger rate	$(12.62 \pm 0.33)hr^{-1}$
Number of random trigger events used to assess the background	1,010

Table **7**.1 : Summary of basic experimental data

7.2 TIME DISTRIBUTION OF RECORDED PULSE HEIGHTS SELECTED BY THE EAS TRIGGER

The measured time distribution (time measured from the start of the oscilloscope time base) of pulses occurring in different ranges of pulse height measured on the oscilloscope are shown in table **7**.2 and figure **7**.2. Also shown is the corresponding range of energy deposition in the scintillator in terms of 'e' where 'e' is the energy loss (10 MeV) produced by a relativistic muon traversing the scintillator at normal incidence. The amplifiers used in conjunction with the delay lines had a non linear response (figure **6**.15) so the range of pulse height is not linearly related to the range of energy loss. In making the conversion from oscilloscope pulse height to pulse height at the output of the head unit the calibration curve shown in figure **6**.15 was used. To write the pulse height at the output of the head unit in terms of 'e' the average pulse height at the output of the head unit produced by relativistic particles traversing the phosphor at normal incidence was taken to be 30 mv. The way in which the figure of 30 mv was established is described

Time range micro seconds	Number of pulses					
	.5mv≤v≤2mv	2mv<v≤4mv	4mv<v≤30mv	30mv<v≤120 mv	v>120 mv	v≥700mv
0 - 10	5	1	0	0	0	0
10 - 20	13	8	3	2	0	0
20 - 30	3	5	2	0	1	0
30 - 40	10	3	0	3	0	0
40 - 50	8	3	0	0	0	0
50 - 60	16	5	0	0	1	0
60 - 70	5	5	1	0	0	0
70 - 80	13	7	3	1	1	0
80 - 90	9	9	2	0	3	0
90 - 100	8	3	1	2	0	0
100 - 110	7	3	3	0	0	0
110 - 120	8	2	1	1	1	0
120 - 130	9	5	0	1	1	0
130 - 140	7	6	1	5	0	0
140 - 150	10	3	0	1	1	0
150 - 160	10	3	1	1	0	0
160 - 170	10	2	2	1	0	0
170 - 180	14	4	0	1	1	0
180 - 190	32	5	0	0	0	0
190 - 200	9	6	0	0	0	0
200 - 210	8	3	0	0	1	0
210 - 220	4	4	2	0	0	0
220 - 230	14	4	2	1	2	0
230 - 240	3	2	0	0	0	0
240 - 250	5	3	0	0	0	0
250 - 260	2	1	0	0	0	0
260 - 270	260	166	250	145	465	172
270 - 280	5	2	2	1	0	0
280 - 290	5	7	2	1	0	0
290 - 300	8	3	3	2	0	0
300 - 310	4	4	1	1	0	0
310 - 320	4	6	4	1	0	0
320 - 330	13	5	5	3	1	0
330 - 340	4	1	3	1	1	0
340 - 350	6	6	2	1	0	0
350 - 360	5	7	2	5	2	0
360 - 370	7	2	3	2	1	0
370 - 380	12	1	6	1	2	0
380 - 390	3	6	2	6	1	0
390 - 400	3	6	2	0	0	0
400 - 410	16	5	3	0	0	0
410 - 420	8	8	4	1	0	0
420 - 430	7	4	4	2	3	0
430 - 440	10	3	1	1	3	1
440 - 450	10	7	5	1	1	1
450 - 460	13	4	3	0	2	0
460 - 470	8	6	5	0	1	0
470 - 480	12	7	1	1	1	0
480 - 490	10	4	0	0	1	0
490 - 500	3	4	1	0	0	0
	418	212	88	51	33	2

Table 7.2 : Tachyon data. Time distribution of events in different ranges of pulse height (measured on the oscilloscope) from a sample of 1443 shower triggers. The data was analysed using the DATABIN program.

No. of EAS triggers = 1443

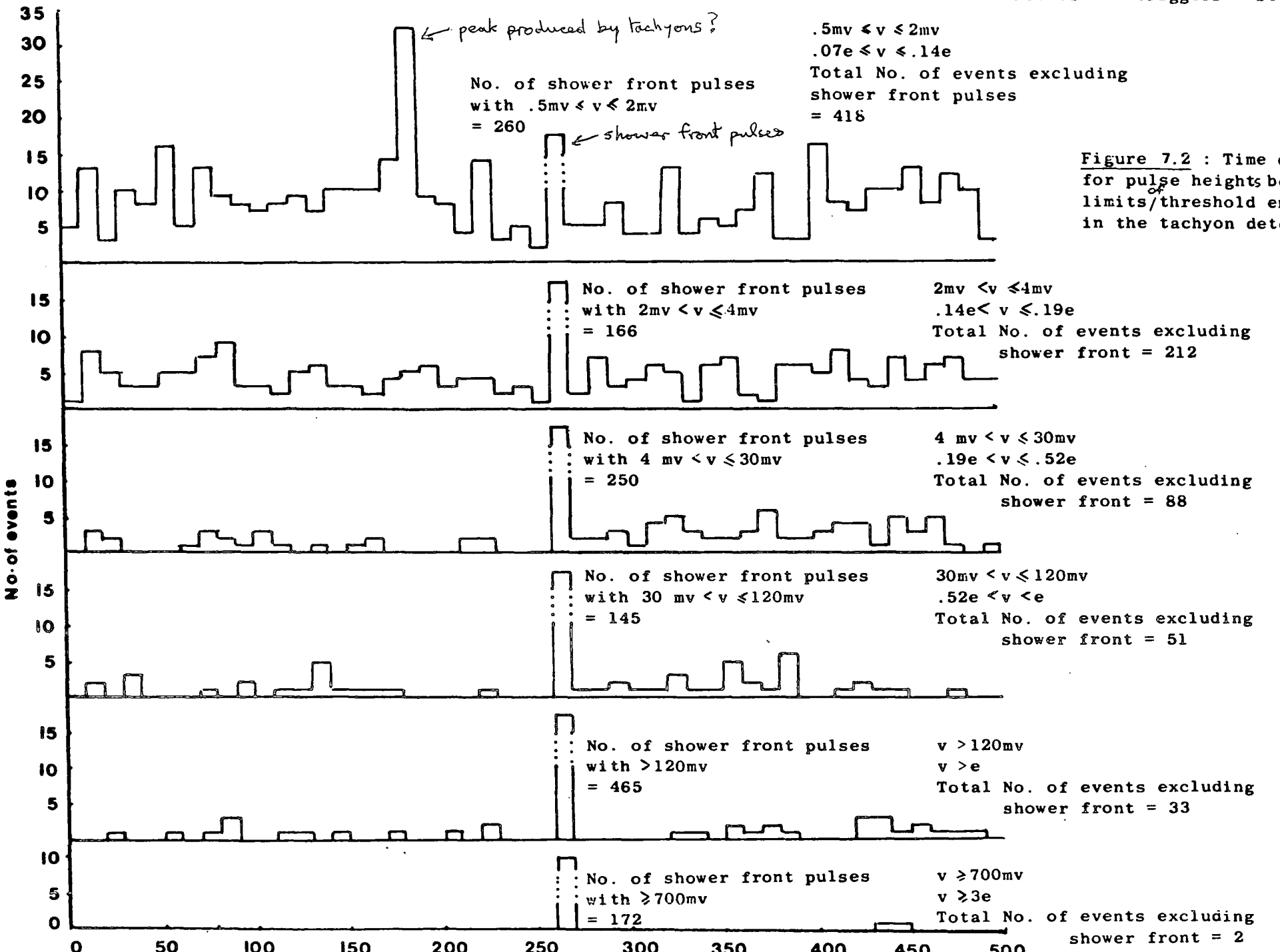

Figure 7.2 : Time distribution for pulse heights between two limits of threshold energy losses in the tachyon detector

in section 7.3. It is shown from figure 7.2 that an excess of events (4.4 standard deviations above the general background level) is observed in the 180-190μs time bin (corresponding to particles that traverse the scintillator in the time domain 75-85μs before the arrival of the shower front) for the smallest range of energy depositions in the tachyon detector investigated. The range of energy deposition of .07e- .14e corresponds to .7 - 1.4 MeV. No other anomalous effects are present in the data. The dip in the general background distribution in the $\sim$30μs time range before the occurrence of the shower front pulse for the .07e- .14e energy loss range is due to an oscillation which precedes the occurrence of large shower front pulses in the tachyon detector. The effect is associated with the properties of the delay lines used in the experiment and has been described previously (Abdullah et al, 1979).

7.3 DISTRIBUTION IN HEIGHT OF THE SHOWER FRONT PULSES

The measured distribution in height of the shower front pulses is shown in table 7.3 and table 7.4 shows how the differential and integral pulse height distributions at the output of the head unit were determined. Plots of the differential and integral pulse height distributions where pulse heights are measured at the output of the head unit are shown in figures 7.3a and 7.3b respectively. It is seen from figure 7.3a that the differential distribution shows a well resolved peak at a pulse height of 30mv and this feature is interpreted as being due to the passage of single muons through the tachyon detector, the muons being part of the air shower front. The value of 30mv established in this way was used in the previous section to obtain an absolute energy calibration in MeV for pulse heights measured in the tachyon detector.

Pulse ht.range on oscillos-cope millivolts	Pulse ht.range at output of head unit millivolts	Frequency
0.5 - 2	2.06 - 4.08	260
2 - 4	4.08 - 5.75	166
4 - 6	5.75 - 7.02	72
6 - 8	7.02 - 8.08	37
8 - 10	8.08 - 9.02	31
10 - 12	9.02 - 9.87	25
12 - 14	9.87 - 10.65	12
14 - 16	10.65 - 11.37	8
16 - 18	11.37 - 12.05	7
18 - 20	12.05 - 12.69	12
20 - 22	12.69 - 13.3	8
22 - 24	13.3 - 13.89	11
24 - 26	13.89 - 14.45	10
26 - 28	14.45 - 14.98	2
28 - 30	14.98 - 15.5	15
30 - 32	15.5 - 16.0	1
32 - 34	16.0 - 16.49	0
34 - 36	16.49 - 16.96	2
36 - 38	16.96 - 17.42	0
38 - 40	17.42 - 17.86	9
40 - 42	17.86 - 18.3	0
42 - 44	18.3 - 18.72	0
44 - 46	18.72 - 19.13	0
46 - 48	19.13 - 19.54	0
48 - 50	19.54 - 19.94	1
50 - 100	19.94 - 28.05	101
100 - 150	28.05 - 34.25	56
150 - 200	34.25 - 39.47	50
200 - 300	39.47 - 48.19	63
300 - 400	48.19 - 61.56	55
400 - 500	61-56 - 72.45	34
500 - 600	72.45 - 82.76	43
600 - 700	82.76 - 92.61	23
700 - 800	92.61 -102.09	12
800 - 900	102.09 -111.26	18
900 - 1000	111.26 -120.15	15
1000 - 1100	120.15 -128.81	17
1100 - 1200	128.81 -146.26	17
1200 - 1400	146.26 -170	51
>1400	>170	42
		1286

"Data bin" is used with

Maximum time	= 530μs
No. of time bins	= 2
Maximum height	= 31.5
No. ht. bin	= 15

Maximum time	= 530μs
No. of time bins	= 2
Maximum height	= 1455
No. of ht. bin	= 29

Table 7.3 : Tachyon data. The distribution in size of the shower front pulse height measured from a sample of 1443 EAS triggers. The DATABIN program was used to analyse the data. The total number of measured pulse heights is shown at the bottom of the column.

Pulse range on oscillos-cope (millivolts)	Pulse ht. range ($\nu_1 \rightarrow \nu_2$) at output of head unit (millivolts)	$\Delta\nu = \nu_2 - \nu_1$ (millivolts)	Mean $\frac{\nu_2+\nu_1}{2}$ (millivolts)	No. of events $N(\nu_1 \rightarrow \nu_2)$ with pulse ht. in range $\nu_1 \rightarrow \nu_2$	Differential frequency $\frac{N(\nu_1 \rightarrow \nu_2)}{\Delta\nu}$ (millivolts)	$N(>\nu_1)$
.5 - 4	2.06 - 5.75	3.69	3.91	$(4.26 \pm .21).10^2$	$(1.15 \pm .06).10^2$	1286
4 - 6	5.75 - 7.02	1.27	6.39	$(7.20 \pm .85).10^1$	$(5.67 \pm .67).10^1$	860
6 - 8	7.02 - 8.08	1.06	7.55	$(3.70 \pm .61).10^1$	$(3.49 \pm .57).10^1$	788
8 - 12	8.08 - 9.87	1.79	8.98	$(5.60 \pm .75).10^1$	$(3.13 \pm .42).10^1$	751
12 - 30	9.87 - 15.50	5.63	12.68	$(8.50 \pm .92).10^1$	$(1.51 \pm .16).10^1$	695
30 - 50	15.50 - 19.94	4.45	17.72	$(1.30 \pm .36).10^1$	$(2.92 \pm .79)$	610
50 - 70	19.94 - 23.53	3.59	21.74	$(3.80 \pm .61).10^1$	$(1.06 \pm .18).10^1$	597
70 - 90	23.53 - 26.63	3.10	25.08	$(3.80 \pm .61).10^1$	$(1.22 \pm .20).10^1$	559
90 - 140	26.63 - 33.11	6.48	29.87	$(8.10 \pm .90).10^1$	$(1.25 \pm .14).10^1$	521
140 - 200	33.11 - 39.47	6.36	36.28	$(5.00 \pm .71).10^1$	(7.86 ± 1.11)	440
200 - 300	39.47 - 48.19	8.73	43.83	$(6.30 \pm .79).10^1$	$(7.22 \pm .91)$	390
300 - 400	48.19 - 61.56	13.37	54.88	$(5.50 \pm .74).10^1$	$(4.11 \pm .55)$	327
400 - 500	61.56 - 72.45	10.89	67.01	$(3.40 \pm .58).10^1$	$(3.12 \pm .53)$	272
500 - 800	72.45 -102.09	29.64	87.27	$(7.80 \pm .88).10^1$	$(2.63 \pm .29)$	238
800 - 1400	102.09 -170	67.91	136.05	$(1.18 \pm .11).10^2$	$(1.73 \pm .16)$	160
>1400	>170					42

Table 7.4 : Shower front pulse height data. Basic data obtained from a sample of 1443 EAS triggers and calculation of the differential and integral spectra of the measured pulse heights.

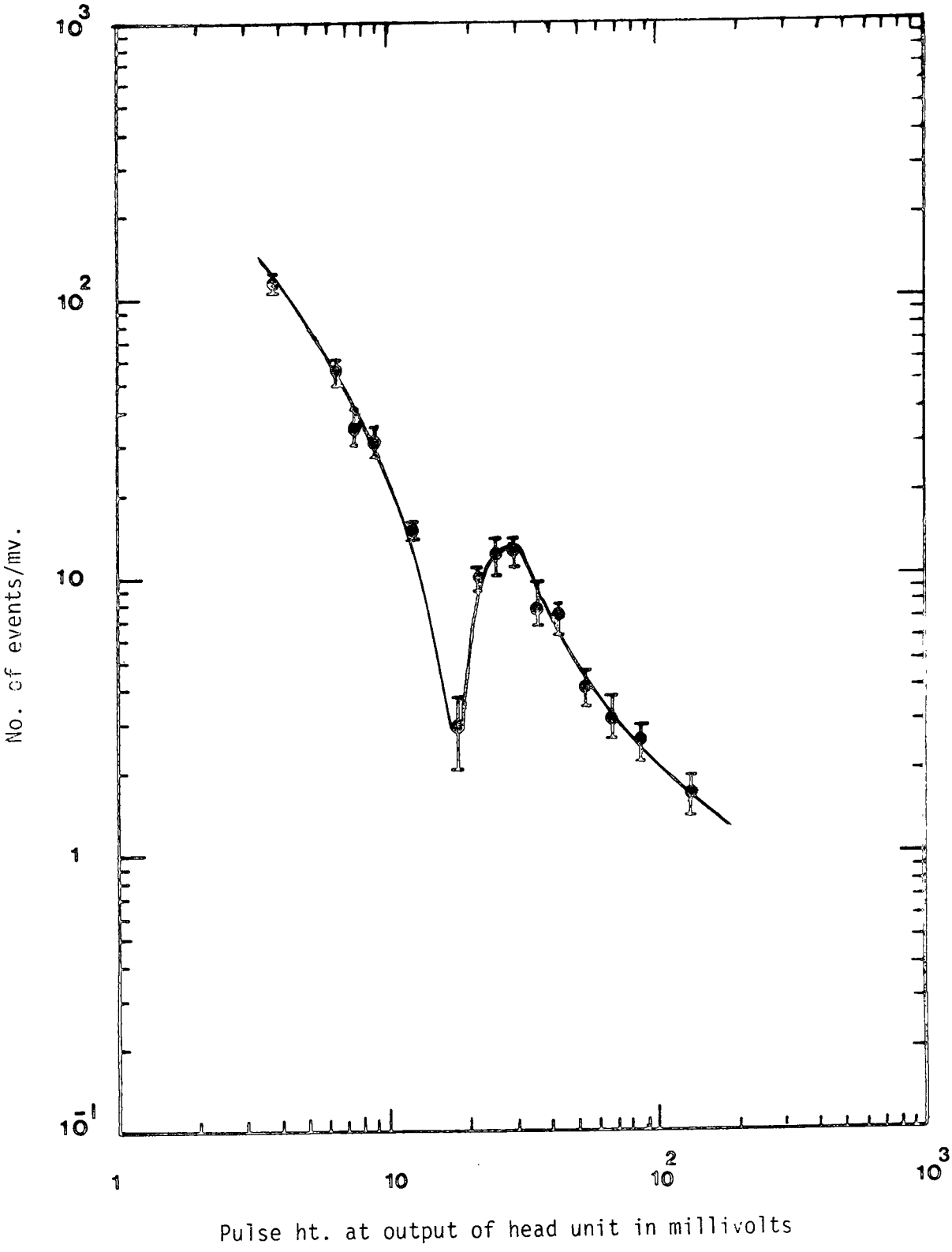

Figure 7.3a Differential distribution of shower front pulse height as measured at the output of the head unit No. of EAS triggers = 1443, total no. of measurable shower front pulse heights = 1286.

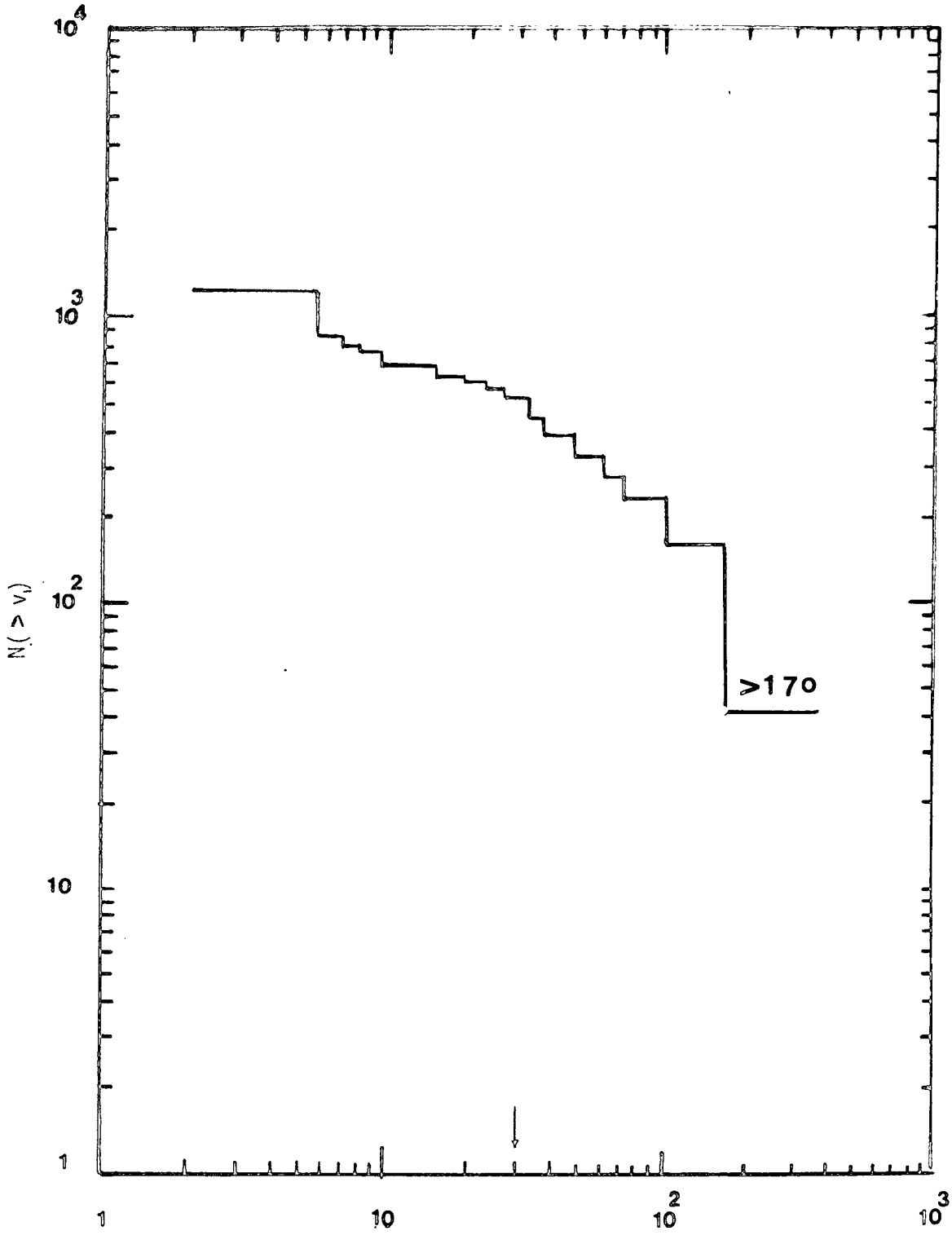

Figure 7. 3b : Integral distribution of shower front pulse ht. as measured at the output of head unit. No. of EAS triggers = 1443, no. of measurable shower front pulse ht. = 1286.

7.4 DISTRIBUTION IN HEIGHT OF PULSES OCCURRING IN THE 265μs TIME DOMAIN BEFORE AND THE 235μs AFTER THE ARRIVAL OF THE EAS SHOWER FRONT

The measured distribution in height of pulses occurring in the 265μs time period before the arrival of the shower front and the 235μs time period after the arrival of the shower front are shown in table 7.5. Using the data in table 7.5 the differential and integral pulse height distributions for the two time domains separately and for both of them lumped together are evaluated in tables 7.6, 7.7 and 7.8. These results are plotted in figures 7.4, 7.5 and 7.6 and it is seen that in each case there is a well resolved peak occurring at a pulse height of 30 mv at the output of the head unit. This is consistent with the events in the peak being produced by cosmic ray muons which are not correlated with the EAS trigger traversing the detector in the relevant time periods. Figures 7.7 and 7.8 show similar plots for the integral distributions in the time domains indicated on the figures. It is noted that if n pulses of size $>\nu$ at the output of the head unit are observed to occur in the time domain Δt in a sample of N time base triggers then the absolute rate of pulses from the detector of size $>\nu$ is given by $R(>\nu) = \frac{n}{N.\Delta t}$ sec^{-1}. In this way the integral pulse height distribution at the output of the head unit found using the background measurements can be compared directly with that found using an amplifier, discriminator and scaler. Such a comparison is shown in figure 7.8 and the two methods of obtaining the absolute integral pulse height distribution at the output of the head unit are seen to be in good agreement.

Pulse ht.range on oscillos-cope millivolts	Pulse ht.range at output of head unit millivolts	N(<265 μs)	N(>265 μs)	N(0 - 500 μs)
0.5 - 2	2.06 - 4.08	243	175	418
2 - 4	4.08 - 5.75	104	108	212
4 - 6	5.75 - 7.02	12	22	34
6 - 8	7.02 - 8.08	6	11	17
8 - 10	8.08 - 9.02	1	9	10
10 - 12	9.02 - 9.87	1	8	9
12 - 14	9.87 - 10.65	0	3	3
14 - 16	10.65 - 11.37	1	1	2
16 - 18	11.37 - 12.05	1	0	1
18 - 20	12.05 - 12.69	0	3	3
20 - 22	12.69 - 13.3	1	2	3
22 - 24	13.3 - 13.89	1	0	1
24 - 26	13.89 - 14.45	0	3	3
26 - 28	14.45 - 14.98	0	2	2
28 - 30	14.98 - 15.5	1	3	4
30 - 32	15.5 - 16.0	0	1	1
32 - 34	16.0 - 16.49	0	1	1
34 - 36	16.49 - 16.96	0	0	0
36 - 38	16.96 - 17.42	0	0	0
38 - 40	17.42 - 17.86	1	2	3
40 - 42	17.86 - 18.3	0	1	1
42 - 44	18.3 - 18.72	0	0	0
44 - 46	18.72 - 19.13	0	0	0
46 - 48	19.13 - 19.54	0	0	0
48 - 50	19.54 - 19.94	0	0	0
50 - 100	19.94 - 28.05	16	25	41
100 - 150	28.05 - 34.25	2	3	5
150 - 200	34.25 - 39.47	1	10	11
200 - 300	39.47 - 48.19	3	1	4
300 - 400	48.19 - 61.56	3	1	4
400 - 500	61-56 - 72.45	0	3	3
500 - 600	72.45 - 82.76	2	2	4
600 - 700	82.76 - 92.61	0	1	1
700 - 800	92.61 -102.09	0	0	0
800 - 900	102.09 -111.26	0	1	1
900 - 1000	111.26 -120.15	0	0	0
1000 - 1100	120.15 -128.81	0	0	0
1100 - 1200	128.81 -146.26	0	0	0
1200 - 1400	146.26 -170	0	0	0
>1400	>170	0	0	0
		400	402	802

"Data bin" is used with

Maximum time	= 530μs	Maximum time	= 530μs
No. of time bins	= 2	No. of time bins	= 2
Maximum height	= 31.5	Maximum height	= 1455
No. ht. bin	= 15	No. of ht. bin	= 29

Table 7.5 : Tachyon data. Pulse height distribution obtained from a sample of 1443 EAS triggers, N(<265μs) is the number of events observed in the first 265μs of the oscilloscope sweep of 500μs and N(>265μs) is the number observed in the final 235μs. N(0-500μs) = N(<265μs) + N(>265 μs). The total number of measured pulse heights is shown at the bottom of each column. The data was analysed using the DATABIN program. Shower front pulse heights (whose leading edge starts at 265μs from the start of the trace) are not included in the data presented in the table.

Pulse ht. range on oscillos-cope (millivolts)	Pulse ht. range ($\nu_1 \rightarrow \nu_2$) at output of head unit (millivolts)	$\Delta\nu = \nu_2 - \nu_1$ (millivolts)	Mean $= \frac{\nu_2 + \nu_1}{2}$ (millivolts)	No. of events $N(\nu_1 \rightarrow \nu_2)$ with pulse ht. in range $\nu_1 \rightarrow \nu_2$	Differential frequency $= \frac{N(\nu_1 \rightarrow \nu_2)}{\Delta\nu}$ per millivolt	$N(>\nu_1)$	Integral rate $>\nu_1$ per sec.
.5 - 4	2.06- 5.75	3.69	3.91	347 ± 18.62	(9.40±.50).10	400	(1.05±.05)·10^3
4 - 6	5.75- 7.02	1.27	6.39	12 ± 3.46	(9.45±2.72)	53	(1.39±.02).10^2
6 - 8	7.02- 8.08	1.06	7.55	6 ± 2.44	(5.66±2.31)	41	(1.07±.16).10^2
8 - 12	8.08- 9.87	1.78	8.98	2 ± 1.41	(1.12±.79)	35	(9.15±1.53).10^1
12 - 20	9.87-12.69	2.83	11.28	2 ± 1.41	(7.07±4.98).10^{-1}	33	(8.61±1.50).10^1
20 - 50	12.69-19.94	7.25	16.32	4 ± 2.00	(5.52±2.76).10^{-1}	31	(8.11±1.46).10^1
50 - 90	19.94-26.63	6.69	23.29	14 ± 3.74	(2.09±.56)	27	(7.06±1.36).10^1
90 - 100	26.63-28.05	1.42	27.34	2 ± 1.41	(1.41±.99)	13	(3.41±.94).10^1
100 - 200	28.05-39.47	11.42	33.76	3 ± 1.73	(2.63±1.51).10^{-1}	11	(2.88±.86).10^1
200 - 300	39.47-48.19	8.72	43.83	3 ± 1.73	(3.44±1.98).10^{-1}	8	(2.09±.74).10^1
300 - 400	48.19-61.56	13.38	54.87	3 ± 1.73	(2.24±1.29).10^{-1}	5	(1.31±.58).10^1
400 - 800	61.56-102.09	40.53	81.83	2 ± 1.41	(4.93±3.48).10^{-2}	2	(5.23±3.70)
800 - 1400	102.09-170	44.17	124.18	0			
>1400	>170			0			

Table 7.6 : The measured pulse height distribution of pulses observed in the 265 μs period before the arrival of the shower front pulse and determination fo their differential size distribution and their integral rate distribution

Pulse ht. range on oscillos-cope (millivolts)	Pulse ht. range ($\nu_1 \rightarrow \nu_2$) at output of head unit (millivolts)	$\Delta\nu = \nu_2 - \nu_1$ (millivolts)	Mean $= \frac{\nu_2 + \nu_1}{2}$ (millivolts)	No. of events $N(\nu_1 \rightarrow \nu_2)$ with pulse ht. in range $\nu_1 \rightarrow \nu_2$	Differential frequency $= \frac{N(\nu_1 \rightarrow \nu_2)}{\Delta\nu}$ per millivolt	$N(>\nu_1)$	Integral rate $>\nu_1$ per sec.
.5 - 4	2.06- 5.75	3.69	3.91	283 ± 16.83	$(7.67\pm.46).10^1$	402	$(1.19\pm.06).10^3$
4 - 6	5.75- 7.02	1.27	6.39	22 ± 4.69	$(1.73\pm.37).10^1$	119	$(3.51\pm.32).10^2$
6 - 8	7.02- 8.08	1.06	7.55	11 ± 3.31	$(1.04\pm.31).10^1$	97	$(2.86\pm.29).10^2$
8 - 12	8.08- 9.87	1.78	8.98	17 ± 4.12	(9.55 ± 2.3)	86	$(2.54\pm.27).10^2$
12 - 20	9.87-12.69	2.83	11.28	7 ± 2.64	$(2.47\pm.90)$	69	$(2.03\pm.08).10^2$
20 - 50	12.69-19.94	7.25	16.32	15 ± 3.87	$(2.07\pm.53)$	62	$(1.83\pm.23).10^2$
50 - 90	19.94-26.63	6.69	23.29	18 ± 4.24	$(2.69\pm.63)$	47	$(1.39\pm.20).10^2$
90 - 100	26.63-28.05	1.42	27.34	7 ± 2.64	(4.93 ± 1.86)	29	$(8.55\pm1.59).10^1$
100 - 150	28.05-34.25	6.20	31.15	3 ± 1.73	$(4.84\pm2.79).10^1$	22	$(6.49\pm1.38).10^1$
150 - 200	34.25-39.47	5.22	36.85	10 ± 3.16	$(1.92\pm.61)$	19	$(5.60\pm1.29).10^1$
200 - 400	39.47-61.56	22.09	50.51	2 ± 1.41	$(9.05\pm6.38).10^2$	9	$(2.65\pm.88).10^1$
400 - 800	61.56-102.09	40.53	81.83	6 ± 2.45	$(1.48\pm.59).10^1$	7	$(2.06\pm.78).10^1$
800 - 1400	102.09-170	44.17	124.18	1 ± 1.00	$(2.26\pm2.26).10^2$	1	(2.95 ± 2.95)
>1400	>170			0			

Table 7.7 : The measured pulse height distribution of pulses observed in the 235 μs period after the arrival of the shower front pulse and determination of their differential size distribution and their integral rate distribution.

Pulse ht. range on oscillos-cope (millivolts)	Pulse ht. range ($\nu_1 \rightarrow \nu_2$) at output of head unit (millivolts)	$\Delta\nu = \nu_2 - \nu_1$ (millivolts)	Mean $= \frac{\nu_2 + \nu_1}{2}$ (millivolts)	No. of events $N(\nu_1 \rightarrow \nu_2)$ with pulse ht. in-range $\nu_1 \rightarrow \nu_2$	Differential frequency $= \frac{N(\nu_1 \rightarrow \nu_2)}{\Delta\nu}$ per millivolt	$N(>\nu_1)$	Integral rate $>\nu_1$ per sec.
.5 - 4	2.06- 5.75	3.69	3.91	630±25.10	$(1.71\pm.07).10^2$	802	$(1.11\pm.04).10^3$
4 - 6	5.75- 7.02	1.27	6.39	34±5.83	$(2.68\pm.46).10^1$	172	$(2.38\pm.18).10^2$
6 - 8	7.02- 8.08	1.06	7.55	17±4.12	$(1.60\pm.39).10^1$	138	$(1.91\pm.16).10^2$
8 - 12	8.08- 9.87	1.78	8.98	19±4.35	$(1.07\pm.24).10^1$	121	$(1.68\pm.15).10^2$
12 - 20	9.87-12.69	2.83	11.28	9±3	(3.18 ± 1.06)	102	$(1.41\pm.14).10^2$
20 - 50	12.69-19.94	7.25	16.32	19±4.36	$(2.62\pm.60)$	93	$(1.29\pm.13).10^2$
50 - 90	19.94-26.63	6.69	23.29	32±5.65	$(4.78\pm.84)$	74	$(1.03\pm.12).10^2$
90 - 100	26.63-28.05	1.42	27.34	9±3	(6.33 ± 2.11)	42	$(5.82\pm.89).10^1$
100 - 150	28.05-34.25	6.20	31.15	5±2.24	$(8.06\pm3.61).10^{\bar{1}}$	33	$(4.57\pm.79).10^1$
150 - 200	34.25-39.47	5.22	36.85	11±3.31	$(2.11\pm.63)$	28	$(3.88\pm.73).10^1$
200 - 300	39.47-48.19	8.72	43.83	4±2	$(4.58\pm2.29).10^{\bar{1}}$	17	$(2.36\pm.57).10^1$
300 - 400	48.19-61.56	13.38	54.87	4±2	$(2.99\pm1.49).10^{\bar{1}}$	13	$(1.80\pm.50).10^1$
400 - 800	61.56-102.09	40.53	81.83	8±2.82	$(1.97\pm0.69).10^{\bar{1}}$	9	$(1.25\pm.41).10^1$
800 - 1400	102.09-170	44.17	124.18	1±1	$(2.26\pm2.26).10^{\bar{2}}$	1	(1.39 ± 1.39)
>1400	>170			0			

Table 7.8 : The measured pulse height distribution of pulses observed in the 265 μs period before and the 235 μs period after the arrival of the shower front pulse and determination of their differential size distribution and their integral rate distribution.

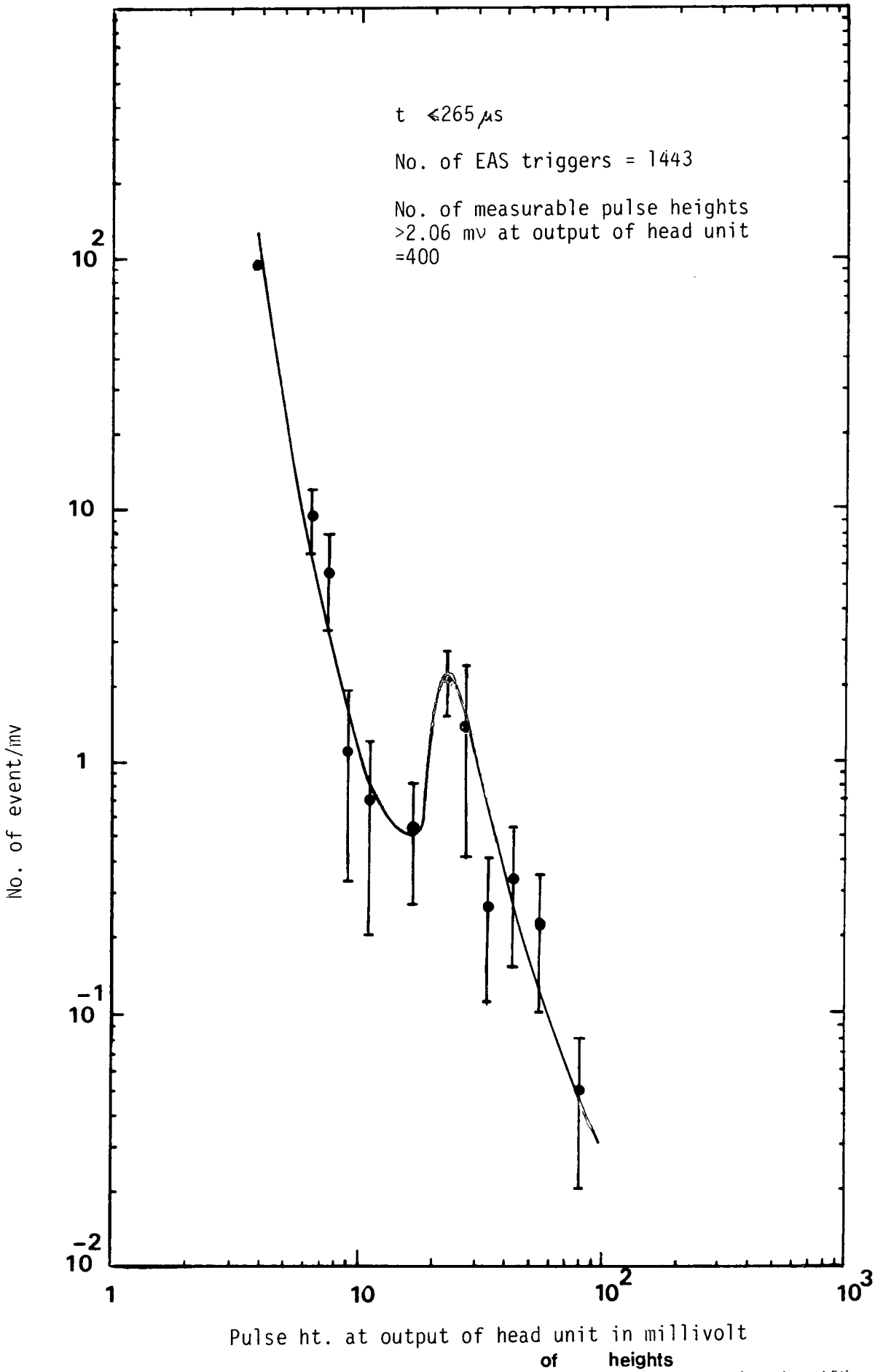

Figure 7.4 : The differential distribution of pulse heights occurring in the 265μs period before the arrival of the shower front pulse at the output of head unit.

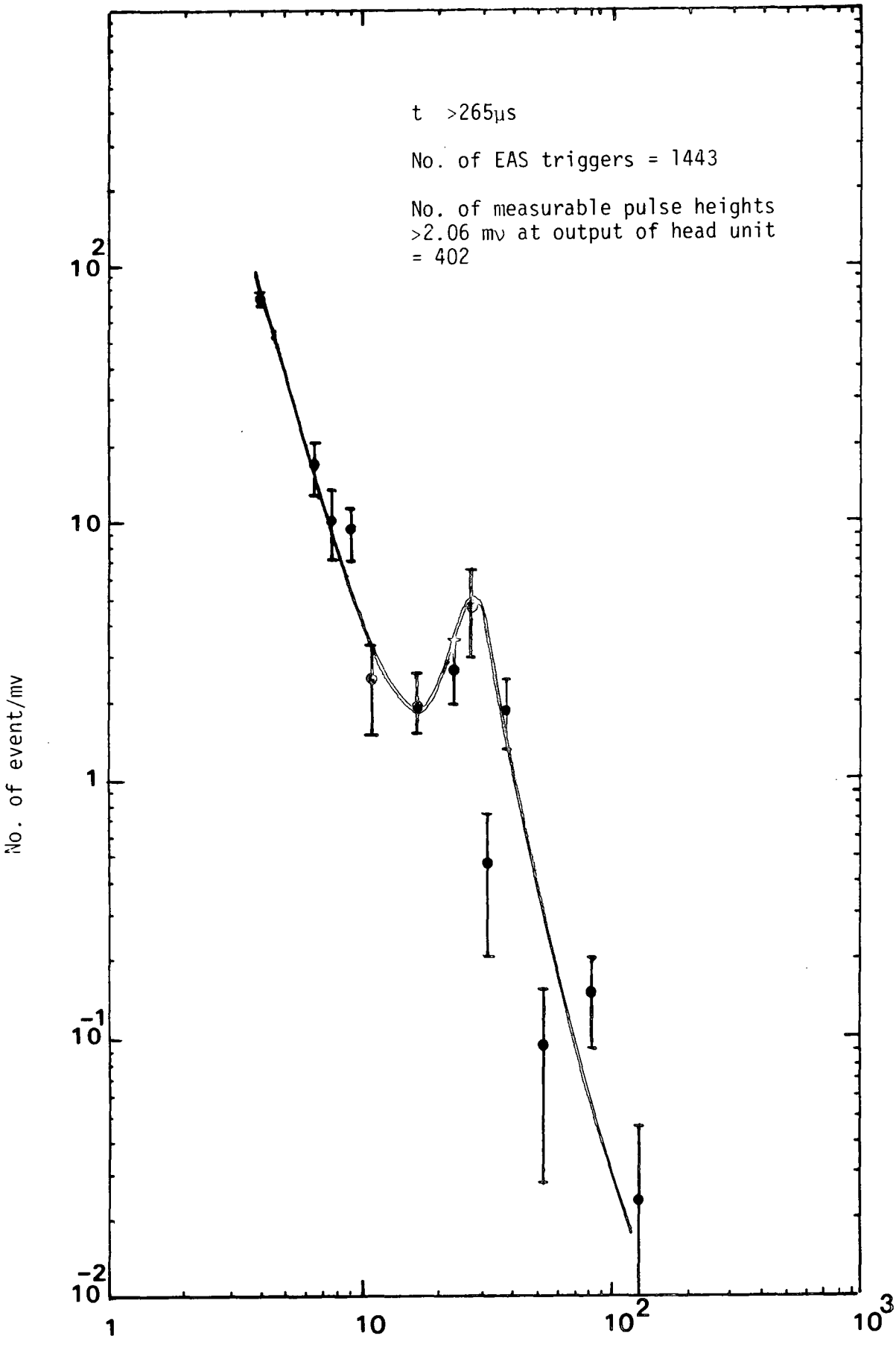

Figure 7.5 : The differential distribution of pulse heights occurring in the 235 μs period after the arrival of the shower front pulse at the output of head unit.

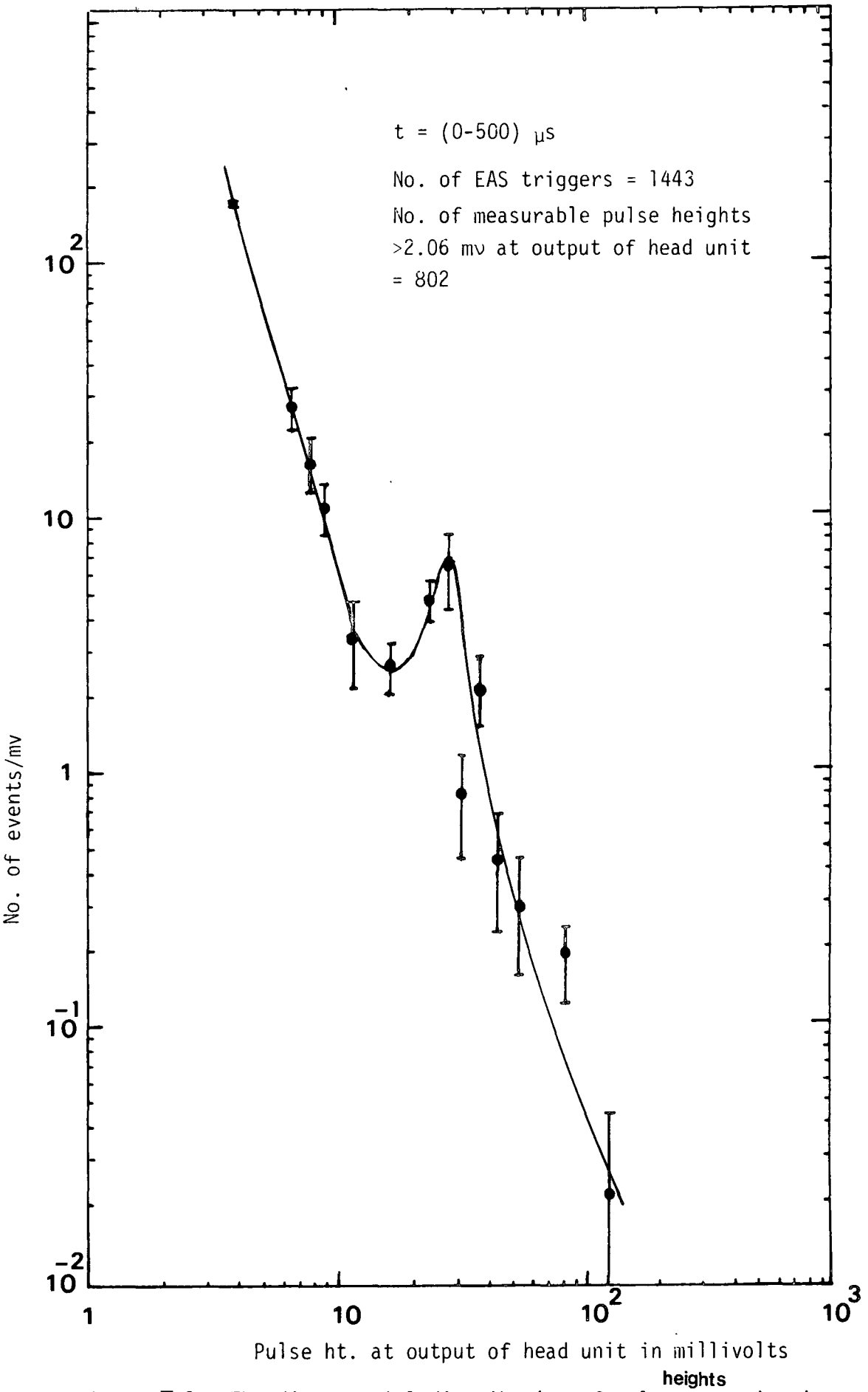

Figure 7.6 : The differential distribution of pulse heights occurring in the 265 μs period before the shower front and 235 μs after the arrival of the shower front at the output of head unit.

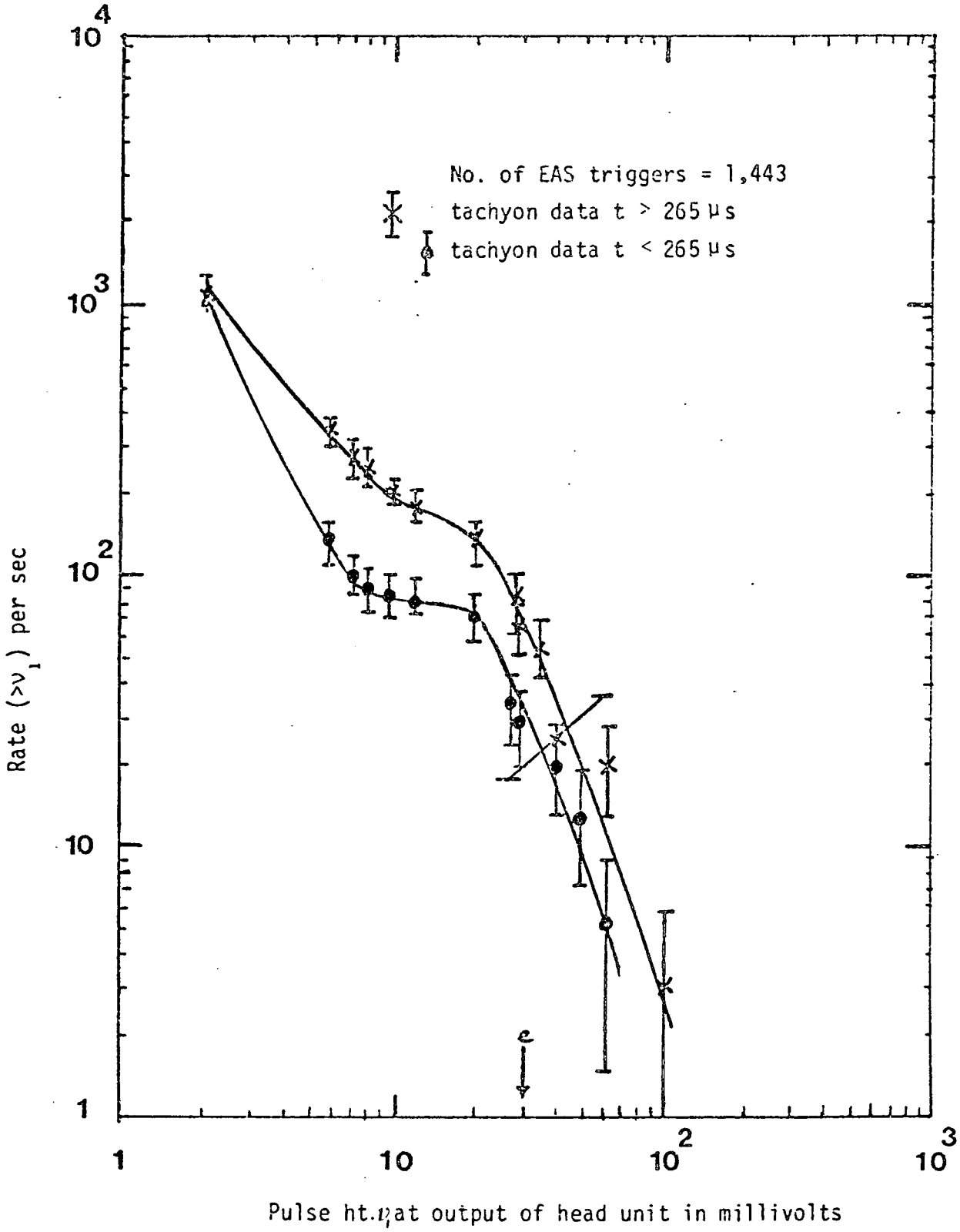

Figure 7.7 The integral rate of pulses of size $>\nu_1$ at the output of the head unit as a function of ν_1 determined from (a) pulses observed in the 265 μs period before the arrival of the shower front and (b) in the 235 μs period after the arrival of the shower front pulse for a sample of 1443 shower triggers. The two distributions should in principle agree exactly (they do for the smallest threshold pulse height of 2mv) and the difference between them is attributed to sampling fluctuations. The pulse height produced by relativistic muons traversing the phosphor at normal incidence is indicated by the arrow.

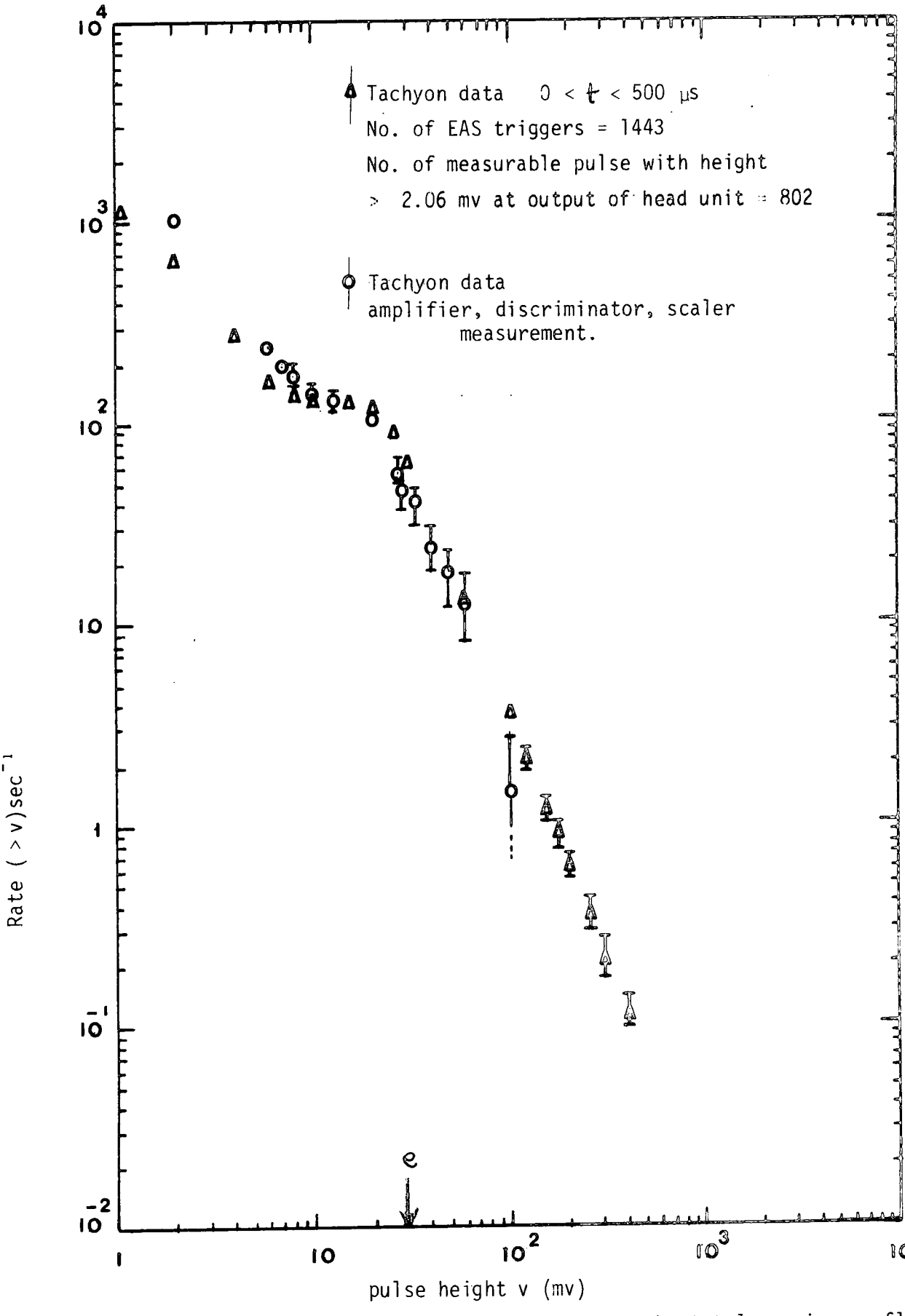

Figure 7.8 : Response of the tachyon detector to the total cosmic ray flux. Integral rate of pulse of height > v millivolts (measured at the output of head unit) versus pulse height v. The average pulse height produced by relativistic muons traversing the detector at normal incidence is 30mv and is indicated on the graph with e.

7.5 RANDOM TRIGGER DATA

As mentioned previously a sample of 1,010 oscillograph photographs were taken in which the oscilloscope time base was triggered at random rather than by using the EAS master coincidence pulse. This work was done to establish the true background and the data has been analysed in exactly the same way as for the EAS trigger data. The time distribution (time measured from the start of the oscilloscope time base) of pulses occurring in different ranges of pulse height measured on the oscilloscope are shown in table 7.9 and figure 7.9. Figure 7.9 also shows the corresponding range of energy deposition in the scintillator in terms of 'e' where 'e' is the energy loss (10 MeV) produced by a relativistic muon traversing the scintillator at normal incidence. It is seen from figure 7.9 that a slight excess above background is observed in the 170-180μs time bin (corresponding to particles that traverse the scintillator in the time domain 85-95μs before the arrival of the shower front) for the smallest range of energy depositions in the tachyon detector investigated. However the excess is of considerably less significance compared to the anomalous peak shown in figure 7.2 for the EAS trigger data which occurs in the 180-190μs time bin. Table 7.10 shows the distribution in pulse height of the observed background pulses over the whole 500μs time range of the oscilloscope sweep, as well as the distribution in the first 265μs and the final 235μs shown separately. The latter distributions were measured so as to give a direct comparison with the tachyon data. Table 7.11 shows details of how the differential and integral pulse height distributions were determined. Figures 7.10 and 7.11 show plots of the measured differential pulse height distribution which shows a well resolved peak produced by the passage of single relativistic particles through the scintillator. It is

Time range micro seconds	Number of pulses					
	.5mv≤v≤2mv	2mv<v≤4mv	4mv< v≤ 30mv	30< v≤ 120 mv	v> 120 mv	v≥700mv
0 - 10	1	5	0	1	0	0
10 - 20	5	13	4	2	0	0
20 - 30	11	11	2	0	1	0
30 - 40	9	4	2	2	0	0
40 - 50	12	9	2	1	1	0
50 - 60	14	9	5	0	1	0
60 - 70	10	12	5	3	0	0
70 - 80	11	8	5	4	0	0
80 - 90	14	16	3	2	1	0
90 - 100	9	7	5	2	3	0
100 - 110	11	13	1	1	0	0
110 - 120	13	9	2	0	1	0
120 - 130	13	14	3	4	2	0
130 - 140	17	14	3	1	3	0
140 - 150	9	10	1	2	0	0
150 - 160	13	8	5	2	2	0
160 - 170	16	12	1	0	0	0
170 - 180	22	17	4	3	0	0
180 - 190	9	13	0	0	0	0
190 - 200	11	8	1	0	1	0
200 - 210	17	10	6	2	1	0
210 - 220	12	4	2	2	4	0
220 - 230	9	14	2	2	1	0
230 - 240	9	9	3	3	0	0
240 - 250	7	12	0	4	0	0
250 - 260	12	13	5	0	1	0
260 - 270	42	17	3	2	4	0
270 - 280	10	5	3	1	2	0
280 - 290	10	14	2	1	1	0
290 - 300	10	11	1	2	1	0
300 - 310	13	16	2	0	0	0
310 - 320	16	14	2	4	3	0
320 - 330	14	16	3	1	1	0
330 - 240	7	8	2	1	2	1
340 - 350	11	8	1	3	0	0
350 - 360	19	17	1	6	2	0
360 - 370	19	11	1	1	2	0
370 - 380	20	13	6	2	1	0
380 - 390	16	7	4	1	2	0
390 - 400	14	7	1	5	1	0
400 - 410	14	14	1	4	2	1
410 - 420	15	10	2	4	1	0
420 - 430	17	14	3	4	3	0
430 - 440	9	17	1	2	0	0
440 - 450	10	12	1	3	1	0
450 - 460	17	8	4	3	2	0
460 - 470	15	15	1	1	1	1
470 - 480	16	14	1	1	3	0
480 - 490	9	7	2	1	1	0
490 - 500	3	6	1	2	0	0
	655	555	117	98	59	3

Table 7.9 : Random trigger data. Time distribution of events in different ranges of pulse ht. (measured on the oscilloscope) from a sample of 1010 random triggers. The data was analysed using the DATABIN program with the following program requirements

Maximum time = 550 μs No. of time bins = 55
Maximum pulse ht. = 31.5 No. of pulse ht. = 15

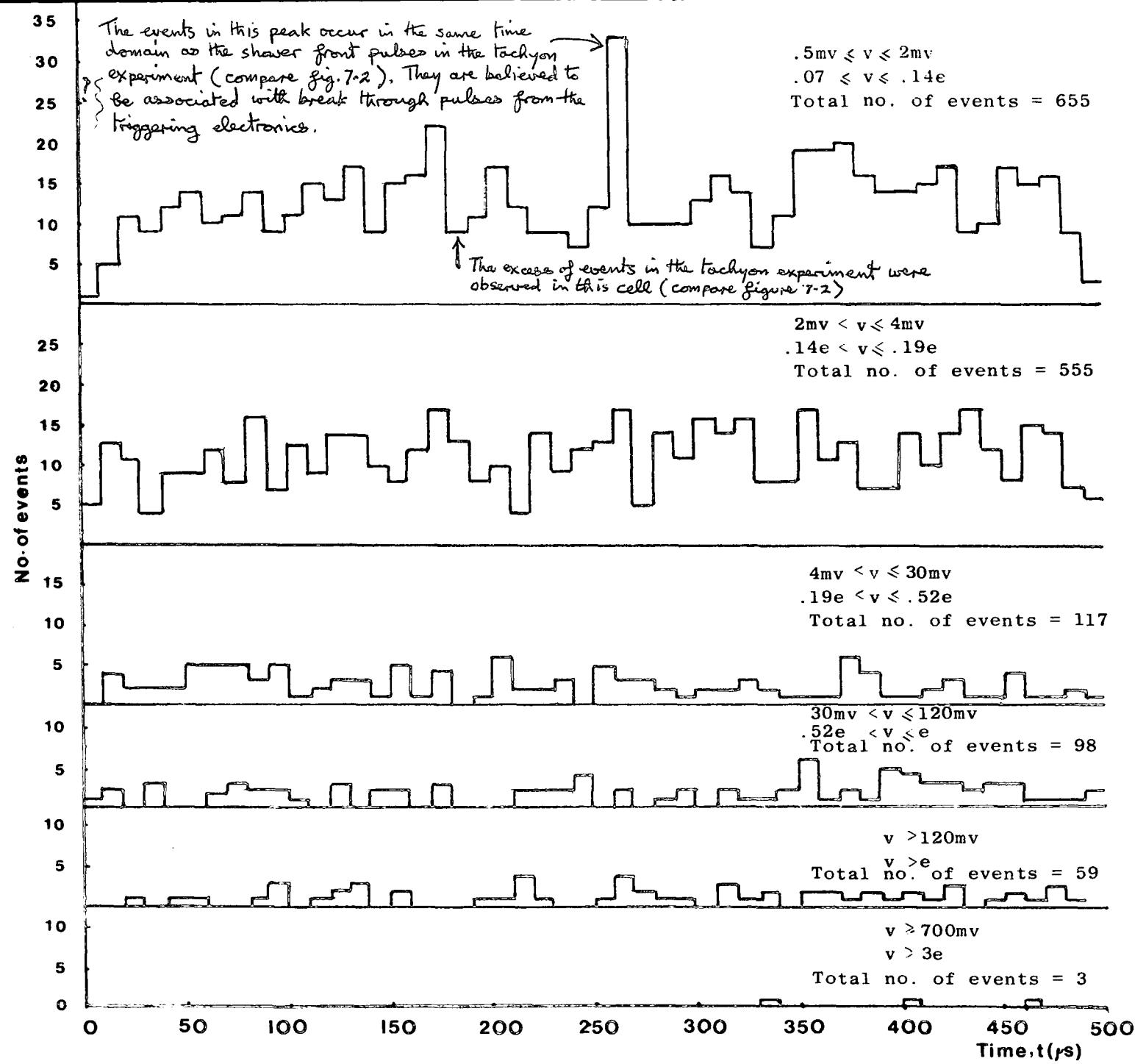

No. of random triggers = 1010

Figure 7.9 : Time distribution for pulse height between two limits of threshold energy losses in the tachyon detector.

Pulse ht.range on oscilloscope millivolts	Pulse ht.range at output of head unit millivolts	N(<265 μs)	N(>265 μs)	N(0 - 500 μs)
0.5 - 2	2.06 - 4.08	324	331	655
2 - 4	4.08 - 5.75	338	217	555
4 - 6	5.75 - 7.02	48	25	73
6 - 8	7.02 - 8.08	10	12	22
8 - 10	8.08 - 9.02	3	6	9
10 - 12	9.02 - 9.87	5	1	6
12 - 14	9.87 - 10.65	1	0	1
14 - 16	10.65 - 11.37	0	0	0
16 - 18	11.37 - 12.05	2	1	3
18 - 20	12.05 - 12.69	1	0	1
20 - 22	12.69 - 13.3	0	1	1
22 - 24	13.3 - 13.89	1	0	1
24 - 26	13.89 - 14.45	0	0	0
26 - 28	14.45 - 14.98	0	0	0
28 - 30	14.98 - 15.5	0	0	0
30 - 32	15.5 - 16.0	0	0	0
32 - 34	16.0 - 16.49	0	0	0
34 - 36	16.49 - 16.96	0	1	1
36 - 38	16.96 - 17.42	0	0	0
38 - 40	17.42 - 17.86	3	4	7
40 - 42	17.86 - 18.3	0	0	0
42 - 44	18.3 - 18.72	0	0	0
44 - 46	18.72 - 19.13	0	0	0
46 - 48	19.13 - 19.54	0	0	0
48 - 50	19.54 - 19.94	3	0	3
50 - 100	19.94 - 28.05	27	40	67
100 - 150	28.05 - 34.25	17	14	31
150 - 200	34.25 - 39.47	9	13	22
200 - 300	39.47 - 48.19	3	5	8
300 - 400	48.19 - 61.56	2	5	7
400 - 500	61-56 - 72.45	3	2	5
500 - 600	72.45 - 82.76	0	0	0
600 - 700	82.76 - 92.61	2	2	4
700 - 800	92.61 -102.09	0	0	0
800 - 900	102.09 -111.26	0	0	0
900 - 1000	111.26 -120.15	0	1	1
1000 - 1100	120.15 -128.81	0	0	0
1100 - 1200	128.81 -146.26	0	1	1
1200 - 1400	146.26 -170	0	0	0
>1400	>170	0	0	0
		802	682	1484

"Data bin" is used with

Maximum time	= 530μs	Maximum time	= 530μs
No. of time bins	= 2	No. of time bins	= 2
Maximum height	= 31.5	Maximum height	= 1455
No. ht. bin	= 15	No. of ht. bin	= 29

Table 7.10 : Random trigger data. Pulse height distribution obtained from a sample of 1,010 random triggers. N(<265μs) is the number of events observed in the first 265 μs of the oscilloscope sweep of 500μs and N(>265 μs) is the number observed in the final 235 μs. N(0-500μs) = N(<265μs) + N(>265μs).

Pulse ht. range on oscillos-cope (millivolts)	Pulse ht. range ($\nu_1 \rightarrow \nu_2$) at output of head unit (millivolts)	$\Delta\nu = \nu_2 - \nu_1$ (millivolts)	Mean $= \frac{\nu_2 + \nu_1}{2}$ (millivolts)	No. of events $N(\nu_1 \rightarrow \nu_2)$ with pulse ht. in range $\nu_1 \rightarrow \nu_2$	Differential frequency $= \frac{N(\nu_1 \rightarrow \nu_2)}{\Delta\nu}$ per millivolt	$N(>\nu_1)$	Integral rate $>\nu_1$ per sec.
5 - 4	2.06- 5.75	3.69	3.91	$(1.21\pm.03).10^3$	$(3.28\pm.09).10^2$	1484	$(2.94\pm.08).10^3$
4 - 6	5.75- 7.02	1.27	6.39	$(7.30\pm.85).10^1$	$(5.75\pm.67).10^1$	274	$(5.43\pm.321).10^2$
6 - 8	7.02- 8.08	1.06	7.55	$(2.20\pm.47).10^1$	$(2.08\pm.44).10^1$	201	$(3.98\pm.28).10^2$
8 - 12	8.08- 9.86	1.78	8.98	$(1.50\pm.38).10^1$	(8.38 ± 2.16)	179	$(3.54\pm.26).10^2$
12 - 20	9.86-12.69	2.83	11.28	(5 ± 2.24)	$(1.77\pm.79)$	164	$(3.25\pm.25).10^2$
20 - 50	12.69-19.94	7.25	16.32	$(1.10\pm.36).10^1$	$(1.79\pm.50)$	159	$(3.15\pm.25).10^2$
50 - 90	19.94-26.63	6.69	23.29	$(4.60\pm.68).10^1$	(6.88 ± 1.02)	146	$(2.89\pm.24).10^2$
90 - 100	26.63-28.05	1.42	27.34	$(2.10\pm.46).10^1$	$(1.48\pm.32).10^1$	100	$(1.98\pm.19).10^2$
100 - 150	28.05-34.25	6.20	31.15	$(3.10\pm.56).10^1$	$(5\pm.90)$	79	$(1.56\pm.17).10^2$
150 - 200	34.25-39.47	5.22	36.85	$(2.00\pm.47).10^1$	$(4.21\pm.90)$	48	$(9.50\pm1.37).10^1$
200 - 300	39.47-48.19	8.72	43.83	(8 ± 2.83)	$(9.17\pm3.25).10^{-1}$	26	$(5.15\pm1.01).10^1$
300 - 400	48.19-61.56	13.38	54.87	(7 ± 2.65)	$(5.23\pm1.98).10^{-1}$	18	$(3.56\pm.84).10^1$
400 - 800	61.56-102.09	40.53	81.83	(9 ± 3)	$(2.22\pm.74).10^{-1}$	11	$(2.18\pm.65).10^1$
800 - 1400	102.09-170	44.17	124.18	(2 ± 1.41)	$(4.53\pm3.19).10^{-2}$	2	(3.96 ± 2.79)
>1400	>170			0			

Table 7.11 : Random trigger data. Bassie data obtained from a sample of 1010 random triggers of the measuring oscilloscope time base of length 500 μs and calculation of the differential and integral spectra of the measured pulse heights.

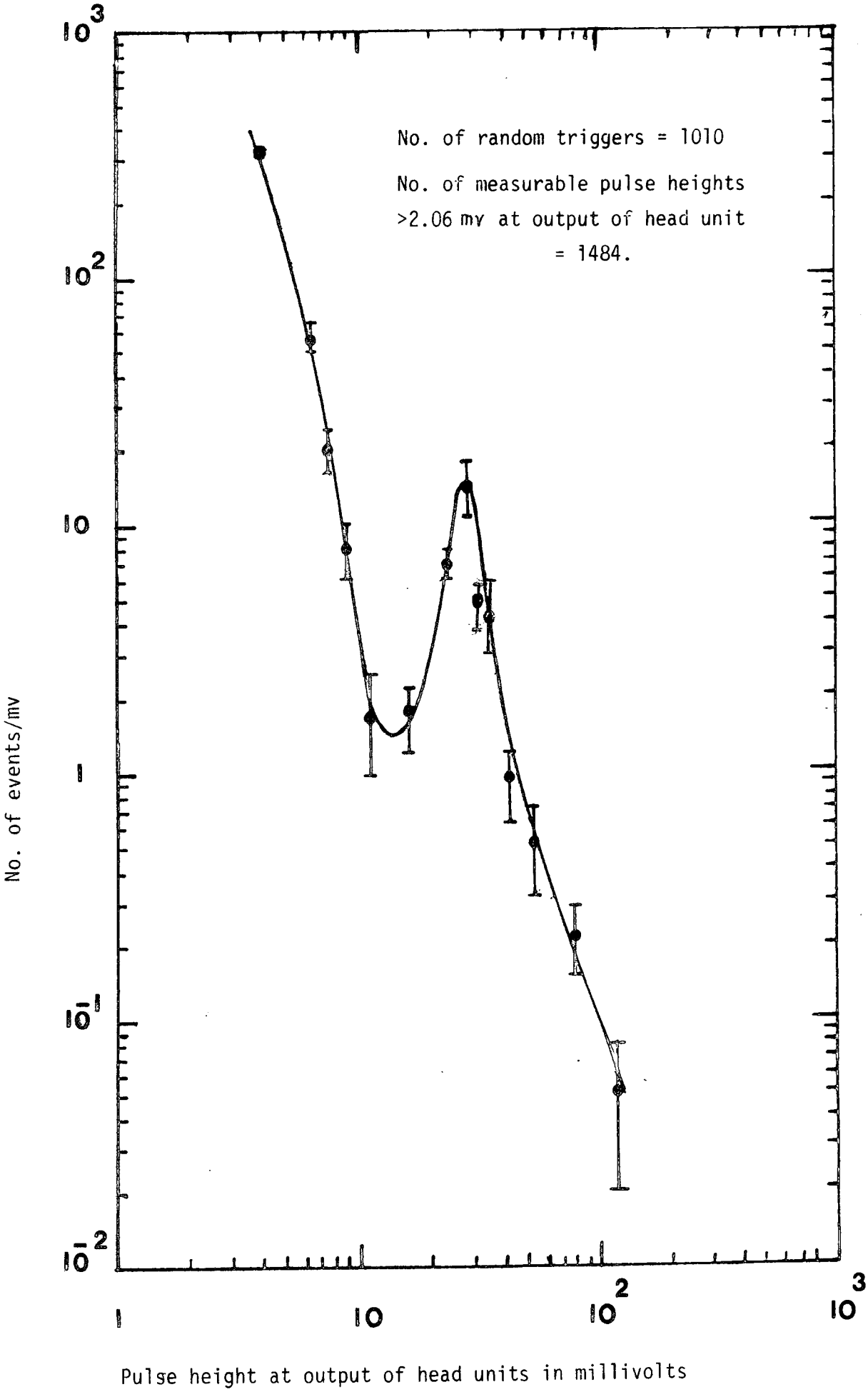

Figure 7.10 : The differential distribution of background pulses determined from a sample of 1010 random triggers of the oscilloscope time bases.

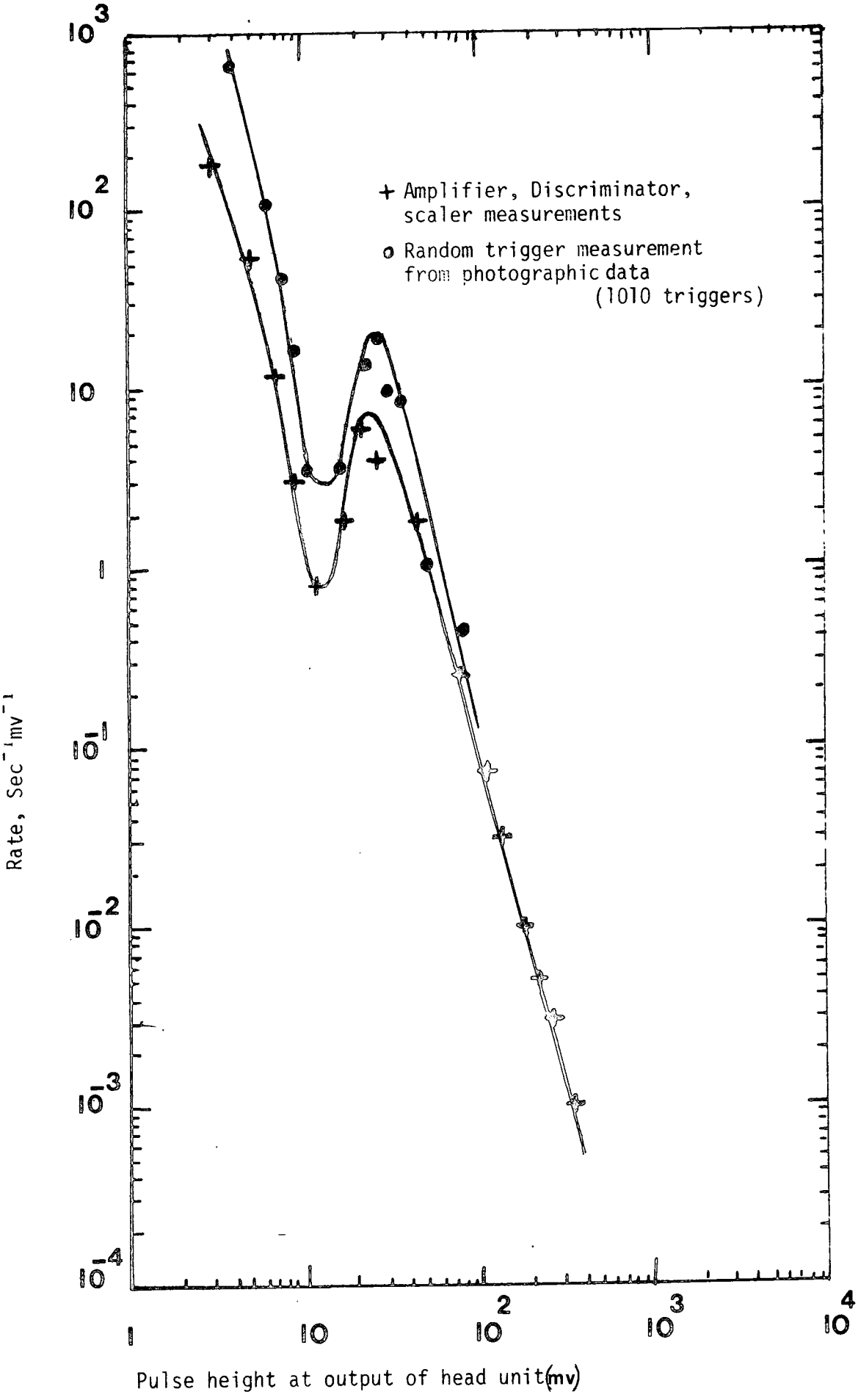

Figure 7.11 : Comparison of the differential pulse height distribution at the output of the head unit as determined from (a) measurements on the photographs of 1010 random triggers and (b) by differentiating the integral rate distribution determined using an amplifier discriminator and scaler.

noted that the peak occurs at a pulse height of 30 mv measured at the output of the head unit which agrees with the value found from the analysis of the tachyon data film for pulses occurring in the time range before and after the shower front. Figures 7.12, 7.13 and 7.14 give pulse height distributions which are relevant in comparing the tachyon data and random trigger data. The differences between the two sets of data are believed to be due to (a) they are integral plots so all the points are not statistically independent (b) sampling fluctuations (c) meteorological changes which affect the low energy cosmic ray flux at sea level.

7.6 MULTIPLE PULSE EVENTS

In both the tachyon data (1,443 EAS triggers) and the random trigger data (1,010 random triggers) multiple pulse events were observed. The multiple pulse events observed in the time domain before the arrival of the shower front in the tachyon data are of particular interest as they could in principle provide evidence for or against a significant tachyon flux. In table 7.12 the frequency distribution of observed multiple pulses are compared with the expected number for different threshold values of energy loss in the tachyon detector. If multiple pulses have a significant non random origin (this would be a background pulse plus a single tachyon pulses occurring in the 150μs preceding the shower front pulse in the present context) then a difference between the expected and observed numbers should be apparent. The expected number of multiple pulse events is expected to obey the Poisson distribution if they are all randomly related. If z is the mean number of pulses then the probability of observing r is $P(r) = \frac{e^{-z} z^{r}}{r!}$. It is seen from table 7.12 and

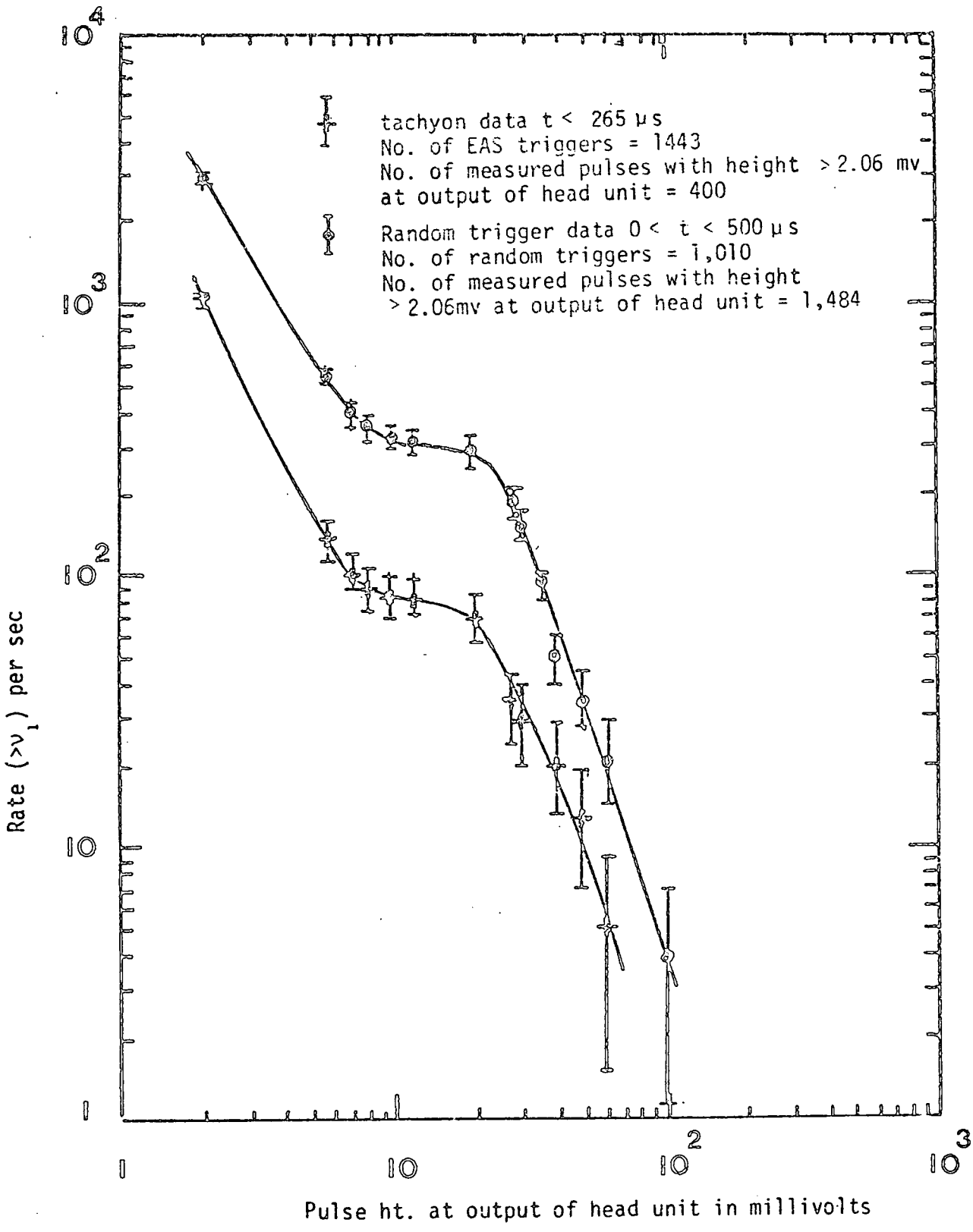

Figure 7.12 : The integral rate of pulses occurring in the 265 μs period before the arrival of the shower front pulse in the tachyon experiment and comparison with the integral rate of background pulses determined from a sample of 1,010 random triggers of the oscilloscope time bases.

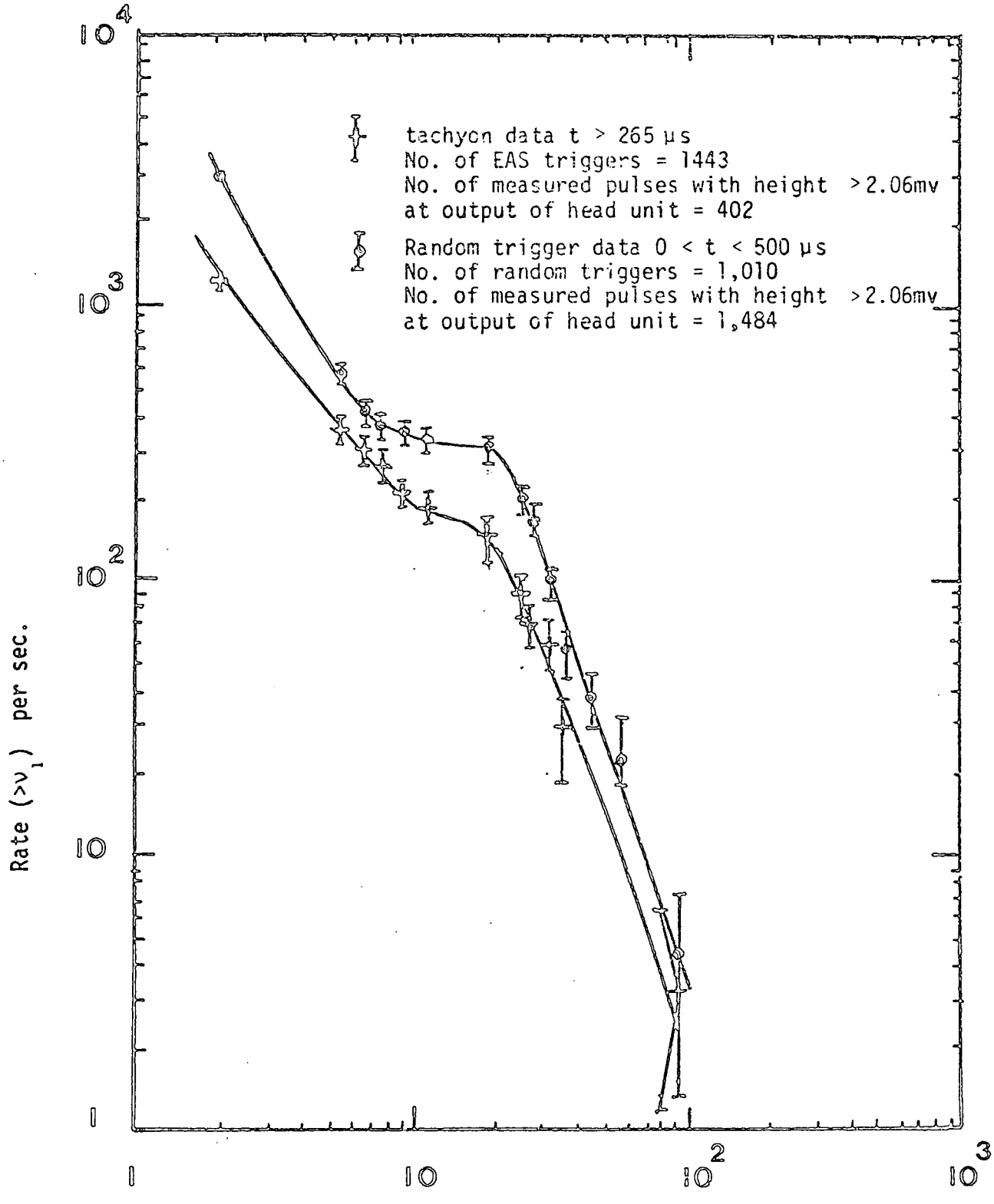

Figure 7.13 The integral rate of pulses occurring in the 235 μs period after the arrival of the shower front pulse in the tachyon experiment and comparison with the integral rate of background pulses determined from a sample of 1,010 random triggers of the oscilloscope time bases.

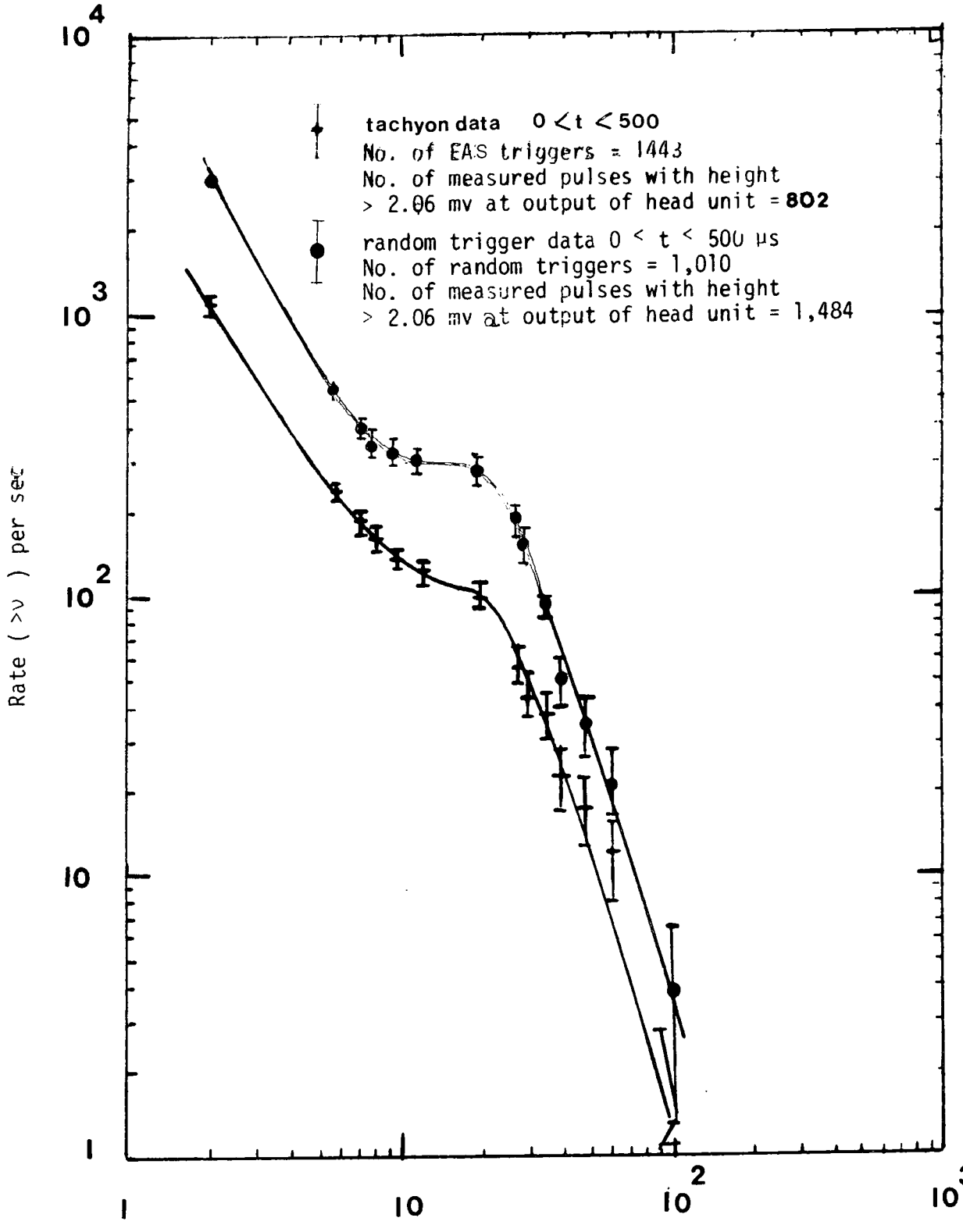

Figure 7.14 : The integral rate of pulses occurring in the 265 μs period before and the 235 μs period after the arrival of the shower front pulse and comparison with the integral rate of background pulses determined from a sample of 1,010 random triggers of the oscilloscope time bases.

t < 265μs				t > 265 μs			
Threshold > .5mv (.07e)				Threshold > .5mv (.07e)			
n	no	ne	no-ne	n	no	ne	no-ne
0	1073	1079.7	-6.7	0	1093	1091.3	+1.7
1	325	313.2	+11.8	1	305	304.8	+0.2
2	42	45.4	-3.4	2	37	42.6	-5.6
3	3	4.4	-1.4	3	8	4.0	+4.0
4	0	0.3	- .3	4	0	.3	-.3
	1443				1443		

t < 265μs				t > 265μs			
Threshold >2mv (.14e)				Threshold > 2mv (.14e)			
n	no	ne	no-ne	n	no	ne	no-ne
0	1239	1243.3	- 4.3	0	1206	1195.9	+10.1
1	193	185.2	+ 7.8	1	209	224.6	-15.6
2	11	13.8	- 2.8	2	22	21.1	+ .9
3	0	0.7	- .7	3	6	1.3	4.7
4	0	0	0	4	0	.1	- .1
	1443				1443		

Table 7.12 : (Tachyon data)

Number of triggers showing n pulses in the tachyon detector in the 265μs time domain (indicated by t < 265μs in the table) prior to the arrival of an EAS shower front pulse and the 235 μs time domain (indicated by t > 265μs in the table) after the shower front pulse.
The number of events with n = 0 increases with threshold energy loss because the rate of the background pulses decreases rapidly with increasing threshold energy loss. no is the observed number of events and ne is the expected number for a Poisson distribution.

t <265 μs				t > 265 μs			
Threshold >4 mv (.19e)				Threshold >4 mv (.19e)			
n	no	ne	no-ne	n	no	ne	no-ne
0	1386	1386.2	- .2	0	1335	1330.6	+4.4
1	56	55.7	+0.3	1	99	107.9	-8.9
2	1	1.1	- .1	2	9	4.4	+4.6
3	0	0	0	3	0	.1	- .1
4	0	0	0	4	0	0	0
	1443				1443		

t <265				t > 265			
Threshold > 30mv (.52e)				Threshold > 30mv (.52e)			
n	no	ne	no-ne	n	no	ne	no-ne
0	1414	1413.3	+ .7	0	1394	1391.1	+2.1
1	28	29.4	-1.4	1	46	50.2	-4.2
2	1	.3	+ .7	2	3	.9	+2.1
3	0	0	0	3	0	0	0
4	0	0	0	4	0	0	0
	1443				1443		

Table 7.12 (continued)

table 7.13 that there is no significant difference between the observed numbers and expected numbers for the time domains and threshold energy loss requirements investigated.

7.7 TIME SEPARATION DISTRIBUTION OF SUCCESSIVE EAS TRIGGERS

As a check on the correct functioning of the EAS selection trigger the differential and integral time separation distribution of successively recorded events has been measured. If a sample of N events are observed in a time T then the mean time separation of events is $\langle T \rangle = {}^{N}/_{T}$ and assuming successive events are unrelated then the number expected with time separation in the range t to t+dt is $n(t)dt = Ne^{-t/\langle T \rangle}\frac{dt}{\langle T \rangle}$ and the number expected with time separation >t is $n(>t) = Ne^{-t/\langle T \rangle}$. In figures 7.15 and 7.16 the measured differential and integral time separation distributions are shown together with the best fit lines representing the above expressions. The results obtained for <T> are summarised in the following table

	Mean time separation <T>	Trigger rate $^{1}/\langle T \rangle$
Differential time separation distribution	(4.56±0.21)min	(13.16±.61)hr^{-1}
Integral time separation distribution	(3.96±0.09)min	(15.15±.35)hr^{-1}

t <265				2 > 265			
Threshold >.5mv (.07e)				Threshold > .5mv (.07e)			
n	no	ne	no-ne	n	no	ne	no-ne
0	461	464.2	-3.2	0	490	493.7	-3.7
1	357	361.1	-4.1	1	360	353.5	+6.5
2	142	140.7	+1.3	2	138	125.9	+11.1
3	47	36.8	+10.2	3	22	30.4	-8.4
4	3	7.2	-4.2	4	0	5.5	-5.5
	1010				1010		

t <265				t> 265			
Threshold >2 mv (.14e)				Threshold> 2 mv (.14e)			
n	no	ne	no-ne	n	no	ne	no-ne
0	607	619.3	-12.3	0	620	629.8	-9.8
1	314	302.9	11.1	1	290	297.6	-7.6
2	79	74.1	4.9	2	88	70.2	17.8
3	10	12.2	-2.2	3	12	11.1	.9
4	0	1.5	-1.5	4	0	1.3	-1.3
	1010				1010		

Table 7.13 (Background data)

Similar table to table 6.12 except that this table refers to the background data measurements (1,010 random triggers of the oscilloscope time base)

t < 265				t > 265			
Threshold > 4mv (.19e)				Threshold > 4mv (.19e)			
n	no	ne	no - ne	n	no	ne	no-ne
0	875	879.3	-4.3	0	881	888.0	-7.0
1	130	121.9	+8.1	1	128	114.3	+13.7
2	5	8.4	-3.4	2	1	7.4	- 6.4
3	0	.4	- .4	3	0	.3	- .3
4	0	0	0	4	0	0	0
	1010				1010		

t < 265				t > 265			
Threshold > 30mv (.52e)				Threshold > 30mv (.52e)			
n	no	ne	no-ne	n	no	ne	no-ne
0	947	946.0	-1.0	0	938	940.5	-2.5
1	62	60.1	+1.9	1	72	67.1	+4.9
2	1	1.9	- .9	2	0	2.4	-2.4
3	0	0	0	3	0	0	0
4	0	0	0	4	0	0	0
	1010				1010		

Table 7.13 (continued)

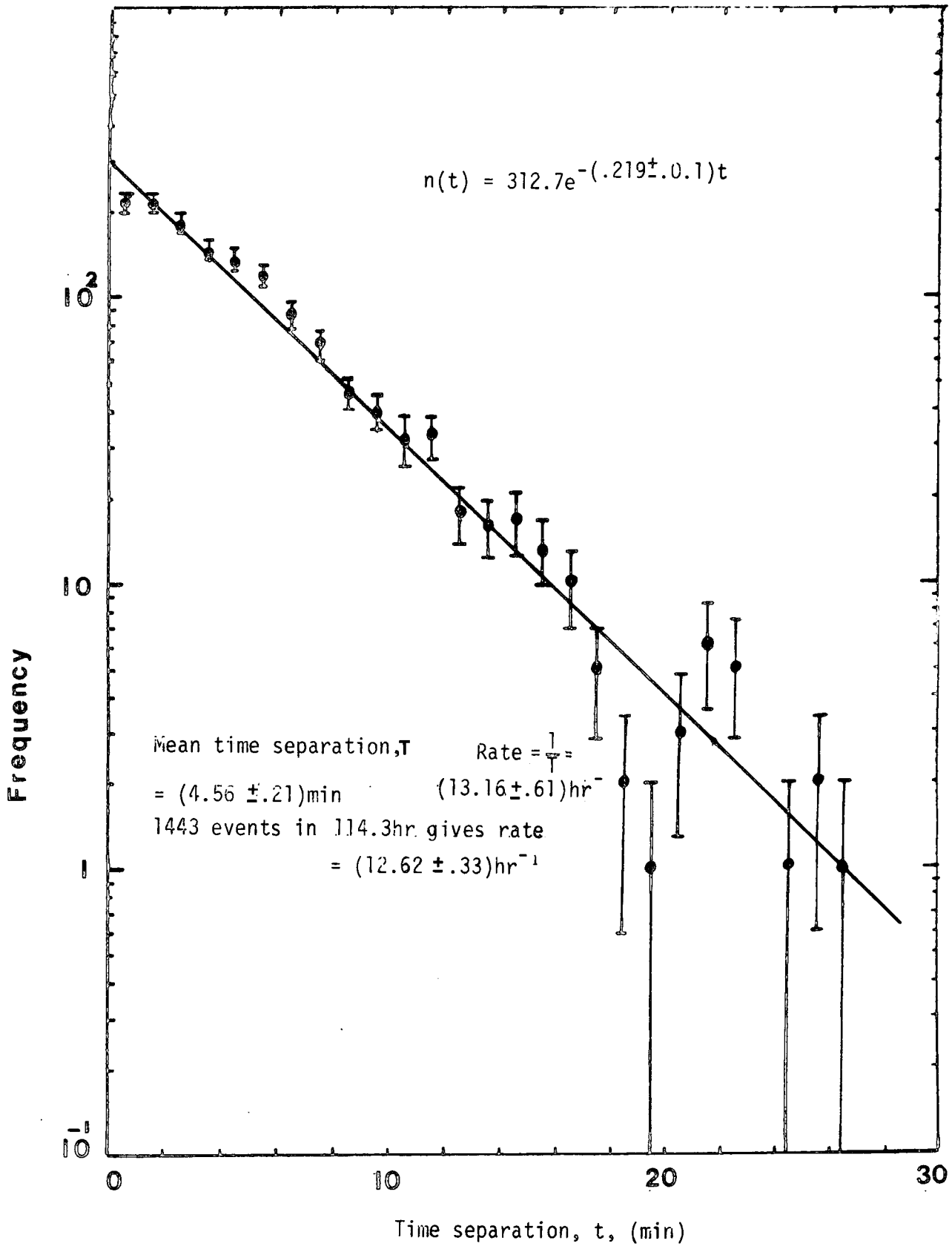

Figure 7.15 : Differential distribution of time separation of 1443 EAS triggers observed in a running time of 114.3 hrs corresponding to a mean time separation T = (4.75 ±.12) mins. The fitted straight line is of the form $n(t) = n(0)e^{-t/T}$ where T = (4.56 ±.21) mins

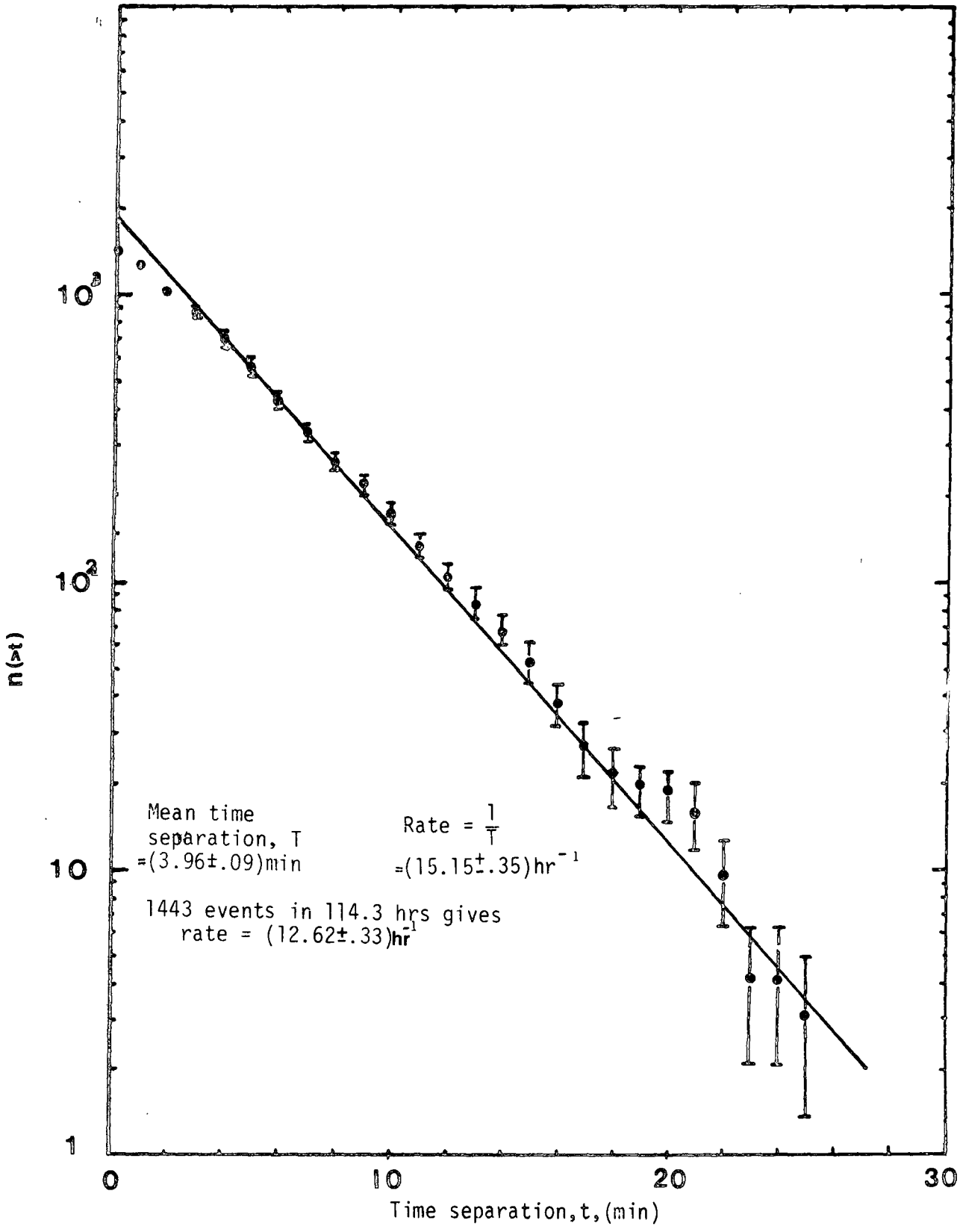

Figure 7.16 : Integral plot of time separation of 1443 EAS triggers observed in a running time 114.3 hrs corresponding to a mean time separation $T = (4.75 \pm .12)$min. The fitted straight line is of the form $n(>t) = n(>0)e^{-t/T}$ where $T = (3.96 \pm .09)$min

The results obtained for the trigger rate obtained in this way should be consistent with the trigger rate determined directly using the fact that 1,443 EAS triggers were observed in 114 hr 21 min 56sec. This gives a trigger rate of $(12.62 \pm 0.37)hr^{-1}$(see table 7·1). It is seen that the differential time separation distribution gives a closer agreement with this figure than the integral distribution. The reason for this is presumably connected with the fact that in experimental data plotted as a differential distribution all the experimental points are statistically independent whereas this is not the case for an integral distribution.

7.8 CONCLUSION

The main conclusion of this work is based on the data shown in figure 7.2 which suggests evidence for a finite flux of tachyons associated with regions of EAS with local electron density $\geqslant 25m^{-2}$. Such showers are generated by primary cosmic ray protons or nuclei of energy $\tilde{>}10^{15}$ ev although it is possible that tachyonic objects are present in the primary cosmic rays and generate the showers themselves. It is noted that the evidence refers to energy deposits in the 5 cm thick scintillation detector of .07-.14 e (.7-1.4 MeV). Obviously further experimental data is required to finally establish whether the observed effect is a real phenomenon or not.

CHAPTER 8

SUMMARY AND CONCLUSION

The work described in this thesis has been concerned with several distinct but related topics. The achievements attained and the conclusions reached will be discussed in turn.

Zenith angle distribution of EAS

The study of the size dependence of the zenith angle distribution of EAS described in Chapter 3 showed that representing the zenith angle distribution by $I(\theta) = I(0)\cos^{n}\theta$ then $n = 8.4 \pm 0.3$ for the size range 5.10^{4}- $1.4.10^{6}$. For the size range 10^{4}- 5.10^{4} the measurements suggest the smaller value of $n = 5.1 \pm 1.3$.

Scintillation counter development

The type of scintillation counter described in Chapter 4. (of which 9 were subsequently constructed) was found to be convenient to use from the point of view that it gives a single particle peak, well resolved from the noise, when its response to the global cosmic ray flux is recorded on a pulse height analyser. This is a considerable improvement on the detectors originally used as all these had to be calibrated using a subsidiary cosmic ray telescope.

Tachyon experiment

Two of the scintillation counters just described were used in twofold concidence to select EAS with local electron density $\geqslant 25 m^{-2}$ in the tachyon experiment. The result of the tachyon experiment suggests that there may be a significant flux of tachyons associated with regions of EAS of local electron density $\geqslant 25 m^{-2}$. This conclusion is based on an excess of events (4.4 standard deviations above back ground) observed in the 85-95μs time domain preceding the arrival of an air shower at sea level. Further experimental data is required to decide whether the effect is real or not.

APPENDIX A

Modifications to the flash tube chamber

As described in chapter 6 the two EAS selection scintillators A and B used in the tachyon experiment were mounted above the flash tube chamber while the tachyon detection scintillator C was mounted inside the chamber (see figure 6.2 and figure A1). Before commencing the tachyon experiment the chamber design was improved upon. Previously all flash tubes (each 2 m long, 1.8 cm external diameter, 1.6 cm internal diameter and filled with neon gas to a pressure of 60 cm of mercury) were mounted with their axes parallel to one another. With this geometry only projected spatial information in one view is available and no visual information is available concerning the spatial position of tracks in the "back plane". The improvement made was to stack the flash tubes in successive double layers of tubes such that the tube axes in successive double layers were orthogonal to one another. Thus a penetrating particle traversing the chamber is expected to produce tracks as illustrated in figure A.1. Figure A2 shows the mirror system used to simultaneously photograph the front and side views of the chamber so that the views appear side by side on 35 mm film and figure A3 shows a photograph taken in this way. Because of high voltage pick up problems the chamber was not operated during the exploratory tachyon experiment described in Chapter 6. To operate it the chamber has to be pulsed with a high voltage pulse ($\sim$10 kv lasting 10μs) while in the tachyon experiment pulses as small as 0.5 mv were measured. If the pick up problem can be solved then an obvious improvement to the tachyon experiment would be to operate in conjunction with the chamber.

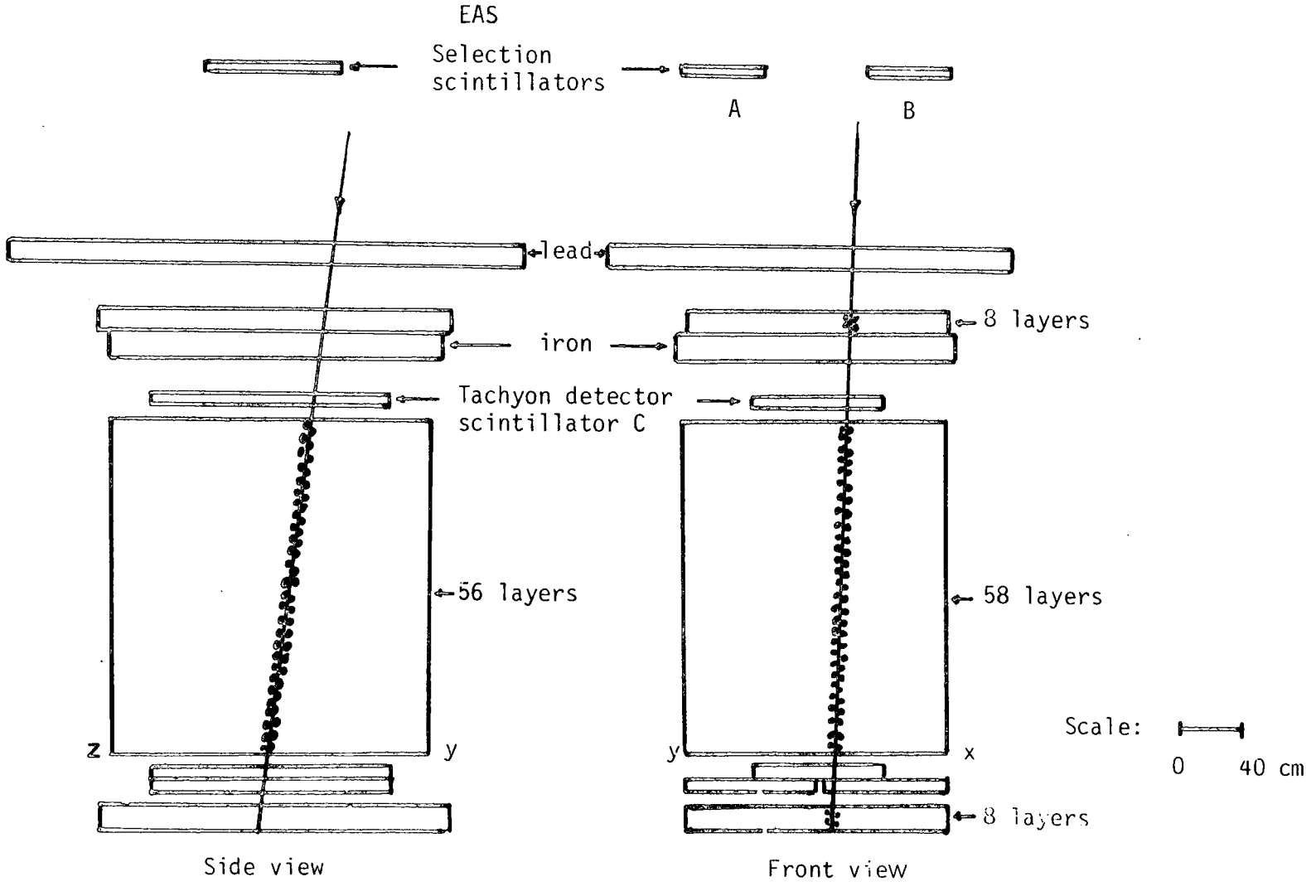

Figure A.1 : Scale diagram of the improved flashtube chamber. A and B are the scintillation counters used to select EAS and C is the tachyon detector scintillator. The track of a single penetrating charged particle through the chamger is added to clarify the positions of the flash tubes.

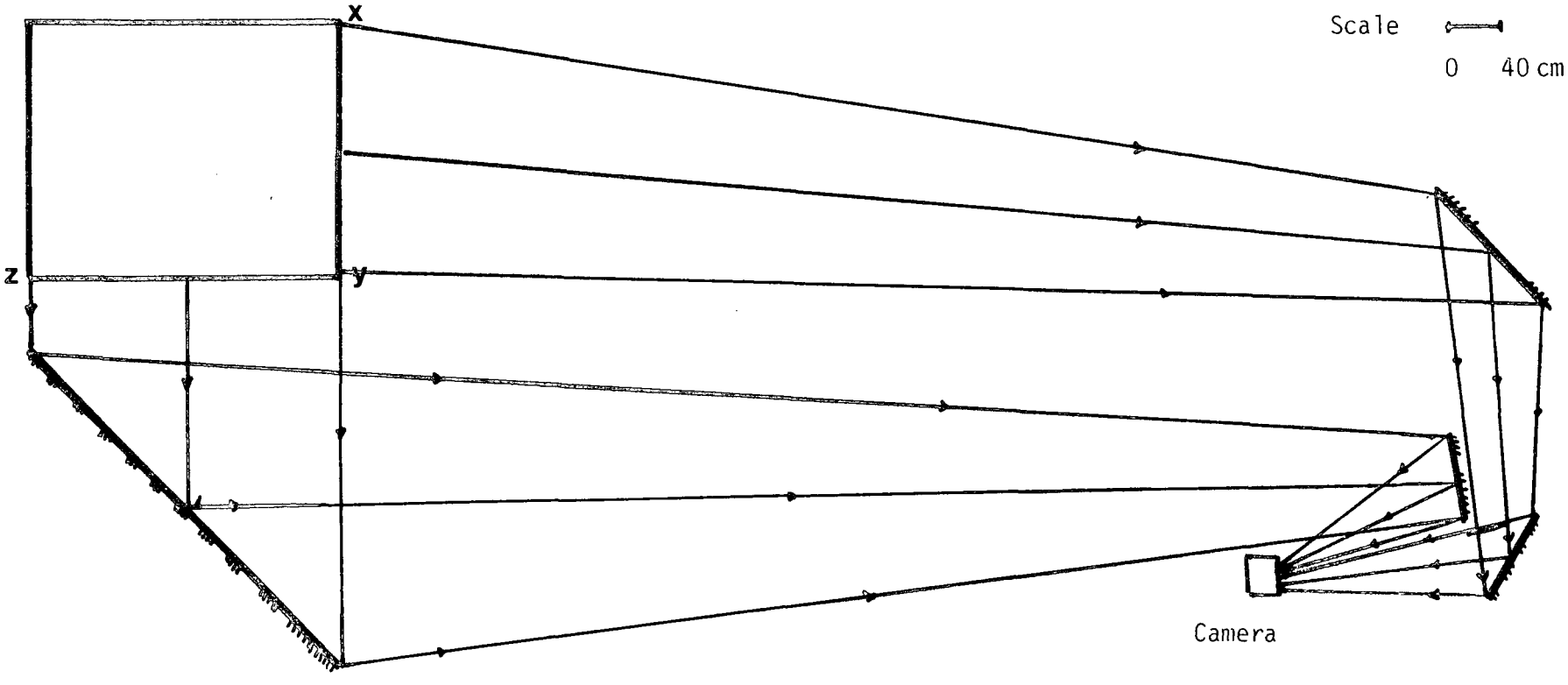

Figure A.2 : The mirror system used to simultaneously photograph the front and side views of the flash tube chamber shown in figure A.1. The points marked x, y and z in this figure (which is a plan view) correspond to the points marked x, y and z in figure A.1.

Figure A.3 : Photograph of the front and side views of the flash tube chamber photographed through the mirror system shown in figure A.2.

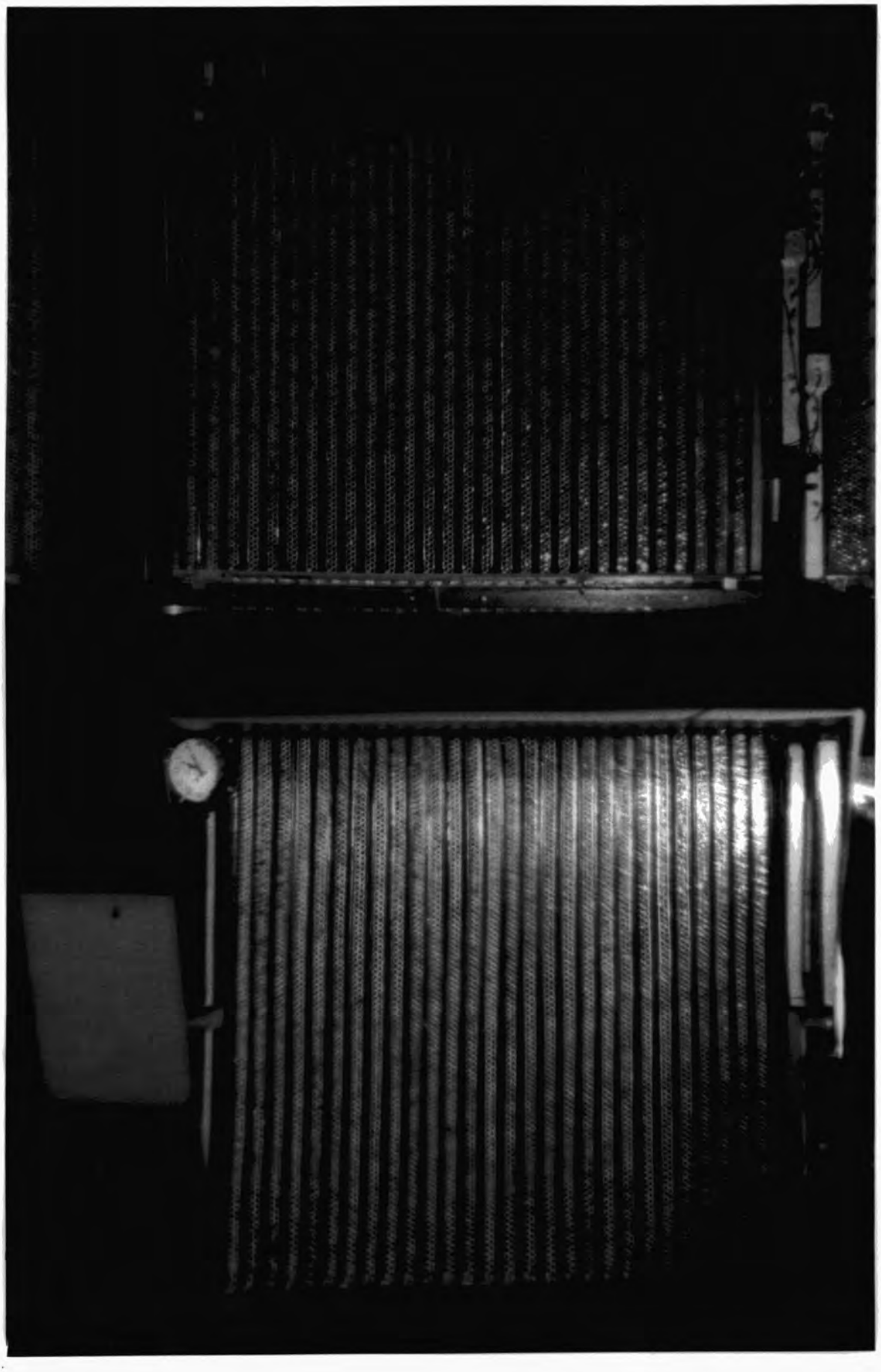

APPENDIX B

DATABIN program

The 35 mm photographic film obtained in the tachyon experiment was analysed using a photographic enlarger. The enlarged oscilloscope record of each event was traced so as to obtain an easily accessible permanent record and the occurrence time (measured from the start of the 500μs oscilloscope sweep) and pulse height of each pulse occurring on the trace was measured. The basic information for each event was 1. The time that the event occurred and 2. pairs of values of occurrence time and pulse height. The problem in analysing the data was to determine the occurrence time distribution for pulses in a given size range in a given range of occurrence time t (pre shower front pulses, $t < 255$ μs; shower front pulses, $t = 265$ μs, post shower front pulses, $t > 265$ μs). To obtain this information the DATABIN program in conjunction with a Commodore PET computer was used. The program serves a dual purpose as it will (a) store information that is input on magnetic tape in a series of files to be specified by the user, and (b) read data from the files, histogram it as requested and display the result. The data from the tachyon experiment was stored in files on magnetic tape as a series of occurrence time, pulse height pairs. The histograms and tables presented in Chapter 7 were then obtained using the program analysis routine. Details of the information obtained using the program are shown in tables B1 and B2.

To obtain the pulse height distribution of the pre and post shower front pulses the DATABIN program was run twice and requirements were set to

Maximum time = 530μs	Maximum time = 530μs
No. of time bins = 2	No. of time bins = 2
Maximum pulse height = 31.5	Maximum pulse height = 1455
No. of pulse height bins = 15	No. of pulse height bins = 29

To obtain the pulse height distribution of the shower front pulses (1443 shower triggers) all occurring at the same time of 265μs the DATABIN program was run twice and the requirements were set to

Maximum time = 265μs	Maximum time = 265μs
No. of time bins = 1	No. of time bins = 1
Maximum height = 31.5	Maximum height = 1455
No. of height bins = 15	No. of height bins = 29

```
READY.

 10 REM TACHYON DATA-BINNING PROGRAM
 20 DIMT(255),H(255),C(99,50)
 21 INPUT"□MAX TIME ";MT
 22 INPUT"MAX HEIGHT";MH
 23 INPUT"# OF TIME BINS (MAX IS 100)";NT
 24 INPUT"# OF HEIGHT BINS (MAX IS 50)";NH
 25 IFNT>100ORNH>100THENGOTO23
 30 PRINT"□WHAT OPTION IS REQUIRED?"
 40 PRINT:PRINT"  1  DATA FROM TAPE"
 50 PRINT"  2  DATA FROM KEYBOARD"
 60 PRINT:INPUT"OPTION #";OP
 70 IF OP<1 OR OP>2 THEN60
 80 INPUT"FILENAME FOR DATA INPUT/OUTPUT";F$
 90 IF OP=1 THEN 120
100 GOSUB300
110 GOTO130
120 GOSUB500
130 GOSUB800
140 STOP
150 END
300 REM KEYBOARD INPUT ROUTINE
310 PRINT"□WIND TAPE TO A CLEAR AREA FOR LOADING"
320 PRINT"DATA":PRINT
330 K=1:E$=F$+STR$(K)
340 PRINT"INPUT TIME(MICROSECONDS),PULSE HEIGHT(MILLIVOLTS)"
350 PRINT"UPTO 256 VALUES PER FILE ALLOWED"
360 PRINT"IF THIS IS EXCEEDED A NEW FILE WILL BE STARTED"
370 PRINT"AT THE END OF DATA INPUT, ENTER 0,0"
380 FORI=0TO255
390 INPUTT(I),H(I)
400 IF T(I)> MT OR H(I)< 0 THEN 410
405 IFT(I)<0ORH(I)>MHTHEN410
406 GOTO420
410 PRINT"ERROR - REDO ENTRY":GOTO 390
420 IF H(I)=0 THEN 440
430 NEXT
440 NO=I
450 GOSUB700
451 OPEN1,1,1,E$
452 FORI=0TONO
453 PRINT#1,T(I)
454 PRINT#1,H(I)
455 NEXT
456 CLOSE1
460 IFI<255THEN490
470 PRINT"NEW FILE BEING STARTED, WAIT FOR PROMPT"
475 PRINT"BEFORE ENTERING FURTHER DATA"
480 K=K+1:E$=F$+STR$(K)
490 RETURN
500 REM TAPE INPUT ROUTINE
510 PRINT"□WIND TAPE TO START OF DATA"
520 PRINT
540 PRINT:INPUT"HOW MANY FILES ARE REQUIRED";N
560 FORK=1TON
570 E$=F$+STR$(K)
580 PRINT"LOADING",E$
590 OPEN1,1,0,E$
600 FORI=0TO255
610 INPUT#1,T(I)
615 INPUT#1,H(I)
620 IFH(I)=0GOTO640
630 NEXT
640 NO=I
650 GOSUB700
660 NEXTK
```

```
 700 REM BINNING ROUTINE
 710 FORI=0TONO-1
 720 X=INT(T(I)/(MT/NT))
 730 Y=INT(H(I)/(MH/NH))
 735 IFX<0ORY<0THENPRINT"ERROR":STOP
 740 IFX>NT  THENX=NT
 750 IFY>NHTHENY=NH+1
 760 C(X,Y)=C(X,Y)+1
 770 NEXT
 780 RETURN
 800 REM OUTPUT ROUTINE
 810 FORI=0TONT-1
 815 XX=MT/NT:YY=MH/NH
 820 PRINT"␣TIME RANGE IS"I*XX"-"I*XX+XX
 830 PRINT:PRINT"HEIGHT RANGE":PRINT
 840 FORJ=0TONH
 845 IFJ<NH+1THEN850
 846 PRINT">"J*YY TAB(20)C(I,J)
 847 GOTO860
 850 PRINTJ*YY "-"(J+1)*YY TAB(20)C(I,J)
 851 IFJ=0THEN860
 852 IFJ/14<>INT(J/14)THEN860
 853 PRINT"PRESS ANY KEY TO CONTINUE"
 854 GETA$:IFA$=""THEN854
 860 NEXTJ
 870 PRINT"PRESS ANY KEY TO CONTINUE"
 880 GETA$:IF A$=""THEN880
 890 NEXTI
 900 RETURN
READY.
```

Pulse ht.range on oscillos-cope millivolts	Pulse ht.range at output of head unit millivolts	N(<265 μs)	N(>265 μs)	N(0 - 500 μs)
0.5 - 2	2.06 - 4.08	243	175	418
2 - 4	4.08 - 5.75	104	108	212
4 - 6	5.75 - 7.02	12	22	34
6 - 8	7.02 - 8.08	6	11	17
8 - 10	8.08 - 9.02	1	9	10
10 - 12	9.02 - 9.87	1	8	9
12 - 14	9.87 - 10.65	0	3	3
14 - 16	10.65 - 11.37	1	1	2
16 - 18	11.37 - 12.05	1	0	1
18 - 20	12.05 - 12.69	0	3	3
20 - 22	12.69 - 13.3	1	2	3
22 - 24	13.3 - 13.89	1	0	1
24 - 26	13.89 - 14.45	0	3	3
26 - 28	14.45 - 14.98	0	2	2
28 - 30	14.98 - 15.5	1	3	4
30 - 32	15.5 - 16.0	0	1	1
32 - 34	16.0 - 16.49	0	1	1
34 - 36	16.49 - 16.96	0	0	0
36 - 38	16.96 - 17.42	0	0	0
38 - 40	17.42 - 17.86	1	2	3
40 - 42	17.86 - 18.3	0	1	1
42 - 44	18.3 - 18.72	0	0	0
44 - 46	18.72 - 19.13	0	0	0
46 - 48	19.13 - 19.54	0	0	0
48 - 50	19.54 - 19.94	0	0	0
50 - 100	19.94 - 28.05	16	25	41
100 - 150	28.05 - 34.25	2	3	5
150 - 200	34.25 - 39.47	1	10	11
200 - 300	39.47 - 48.19	3	1	4
300 - 400	48.19 - 61.56	3	1	4
400 - 500	61.56 - 72.45	0	3	3
500 - 600	72.45 - 82.76	2	2	4
600 - 700	82.76 - 92.61	0	1	1
700 - 800	92.61 -102.09	0	0	0
800 - 900	102.09 -111.26	0	1	1
900 - 1000	111.26 -120.15	0	0	0
1000 - 1100	120.15 -128.81	0	0	0
1100 - 1200	128.81 -146.26	0	0	0
1200 - 1400	146.26 -170	0	0	0
1400	170	0	0	0
		400	402	802

"Data bin" is used with Maximum time = 530μs, No.of time bins = 2, Maximum height = 31.5, No.of height bins = 15

Maximum time = 530μs, No.of time bins = 2, Maximum height = 1455, No. of height bins = 29

Table B.1 : Tachyon data. Pulse height distribution obtained from a sample of 1443 EAS triggers, N(<265μs) is the number of events observed in the first 265 μs of the oscilloscope sweep of 500μs and N(>265μs) is the number observed in the final 235μs. N(0-500μs) = N(<265μs) + N(>265μs). The total number of measured pulse heights is shown at the bottom of each column. The data was analysed using the DATABIN program. Shower front pulse heights whose leading edge starts at 265μs from the start of the trace are not included in the data presented in the table.

Pulse ht. range on oscilloscope millivolts	Pulse ht. range at output of head unit (millivolts)	Frequency
0.5 - 2	2.06 - 4.08	260
2 - 44	4.08 - 5.75	166
4 - 6	5.75 - 7.02	72
6 - 8	7.02 - 8.08	37
8 - 10	8.08 - 9.02	31
10 - 12	9.02 - 9.87	25
12 - 14	9.87 - 10.65	12
14 - 16	10.65 - 11.37	8
16 - 18	11.37 - 12.05	7
18 - 20	12.05 - 12.69	12
20 - 22	12.69 - 13.3	8
22 - 24	13.3 - 13.89	11
24 - 26	13.89 - 14.45	10
26 - 28	14.45 - 14.95	2
28 - 30	14.98 - 15.5	15
30 - 32	15.5 - 16.0	1
32 - 34	16.0 - 16.49	0
34 - 36	16.49 - 16.46	2
36 - 38	16.96 - 17.42	0
38 - 40	17.42 - 17.86	9
40 - 42	17.86 - 18.3	0
42 - 44	18.3 - 18.72	0
44 - 46	18.72 - 19.13	0
46 - 48	19.13 - 19.54	0
48 - 50	19.54 - 19.94	1
50 - 100	19.94 - 28.05	101
100 - 150	28.05 - 34.25	56
150 - 200	34.25 - 39.47	50
200 - 300	39.47 - 48.19	63
300 - 400	48.19 - 61.56	55
400 - 500	61.56 - 72.45	34
500 - 600	72.45 - 82.76	43
600 - 700	82.76 - 92.61	23
700 - 800	92.61 -102.09	12
800 - 900	102.09 -111.26	18
900 - 1000	111.26 -120.15	15
1000 - 1100	120.15 -128.81	17
1100 - 1200	128.81 -146.26	17
1200 - 1400	146.26 -170.0	51
>1400	>170	42
		1286

"Data bin" Program used with	Maximum time bin = 550 No.of time bin = 1 Maximum height = 31.5 No.of ht.bin = 15	Maximum time bin = 530 No.of time bin = 1 Maximum height = 1455 No.of ht. bin = 29

Table B.2 : Tachyon data. The distribution in size of the shower front pulse heights measured from a sample of 1443 EAS triggers. The DATABIN program was used to analyse the data. The total number of measured pulse heights is shown at the bottom of the column.

APPENDIX C

Light emitting diodes

The use of pulsed light emitting diodes (LED) is the most convenient way of testing photomultiplier tubes. Using a light tight box containing the LED and tube to be studied the variation of photomultiplier output pulse height with the voltage applied to the tube can be rapidly measured. Also using the same LED light source the relative sensitivities of a number of tubes can be found and hence the voltage at which each should be operated to have the same sensitivity determined. Small light-emitting diodes based on GaAs that produce yellow, green and red light are now readily available commercially. From a practical point of view one needs to know how large and how wide the voltage and current pulse applied to the diode must be in order to generate a sufficient amount of light to be readily detected. These problems have been investigated and the results are shown in figures C1, C2, C3, C4 and C5. All the measurements refer to the use of a Phillips 53 AVP photomultiplier tube used as a detector. It is concluded that for photomultipliers of this type (i.e. with an S11 photocathode response) light emitting diodes producing yellow light are the most satisfactory to use.

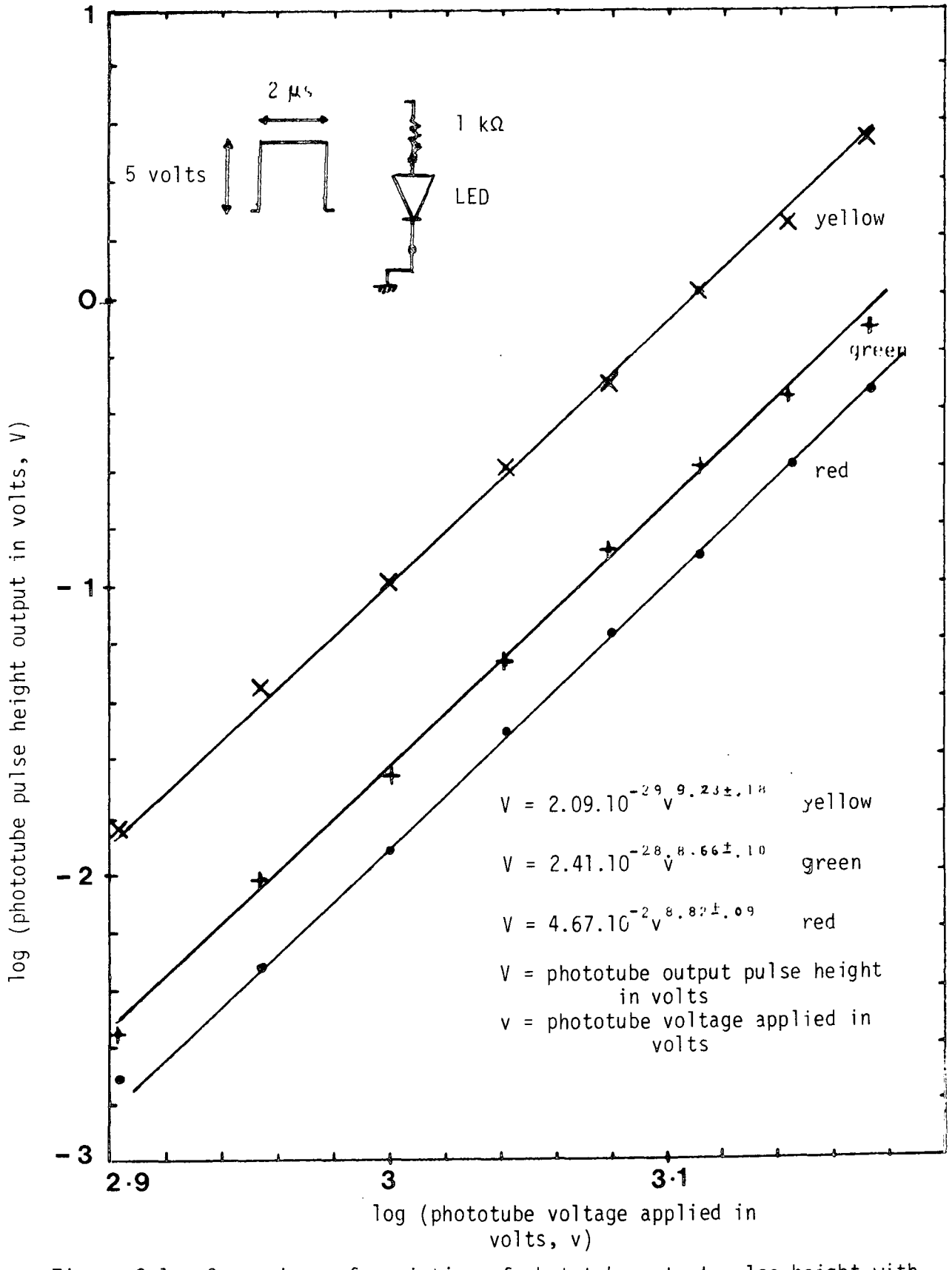

Figure C.1 : Comparison of variation of phototube output pulse height with voltage applied in volts. Different colour LEDs used as light source.

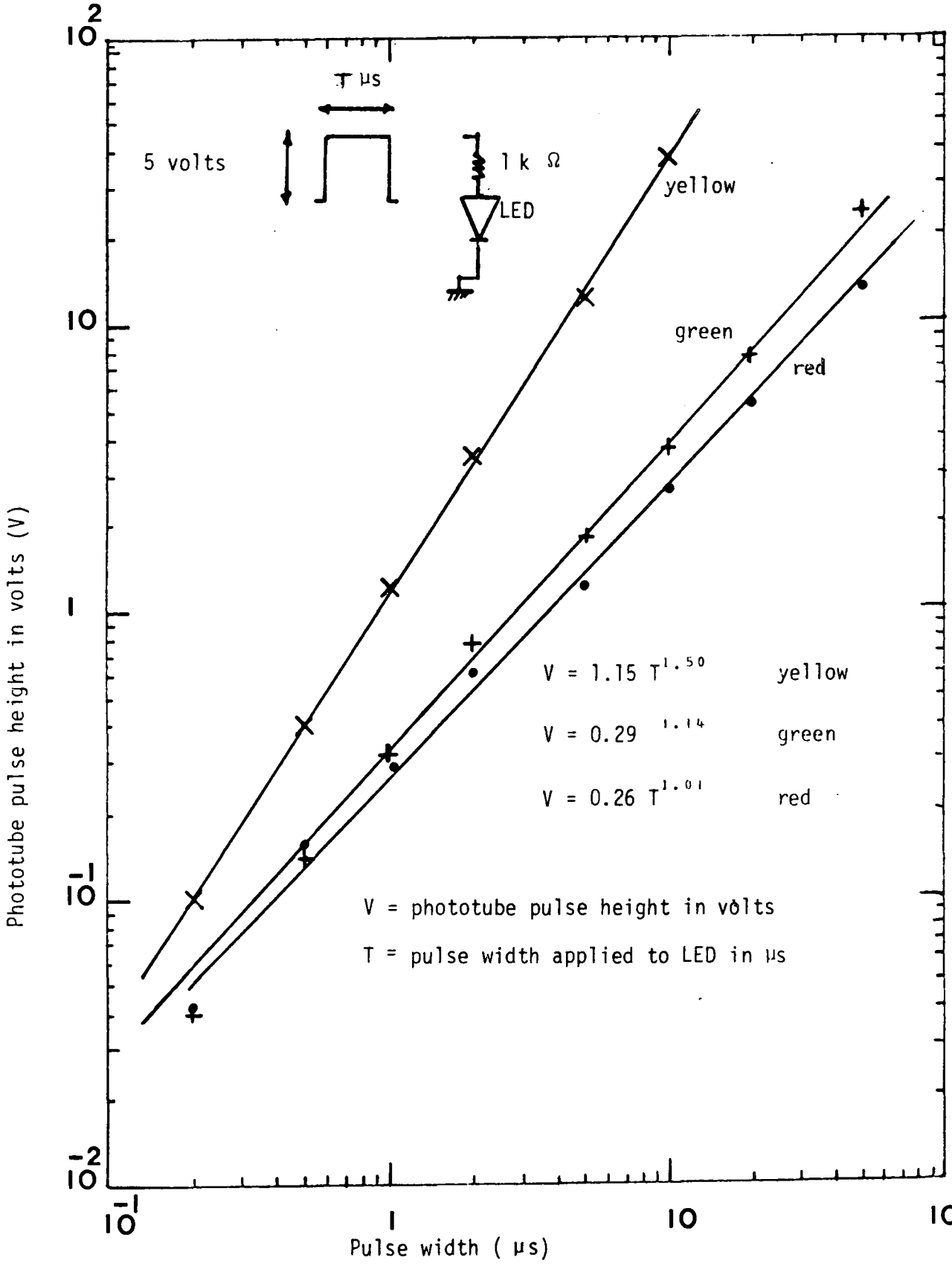

Figure C.2 : Comparison of variation of phototube pulse height with pulse width applied to yellow, green and red light emitting diodes.

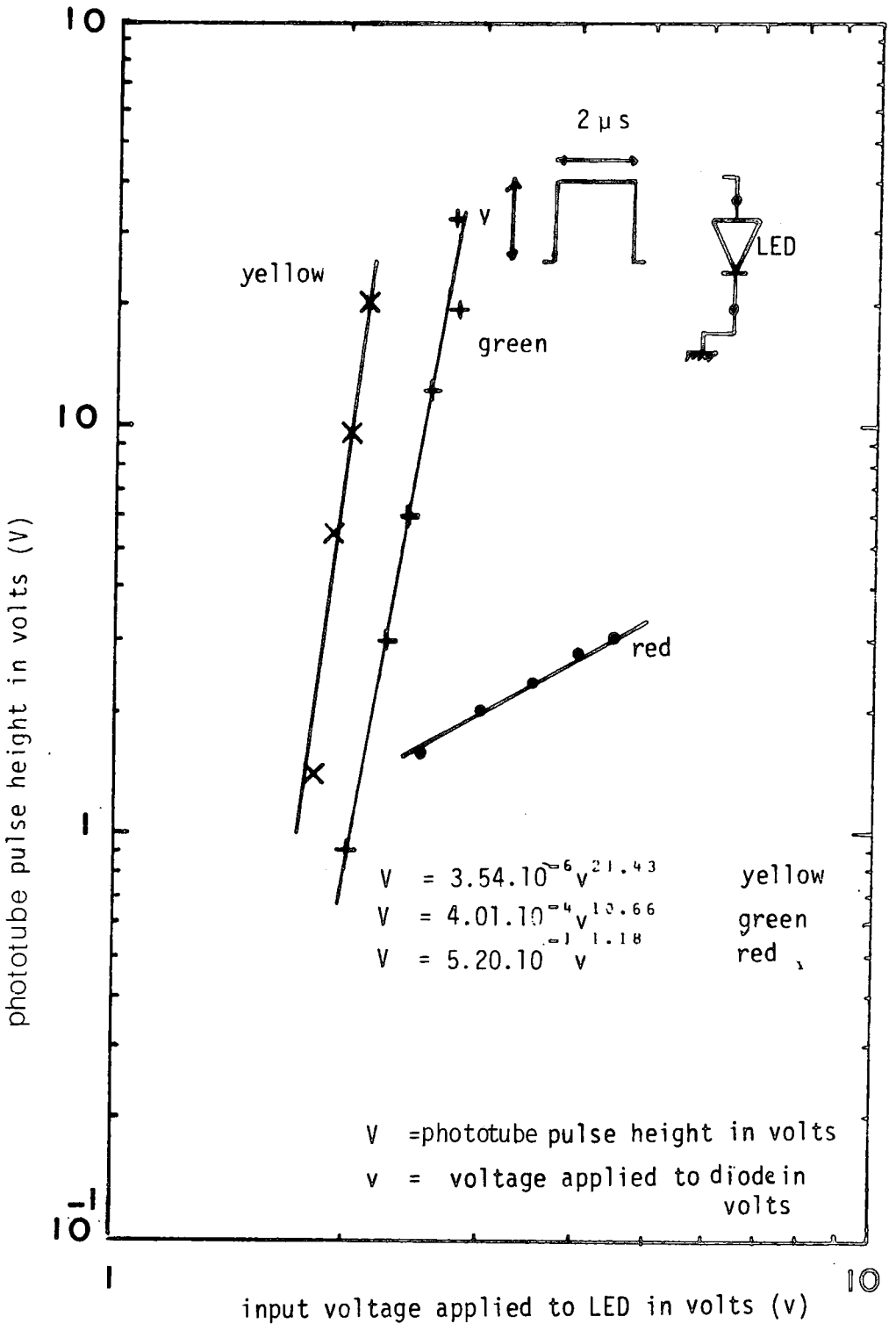

Figure C.3 : Comparison of variation of phototube output pulse height with voltage applied to LEDs of different colours. (yellow, green and red).

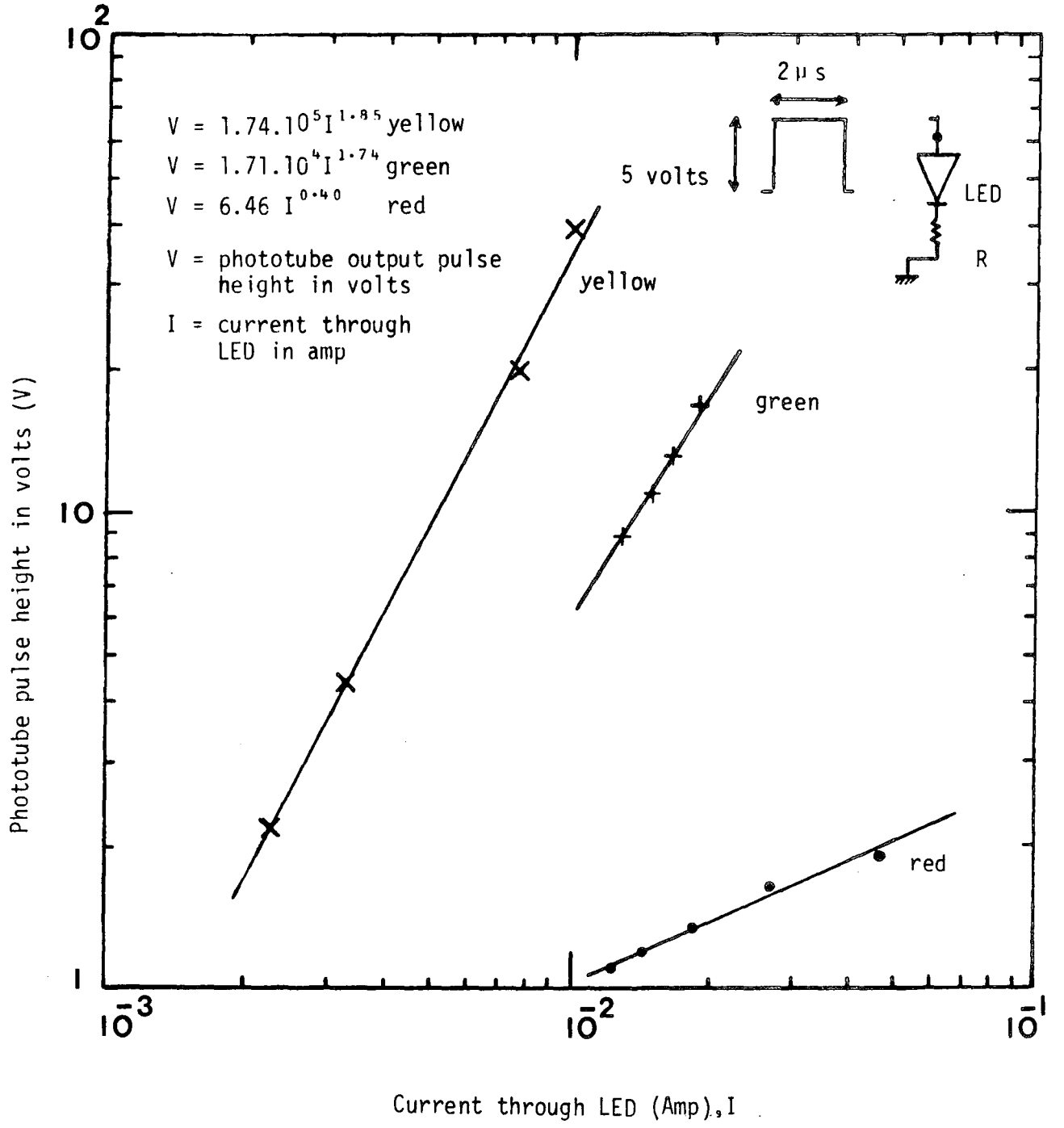

Figure C.4 : Comparison of the variation of phototube pulse height with current applied to the LEDs of different colours. (yellow, green and red).

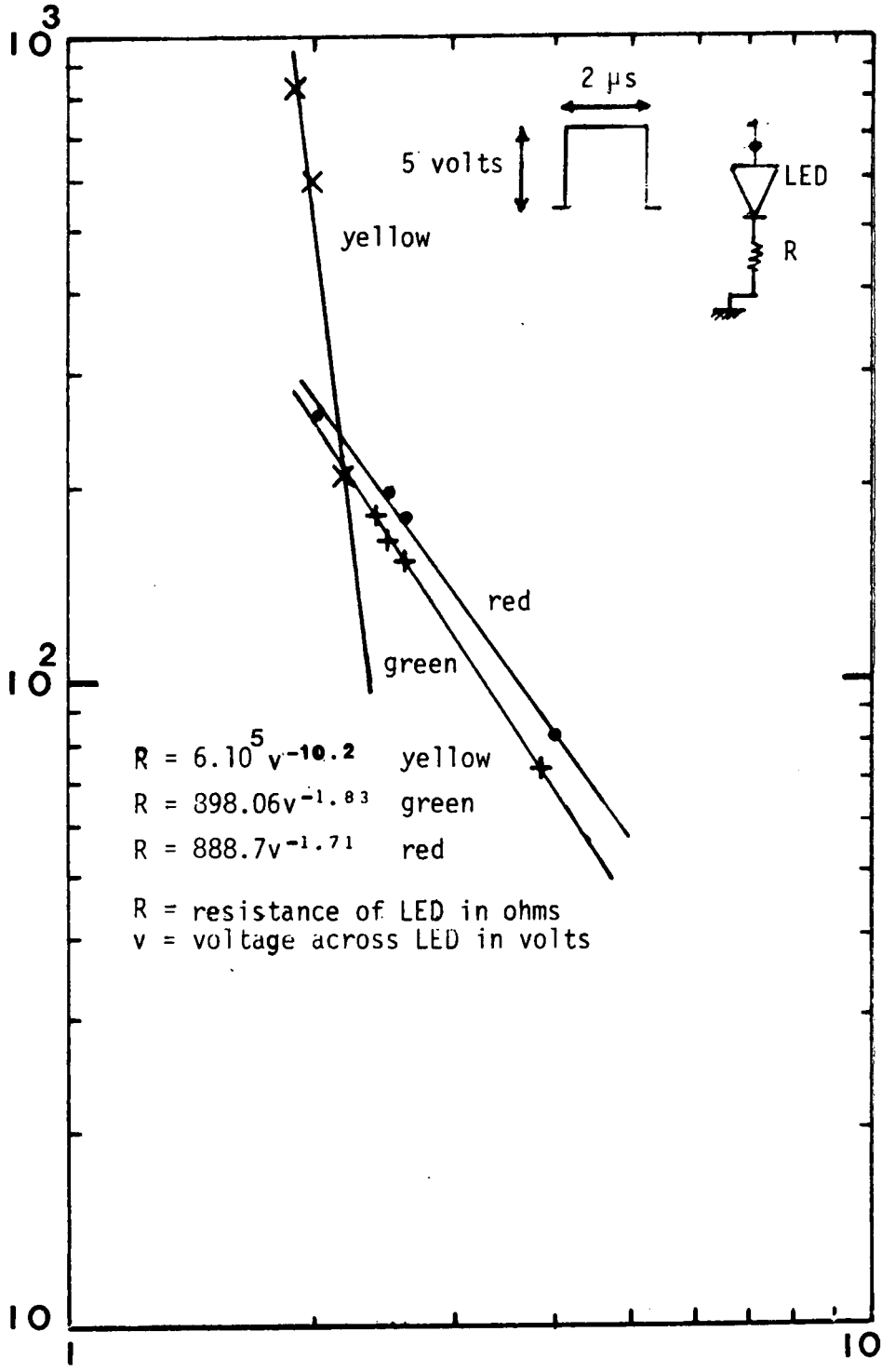

Figure C.5 : Comparison of the variations of the resistance of the LED with voltage applied across the LEDs of different colours. (yellow, green and red)

Appendix D

Correction of the time distribution of recorded pulse heights in the tachyon experiment for experimental bias

In the analysis of the results of the tachyon experiment described in Chapter 7 (Table 7.2 and Figure 7.2) no account was taken of experimental bias as this was believed to be a small effect. Bias arises because large shower front pulses saturate the recording electronics and time domains occur in which small pulses would not be recorded even if present. Figure D1(a) shows a recorded event in which no bias is present. The output of the delay line used in the tachyon experiment (Figure 6.3) was connected to both beams of a dual beam oscilloscope of sweep time 500 μs. The lower beam of the oscilloscope was operated at a sensitivity of 5 mv/cm with a maximum measurable pulse height of 30 mv and the upper beam at a sensitivity of 200 mv/cm with a maximum measurable pulse height of 1400 mv. Figure D1(b) shows a large shower front pulse which saturates the oscilloscope electronics on the lower time base but which is accurately recorded on the upper time base. The shower front pulse on the lower time base is preceded by an oscillation which occupies the ∿90μs time domain preceding the shower front pulse. It is estimated from scanning the film that input pulses in the smallest size range measurable (0.5-2mv) would not be detectable in this type of event in the ∿90μs time domain before the shower front pulse although larger input pulse heights would be. Figure D1(c) shows that small pulse heights can be recorded after the shower front pulse even if the oscilloscope amplifiers overswing. If the overswing goes off scale as shown in Figure D1(d) then no input pulses are recorded by the lower time base but they will be measurable on the upper time base if their height is >30 mv. A correction factor to apply to the

measured number of events in a given size range and a given time range has been found in the following way. Let N be the total number of triggers and X be the number of triggers in which the time range $t_1 \rightarrow t_2$ is not sensitive so N - X is the number of triggers in which the time range $t_1 \rightarrow t_2$ is sensitive. The required correction factor f to give the number of events that should have been recorded if the time domain $t_1 \rightarrow t_2$ was sensitive for all N triggers is $f = \frac{N}{N-X}$. X has been found from scanning the film and figure D2 shows the variation of f with time which is measured from the start of the oscilloscope time base. The correction factor f shown in figure D2 shows the variation of f with time which is measured from the start of the oscilloscope time base. The correction factor f shown in figure D2 is to be applied to pulse heights in the size range 0.5 - 2 mv recorded before the shower front pulse and to pulses in the size range 0.5 - 30 mv after the occurrence of the shower front pulse. Table D1 shows the measured and corrected number of events in different time ranges for different ranges of pulse height. Figure D3 shows the observed and corrected number of events presented in histogram form. It is noted that no correction to the observed number of events is required for input pulse heights >30 mv as these could all be measured on the low sensitivity recording channel where bias effects were zero.

It is seen from figure D3 and table D1 that for the smallest measurable size range of (0.5 - 2)mv the number of events in the time range 180 - 190 μs (corresponding to the time domain 75 - 85 μs preceding the shower front pulse) is increased from 32 ± 5.7 to 37.8 ± 6.7. This is the only cell that gives an anomolously large number of events in the whole of the data and after correction for

bias the excess above the background level expected (10.1 events) if no tachyons are associated with the showers is 4.1 standard deviations which is slightly less than the 4.4 standard deviation excess previously found in Chapter 6. The energy deposit in the tachyons detection scintillator corresponding to pulse height range 0.5 - 2 mv is 0.7 - 1.4 Mev. Again it is concluded that more experimental data is required to determine whether the observed effect is real or merely due to a large statistical fluctuation.

Apart from a search for tachyons associated with extensive air showers the present data can also be used to assess whether there are a significant number of ionising events produced in the tachyon detection scintillator that occur after the arrival of the shower front. Table D2 and D3 give the values of the ratios $\frac{N(120\text{-}260\mu s)}{N(270\text{-}410\mu s)}$ and $\frac{N(0\text{-}260\mu s)}{N(270\text{-}500\mu s)}$ as a function of the energy deposited in the tachyon detection scintillator. The times quoted in the above ratios are measured from the start of the oscilloscope time base with the shower front occurring at a time of 265 μs after the start of the oscilloscope time base. Assuming no significant tachyon flux and that no particles arrive at long time delays ($> 5\mu s$) after the arrival of the shower front the expected values of the above ratios are $\frac{260\text{-}120}{410\text{-}270} = \frac{140}{140} = 1.00$ and $\frac{260\text{-}0}{500\text{-}270} = \frac{260}{230} = 1.13$. It is seen from tables D2 and D3 that all the measured ratios are consistently less than the above values except the one that refers to the smallest range of pulse heights (0.5 - 2 mv) measured. The smallest measured ratio is for pulse heights measured on the recording oscilloscope of (4-30 mv) corresponding to a range of energy deposition in the scintillator of 1.9 Mev - 5.2 Mev. Such delayed pulses could be produced by photons in the EAS electromagnetic cascade which have undergone diffusive scattering or by low energy evaporation neutrons from air nuclei produced in the EAS hadron cascade which subsequently interact in the detection scintillator.

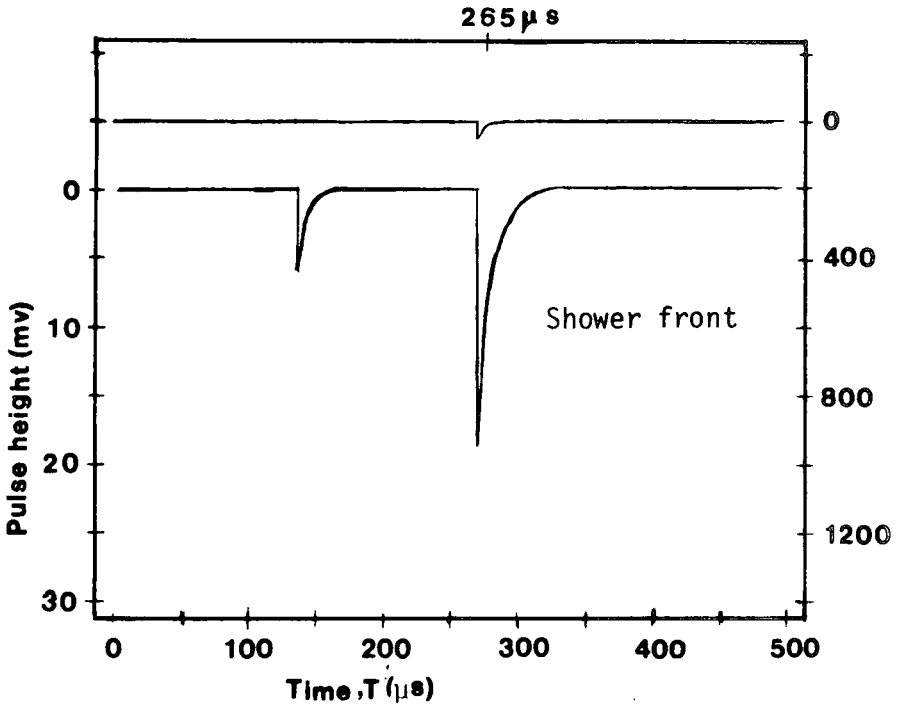

(a) Event with no bias

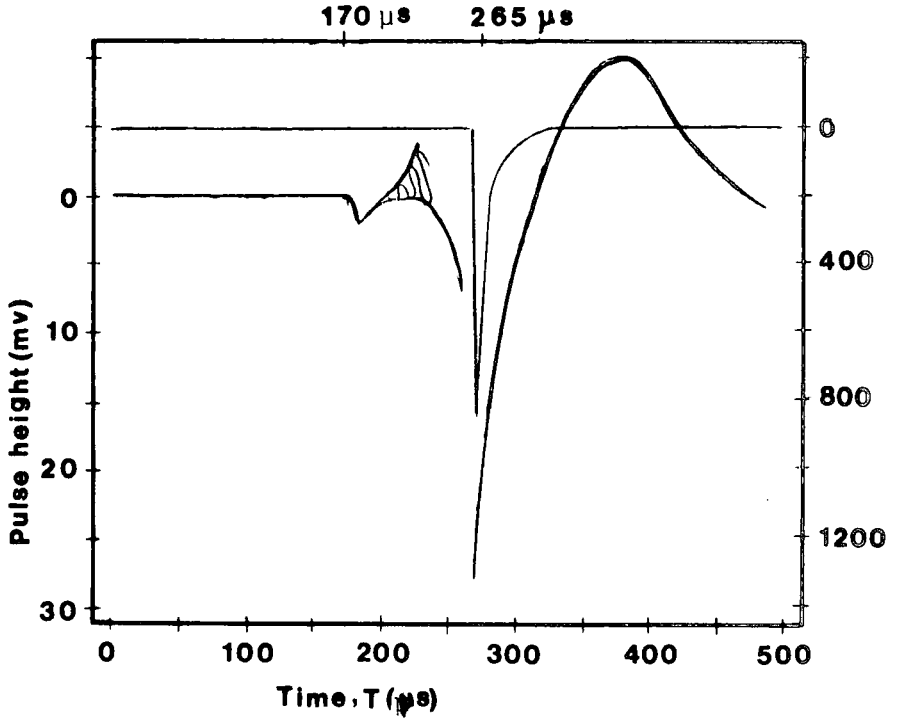

(b) Oscillation that produces bias before the shower front pulse

Fig. D1 : Classification of different types of event

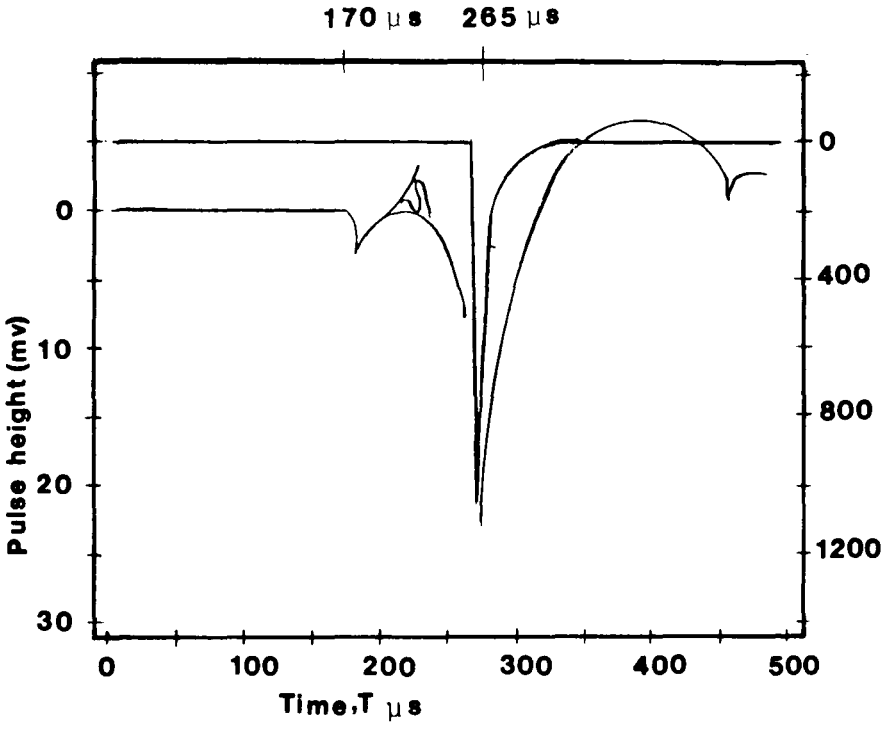

(c) Event measurable after large shower front pulse

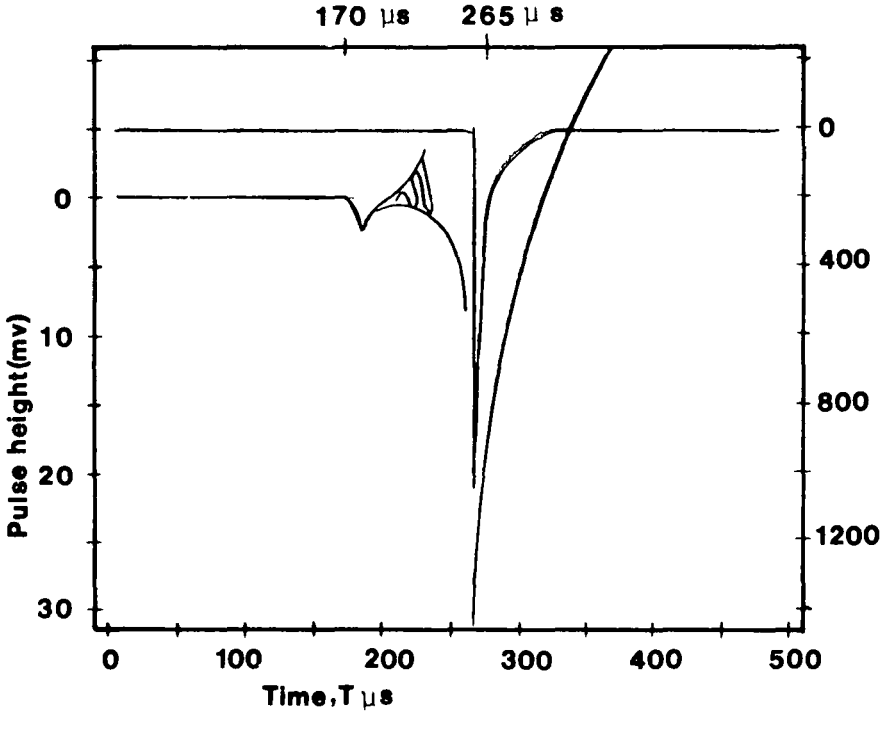

(d) No event measurable after shower front pulse in the time domain 370-500µs

Fig. D1 : Continued

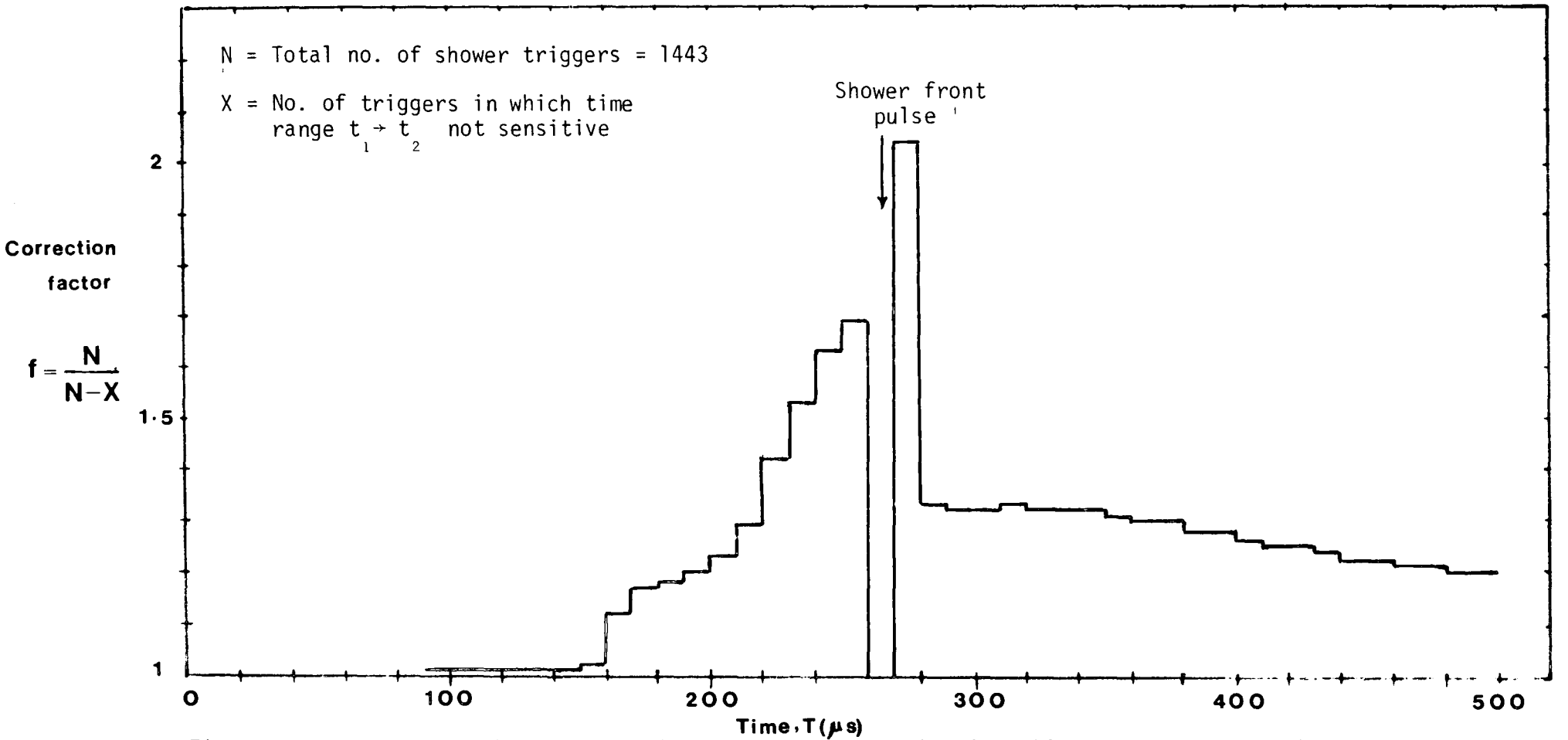

Figure D2. The correction factor f due to experimental bias for different time bins, time being measured from the start of the oscilloscope time base. The shower front pulse occurs at a time of 265μs. For times < 260 μs the correction factor applies only to pulse heights in the range .5-2mv. For times >270μs the correction factor applies only to pulse heights in the range .5-30mv, there being no bias correction for pulse heights >30mv.

Time range micro seconds	Correc-tion factor	.5≤v≤2mv		2<v≤4mv		4<v≤30mv	
		No.of ev. before correc.	No. of ev. after correc.	No.of.ev. before correc.	No.of ev. after correc.	No.of ev. before correc.	No.of ev. after correc.
0- 10	1.00	5	5	1	1	0	0
10- 20	1.00	13	13	8	8	3	3
20- 30	1.00	3	3	5	5	2	2
30- 40	1.00	10	10	3	3	0	0
40- 50	1.00	8	8	3	3	0	0
50- 60	1.00	16	16	5	5	0	0
60- 70	1.00	5	5	5	5	1	1
70- 80	1.00	13	13	7	7	3	3
80- 90	1.00	9	9	9	9	2	2
90-100	1.01	8	8.1	3	3	1	1
100-110	1.01	7	7.1	3	3	3	3
110-120	1.01	8	8.1	2	2	1	1
120-130	1.01	9	9.1	5	5	0	0
130-140	1.01	7	7.1	6	6	1	1
140-150	1.01	10	10.1	3	3	0	0
150-160	1.02	10	10.2	3	3	1	1
160-170	1.12	10	11.2	2	2	2	2
170-180	1.17	14	16.4	4	4	0	0
180-190	1.18	32	37.8	5	5	0	0
190-200	1.20	9	10.8	6	6	0	0
200-210	1.23	8	9.8	3	3	0	0
210-220	1.29	4	5.2	4	4	2	2
220-230	1.42	14	19.9	4	4	2	2
230-240	1.53	3	4.6	2	2	0	0
240-250	1.63	5	8.2	3	3	0	0
250-260	1.69	2	3.4	1	1	0	0
260-270							
270-280	2.04	5	10.2	2	4.1	2	4.1
280-290	1.33	5	6.7	7	9.3	2	2.7
290-300	1.32	8	10.6	3	4.0	3	4.0
300-310	1.32	4	5.3	4	5.3	1	1.3
310-320	1.33	4	5.3	6	8.0	4	5.3
320-330	1.32	13	17.2	5	6.6	5	6.6
330-340	1.32	4	5.3	1	1.3	3	4.0
340-350	1.32	6	7.9	6	7.9	2	2.6
350-360	1.31	5	6.6	7	9.2	2	2.6
360-370	1.30	7	9.1	2	2.6	3	3.9
370-380	1.30	12	15.6	1	1.3	6	7.8
380-390	1.28	3	3.8	6	7.7	2	2.6
390-400	1.28	3	3.8	6	7.7	2	2.6
400-410	1.26	16	20.2	5	6.3	3	3.8
410-420	1.25	8	10.0	8	10.0	4	5.0
420-430	1.25	7	8.8	4	5	4	5.0
430-440	1.24	10	12.4	3	3.7	1	1.2
440-450	1.22	10	12.2	7	8.5	5	6.1
450-460	1.22	13	15.9	4	4.9	3	3.7
460-470	1.21	8	9.7	6	7.3	5	6.1
470-480	1.21	12	14.5	7	8.5	1	1.2
480-490	1.20	10	12.0	4	4.8	0	0
490-500	1.20	3	3.6	4	4.8	1	1.2
Total		418	495.8	212	243.8	88	107.4

Table D1 : Tachyon data based on a sample of 1443 air shower triggers. Time distribution of events in three different ranges of pulse height (measured on the oscilloscope) before and after correction for experimental bias. Time is measured from the start of the oscilloscope time base and the shower front pulse occurs at 265μs. The bias correction shown in Fig.D2 applies to only the pulse height range .5-2mv for times < 260μs and for times > 270μs it applies to the pulse height range .5-30 mv. For large pulse heights there is no bias correction.

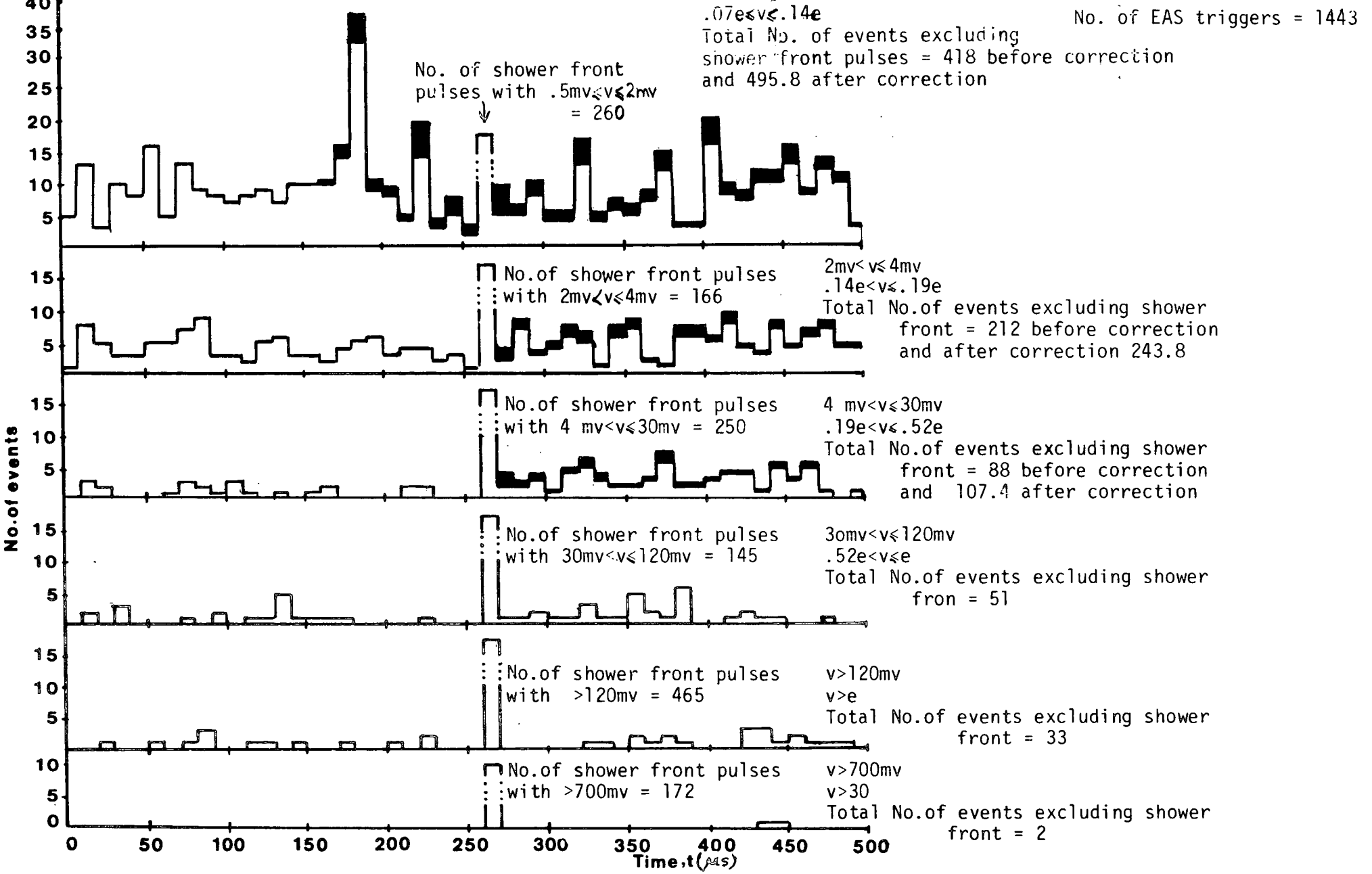

Figure D3. Occurrence time distribution of pulse heights between the two stated pulse height limits and energy deposit limits expressed in terms of e where e = 10 Mev in the tachyon detector. e is the energy deposited in the tachyon detector by a relativistic muon traversing it at normal incidence. Time is measured from the start of the oscilloscope time base and the shower front pulse occurs at 265μs. The effect of applying the correction

Pulse height range	N(120-260μs)		N(270-410)		$\frac{N(120\text{-}260\mu s)}{N(270\text{-}410\mu s)}$	
	Before correction	After correction	Before correction	After correction	Before correction	After correction
.5≤ν≤2mv .07e≤ν≤.14e	137	163.8	95	127.6	1.44±.19	1.28±.15
2<ν≤4mv .14e<ν≤.19e	51	51	61	81.3	.84±.15	.63±.11
4<ν≤30 .19e<ν≤.52e	8	8	40	53.9	.20±.08	.15±.06
30<ν≤120mv .52<ν≤e	11	11	25	25	.44±.16	.44±.16
ν>120mv ν>e	6	6	8	8	.75±.41	.75±.41
ν≥700mv ν≥3e	0	0	0	0	0	0

Table D2. The ratio of the number of events $\frac{N(120\text{-}260\mu s)}{N(270\text{-}410\mu s)}$ occurring in time regions 120-260 μs and 270-410 μs with the times measured from the start of the oscilloscope time base. The shower front pulse occurs at 265 μs from the start of the oscilloscope time base.

Pulse Height range	N(0-260μs)		N(270-500μs)		$\frac{N(0-260\mu s)}{N(270-500\mu s)}$	
	Before correction	After correction	Before correction	After correction	Before correction	After correction
.5≤v≤2mv .07e≤v≤.14e	242	269.1	176	226.7	1.38±.14	1.19±.11
2<v≤4mv .14e<v≤.19e	105	105	107	138.8	.98±.13	.76±.10
4<v≤3omv .19<v≤.52e	24	24	64	83.4	.38±.09	.29±.07
30<v≤120mv .52<v<e	20	20	31	31	.65±.19	.65±.19
v>120mv v>e	13	13	20	20	.65±.23	.65±.23
v>700mv v<3e	0	0	2	2	0	0

Table D3. The ratio of the number of evens $\frac{N(0-260\mu s)}{N(270-500\mu s)}$ occurring in the time regions 0-260μs and 270-500μs with the times measured from the start of the oscilloscope time base. The shower front pulse occurs at 265μs from the start of the oscilloscope time base.

REFERENCES

Abdullah, M.M. et al., (1979), PICCR, Kyoto, 13, 254.
Alvager, T. and Kreisler, M.N.(1968). Phys.ReV., 171, 1357

Anderson, C.D., (1932), Science, 76, 238.

Anderson, C.D., et al., (1938), Phys. Rev., 54, 88.

Aquilar-Benitez, M., et al., (1982), Phys. Letter 111B, (April)

Ashton, F., Coats, R.B., and Simpson, D.A., (1965), Proc. Int. Cosmic Ray Conf. (London), 2, 1079-1081.
Ashton, F., et.al (1970), Acta.Phys.Hung., 29, Suppl., 3, 29

Ashton, F., Parvaresh, A., and Salleh, A.J., 1975, Proc. Int. Conf. Cosmic Rays (Munich), 8, 2831-2836.

Ashton, F., et al., (1977), Proc. 15th Int. Conf. Cosmic Rays, Provdiv 7, 370.
Ashton, F., et al., (1979), PICCR, Kyoto, 13, 238
Baltay, C., et al)1970), Phys. Rev., D1, 759
Bassi, P., Clark, G., and Rossi, B., 1953, Phys.,Rev., 92, 441-451.
Bartlett, D.F. and Lahang, M.D. (1972) Phys.Rev., D6, 1817
Birk, J.B. "The theory and practice of scintillation counting" Pergamon Press, Oxford,1964
Bhat, P.N., Gopolakrishnan, N.V., Gupta, S.K. and Tonwar, S.C., 1979, J.Phys. G., 5, L13 - L18.
Bilaniuk, O.M.P. and Sudarshan, E.C.G. (1962), Am.J.Phys.,30, 718.

Clay, J. (1927), Proc. Roy. Acad. Amsterdam, 30., 1115.
Clay, R.W. and Crouch, P.C. 1974, Nature, 248, 28.

Crouch, P.C., Kahlmann, J.D., Clay, R.W., Gregory, A.G., Patterson, J.R., and Thorton, G.J., (1977), Proc. Int. Conf. Cosmic Rays (Plovdiv), 12, 166-171.
Davis, M.B., et al (1969), Phys. Rev., 183, 1132.

Earnshaw, J.C., Machin, A.C., Pickersgill, D.R., and Turver, K.E., (1973), J.Phys. A., 6, 1244-1261.

Einstein,Ann.Phys. 17, 891 (1905)

Elster, J. and Geitel, H. (1899), Phys.Z., 1, 11.

Emery, M.W., et al (1975), PICCR, Munich, 7.2486.

Fegan, D.J., et al (1975), PICCR, Munich, 7, 2480

Fegan, D.J., (1981), PICCR, Paris, 5, 55.

Fermi, E. (1949), Phys., Rev., 75, 1169.

Feinberg, G. (1967), Phys. Rev., 159, 1089

Feynman, R.P. (1949), Phys. Rev., 76, 749

Galliraith, W., 1958, "Extensive Air Showers", Published by Butterworths.

Gerasimova, N.M. and Zatsepin, G.T. (1960), Sov.Phys. JETP, 11, 899

Greisen, K., (1942), Phys. Rev., 61, 212-221.

Greisen, K., (1960), Ann. Rev. Nucl., Sci. 10, 63.

Greisen, K., (1965), PICCR, London, 609.

Greisen, K., (1966), Phys., Rev., Lett., 16, 748.

Grigorov, N.L., et al. (1971), Sov. J. Nucl. Phys., 11, 588.

Hayakawa, S., 1969, "Cosmic Ray Physics", Published by Wiley - Int. Science.

Hess, V.F., (1912). Phys., Zeitschr, 13, 1084.

Hillas, A.M., (1981), PICCR, Paris, 6, 244.

Jelley, J.V., "Cerenkov Radiation", Published by Pergamon Press 1958.

Johnson, H.T., (1932), Phys. Rev., 41, 545.

Julliusson, E. (1975), PICCR, Munish, 8, 2689.

Kalmykov, N.N., Fomin, Yu, A., and Khristiansen, G.B., 1973, Proc. Int. Conf. Cosmic Rays (Denver), 4, 2633-2638.

Kempa, J. 1976, Nuovo Cimento, 31A, 568-580

Kolhorster, W. (1913), Phys. Zeits., 14, 1153.

Linsley, J., and Scarsi, L., 1962, Phys. Rev., 128, 2384-2392.

Meyer, P., Ramaty, R., and Webber, W.R., (1974), Phys. Today, 27, 23.

Millikan, R.A., and Camerson, G.H., (1926), Phys. Rev., 28, 851.

Morrison, P., Ullert, S., and Rossi, B., (1954), Phys.Rev. ,94, 440

Morrison, P, 1961, Handuch der Physik, XLVI/1, 1-87.

Pathak, K.M., and Subba, L.N., 1981, Proc. Int. Cosmic Ray Conf. (Paris), 7, 11-14.

Prescott, J.R. (1975), PICCR, Munich, 7, 2474

Ramana Murty, P.V. (1971) Lett. Nuov. Cim., 1, 908

Rochester, G.D. and Butler, C.C., (1947), Nature, 160, 855.

Rossi, B. (1952) "High energy particles" published by Prentice-Hall.

Smith, A.C., (1976), Ph.D. Thesis, University of Durham.

Smith, A.C., and Thompson, M.G., 1977, Nuc-Inst and Meth.,145, 289-293

Smith, G.R., and Standil, S., 1976, Canadian Journal of Physics, 54, 176-185.

Street, J.C. and Steven, E.C., (1937), Phys. Rev., 52, 1003.

Turver, K.E., 1973, "Cosmic Rays at Ground Level", Published by the Institute of Phys. (London).

Van Allen, J.A. and Singer, S.F. (1950) Phys. Rev. 78, 819; Correction, 80, 116

Woidneck, C.P., and Bohm, E., 1975, J. Phys. A., 8, 997-1004.

Wolfendale, A.W., (1973), "Cosmic Rays at Ground Level, published by the Institute of Phys. (London).

Wilson, C.T.R. (1901), Proc. Roy. Soc., 68, 151.